LONG WAVELENGTH FLUORESCENT REPORTERS FOR PROTEIN KINASES AND DESIGN OF LIGHT-ACTIVATABLE BIOAGENTS

Luong Tien Nguyen

A dissertation submitted to the faculty at the University of North Carolina at Chapel Hill in partial fulfillment of the requirements for the degree of Doctor of Philosophy in the UNC Eshelman School of Pharmacy
(Division of Chemical Biology and Medicinal Chemistry)

Chapel Hill
2014

Approved by:

David S. Lawrence

Christopher E. Sims

Leslie Parise

Michael B. Jarstfer

Qisheng Zhang

© 2014
Luong Tien Nguyen
ALL RIGHTS RESERVED

ABSTRACT

LUONG TIEN NGUYEN: Long Wavelength Fluorescent Reporters for Protein Kinases and Design of Light-Activatable Bioagents
(Under the direction of David S. Lawrence)

The first part of this dissertation describes the development of wavelength-tunable fluorescent reporters for monitoring protein kinase activity. The probing wavelength is preprogrammed by using a variety fluorophores which are commercially available. Specifically, we develop fluorescent sensors sensing in the far-red and near-IR region and use them to monitor endogenous cAMP-dependent protein kinase activity in erythrocyte lysates and in erythrocytes. Stabilization of the peptide sensor in erythrocyte lysate is also reported. The study provides powerful tools to investigate the roles of protein kinase A activity in erythrocyte biochemistry, for example, in *Plasmodium Falciparum* infection and propagation.

In the second part of the dissertation, we describe the design of light-activatable bioagents based on lipidation and membrane sequestration. A lipidated bioagent upon binding to cells/organelles' membrane is biologically inert. A photolabile group placed between the lipid and bioagent furnishes a means to release the bioagent from the membrane and activate it. The strategy provides a way to fine-tune the presence of an "active" bioagent using light. For example, a peptide sensor can be introduced into a biological system and remains "silent" until controllably activated with light; a protein can be activated or inhibited by the light-triggered release of the corresponding active activator or inhibitor that is hidden in the membrane.

Additionally, the use of erythrocytes as carriers and protectors of photoactivatable peptide therapeutics is also discussed. The study is aim to develop a way to controllably deliver active therapeutics to a specific region of the body to increase their potency and reduce their toxicity.

This work is dedicated to my daughter, Trang Phuong Nguyen, and my wife, Bong Nguyen, for all the time being here with me. We have such a memorable time here at Chapel Hill.

ACKNOWLEDGEMENTS

I would like express the deepest appreciation to my advisor, Dr. David Lawrence, for his guidance, patience, and insightful discussions about research during my time here in the group. I want to thank my committee members, Dr. Christopher E. Sims, Dr. Leslie Parise, Dr. Michael B. Jarstfer, and Dr. Qisheng Zhang for supporting me during the training and for advice regarding future career. I am also very grateful to Dr. Nancy Allbritton for her insightful comments and support during the past few years.

I especially would like to thank Dr. Melanie Priestman for the help with microscopy, for all supporting arguments, and helping me with the dissertation writing. I want to thanks Nathan Oien for the PKA project. I greatly appreciate Dr. Qunzhao Wang for his help regarding peptide chemistry and instrumentation. I also would like to thank Collin O'Banion for his assistance (together with Dr. Qunzhao Wang) in continuing the unfinished project and for helping me with the dissertation writing. I am so fortunate to have many colleagues who help me tremendously when I am in the laboratory. I would like to thanks Weston Smith for helping me with the writing and for all the discussion we have. I greatly appreciate Dr. Hsien-ming Lee, Dr. Vyas Sharma, Dr Finith Jernigan, Dr. Jennifer Shell, Dr. Thomas Shell, Dr. Robert Hughes, Nathan Oien, and Zach Rodgers for helping me during the progression of my research projects.

I would also like to thank members in Allbritton's Lab, Angie Proctor, Ryan Phillips, and Abby Turner for helping with CE experiments.

There are numerous people I would like to thank for helping me during my five-year here at Chapel Hill, but after days of focusing on writing this dissertation, lots of the neurons involving in name memory have lost contact with each other or died.

I also thank Vietnam Education Foundation (VEF) for encouraging and giving me the opportunity to come here to pursue the graduate program and experience American culture. I would like to thank NIH for funding my research.

PREFACE

Chapter 2 represents work done by myself and work done in collaboration with Nathan Oien. All experiments with erythrocytes in Chapter 2 were done in collaboration with Nathan Oien. The work has been published before writing this dissertation with the following citation:

> Oien, N. P.; Nguyen, L. T.; Jernigan, F. E.; Priestman, M. A.; Lawrence, D. S., Long-wavelength fluorescent reporters for monitoring protein kinase activity. *Angew Chem Int Ed Engl* **2014,** *53* (15), 3975-8.

Chapter 3 describes unpublished research that was designed and performed by myself.

Chapter 4 describes work performed by myself under the direction of Dr. David Lawrence and Dr. Nancy Allbritton and in collaboration with Nathan Oien. The work has been published previous to writing this dissertation with the following citation:

> Nguyen, L. T.; Oien, N. P.; Allbritton, N. L.; Lawrence, D. S., Lipid Pools As Photolabile "Protecting Groups": Design of Light-Activatable Bioagents. *Angew Chem Int Ed Engl* **2013,** *52* (38), 9936-9939.

Chapter 5 describes unpublished work that has been done in collaboration with Dr. Melanie Priestman, Dr. Qunzhao Wang, and Collin O'Banion.

All copyrighted materials included in this dissertation are used with permission from the relevant copyright holders.

TABLE OF CONTENTS

LIST OF TABLES

LIST OF FIGURES

LIST OF SCHEMES

LIST OF ABBREVIATIONS

5Fam	5-carboxyfluorescein
5Tam	5-carboxytetramethylrhodamine
5Fam-α-MSH-amide	See structure in page 151
5Fam-α-MSH-nb-Cys-amide	See structure in page 150
MSH-nb-Dipal	See structure in page 138
5Tam-Aoc-GRTGRRFSY-amide	See structure in page 130
CP-nb-Cys	See structure in page 148
CP-nb-Stear	See structure in page 130
CP-nb-Dipal	See structure in page 134
5Tam-EEK(Chol)-nb-R-AMC	See structure in page 95
5Tam-EEK(Stear)-nb-R-AMC	See structure in page 95
5Tam-K(Chol)-nb-R-AMC	See structure in page 119
5Tam-K(Stear)-nb-R-AMC	See structure in page 95, 122
Abl	An tyrosine kinase in human encoded by ABL gene
Akt a.k.a. PKB	Protein kinase B
anp	3-(fmoc-amino)-3-(2-nitrophenyl)propanoic acid
Aoc	8-amino octanoyl linker
ATP	Adenosine triphosphate
Atto633-Aoc-GRTGRRFS(DMNB)Y-amide	See structure in page 42
C12-bn-COOH	See structure in page 123
C12-bn-PKA	See structure in page 123
C18-bn-COOH	See structure in page 112
C18-bn-K(5Tam)	See structure in page 114
C18-bn-K(5Tam)--K(5Fam)	See structure in page 116
C8-K(5Tam)-α-MSH-nb-Cys-amide	See structure in page 151
C8-K(5Tam)-α-MSH-nb-Dipal	See structure in page 151
cAMP	Cyclic adenosine monophosphate
cAMP	Cyclic adenosine monophosphate
CE	Capillary electrophoresis
CE-LIF	Capillary electrophoresis with laser induced fluorescence detection
Cys-Hex1-Cys	See structure in page 126
Cys-Hex2-Cys	See structure in page 126
Dap	2,3-diaminopropionic acid
DIC	N,N'-diisopropylcarbodiimide
DIC image	Image produced by differential interference contrast

Dipal-Mal	See structure in page 147
DIPEA	N,N-diisopropylethylamine
DMNB	4,5-dimethoxy-2-nitrobenzyl
DNA	Deoxyribonucleic acid
EGFR	Epidermal growth factor receptor
ERK	Extracellular signal-regulated kinase
FBS	Fetal bovine serum
Fmoc	Fluorenylmethyloxycarbonyl
Fmoc-anp-OH	See structure in page 125
Fmoc-L-Ser(DMNB)-OH	See structure in page 47
Fmoc-nb-COOH	See structure in page 112
FRET	Fluorescence Resonance Energy Transfer
GFP	Green fluorescent protein
HCTU	O-(6-chlorobenzotriazol-1-yl)-N,N,N′,N′-tetramethyluronium hexafluorophosphate
HOBt	1-hydroxybenzotriazole
HPLC	High performance chromatography
ivDde	1-(4,4-dimethyl-2,6-dioxocyclohex-1-ylidene)-3-methylbutyl
JNK	C-Jun N-terminal kinase
Lck	A tyrosine kinase, a member of Src
LC-MS	Liquid chromatography with mass detection
Mal-anp-K(5Tam)RRRLAALAA-amide	See structure in page 127
min	minute(s)
Mtt	4-methyltrityl
p38α	P38 mitogen-activated protein kinase alpha
PBS	Phosphate buffered saline
P-H1-P	See structure in page 127
P-H2-P	See structure in page 127
Pim	A group of serine/threonine kinases
PKA	cAMP-dependent protein kinase
PKC	Protein kinase C
PMT	Photomultiplier tubes
PRCP	A prolylcarboxypeptidase
RF-HPLC	Reverse phase-high performance chromatography
RNA	Ribonucleic acid

RSK	Ribosomal S6 kinase
S6K	p70 ribosomal S6 kinase
SDS	Sodium dodecyl sulfate
sec	second(s)
SH1	Src homology 1
SH2	Src homology 2
Src	A tyrosine kinase
TFA	Trifluoroacetic acid

CHAPTER 1: BACKGROUND AND SIGNIFICANCE

Fluorescence Techniques and the Optical Windows of Tissue

Fluorescence Techniques

Since first reported by Sir John Herschel in 1845 and named by Sir George Stockes in 1852, fluorescence has now become a powerful tool in biomedical research.[1, 2] The techniques provide excellent sensitivity as well as a continuous and nondestructive detection with a high degree of spatial and temporal resolution when applied in living systems.

Small fluorescent molecules (fluorophores) and fluorescent proteins are two major classes of fluorescent molecules that are commonly used. For small molecule fluorophores, scientists have not only relied on naturally-occurring substances, but also developed a huge collection of fluorescent molecules derived from variety of structural scaffolds, i.g., coumarin, xanthene, cyanine, oxazine, and so on.[3] The excitation and emission wavelengths of those fluorophores now cover from 300 nm - 800 nm (Figure 1.1).[4] The discovery of a fluorescent protein in 1962 together with genetic manipulating technologies has brought fluorescence to a new level of applicability when the fluorescent probes can be generated continuously *in situ*.[5-11] In term of excitation and emission wavelength, a number of fluorescent proteins have been reported working at various excitation and emission wavelengths, however the selection is somehow limited compared to that of small molecule fluorophores due to the strict folding requirement of fluorescent proteins.[6, 7]

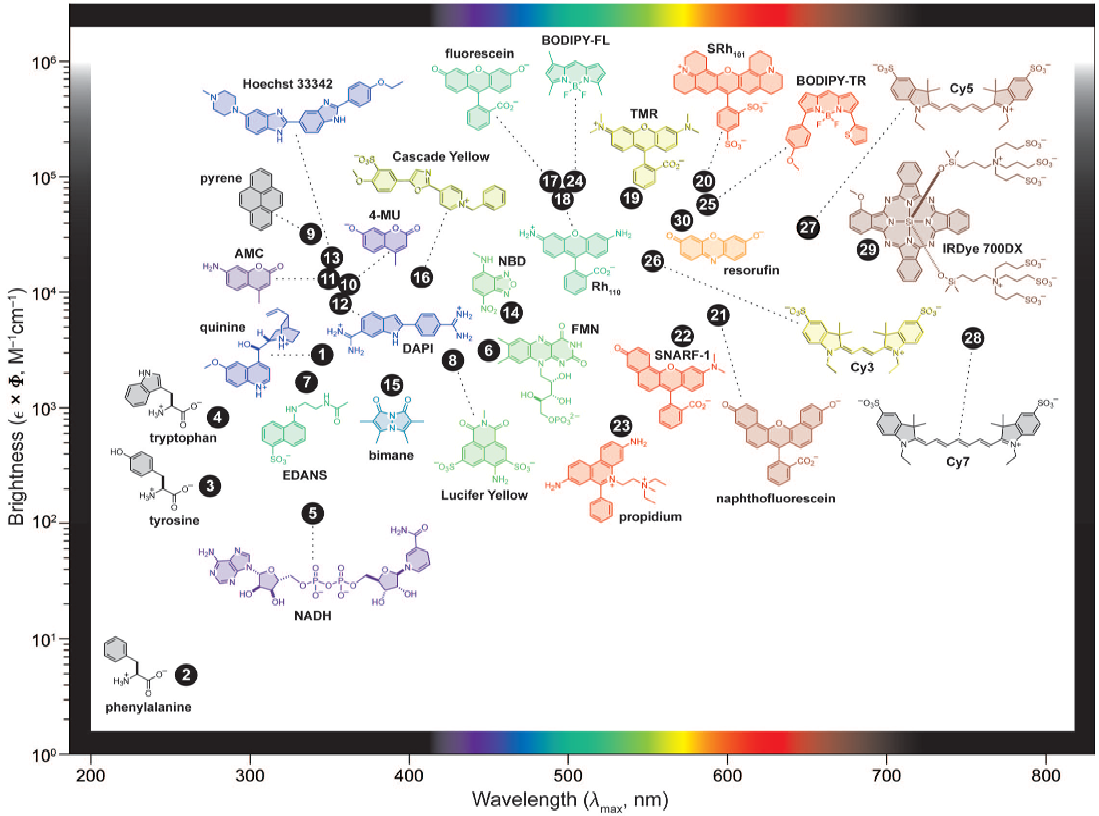

Figure 1.1: Plot of fluorophore brightness (ε x ϕ) vs the wavelength of maximum absorption (λ_{max}) for the major classes of fluorophores. The color of the structure indicates its wavelength of maximum emission (λ_{em}). For clarity, only the fluorophoric moiety of some molecules is shown.

Reprinted with permission from Lavis, L. D.; Raines, R. T., Bright ideas for chemical biology. *ACS Chem Biol* **2008,** *3* (3), 142-55. © 2008 American Chemical Society.

Based on those fluorescent molecules, scientists have developed numerous applications including in, but not limited to, cell and organelle staining, molecular dynamic and function sensing, gene expression reporting, enzymatic activity measurements, disease markers, tumor surgery, etc.[3, 11-17]

Optical Windows of Tissue

When a fluorescent technique is used, selection of wavelengths which can provide clear images is one of the most important parameters. Signal attenuation and auto-fluorescence are two major causes of poor images. Typically in tissue imaging, excitation photons need to travel through tissue and reach the target fluorescent contrast agent and emission photons need to travel the same pathway to reach a detector. During this propagation, photons can be absorbed or scattered by tissue's components. Light absorption can be due to selected biomolecules in tissue, such as collagen, elastin, lipids, hemoglobin, while scattering can come from cells or intracellular matrix.[18, 19] This interference is also applied to *in vitro* assay when strong absorption of assay components can eliminate the signal. In addition to tissue scattering and absorption, autofluorescence can also severely affect the signal. For example, Frangioni took fluorescent images of a sacrificed mouse using three different excitation/emission filter sets: blue/green ($\lambda_{ex}/\lambda_{em}$: 460 - 500 nm/505 - 560 nm); green/red (525 - 555 nm/590 - 650 nm); and near-infrared (NIR) (725 - 775 nm/790 - 830 nm). In the images taken in blue/green and green/red regions, significant background from tissue autofluorescense was observed suggesting the potential challenge if using fluorescent contrast agents working in those regions. However, in the near IR image, autofluorescence was essentially eliminated.[20] This observation together with other data suggests an optical window of tissue (600-1000 nm), in which the fluorescence signals are least interfered (Figure 1.2).[18, 21, 22]

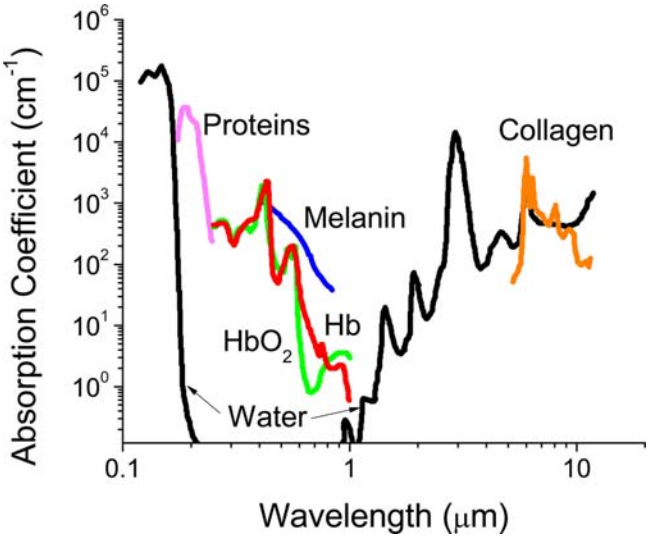

Figure 1.2: Absorbance of various tissue and blood components from 200 nm to 10 μm.

Reprinted with permission from Pansare, V.; Hejazi, S.; Faenza, W.; Prud'homme, R. K., Review of Long-Wavelength Optical and NIR Imaging Materials: Contrast Agents, Fluorophores and Multifunctional Nano Carriers. *Chem Mater* **2012,** *24* (5), 812-827. © 2012 American Chemical Society.

Protein Kinase and Protein Kinase Activity Probes

Protein Kinases

Protein kinases are enzymes that catalyze the transfer of the γ-phosphoryl group from ATP to specific sites in proteins in a process called phosphorylation. In eukaryotes, these sites are usually the free hydroxyl groups of serine, threonine, and tyrosine residues in proteins. It has been estimated that about 500 genes in human genome encode for protein kinases and up to 30% of all cellular proteins contain a phosphate group. Protein kinases are involved in every basic cellular process, including metabolism, growth, division, differentiation, motility, cellular transport. Numerous studies suggest the roles of protein kinases in many human diseases such as cancer, inflammatory diseases, neurological disorders, etc.[23-26]. Protein kinases are currently a major drug target.

Given the important role of protein kinases in human diseases, it is crucial to be able to monitor the activity of a kinase of interest. To date, a number of protein kinase sensors have been developed. The majority of them are fluorescent sensors and can be categorized into two major classes: genetically encoded protein based sensors and small molecule peptide-based sensors.[27]

Protein-Based Kinase Probes

The majority of the protein-based kinase probes function through phosphorylation induced conformational change leading to Fluorescence Resonance Energy Transfer (FRET). Basically, the probes contain a donor fluorescent domain, an acceptor fluorescent domain, and a domain of which conformation is phosphorylation sensitive. The donor/acceptor pair are selected so that the emission spectrum of the donor domain sufficiently overlaps with the excitation spectrum of the acceptor. When phosphorylation occurs, the relative orientation between the two are altered, which leads to the change in the excitation-emission profile of the pair (Figure 1.3).[28] This type of sensors have been developed for variety of kinases, such as PKA, Akt, RSK, S6K, ERK, JNK, EGFR/Abl, to name a few .[27, 29]

The protein-based probes have both advantages and disadvantages. An advantage is that the protein probes can be synthesized continuously *in situ* thus can be customized to provide spatiotemporal information regarding signaling in living cells. Additionally, they are usually reversible probes, and thus can provide information about the dynamic interplays between the activity of kinases and phosphatases. On the other hand, however, the protein probes have limitations in term of signal gain and the flexibility of wavelength used. Even after significant effort of optimization, the FRET-based sensors typically only give from 10 - 60% and rarely get to 100% signal gain.[27, 29] Additionally, the fluorescence

bleed-through and limited options of FRET fluorescent protein pairs also lead to difficulties when designing and using FRET-based kinase sensors.

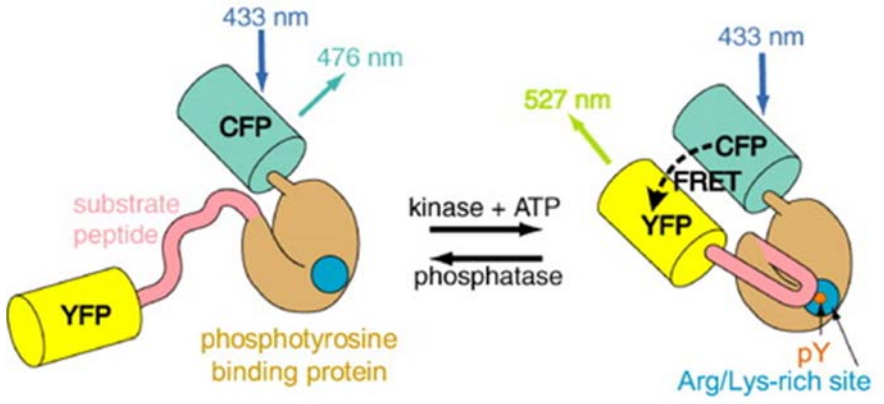

Figure 1.3: General design of FRET-based protein kinase sensors. Once phosphorylated by a kinase of interest, the phosphopeptide binding domain forms an intramolecular complex with the phosphopeptide, giving rise to a distance change between the two flanking fluorescent proteins that alters the FRET.

> Reprinted with permission from Ting, A. Y.; Kain, K. H.; Klemke, R. L.; Tsien, R. Y., Genetically encoded fluorescent reporters of protein tyrosine kinase activities in living cells. *Proc Natl Acad Sci U S A* **2001,** 98 (26), 15003-8. Copyright (2001) National Academy of Sciences, U.S.A.

Peptide-Based Kinase Probes

In the last two decades, there has been significant progress in developing fluorescent probes for sensing kinase activity based on short peptides. Basically, this type of probe contains a fluorophore appended to a short peptide sequence which, upon phosphorylation by a kinase of interest, leads to a fluorescence change by different mechanisms. These probes can be categorized into groups based on working mechanism: chelation induced fluorescent increase, environment sensitive fluorescence, phosphorylation disrupting quenching mechanism, or capillary electrophoresis coupled with laser induced fluorescence detection.

Lawrence and colleagues were the first created a peptide sensor for protein kinases based on chelation induced fluorescence increase. Specifically, the probe contains a peptide substrate for PKC to which is appended a fluorophore bearing two carboxylate groups. Phosphorylation of the peptide substrate generates a M^{2+} binding site which consists of the newly introduced phosphate group and the two carboxylate moieties from the fluorophore. The fluorescence signal is gained from phosphorylation followed by divalent cation coordination (Figure 1.4).[30]

An analogous approach was exploited by Imperiali and co-workers to develop kinase sensors based on the chelation of 8-hydroxy-5-(*N,N*-dimethylsulfonamido)-2-methylquinoline (Sox) moiety and phosphate group to Mg^{2+} (Figure 1.5).[31] The probes comprise a Sox moiety appended to an optimized peptide substrate for the target kinase. Upon phosphorylation and in the presence of Mg^{2+}, the Sox and phosphate groups coordinate the divalent magnesium ions leading to fluorescence enhancement. Employing this strategy, Imperiali and colleagues have developed sensors targeting a number of kinases such as Akt, Abl, ERK1/2, PKA, PKC, p38α, Pim, etc.[32, 33]

Using environmentally sensitive fluorophores is another strategy for making peptide-based kinase sensors. For example, Lawrence and co-workers designed a PKC probe in which an environmentally sensitive fluorophore is placed on a peptide substrate close to the phosphorylation site. Phosphorylation of the peptide changes the environment around the fluorophore leading to the fluorescence change (Figure 1.6).[34]

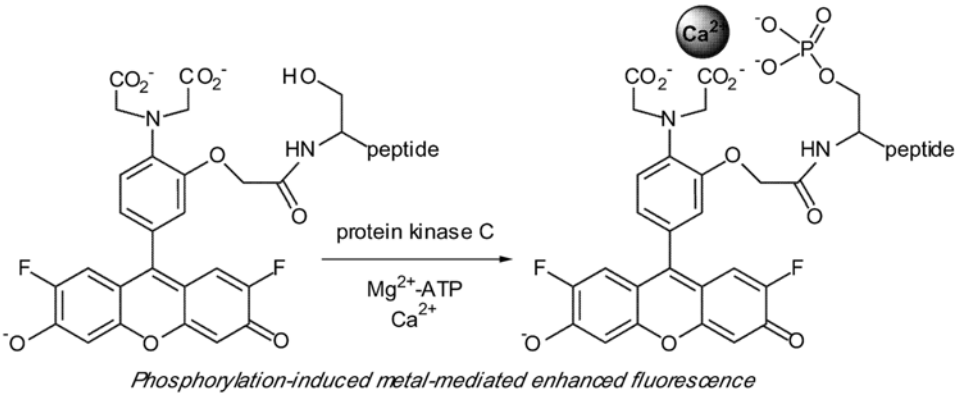

Figure 1.4: Structure of a PKC fluorescent sensor based on chelation induced fluorescence change.

Reprinted with permission from Chen, C. A.; Yeh, R. H.; Lawrence, D. S., Design and synthesis of a fluorescent reporter of protein kinase activity. *J Am Chem Soc* **2002,** 124 (15), 3840-1. Copyright (2002) American Chemical Society.

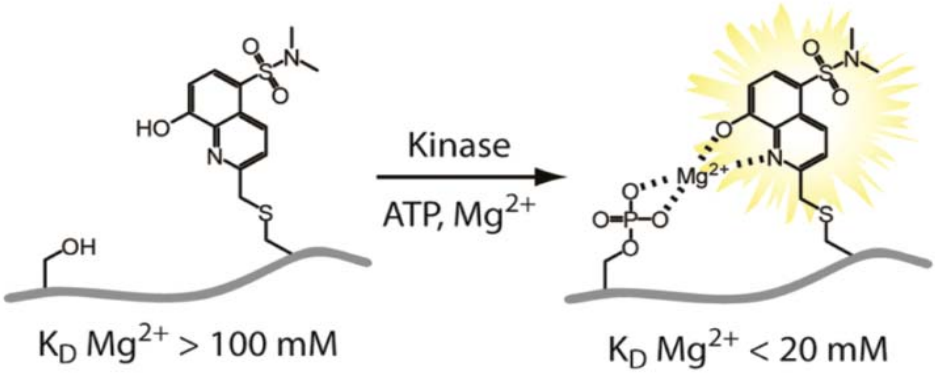

Figure 1.5: General design of Sox kinase sensors developed by Imperiali and coworkers.

Reprinted with permission from Stains, C. I.; Lukovic, E.; Imperiali, B., A p38α-Selective Chemosensor for use in Unfractionated Cell Lysates. *ACS Chem Biol* **2010,** *6* (1), 101-105. Copyright (2010) American Chemical Society.

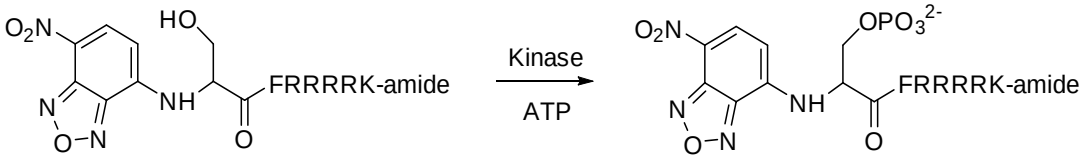

Figure 1.6: PKC fluorescent sensor developed by Lawrence and coworkers. Phosphorylation of the serine residue which is in proximity of an environmentally sensitive fluorophore results in a fluorescence signal.

Figure adapted from Yeh, R. H.; Yan, X.; Cammer, M.; Bresnick, A. R.; Lawrence, D. S., Real time visualization of protein kinase activity in living cells. *J Biol Chem* **2002,** *277* (13), 11527-32. Copyright the American Society for Biochemistry and Molecular Biology.

The strategy of using environmentally sensitive fluorophores was further developed by Lawrence and co-workers using a phosphopeptide binding domain. The Src peptide substrate tagged with an environmentally sensitive fluorophore, following phosphorylation, binds to the phosphopeptide binding protein (Lck SH2 domain). The change in the environment due to binding event leads to fluorescence signal (Figure 1.7).[35]

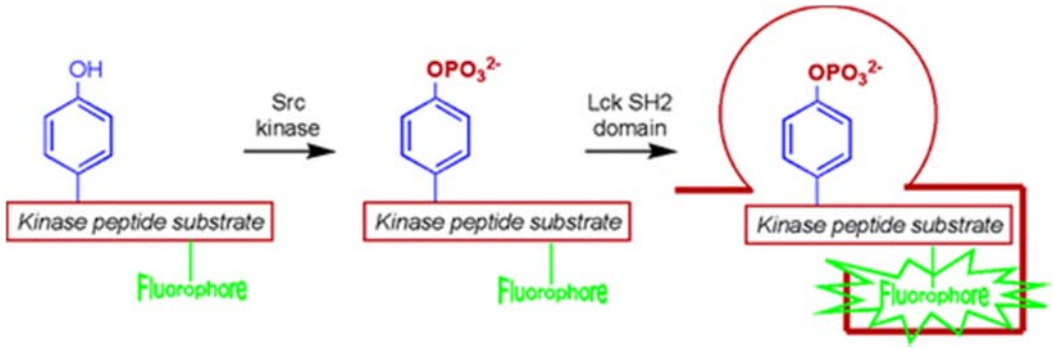

Figure 1.7: An alternative design of kinase fluorescent sensor based on an environmentally sensitive fluorophore. Phosphorylation followed by protein binding leads to a fluorescence response.

Reprinted with permission from Wang, Q.; Lawrence, D. S., Phosphorylation-driven protein-protein interactions: a protein kinase sensing system. *J Am Chem Soc* **2005,** *127* (21), 7684-5. Copyright (2005) American Chemical Society.

Another type of peptide kinase sensor was developed based on phosphorylation induced fluorescence dequenching mechanism. Lawrence et al. designed a Src kinase

peptide sensor in which a pyrene is attached to the peptide near the phosphorylated tyrosine residue. While the fluorescence of the flurophore is quenched by the tyrosine residue, phosphorylation of the residue disrupts the interaction leading to a fluorescence increase (Figure 1.8).[36, 37] The strategy has been applied to develop tyrosine kinases sensor working at long wavelengths for multicolor monitoring experiments.[38]

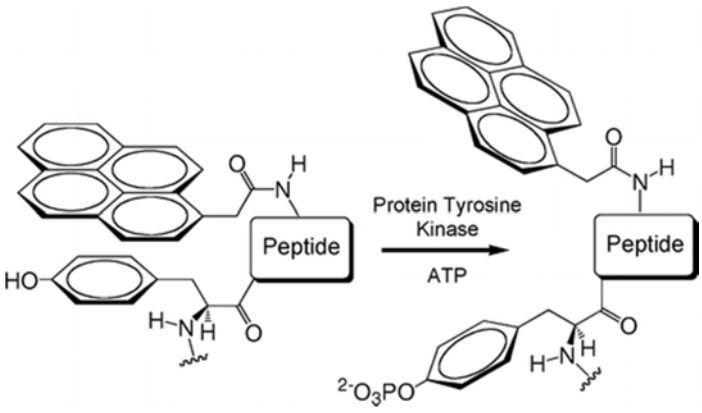

Figure 1.8: Tyrosine kinase fluorescent sensor based on a phosphorylation induced fluorescence dequenching mechanism developed by Lawrence and coworkers.

Reprinted with permission from Wang, Q.; Cahill, S. M.; Blumenstein, M.; Lawrence, D. S., Self-Reporting Fluorescent Substrates of Protein Tyrosine Kinases. *J Am Chem Soc* **2006,** *128* (6), 1808-1809. Copyright (2006) American Chemical Society.

Alternatively, Sharma and Lawrence reported an elegant design named “Deep Quench” technique which provides an excellent fluorescence response upon phosphorylation (up to 65 fold fluorescence increase). Basically, the sensor system contains a fluorescently labelled peptide substrate and a quencher which can interact and quench the peptide fluorescence. Upon phosphorylation, in the presence of a phosphoserine recognition domain, the binding of phosphopeptide to the receptor disrupts quencher-peptide interaction, thus leading to fluorescence increase (Figure

1.9).[39] Lawrence and colleagues demonstrated the applicability of the technique to measure the activity of PKA in different mitochondrial sub-compartments.[40]

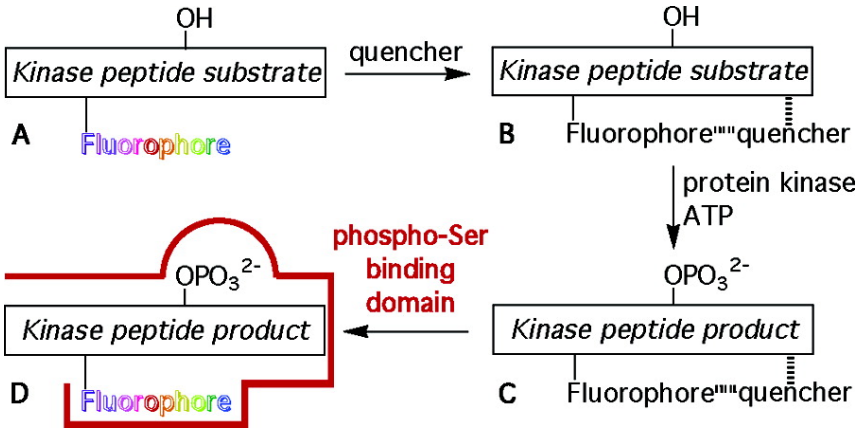

Figure 1.9: General design of "Deep Quench" kinase sensor developed by Lawrence and colleagues.

Reprinted with permission from Sharma, V.; Agnes, R. S.; Lawrence, D. S., Deep Quench: An Expanded Dynamic Range for Protein Kinase Sensors. *J Am Chem Soc* **2007,** 129 (10), 2742-2743. Copyright (2007) American Chemical Society.

Another kinase activity measurement system based on fluorescent peptides was pioneered by Allbritton and coworkers employing capillary electrophoresis with laser induced fluorescence detection (CE-LIF). A fluorescently labelled peptide substrate of a kinase of interest is introduced into cell lysates or living cells. At various time points, aliquots/cells are analyzed by CE-LIF in which the nonphosphorylated peptide and the phosphorylated product are separated and quantified. Using this technique, numerous peptide-based sensors have been developed, for example for PKA, PKB, PKC, CamKII, cdc2K, Src and EGFR.[41-44]

Even though rapidly developed in the last two decades and provides excellent fluorescence response upon phosphorylation, peptide-based kinase sensors possess two major challenges: cellular delivery and stability inside living cells. Technologies dealing

with these two issues are important for further development of the peptide-based sensors.

Spatiotemporal Control and the Creation of Light-Activatable Bioagents

In studying of complex biological processes and medical applications, controlling the presence as well as the amount of an active species in a spatiotemporal manner is crucial. For example, the function of a specific protein in a biological context can be revealed by keeping it in an inactive state for a necessary amount of time then quickly activating it followed by phenotypic observation. Another example is measuring the activity of an enzyme of which the catalytic process is fast. A sensor used to report the activity when introduced into the system would be completely processed before the system gets equilibrated. It would be beneficial if the sensor is delivered into the system in an inert state and quickly converted to active state followed by necessary detection when the system is ready. Another circumstance is in medical applications when a drug is absolutely beneficial if it is active at only one or a few specific locations rather than the whole body. Hence, it is desired to have a "drug" that can circulate in the body in an inert form and can be activate at the specific locations in a controlled manner.

For that purpose, researchers have been developing photoactivatable agents for many years. Based on the characteristic of the activation, those agents can be categorized into either reversible or irreversible light-activatable agents. Reversible agents all contain groups which can absorbed light and undergo a reversible conformational change while irreversible agents typically have one or a few photocleavable groups. Examples of reversible light-activatable agents include azobenzene or analogous compounds[45-48] and genetically encoded light-activatable proteins which have been developed and optimized

recently.[49] Those reversible agents have found great applications in cellular molecular biology.[49, 50]

In contrast to the former group in which the activated agent can turn itself off after activation, the irreversible light-activatable agents furnish a way to permanently release an active species. These agents usually contain one or a few photocleavable groups.[51] Typically, an essential functional group/groups on the bioagent of interest is/are identified and chemically modified with photoremovable group(s). This modification, therefore, renders the bioagent functionally inactive. The inactive bioagent is then introduced into the biological system and converted from inactive to active form upon exposure to light. In some circumstances, however, the photoactivatable bioagents can be considered as generated in an indirect manner through photocleavage-induced molecular interaction disruption. In those cases, a molecule that contains a photolabile group can interact intra- or inter-molecularly and "inhibit" a bioactive molecule. Photolysis triggers cleavage of that photolabile group, and thus disrupts the interactions which results in the release of the active biomolecule (Figure 1.16).

Using both direct and indirect approaches, various photoactivatable bioagents, ranging from ions and small molecules to macromolecules such as proteins and nucleotides, have been developed.[50, 52, 53] The following lists just a few of them.

Kaplan, Forbush, and Hoffman were among the first to report the development of light activatable ATP utilizing a photocleavable 2-nitrobenzyl moiety and demonstrated the ability to activate Na/K-ATPase in ATP-depleted erythrocyte ghosts using light (Figure 1.10a).[54] Hess and colleagues reported the synthesis of light-activatable acetylcholine analog (Figure 1.10c)[55], glutamate (Figure 1.10b).[56] Koh and colleagues synthesized photoactivatable estradiol and controlled gene expression with light using this estrogen

analog (Figure 1.11a).[57] Lawrence and coworkers utilizes a similar approach to gain control over gene expression using photoactivatable β-ecdysone (Figure 1.11b).[58]

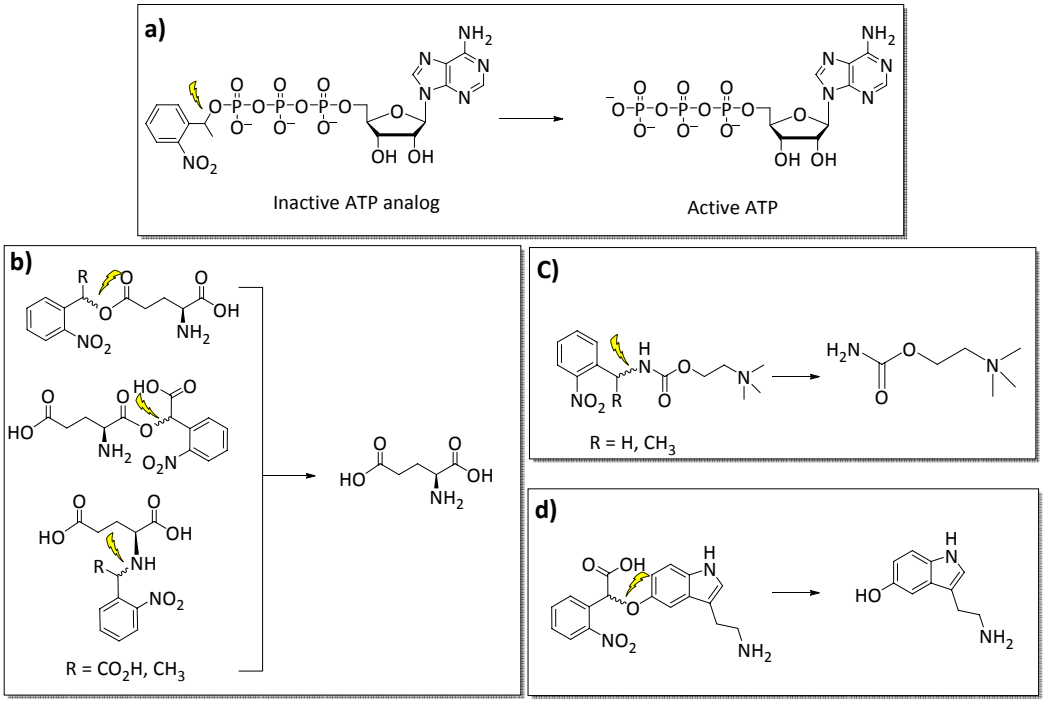

Figure 1.10: Structures of light-activatable ATP (a), glutamate (b), acetylcholine analog (c), and serotonin (d).

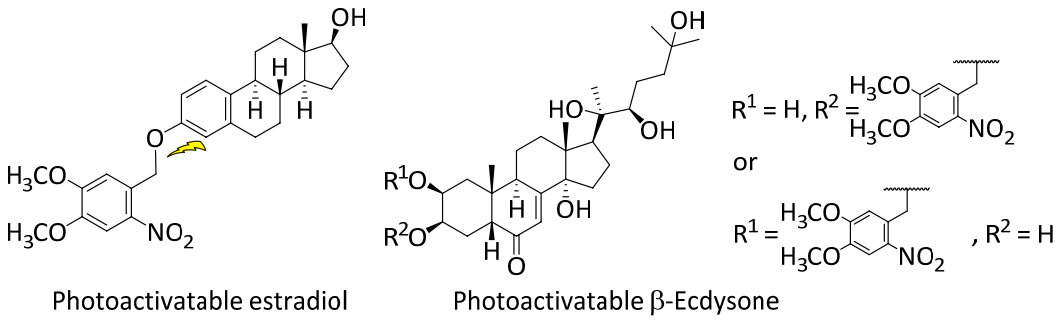

Figure 1.11: Structures of photoactivatable estradiol and photoactivatable β-ecdysone. Redraw from Ref. 57, 58.

Kaplan and Tsien groups at the same time reported the creation of calcium ion releaser upon exposed to light (Figure 1.12).[59, 60]. Ellis-Davies and Kaplan reported a construct that selectively binds to calcium with high affinity (80 nM) in the dark. Upon

exposure to UV-irradiation (~350 nm), this binding is eliminated, leading to the release of calcium (Figure 1.13).[61]

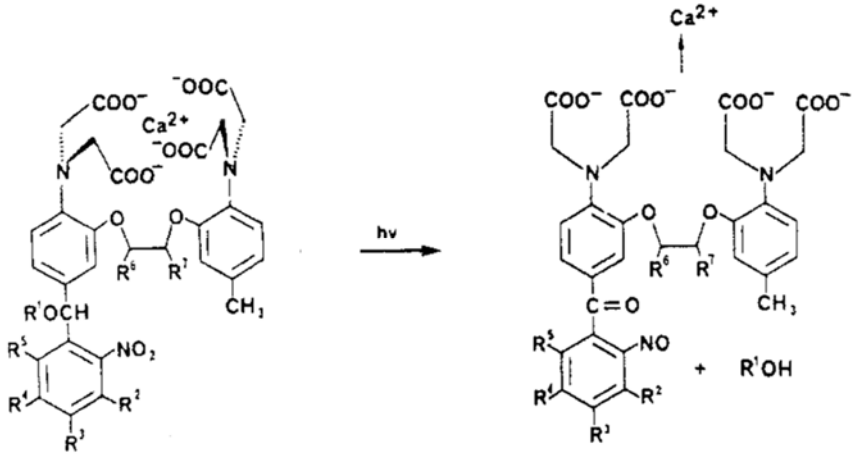

Figure 1.12: Light-mediated calcium release designed by Tsien et al.

Adapted with permission from Adams, S. R.; Kao, J. P. Y.; Grynkiewicz, G.; Minta, A.; Tsien, R. Y., Biologically useful chelators that release Ca^{2+} upon illumination. *J Am Chem Soc* **1988,** *110* (10), 3212-3220. Copyright (1988) American Chemical Society.

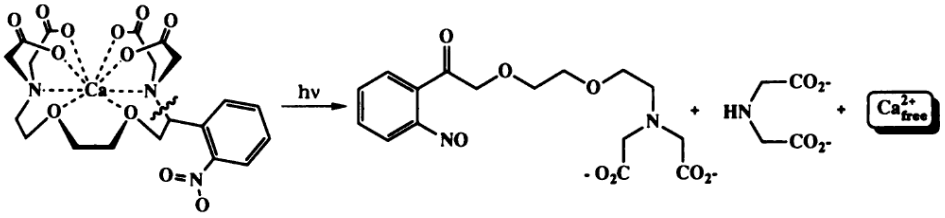

Figure 1.13: Light-mediated calcium release designed by Ellis-Davies and Kaplan.

Reprinted from Ellis-Davies, G. C.; Kaplan, J. H., Nitrophenyl-EGTA, a photolabile chelator that selectively binds Ca^{2+} with high affinity and releases it rapidly upon photolysis. *Proc Natl Acad Sci* U S A **1994,** *91* (1), 187-191.

For macromolecules, a variety of photoactivatable peptides, proteins, RNAs, and DNA, have been synthesized and used in biology.[27, 50, 53, 62]. Fay and coworkers reported photoactivatable peptide inhibitors of calmodulin and myosin light chain kinase (MLCK).[63] Imperiali and colleagues synthesized a phosphorylated peptide bearing a photolabile group on the phosphate moiety (Figure 1.14) and used the peptide to study the global

function of phosphopeptide binding protein in cell cycle. The peptide with a photolabile group on the phosphate moiety binds poorly to a 14-3-3 protein (K_d ~ 900 μM). Upon the removal of the photolabile group with UV light, the peptide tightly binds to the 14-3-3 protein (K_d of 25 nM), thus depletes the 14-3-3 from binding to endogenous proteins. With this technique, Imperiali, Yaffe, and coworkers demonstrated the role of 14-3-3 binding in various phases of cell cycle and the consequence, e.g., premature cell cycle entry, release of G1 cells from interphase arrest, and cells death, when such binding is compromised.[64]

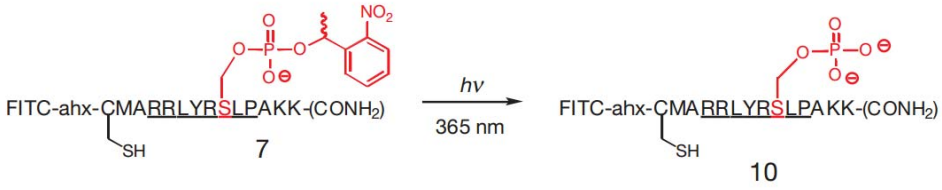

Figure 1.14: Structure of light-activatable phosphopeptide designed by Imperiali and coworkers.

> Adapted by permission from Macmillan Publishers Ltd: [Nature Biotechnology], Nguyen, A.; Rothman, D. M.; Stehn, J.; Imperiali, B.; Yaffe, M. B., Caged phosphopeptides reveal a temporal role for 14-3-3 in G1 arrest and S-phase checkpoint function. *Nat Biotechnol* **2004,** *22* (8), 993-1000. Copyright 2004.

Lawrence and coworkers applied the light-activatable strategy to kinase peptide reporters and demonstrated the applicability of the sensor in studying cellular biochemistry (Figure 1.15).[65, 66] Additionally, Lawrence et al. reported the design of a light-deativatable peptide inhibitor to activate Src protein tyrosine kinase.[67] A divalent peptide inhibitor was designed to bind to both SH1 and SH2 domains of Src and inhibits the enzyme (Figure 1.16). A photolabile moiety was placed in between the two binding motifs so that photolysis cuts the peptide in half and restores the kinase activity.

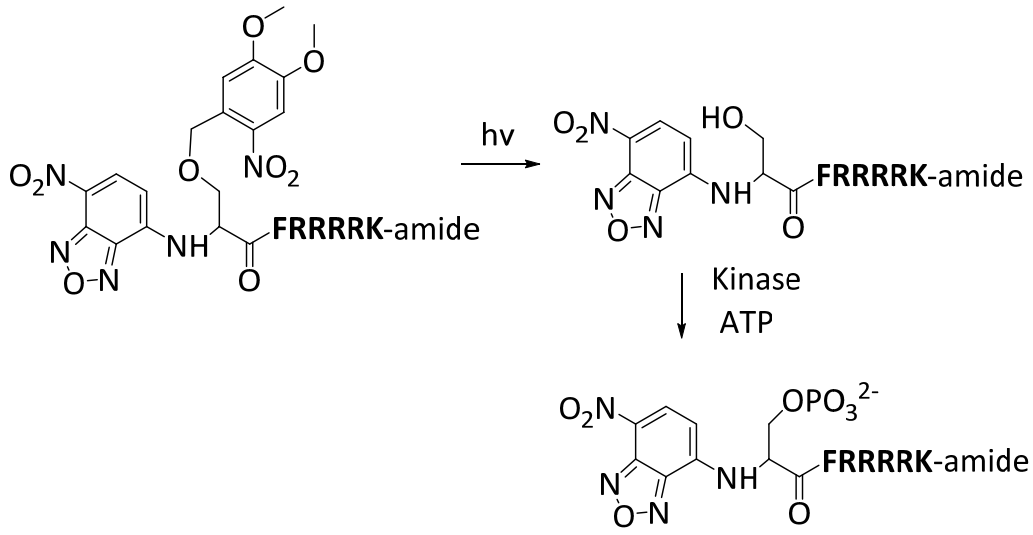

Figure 1.15: Structure of light-activatable PKC fluorescent sensor reported by Lawrence et al.

Adapted with permission from Veldhuyzen, W. F.; Nguyen, Q.; McMaster, G.; Lawrence, D. S., A light-activated probe of intracellular protein kinase activity. *J Am Chem Soc* **2003,** *125* (44), 13358-9. Copyright (2003) American Chemical Society.

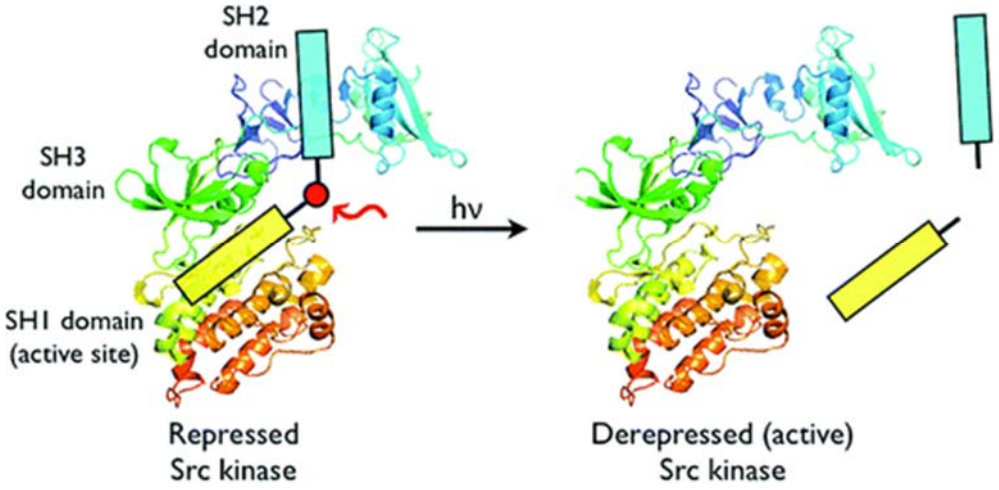

Figure 1.16: Design of photocleavable peptide inhibitor to control Src kinase activity reported by Lawrence and coworkers.

Li, H.; Hah, J. M.; Lawrence, D. S., Light-mediated liberation of enzymatic activity: "small molecule" caged protein equivalents. *J Am Chem Soc* **2008,** *130* (32), 10474-5. Copyright (2008) American Chemical Society.

For protein, Bayley and coworkers reported the synthesis of light-activatable version of c-AMP-dependent protein kinase's catalytic subunit by chemically targeted modification.[68, 69] In the similar strategy and around the same time, Ghosh and coworkers reported the construct of a light-activatable cofilin analog and used it to demonstrate cofilin's function in cell migration.[70, 71] Imperiali and colleagues reported the synthesis of photoactivatable myosin by chemical synthesis and protein ligation and tried to use the construct to study the function of myosin inside living cells.[72] Lawrence and colleagues reported an elegant design of photoactivatable profluorescent PKA which is inactive and nonfluorescent before photolysis. Illumination not only activates the enzyme but also renders it fluorescent, and thus provides a means to monitor the activation using the fluorescence readout.[73] In addition to chemically targeted modification, a number of light-activatable proteins (caspase-3,[74, 75] endonuclease,[76] β-galactosidase,[77] MAP kinase kinase (MEK1)[78]) were synthesized employing technology pioneered by Schultz and coworkers, which allows the genetic insertion of unnatural amino acids into protein. For polynucleotides, for example, Monroe and colleagues chemically synthesized photoactivatable DNAs and demonstrated the ability to induce expression of luciferase and GFP in rat skin and HeLa cells, respectively.[79] Ando and coworkers synthesized a light-activatable version of mRNAs of GFP and β-galactosidase and demonstrated the ability to drive the expression of the corresponding proteins in zebrafish embryos. The group then further synthesized a light-activatable mRNA version of the transcription factor Engrailed2a, injected it into the embryos and showed the ability to locally activate, express Enggrailed2a, and observe subsequent effects (Figure 1.17).[80]

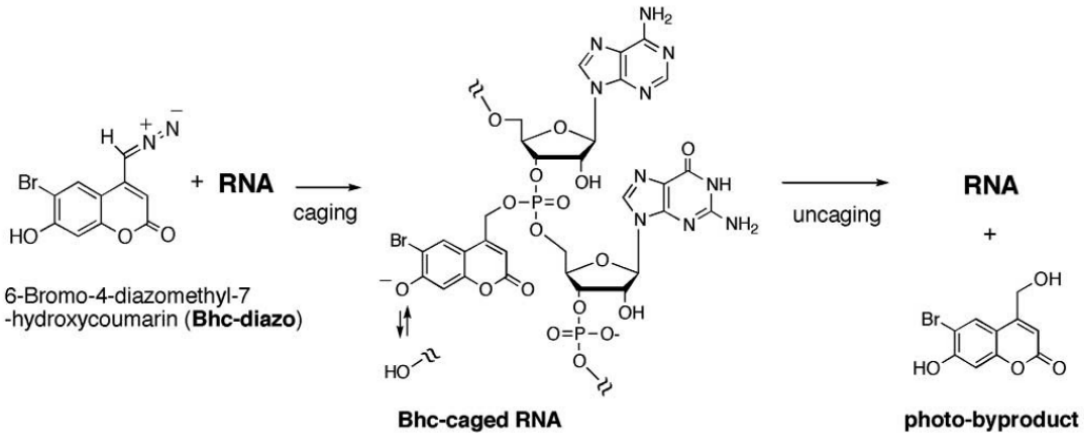

Figure 1.17: General design, synthesis, and photoactivation of RNA reported by Ando and coworkers.

> Reprint with permission from Ando, H.; Furuta, T.; Tsien, R. Y.; Okamoto, H., Photo-mediated gene activation using caged RNA/DNA in zebrafish embryos. *Nat Genet* **2001,** *28* (4), 317-325.

Even though various types of light-activatable biomolecules have been synthesized and used in numerous biological studies, the applicability of current strategies poses challenges. For example, when interactions between two or more biomolecules (i.e., nucleic acid-nucleic acid, protein-protein, nucleic acid-protein interactions) are the targets of light-activation designs. There is usually no defined functional group that is absolutely essential for the binding. One strategy that has been employed is to block a number of functional groups with photocleavable moieties. However, this strategy either results in a construct with high "dark background" when few functional groups are modified or a construct that is photolysis-demanding when too many photolabile groups are incorporated as these need to be removed in order to restore the original interactions.

CHAPTER 2: LONG-WAVELENGTH FLUORESCENT REPORTERS FOR PROTEIN KINASES

Fluorescent techniques have become powerful tools in biomedical research. Their *in vivo* applications, however, reveal an intrinsic limitation brought by tissue opacity. The presence of hemoglobin and melanin limits the use of wavelengths below 600 nm whereas water interferes with the use of wavelength greater than 1000 nm. The problem is exemplified when researchers aim to study biochemistry inside erythrocytes. These cells, unlike other mammalian cells, contain a high percentage of hemoglobin (about 97% by dry weight). The strong absorption of hemoglobin from UV to 600 nm makes it difficult to monitor subcellular biochemical processes in this region (Figure 2.1).

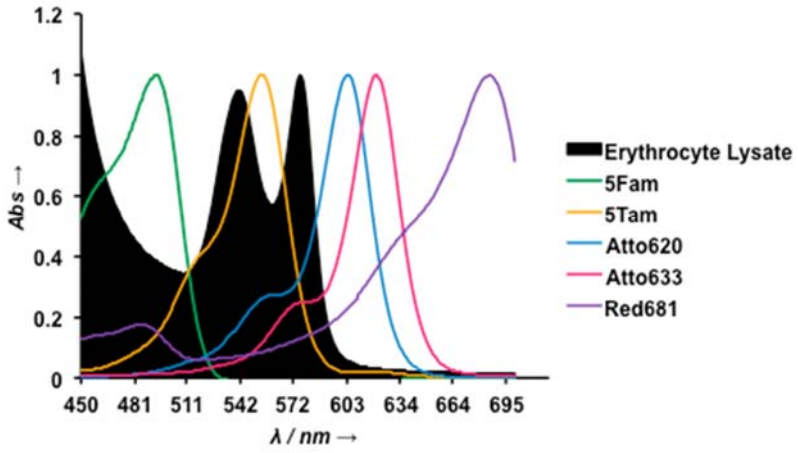

Figure 2.1: Relative wavelength absorbances of erythrocyte lysate and fluorophore-Aoc-GRTGRRFSY-amide peptides.

Among numerous proteins associated with erythrocytes, we were specifically interested in cAMP-dependent protein kinase (PKA) since it plays a central role in erythrocyte behavior and the life cycle of the malarial parasite *Plasmodium Falciparum*. For example, it is of great benefit to be able to quickly profile the PKA activity in

erythrocytes during *Plasmodium Falciparum* infection and determine the roles of PKA-induced phosphorylation during the infection and propagation of *Plasmodium Falciparum*. While a number of fluorescent sensors for protein kinases have been developed, none are compatible with the optical challenges associated with erythrocytes. In this chapter, we describe an approach which takes advantage of the commercial availability of various fluorophores to create wavelength-tunable protein kinase sensors. Especially, we report the development of far-red and near-IR fluorescent sensors for protein kinases and demonstrate the applicability of these sensors to monitor endogenous PKA activity in erythrocyte lysates and in erythrocytes when using a light-activatable reporter.

Results and Discussion

Design and Synthesis

Sharma *et al.* previously reported a strategy for creating fluorescent sensor for kinases based on a phosphorylation-induced dequenching mechanism. The strategy, however, requires the presence of a phosphopeptide binding protein, 14-3-3τ, which only binds tightly to phosphopeptides and sequesters them from interacting with quenchers (Figure 1.9).[39] However, Dr. Melanie Priestman found that, despite the lack of the phosphopeptide binding protein, modest fluorescent increases are observed when PKA is added to the assay mixture containing fluorescently labeled peptide, quencher, ATP, and $MgCl_2$. We hypothesized that, upon phosphorylation by PKA, the newly introduced negatively charged phosphate group serves as a molecular trigger that drives the release of the fluorescent quenchers. Therefore, we pursued a screening approach to take advantage of the commercial availability of far-red/near-IR fluorophores and create tunable fluorescent sensors for protein kinase activity.

Our initial efforts focused on two serine-containing positively charged peptides, Aoc-GRTGRRFSY-amide and KRRRLASLAA-amide, which are known to be phosphorylated by PKA.[81] Fluorophores were appended to the N termini of both peptides. The amino octanoyl (Aoc) moiety was used as a spacer in one of these to reduce any potential unfavorable steric effect of the large fluorophores on phosphorylation process. The strategy is outlined in Figure 2.2.

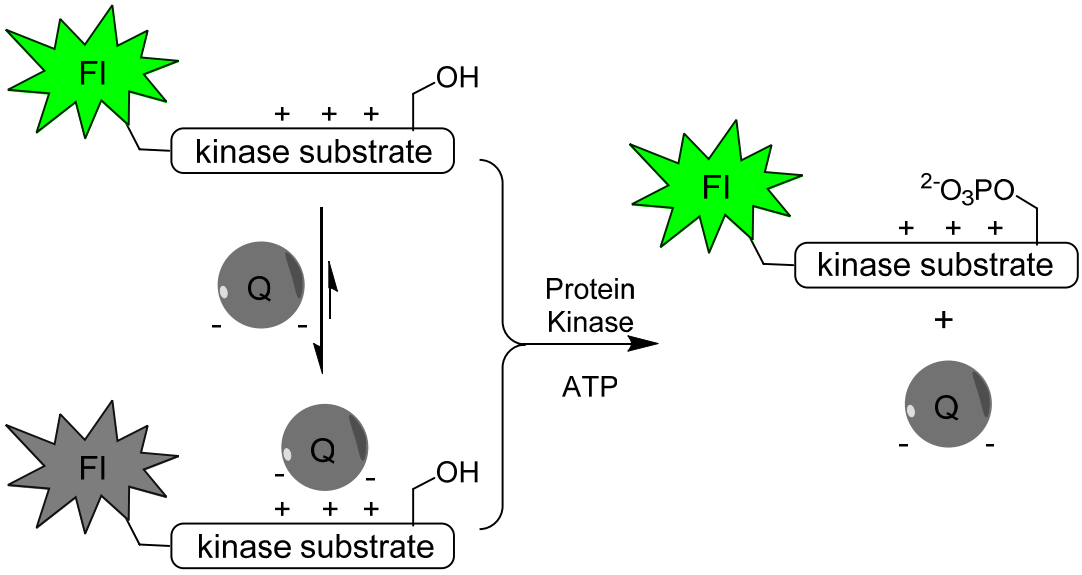

Figure 2.2: General strategy for the protein kinase catalyzed dequenching of fluorescent kinase substrates. A positively charged fluorescent kinase substrate is quenched upon exposure to a negatively charged quencher dye (Q). Kinase-catalyzed phosphorylation releases Q as a result of favorable intramolecular electrostatic interactions between the newly introduced phosphate and positively charged substrate residues.

We examined a total of fourteen fluorophores that encompass a nearly 250 nm wavelength range throughout the red/far-red region (λ_{ex} = 494 - 727 nm, λ_{em} = 530 - 752 nm). The structures of these fluorophores were selected from different scaffolds (Figure 2.3). Fluorophores were coupled to the peptide on resin, cleaved by TFA, and then purified by RF-HPLC (Table 2.1).

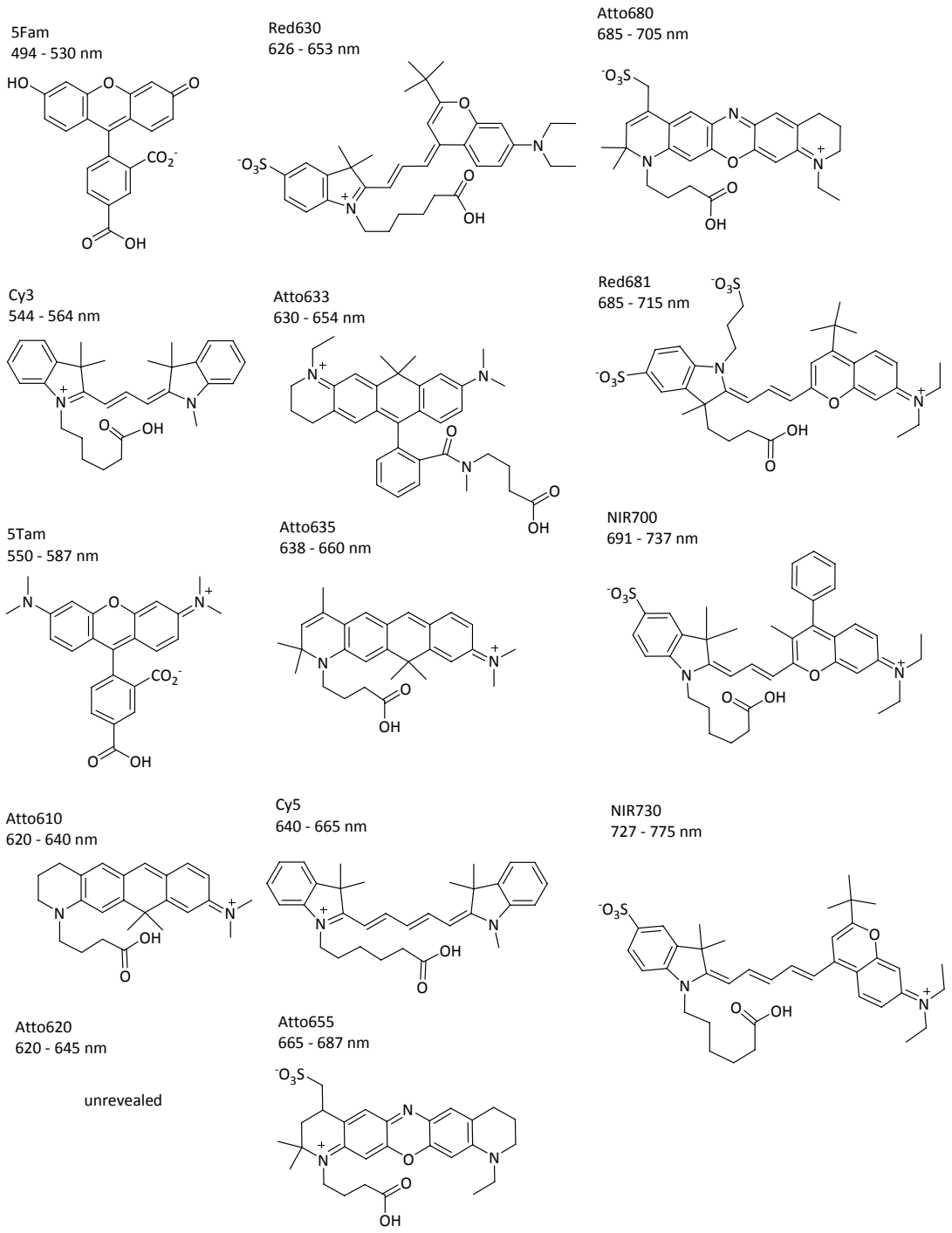

Figure 2.3: Structures and excitation - emission wavelengths of fluorophores.

Table 2.1: Peptide ESI+ mass data.

Peptide	Molecular formula	Calculated mass	Found (ESI+, m/z)
5Fam-KRRRLASLAA	$C_{69}H_{102}N_{21}O_{17}^-$	1496.78	750.0 ([M + 3 H]$^{2+}$), 500.4 ([M + 4 H]$^{3+}$), 375.6 ([M + 5 H]$^{4+}$)
Cy3-KRRRLASLAA	$C_{78}H_{128}N_{23}O_{12}^+$	1579.01	527.2 ([M + 2 H]$^{3+}$), 395.7 ([M + 3 H]$^{4+}$)
5Tam-KRRRLASLAA	$C_{73}H_{113}N_{23}O_{15}$	1551.88	777.1 ([M + 2 H]$^{2+}$), 518.5 ([M + 3 H]$^{3+}$), 389.2 ([M + 4 H]$^{4+}$)
Atto610-KRRRLASLAA	$C_{73}H_{122}N_{23}O_{12}^+$	1512.96	757.2 ([M + H]$^{2+}$), 505.2 (M + 2 H]$^{3+}$), 379.1 ([M + 3 H]$^{4+}$)
Atto620-KRRRLASLAA	unknown	unknown	817.9 ([M + 2 H]$^{2+}$), 545.6 ([M + 3 H]$^{3+}$), 409.5 ([M + 4 H]$^{4+}$)
Red630-KRRRLASLAA	$C_{84}H_{137}N_{23}O_{16}S$	1756.03	879.6 ([M + 2 H]$^{2+}$), 586.5 ([M + 3 H]$^{3+}$), 440.2 ([M + 4 H]$^{4+}$)
Atto635-KRRRLASLAA	$C_{76}H_{126}N_{23}O_{12}^+$	1553.00	777.0 ([M + H]$^{2+}$), 518.5 ([M + 2 H]$^{3+}$), 389.1 ([M + 3 H]$^{4+}$)
Cy5-KRRRLASLAA	$C_{80}H_{130}N_{23}O_{12}^+$	1605.03	803.1 ([M + H]$^{2+}$), 535.8 ([M + 2 H]$^{3+}$), 402.2 ([M + 3 H]$^{4+}$), 321.9 ([M + 4 H]$^{5+}$)
Atto655-KRRRLASLAA	$C_{75}H_{124}N_{24}O_{16}S$	1648.93	825.4 ([M + 2 H]$^{2+}$), 550.9 ([M + 3 H]$^{3+}$), 413.4 ([M + 4 H]$^{4+}$)
Atto680-KRRRLASLAA	$C_{75}H_{122}N_{24}O_{16}S$	1646.92	824.6 ([M + 2 H]$^{2+}$), 550.2 ([M + 3 H]$^{3+}$), 412.9 ([M + 4 H]$^{4+}$)
Red681-KRRRLASLAA	$C_{84}H_{136}N_{23}O_{19}S_2^-$	1834.98	919.2 ([M + 3 H]$^{2+}$), 613.2 ([M + 4 H]$^{3+}$), 460.1 ([M + 5 H]$^{4+}$)
NIR700-KRRRLASLAA	$C_{87}H_{135}N_{23}O_{16}S$	1790.02	896.3 ([M + 2 H]$^{2+}$), 597.9 ([M + 3 H]$^{3+}$), 448.7 ([M + 4 H]$^{4+}$)
NIR730-KRRRLASLAA	$C_{86}H_{139}N_{23}O_{16}S$	1782.05	892.2 ([M + 2 H]$^{2+}$), 595.3 ([M + 3 H]$^{3+}$), 446.7 ([M + 4 H]$^{4+}$)
5Fam-Aoc-GRTGRRFSY	$C_{76}H_{99}N_{20}O_{19}^-$	1595.74	799.7 ([M + 3 H]$^{2+}$), 533.5 ([M + 4 H]$^{3+}$), 400.3 ([M + 5 H]$^{4+}$)
5Tam-Aoc-GRTGRRFSY	$C_{80}H_{110}N_{22}O_{17}$	1650.84	826.7 ([M + 2 H]$^{2+}$), 551.5 ([M + 3 H]$^{3+}$), 413.8 ([M + 4 H]$^{4+}$)
Atto620-Aoc-GRTGRRFSY	unknown	unknown	867.3 ([M + 2 H]$^{2+}$), 578.6 ([M + 3 H]$^{3+}$), 434.1 ([M + 4 H]$^{4+}$)
Atto633-Aoc-GRTGRRFSY	$C_{90}H_{130}N_{23}O_{15}^+$	1773.01	887.1 ([M + H]$^{2+}$), 591.9 ([M + 2 H]$^{3+}$),444.2 ([M + 3 H]$^{4+}$)
Red681-Aoc-GRTGRRFSY	$C_{91}H_{133}N_{22}O_{21}S_2^-$	1933.95	1291.4 ([2 M + 5 H]$^{3+}$), 968.6 ([M + 3 H]$^{2+}$), 646.2 ([M + 4 H]$^{3+}$)
Atto633-Aoc-GRTGRRF(DMNB)SY	$C_{99}H_{139}N_{24}O_{19}^+$	1968.06	984.6 ([M + H]$^{2+}$), 656.9 ([M + 2 H]$^{3+}$), 493.0 ([M + 3 H]$^{4+}$)

Table 2.2: Dye library.

	A	B	C	D
1	Acid Green 27	Ethyl Orange	Aniline Blue WS	Naphthol Blue Black
2	Acid Blue 40	Methylene Blue	Azure A	Methylthymol Blue
3	Evans Blue	Brilliant Blue R	Azure B bromide	Methyl Violet
4	Acid Alizarin Violet N	Eriochrome Black T	Basic Fuchsin	Ponceau S
5	Acid Blue 80	Alizarin Red	Bismark Brown Y	Rose Bengal
6	N,N-dimethylnitrosoaniline	Malachite Green Oxalate	Brilliant Yellow	Rosolic Acid
7	Cresol Red	Phenolphthalein	Bromocresol Purple	Safranin O
8	Phenol Red	Carminic Acid	Chlorazol Black E	Tartrazine
9	Methyl Orange	Nuclear Fast Red	Chlorophenol Red	Trypan Blue
10	Bromophenol Blue	Acid Fuchsin	Chrysoidine Y	Acid Green 25
11	Xylene Cyanol FF	Acridine Orange	Erythrosin	Acid Blue 129
12	Disperse Yellow 3	Acridine Yellow G	Ethyl Violet	Acid Red 27

Screening Dye Library

The fluorescence increase induced by phosphorylation in the presence of a library of forty eight dyes (Table 2.2) was investigated. To ensure the coverage of all potential peptide-quencher hits, initial screening was carried out in Tris-HCl buffer (25 mM, pH 7.5) at peptide concentration of 2.5 µM and 5 µM; and quencher concentration varied from 5 µM to 60 µM. Upon the addition of PKA to the solution of fluorescently quenched peptide (Tris-HCl buffer containing peptide, quencher, $MgCl_2$, and ATP), fluorescence dequenching ranging from modest to dramatic was observed (Table 2.3, Figure 2.4-2.6).

Table 2.3: The PKA-catalyzed fluorescence increase of the fluorophore-substituted peptides in buffer Tris-HCl pH 7.5 (25 mM), $MgCl_2$ (1 mM) containing various quenchers. Fluorescence monitored in a plate reader at maximum wavelengths of the fluorohores except (**) were done in a spectrofluorometer.

Peptide (2.5 μM)	Quencher (μM)	Fluorescence fold increase
5Fam-KRRRLASLAA	Acid green 27 (30)	3.7 ± 0.8
Cy3-KRRRLASLAA	Bromophenol blue (20)	5.1 ± 0.1
5Tam-KRRRLASLAA	Acid blue 80 (15)	24.5 ± 1.4
Atto610-KRRRLASLAA	Bromophenol blue (35)	5.5 ± 0.2
Atto620-KRRRLASLAA	Acid blue 80 (7.5)	21.9 ± 0.5
Red630-KRRRLASLAA	Bromophenol blue (30)	4.0 ± 0.5
Atto635-KRRRLASLAA	Bromophenol blue (35)	4.2 ± 0.2
Cy5-KRRRLASLAA*	Bromophenol blue (20)	5.8 ± 0.2
Atto655-KRRRLASLAA	Acid blue 80 (10)	16.7 ± 0.5
Atto680-KRRRLASLAA	Acid blue 80 (15)	22.5 ± 2.7
Red681-KRRRLASLAA	Acid blue 80 (5)	13.8 ± 0.7
NIR700-KRRRLASLAA**	Bromocresol purple (80)	2.7 ± 0.1
NIR730-KRRRLASLAA**	Bromocresol purple (80)	2.6 ± 0.2
5Fam-Aoc-GRTGRRFSY	Acid green 27 (30)	21.2 ± 0.4
5Tam-Aoc-GRTGRRFSY	Acid blue 80 (15)	100 ± 27
Atto620-Aoc-GRTGRRFSY	Acid blue 80 (7.5)	31.4 ± 1.0
Atto633-Aoc-GRTGRRFSY	Acid blue 80 (5)	30.9 ± 4.9
Red681-Aoc-GRTGRRFSY	Acid blue 80 (5)	11.2 ± 0.6

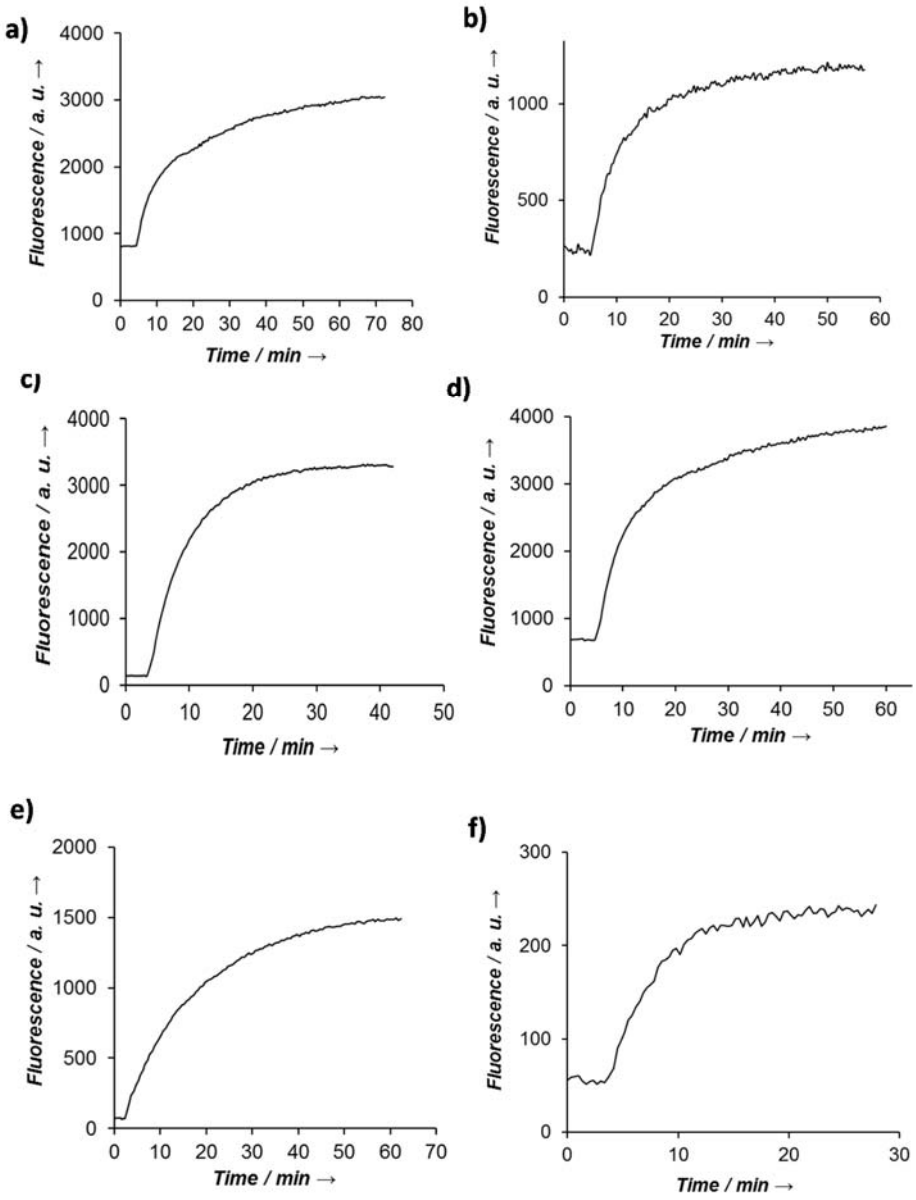

Figure 2.4: PKA-catalyzed fluorescence dequenching. (a) 5Fam-KRRRLASLAA-amide (2.5 µM) with Acid Green 27 (30 µM), (b) Cy3-KRRRLASLAA-amide (2.5 µM) with Bromophenol Blue (20 µM), (c) 5Tam-KRRRLASLAA-amide (2.5 µM) with Acid Blue 80 (15 µM), (d) Atto610-KRRRLASLAA-amide (2.5 µM) with Bromophenol Blue (35 µM), (e) Atto620-KRRRLASLAA-amide (2.5 µM) with Acid Blue 80 (7.5 µM), (f) Red630-KRRRLASLAA-amide (2.5 µM) with Bromophenol Blue (30 µM). PKA (10 nM) was added to buffer (200 µL), containing Tris-HCl pH 7.5 (25 mM), $MgCl_2$ (1 mM), ATP (1 mM), peptide, and quencher. Fluorescence change was followed in a plate reader.

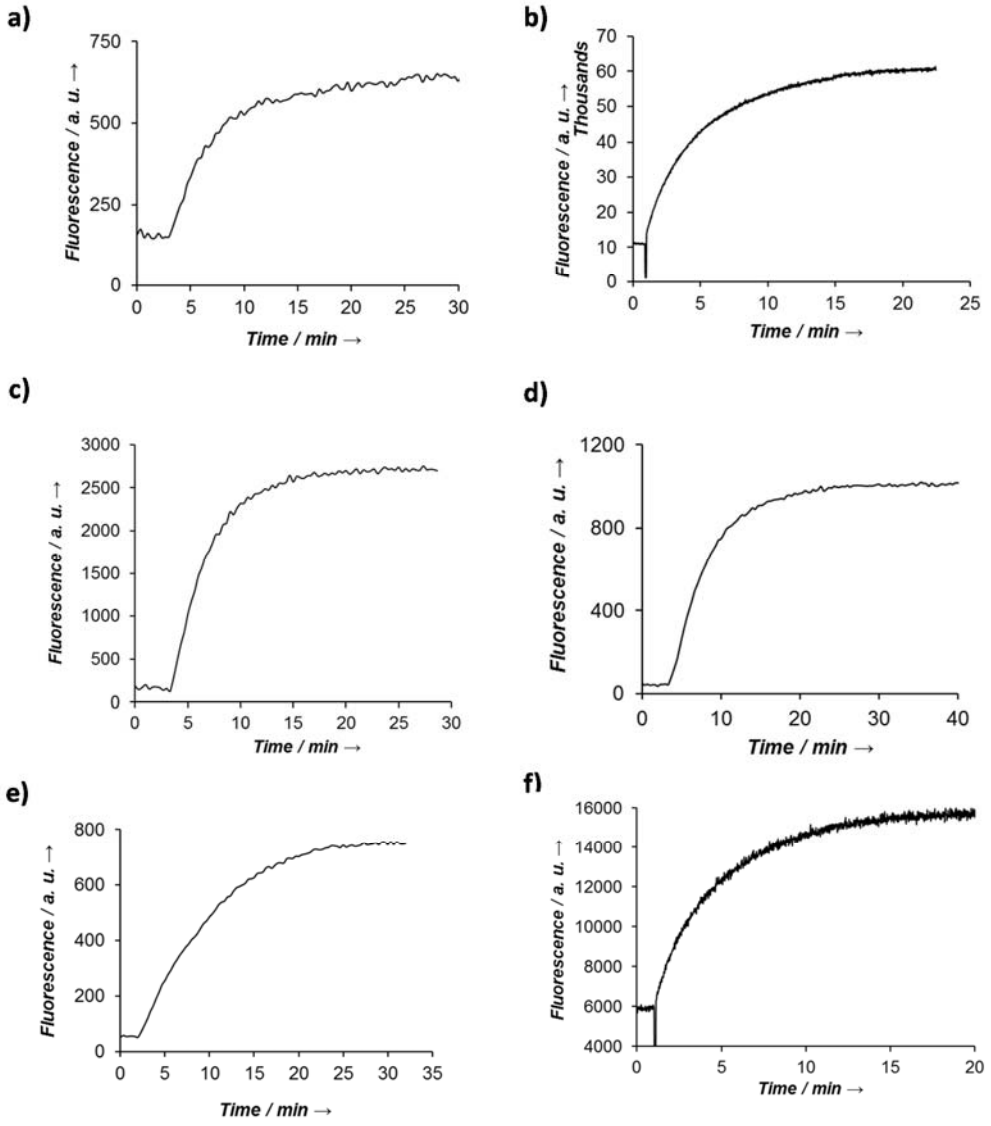

Figure 2.5: PKA-catalyzed fluorescence dequenching (continued). (a) Atto635-KRRRLASLAA-amide (2.5 µM) with Bromophenol Blue (35 µM), (b) Cy5-KRRRLASLAA-amide (2.5 µM) with Bromophenol Blue (20 µM), (c) Atto655-KRRRLASLAA-amide (2.5 µM) with Acid Blue 80 (10 µM), (d) Atto680-KRRRLASLAA-amide (2.5 µM) with Acid Blue 80 (15 µM), (e) Red681-KRRRLASLAA-amide (2.5 µM) with Acid Blue 80 (5 µM), (f) NIR700-KRRRLASLAA-amide with Bromocresol Purple (80 µM). PKA (10 nM) was added to buffer (200 µL), containing Tris-HCl pH 7.5 (25 mM), $MgCl_2$ (1 mM), ATP (1 mM), peptide, and quencher. Fluorescence change was followed in a spectroflurometer (b, f) or in a plate reader for all others.

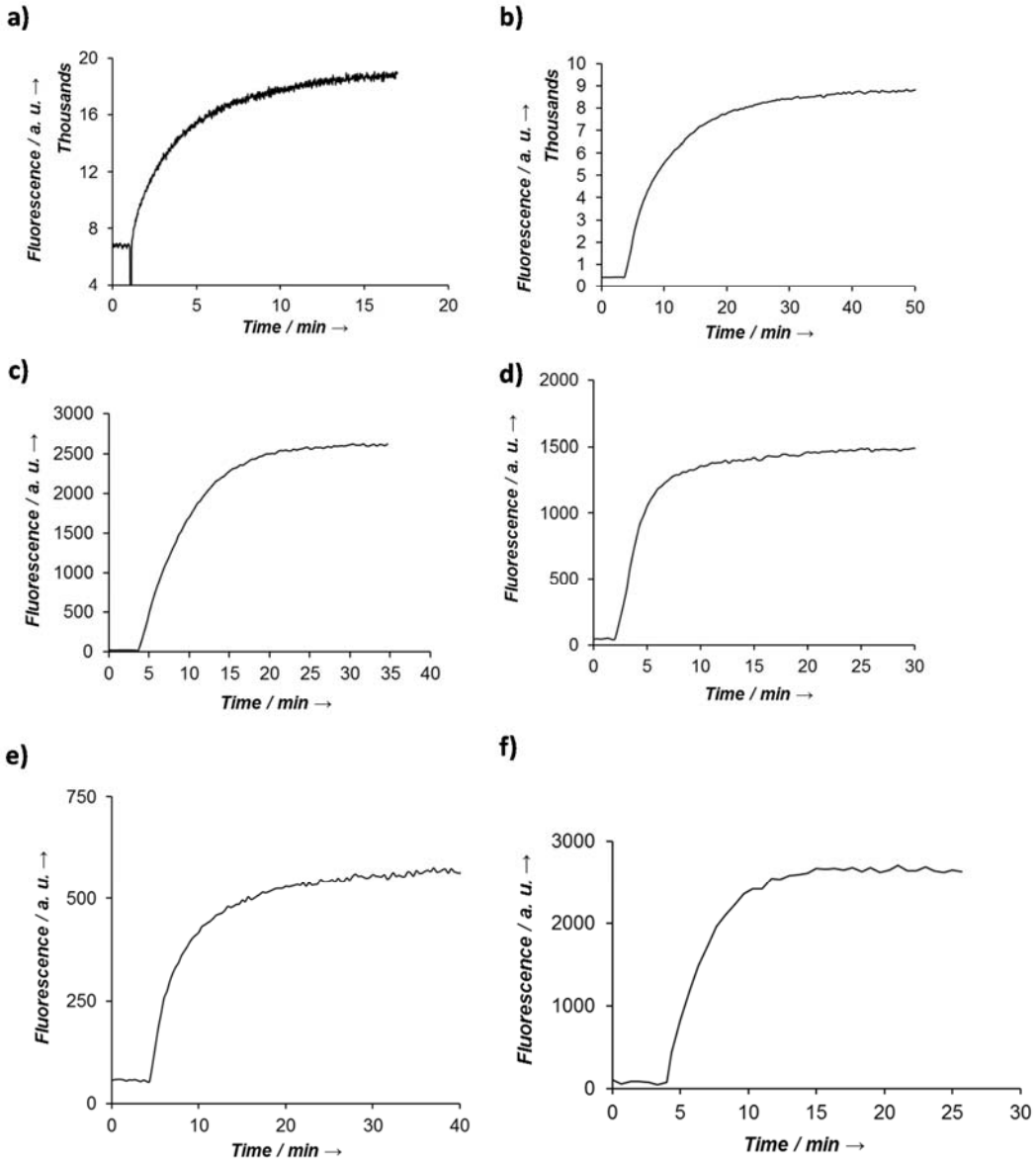

Figure 2.6: PKA catalyzed fluorescence dequenching (continued). (a) NIR730-KRRRLASLAA-amide with Bromocresol Purple (80 µM), (b) 5Fam-Aoc-GRTGRRFSY-amide (2.5 µM) with Acid Green 27 (30 µM), (c) 5Tam-Aoc-GRTGRRFSY-amide (2.5 µM) with Acid Blue 80 (15 µM), (d) Atto620-Aoc-GRTGRRFSY-amide (2.5 µM) with Acid Blue 80 (7.5 µM), (e) Red681-Aoc-GRTGRRFSY (2.5 µM) with Acid Blue 80 (5 µM), (f) Atto633-Aoc-GRTGRRFSY-amide (2.5 µM) with Acid Blue 80 (5 µM). PKA (10 nM) was added to buffer (200 µL), containing Tris-HCl pH 7.5 (25 mM), $MgCl_2$ (1 mM), ATP (1 mM), peptide, and quencher. Fluorescence was followed in a spectroflurometer (a) or in a plate reader for all others.

Fluorescent Fold Change and Fluorescent Recovery

We investigated the PKA-catalyzed fluorescence fold change and fluorescence recovery of the best reporters at a fixed concentration of peptide and varied concentrations of quencher. The fluorescence recovery is calculated by dividing fluorescence increase induced by phosphorylation by fluorescence before the addition of quencher. Examples are shown in Figure 2.7. At the fixed peptide concentration of 2.5 μM, the fluorescent fold change tends to approach maximal value while the fluorescence recovery tends to reduce as the quencher concentration increases (Figure 2.7).

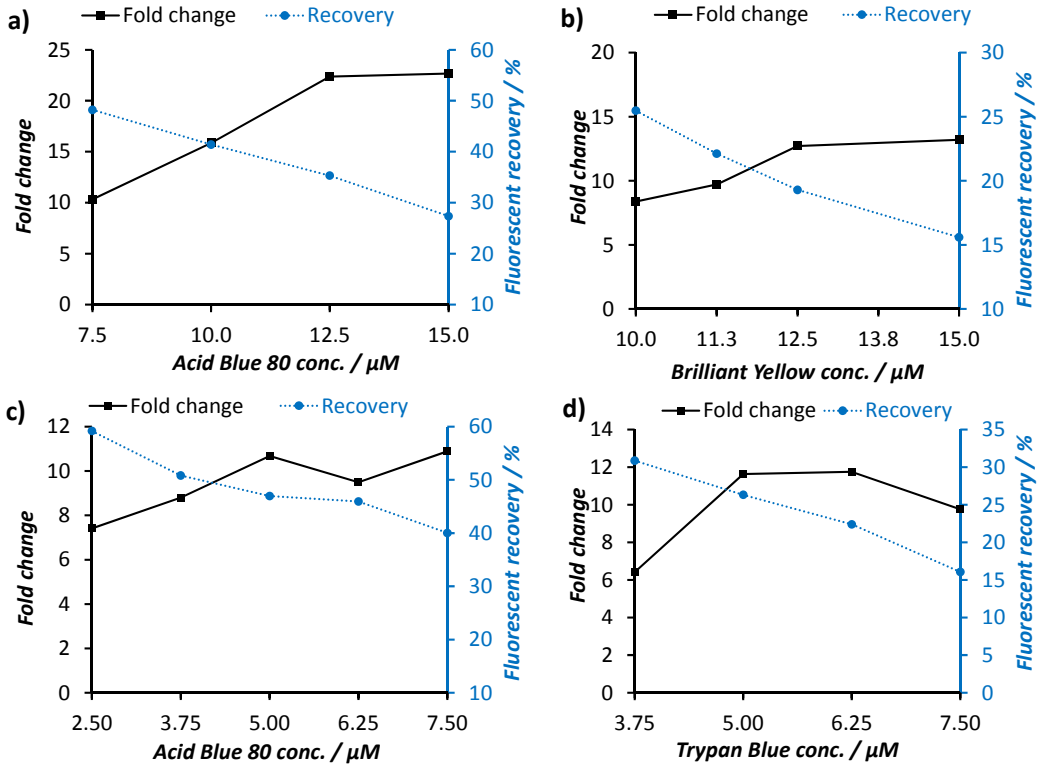

Figure 2.7: Dependence of fluorescence fold change and fluorescence recovery on the concentration of quencher. (a, b) Atto680-KRRRLASLAA amide; (c, d) Red681-KRRRLASLAA-amide. Data was acquired in a spectroflurometer.

Peptide Quencher Binding Investigation

We investigated the dependency of fluorescence fold change and fluorescence recovery at various peptide and quencher concentrations. Variations of the fluorescence response were observed when the peptide concentration was varied and the quencher concentration was fixed or when the peptide concentration was varied and the quencher/peptide concentration ratio was fixed. For example, for 5Tam-KRRRLASLAA-amide and quencher Acid Blue 80, at 100 nM of peptide exhibits little or no fluorescence increase at either quencher/peptide concentration ratio of 6 or quencher concentration of 15 µM. Since Job plot analyses of several quencher/fluorophore-peptide pairs reveals no defined binding stoichiometry, we reasoned that there might be complexity in the interaction of the peptide/quencher pairs (Figure 2.8). A good explanation would be the formation of quencher/fluorophore-peptide aggregates and phosphorylation of the peptide disrupts aggregate formation, resulting in the fluorescence increase. Dynamic light scattering (DLS) experiments were carried out but we were unable to confirm any high-molecular-weight aggregate formation (Figure 2.9). We, however, note that the concentration of peptide and quencher used in DLS experiments were in µM range. Aggregates, if formed, might be too dilute to be detected by the DLS equipment.

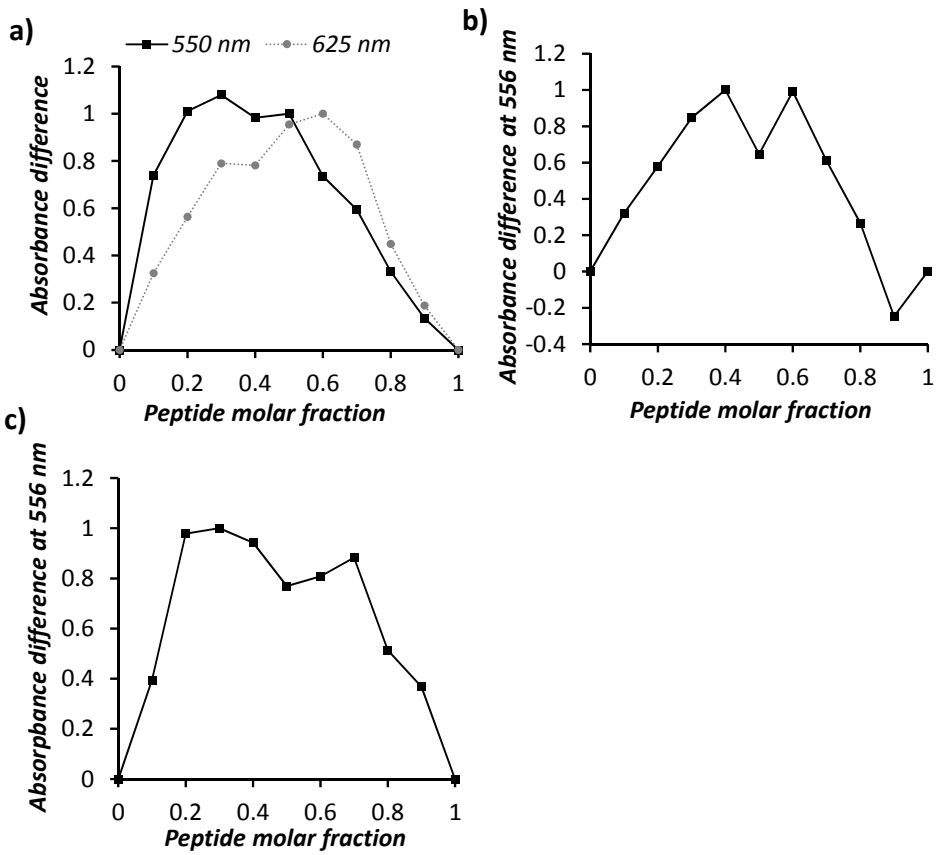

Figure 2.8: Job plot of complex formation of 5Tam-KRRRLASLAA-amide with acid blue 80 (a), 5Tamra-Aoc-GRTGRRFSY-amide with Acid Blue 80 (b) and 5Tam-Aoc-GRTGRRFSY with Evans Blue (c). The peptide and quencher [total concentration of peptide and quencher was 10 µM in (a) and 5 µMin (b, c)] were added to buffer (200 µL) containing Tris-HCl pH 7.5 (25 mM), $MgCl_2$ (1 mM), and ATP (1 mM) in (a) or Tris-HCl pH 7.5 (25 mM), $MgCl_2$ (1 mM), ATP (1 mM), and NaCl (150 mM) in (b, c). Mixtures were incubated at room temperature for 10 min before the absorbance measurements.

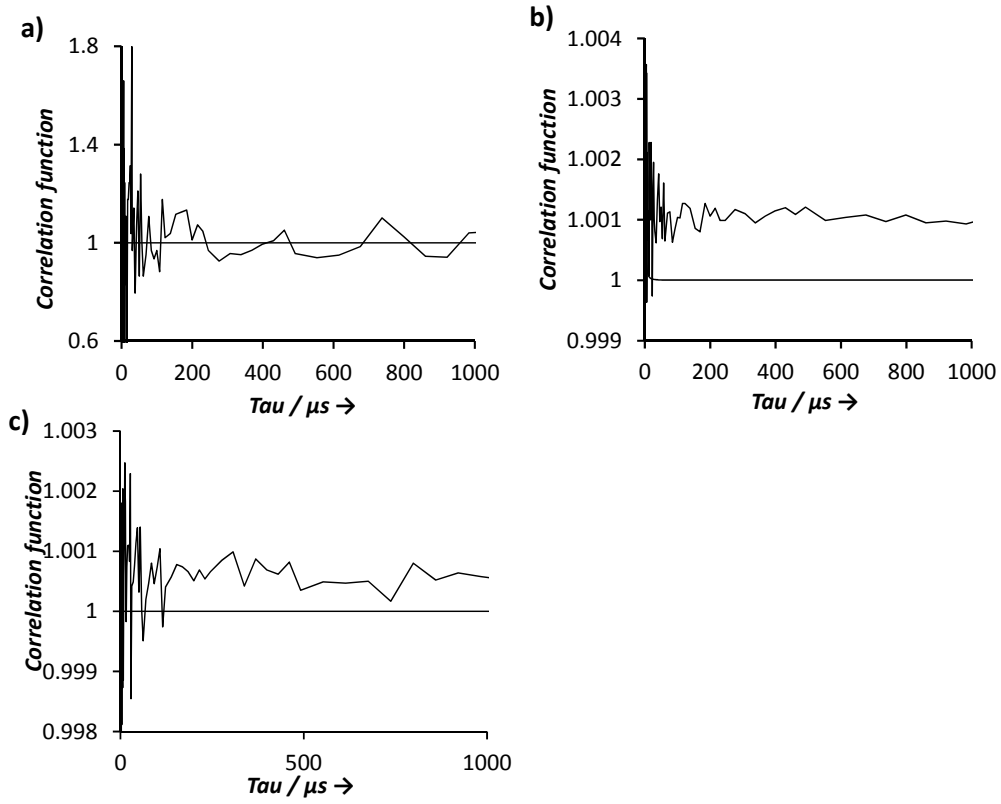

Figure 2.9: Dynamic light scattering analysis did not reveal detectable aggregate formation. Correlation function of 5Tam-Aoc-GRTGRRFSY-amide (1 µM) solution (a), Evans Blue (2 µM) solution (b), and 5Tam-Aoc-GRTGRRFSY-amide (1 µM) + Evans Blue (2 µM) solution.

Initial Phosphorylation Rate and Kinase Inhibitor IC_{50} Determination

We investigated the feasibility of using our reporters to detect phosphorylation at different wavelengths. We first used five reporters (5Fam: λ_{ex} - λ_{em} = 494 nm - 530 nm, 5Tam: 550 nm - 587 nm, Atto620: 620 nm - 645 nm, Atto680: 685 nm - 705 nm, and Red681: 685 nm - 715 nm) to determine the initial phosphorylation rates based on the assumption that the formation of the phosphopeptides is linear with respect to fluorescence increase. A standard value was acquired employing 5Fam-KRRRLASLAA-amide peptide and capillary electrophoresis with laser induced fluorescence detection

(CE-LIF). As shown in the Table 2.4, the obtained values from various peptide/quencher pairs are comparable to the standard value obtained by capillary electrophoresis.

In addition to the initial rate determination, we further investigated the ability of our reporters for determining the IC_{50} of kinase inhibitors. H9 and H89 were selected as examples of PKA inhibitors since their IC_{50} values for PKA have been well documented in literatures. As shown in Figure 2.10, IC_{50} value of H9 and H89 determined by various reporters are comparable to the values reported in literatures.[82] The assay is flexible in term of excitation and emission wavelengths since they can be selected if desired from λ_{ex}: 494 nm - 730 nm and λ_{em}: 530 nm - 750 nm.

Effect of High Salt Concentration on the Fluorescence Response

We hypothesized that this electrostatic interaction prevents the quencher from interacting with the peptide which results in the observed fluorescence increase. This electrostatic interaction, therefore, is likely affected by ionic strength of the assay buffer. We set out to investigate the interference of the fluorescence response under low and high salt concentration. As expected, the addition of NaCl reduces quenching efficiency of all quenchers investigated (Table 2.5, 2.6). The fluorescence fold increase, in most of the cases, is also reduced when 150 mM NaCl is introduced into the buffer. To our surprise, however, in some instances, the fluorescence fold increase is enhanced in the presence of 150 mM NaCl compared to that in the absence of the salt (5Tam-Aoc-GRTGRRFSY-amide and Atto633-Aoc-GRTGRRFSY-amide with Evans blue, Atto620-Aoc-GRTGRRFSY-amide with Acid Blue 80) (Table 2.5, 2.6). This suggests that other types of interactions, in addition to electrostatic interaction, might play a role in the quenching and dequenching

mechanism; and that the presence of positively charged residues in the peptide sequence might not be absolutely required for the fluorescence increase to be observed.

Table 2.4: Initial phosphorylation rate of various peptide/dye quencher pairs. (#) value determined by CE-LIF.

Peptide	Quencher (µM)	Initial rate µmol*min^{-1}*mg^{-1} (mean ± std)
5Fam-KRRRLASLAAamide	Acid green 27 (20)	4.6 ± 0.4 2.1 ± 0.2 #
5Tam-KRRRLASLAAamide	Acid Blue 80 (10)	2.7 ± 0.1
Atto620-KRRRLASLAAamide	Acid Blue 80 (10)	3.8 ± 0.1
Red681-KRRRLASLAAamide	Acid Blue 80 (5)	1.8 ± 0.1
Atto680-KRRRLASLAAamide	Acid Blue 80 (10)	3.2 ± 0.2

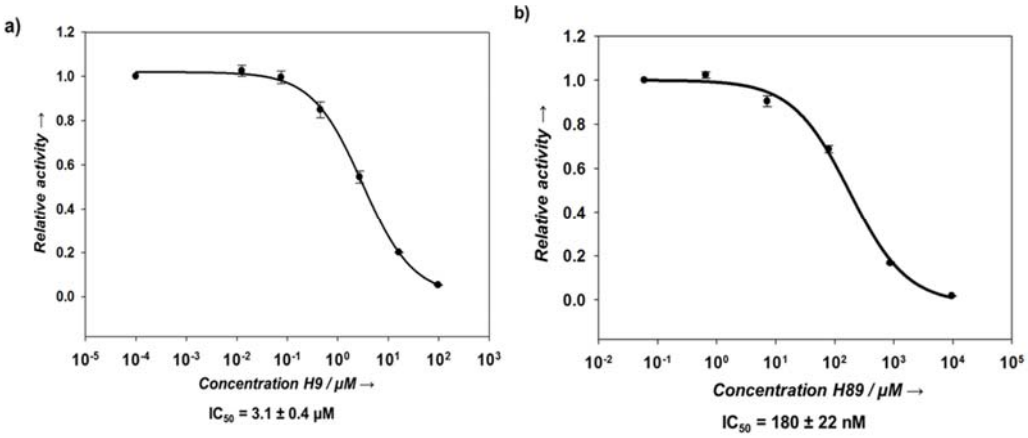

Figure 2.10: *IC_{50}* curve of H9 and H89 toward PKA. PKA (10 nM) was added to buffer (200 µL) containing Tris-HCl (25 mM, pH 7.5), $MgCl_2$ (1 mM), ATP (100 µM), 5Tam-KRRRLASLAA-amide (5 µM), acid blue 80 (10 µM), and the designated concentration of inhibitor H9 or H89 to initiate the phosphorylation. The relative activity was determined by the slope of the fluorescence change over that of the control without inhibitor.

Table 2.5: Effect of salt on the fluorescence response upon phosphorylation. Peptides (2.5 μM) and various dye quenchers were incubated under either "no salt" buffer containing Tris-HCl (25 mM, pH 7.5), $MgCl_2$ (1 mM), ATP (1 mM) or "with salt" buffer containing Tris-HCl (25 mM, pH 7.5), $MgCl_2$ (1 mM), ATP (1 mM), and 150 mM NaCl. The reaction was initiated by addition of PKA (10 nM).

Buffer condition	Peptide (2.5 μM)	Quencher (μM)	Fluorescent quenching (%)	Fluorescent fold increase
No salt	5Fam-Aoc-GRTGRRFSY	Acid green 27 (30)	97.2 ± 0.3	18.5 ± 3.4
With salt	5Fam-Aoc-GRTGRRFSY	Acid green 27 (30)	97.0 ± 0.1	3.5 ± 0.5
No salt	5Tam-Aoc-GRTGRRFSY	Acid Blue 80 (15)	99.8 ± 0.1	103.7 ± 24.4
With salt	5Tam-Aoc-GRTGRRFSY	Acid Blue 80 (15)	99.7 ± 0.0	41.0 ± 1.2
No salt	Atto620-Aoc-GRTGRRFSY	Acid Blue 80 (7.5)	99.1 ± 0.1	16.6 ± 0.8
With salt	Atto620-Aoc-GRTGRRFSY	Acid Blue 80 (7.5)	98.6 ± 0.0	18.2 ± 0.1
No salt	Atto633-Aoc-GRTGRRFSY	Acid Blue 80 (5)	99.4 ± 0.3	30.2 ± 9.1
With salt	Atto633-Aoc-GRTGRRFSY	Acid Blue 80 (5)	98.6 ± 0.2	23.6 ± 3.0

Table 2.6: Effect of salt on the fluorescence response upon phosphorylation of peptides with Evans Blue. Peptides (2.5 μM) and Evans Blue (2.5 μM) were incubated under either "no salt" buffer containing tris-HCl (25 mM, pH 7.5), $MgCl_2$ (1 mM), ATP (1 mM) or "with salt" buffer containing tris-HCl (25 mM, pH 7.5), $MgCl_2$ (1 mM), ATP (1 mM), and 150 mM NaCl. The reaction was initiated by addition of PKA (10 nM).

Buffer condition	Peptide (2.5 μM)	Fluorescent quenching (%)	Fluorescent fold increase
No salt	5Fam-Aoc-GRTGRRFSY	80.9 ± 1.5	2.9 ± 0.5
With salt	5Fam-Aoc-GRTGRRFSY	62.1 ± 1.1	1.4 ± 0.0
No salt	5Tam-Aoc-GRTGRRFSY	99.8 ± 0.0	20.6 ± 2.9
With salt	5Tam-Aoc-GRTGRRFSY	99.8 ± 0.0	34.6 ± 14.5
No salt	Atto633-Aoc-GRTGRRFSY	98.0 ± 0.4	2.0 ± 0.3
With salt	Atto633-Aoc-GRTGRRFSY	94.6 ± 1.3	3.0 ± 0.5

Monitoring PKA Activity in Erythrocyte Lysates

As mentioned before, PKA plays important roles in erythrocyte biochemistry and the infection of malarial parasite *Plasmodium Falciparum*. However, the high hemoglobin concentration (5 mM) is likely to obscure fluorescence monitoring at wavelengths below

600 nm. To confirm the feasibility of using our reporters in erythrocytes, we investigated the loss of fluorescence signals from three peptides in erythrocyte lysate: 5Fam-Aoc-GRTGRRFSY-amide, 5Tam-Aoc-GRTGRRFSY-amide, and Atto633-Aoc-GRTGRRFSY-amide. As expected, while 90% of the fluorescence signal is lost for the 5Fam-peptide and 98% for the 5Tam-peptide, only 10% of the signal is compromised in the case of the Atto633-peptide in 10% lysate (Figure 2.11, blue and red). Additionally, the fluorescence signals from 5Fam and 5Tam labeled peptides are completely blocked, whereas 50% of the original Atto633-peptide signal is still detected in 100% erythrocyte lysate (Figure 2.11, blue and green).

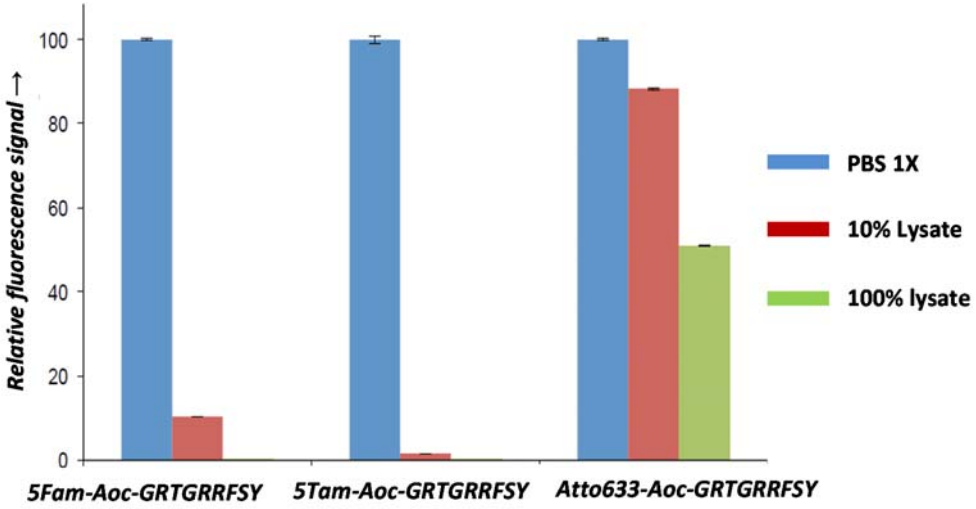

Figure 2.11: Relative fluorescence of 5Fam-, 5Tam-, and Atto633 - labeled petides (1μM) in the presence of PBS 1X, 10% erythrocyte lysate, and 100% erythrocyte lysate.

Adapted with permission from Oien, N. P.; Nguyen, L. T.; Jernigan, F. E.; Priestman, M. A.; Lawrence, D. S., Long-wavelength fluorescent reporters for monitoring protein kinase activity. *Angew Chem Int Ed Engl* **2014**, 53 (15), 3975-8.

We further investigated the fluorescence response upon phosphorylation of 5Tam- and Atto633-labeled Aoc-GRTGRRFSY peptides in erythrocyte lysates. When phosphorylated in buffer and in the presence of Evan blue, the 5Tam-peptide shows a

greater fluorescence response (34 fold) compared to the response of the Atto633-peptide (3 fold) (Table 2.5, 2.6). However, no fluorescence response is detected when the 5Tam-peptide is phosphorylated in erythrocyte lysates in the presence of Evans Blue while profound response is still observed when the Atto633-peptide is used (Figure 2.12).

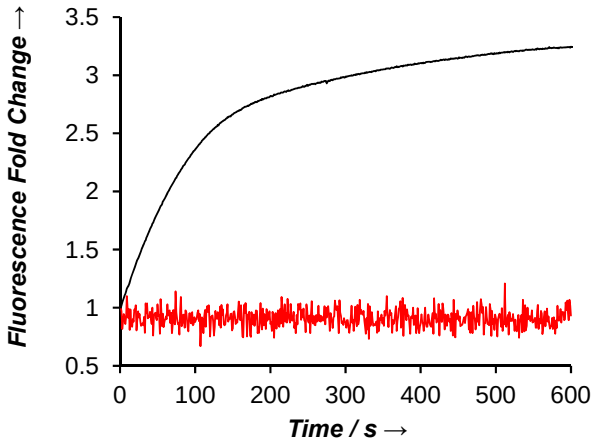

Figure 2.12: Reaction progress curve of the PKA-catalyzed phosphorylation of fluorophore-Aoc-GRTGRRFSY-amide (1 µM) with Evans Blue (2 µM) in 100% erythrocyte lysates where the fluorophore is Atto633 (black) or 5Tam (red).

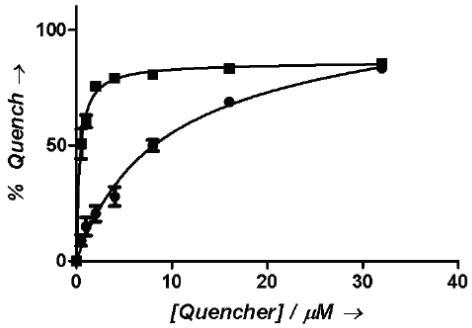

Figure 2.13: Quenching of Atto633-Aoc-GRTGRRFSY (1 µM) fluorescence by Acid Blue 80 (circles, EQ_{50} = 8.1 ± 1.7 µM) and Evans Blue (squares, EQ_{50} = 0.35 ± 0.03 µM) in the presence of 10% erythrocyte lysate. EQ_{50} is the concentration of quencher at which fluorescence is quenched by 50%.

We also examined the quenching efficiency of quenchers in erythrocyte lysates. Quencher Evans Blue is significantly more effective than Acid Blue 80 in term of quenching

Atto633-peptide fluorescence (Figure 2.13). Furthermore, erythrocyte cellular integrity is markedly reduced upon exposure to Acid Blue 80 (30 µM), but remains unperturbed in the presence of Evans Blue (30 µM). Therefore, further phosphorylation studies were performed with the Atto633-peptide and Evans blue quencher.

Selectively Detect PKA Activity in Erythrocyte Lysate

Erythrocytes possess a number of protein kinases.[83] Therefore we investigated whether the observed fluorescence response is due to endogenous PKA activity. The PKA inhibitor H89 blocks the observed fluorescence change with an IC_{50} of 1.14 ± 0.17 µM in 10% lysates. The more selective PKA inhibitor KT5720 prevents the phosphorylation-induced fluorescence response with an IC_{50} of 1.59 ± 0.36 µM.

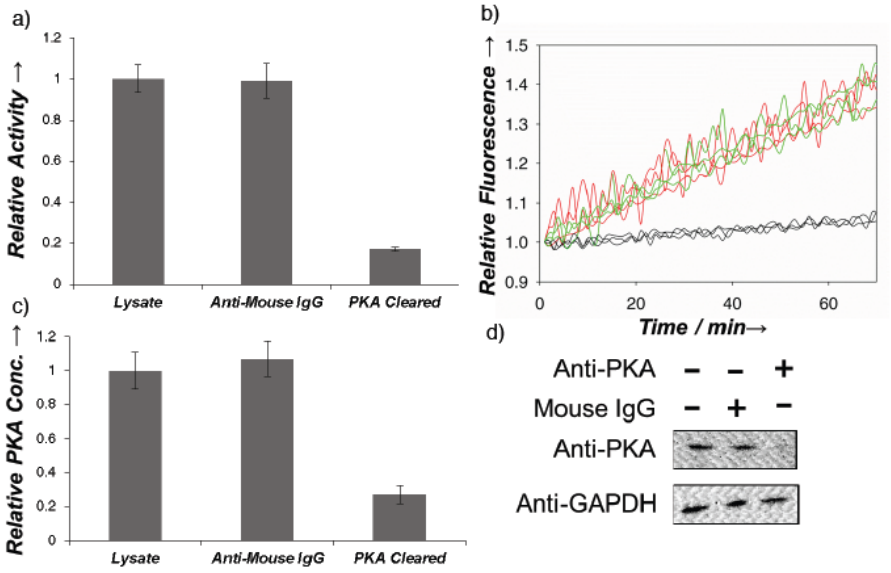

Figure 2.14: Erythrocyte PKA activity (a-b) in lysates, lysates pre-cleared with a control anti-mouse IgG, and lysates pre-cleared with an antibody against the catalytic subunit of PKA. Erythrocyte PKA levels (c-d) in lysates (red), lysates pre-cleared with a control anti-mouse IgG (green), and lysates pre-cleared with an antibody against the catalytic subunit of PKA (black).

Furthermore, PKA was cleared from the erythrocyte lysates by a PKA-specific antibody and kinase activity was then assessed. The precleared lysate showed an 80% decrease in

the rate of fluorescence response compared to control lysates. This directly corresponds with the amount of PKA removed from the lysate (Figure 2.14). These results confirm that the fluorescence response in the lysate is due to PKA activity.

Light-activatable sensor and the monitoring PKA activity inside erythrocytes

After we succeeded in measuring PKA activity in erythrocyte lysates, we investigated the Atto633-Aoc-GRTGRRFSY/Evans Blue as a sensor to measure PKA activity inside erythrocytes. One of the challenges associated with assessing intracellular enzymatic activity in cells is the control of the starting point (t= 0) of the phosphorylation. Veldhuyzen demonstrated one strategy to do so by using a light-activatable peptide substrate.[65] We, therefore, synthesized the light-activatable **Fmoc-Ser(DMNB)-OH** amino acid and incorporated it into the solid phase peptide synthesis to make the light-activatable version of the Atto633-Aoc-GRTGRRFSY-amide. LC-MS analysis shows that the light-activatable peptide analog, **Atto633-Aoc-GRTGRRFS(DMNB)Y-amide** is efficiently converted to Atto633-Aoc-GRTGRRFSY-amide peptide upon irradiation with UV light (Figure 2.15). Additionally, PKA cannot phosphorylate the peptide bearing the photolabile group in the absence of photolysis. Upon illumination, however, a time-dependent fluorescence increase is observed. The fluorescence response of the photochemically activated sensor is blocked in the presence of a PKA inhibitor, which further confirms the light-activation and subsequent phosphorylation of the sensor (Figure 2.16).

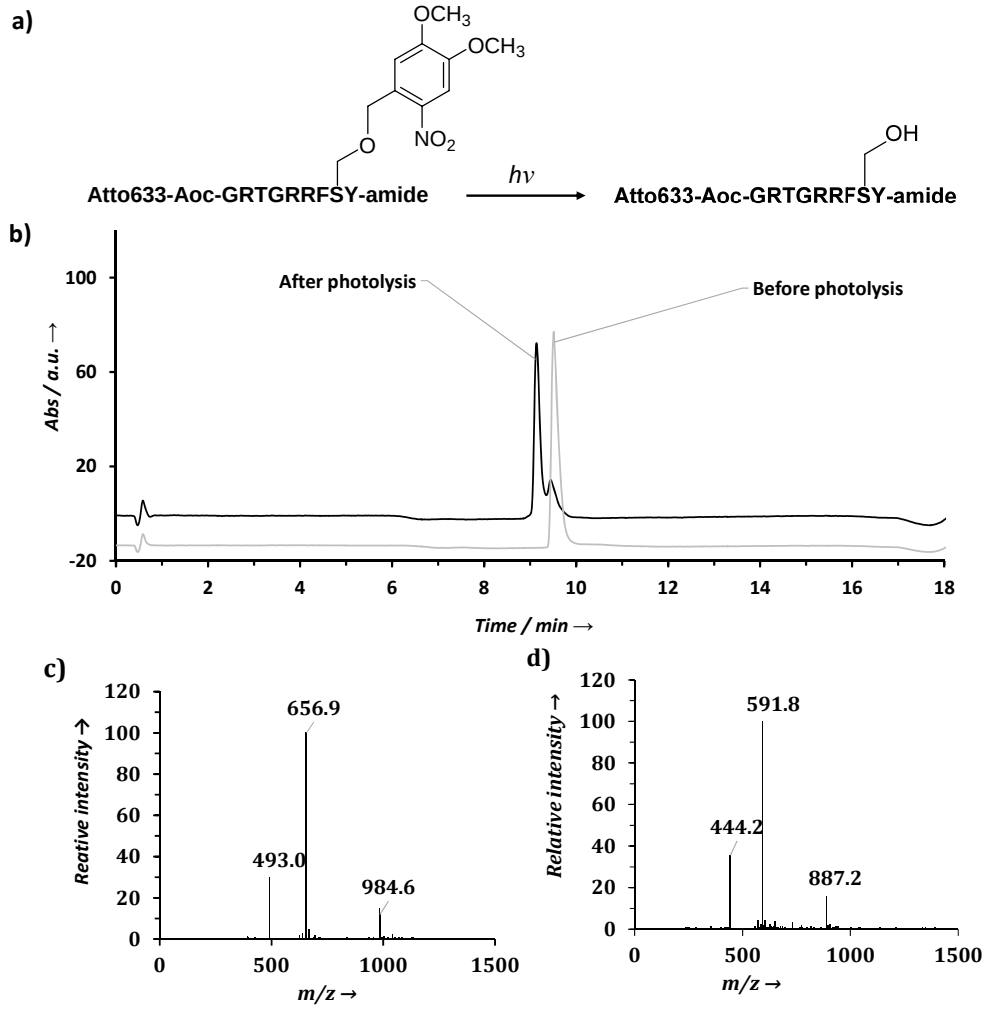

Figure 2.15: Photolysis of Atto633-Aoc-GRTGRRFS(DMNB)Y-amide (a) Structure of peptide before and after photolysis (b) UV traces at 600 nm of Atto633-Aoc-GRTGRRFS(DMNB)Y-amide before (grey) and after photolysis (black). (c, d) ESI+ mass data of before and after photolysis in (b) respectively. Atto633-Aoc-GRTGRRFS(DMNB)Y-amide (5 µM) in PBS 1x was kept in dark or underwent 2 min illumination before analyzed by LC-MS. LC-MS analytical characterizations were run on an Agilent instrument equipped with UV-VIS and quadrupole mass detectors using either a Viva C4 column (5 µM, 50 x 2.1 mm) from Restek. All LC-MS experiments were conducted using H_2O-CH_3CN solvents with 0.1% formic acid. Photolysis was performed using an Oriel 200 W Hg-arc lamp (model 66901) equipped with a beam splitter and a UV bandpass 360 ± 50 nm filter (Newport, FSQ-UG1).

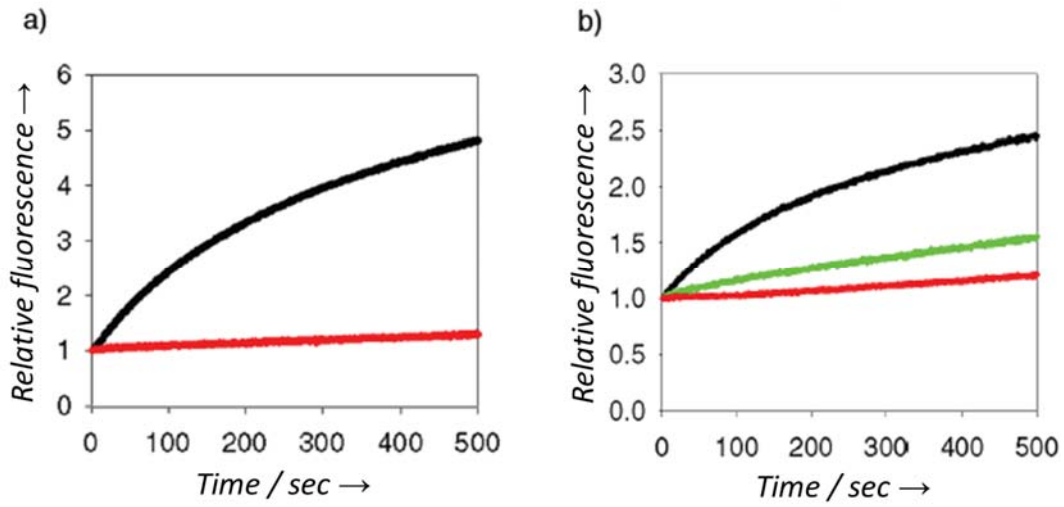

Figure 2.16: Photoactivation of Atto633-Aoc-GRTGRRFS(DMNB)Y-amide. (a) Atto633-Aoc-GRTGRRFS(DMNB)Y-amide (1 µM) and Evans Blue (2 µM) in PBS 1X in the absence (red) and presence (black) of illumination (365 nm, 5 min). Protein kinase-catalyzed phosphorylation was initiated following illumination by the addition of PKA (10 nM). (b) Atto633-Aoc-GRTGRRFS(DMNB)Y-amide (1 µM) and Evans Blue (2 µM) in 10% erythrocyte lysate/PBS buffer upon illumination (365 nm, 5 min) in the absence (black, 5 min) and presence of KT5720 (green, 5 µM) and in the absence of illumination (red). Protein kinase-catalyzed phosphorylation was initiated by the addition of ATP (1 mM).

Light-Activation and Monitoring PKA Activity in Erythrocytes

The light-activatable peptide and Evans Blue quencher were introduced into erythrocytes using hypotonic loading condition. PKA activity in erythrocytes was assessed by confocal microscopy. A 405 nm laser was used to convert the DMNB-bearing peptide to its phosphorylatable counterpart. Upon photolysis, a rapid fluorescence response is observed in the interior of erythrocytes (Figure 2.17). By contrast, no fluorescence response is observed when either the intracellular content of the erythrocytes is depleted of ATP or the PKA-selective cell-permeable inhibitor KT5720 is included in the media.

These results confirm that Atto633-GRTGRRFSY-amide peptide is phosphorylated by PKA upon photolysis.

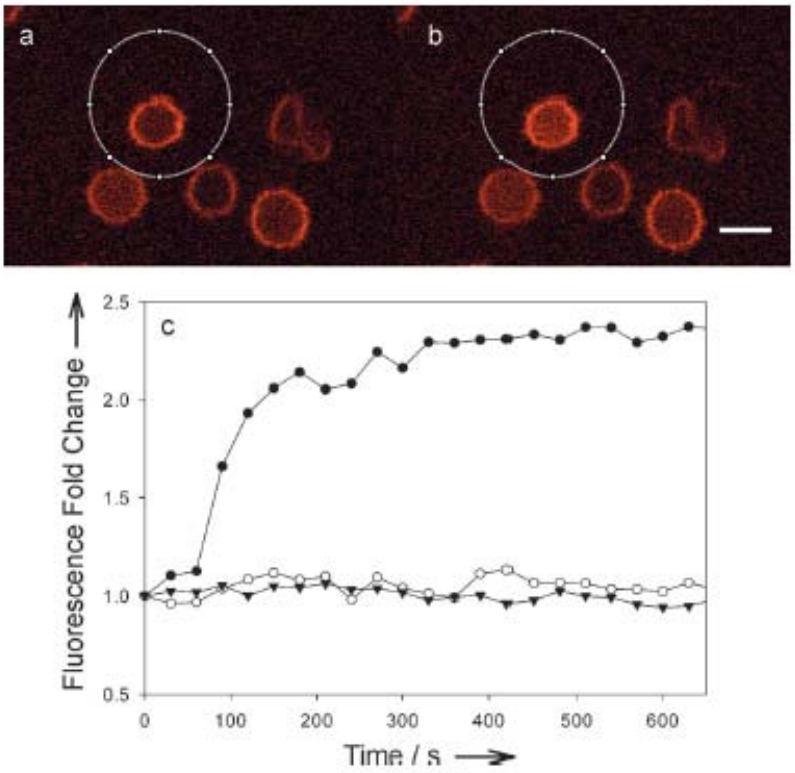

Figure 2.17: Confocal images of Atto633-Aoc-GRTGRRFS(DMNB)Y-amide loaded erythrocytes a) before photolysis and b) 300 sec after photolysis of the encircled cell. Photolysis was performed with a 50 mW, 405 nm laser (2% power level) in tornado mode with a dwell time of 20 µs/pixel and 25 frames. Imaging was performed with a 100X objective by using 635 nm at 4% laser power. Scale bar: 5 µm. c) Fluorescence fold change as a function of time where photolysis at 405 nm is applied at the third time point (filled circles), in the presence of KT5720 (triangles), and under depleted ATP (open circles).

Conclusion

We have developed a series of red and far-red sensors for protein kinase activity by a convenient quenching and dequenching screening approach. The desired wavelength of visualization is easily tuned by appending appropriate commercially available

fluorophores. We have demonstrated the applicability of the approach to develop long wavelength fluorescent reporters for PKA and illustrated visualization of the protein kinase activity in erythrocytes.

Materials and Method

General reagents and solvents were purchased from Fisher or Sigma-Aldrich. 2-(6-chloro-1H-benzotriazole-1-yl)-1,1,3,3-tetramethylaminium hexafluorophosphate (HCTU), 5-carboxyfluorescein (5Fam), 5-carboxytetramethylrhodamine (5Tam), Fmoc protected amino acids, and NovaSyn TGR resin were purchased from Chempep, Inc (Wellington, FL) and NovaBiochem. Fmoc-8-aminooctanoic acid (Fmoc-Aoc-OH) was purchased from Advanced Chemtech (Louisville, KY). All fluorophores, other than Cy3 and Cy5, were purchased from Sigma-Aldrich as either the free carboxylic acid or as the NHS ester pre-activated form. Cy3 and Cy5 carboxylic acids were purchased from Lumiprobe. All reagents for the synthesis of the 4,5-dimethoxy-2-nitrobenzyl ether of Fmoc-Ser-OH [Fmoc-Ser(DMNB)-OH] were purchased from Sigma-Aldrich. The cAMP dependent protein kinase (PKA) inhibitors H89 and KT5720 were purchased from Sigma-Aldrich and Calbiochem (EMD), respectively. Peripheral red blood cells were purchased from AllCells. 8-(4-chlorophenylthio) adenosine-3',5'-cyclic monophosphorothioate (CPT-cAMP), ATP, and cAMP were purchased from Sigma-Aldrich. PKA was obtained either from Promega (for initial screening of dyes) or Sigma (all other studies). Halt Protease and Phosphotase inhibitors were obtained from Thermo Scientific. PKA and IgG antibodies as well as secary goat ant-rabbit antibodies were obtained from Abcam.

Syntheses

Synthesis of ***Fmoc-L-Ser(DMNB)-OH***

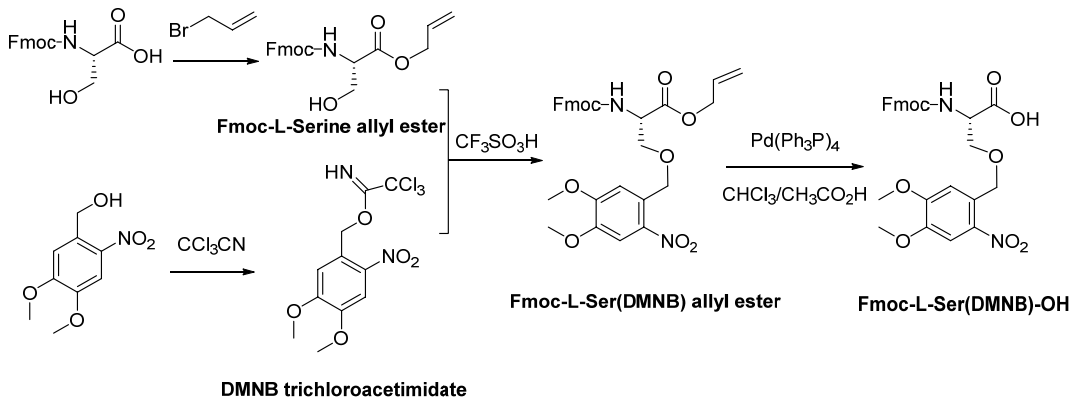

Scheme 2.1: Synthesis of Fmoc-L-Ser(DMNB)-OH.

Fmoc-L-Serine allyl ester

Water (150 mL) containing N-α-Fmoc-L-serine (10.22 g, 31.2 mmol) and $NaHCO_3$ (14.36 g, 31.8 mmol) were combined with CH_2Cl_2 (60 mL) containing tricaprylmethylammonium chloride (~11 g) and allyl bromide (16 mL, 184.89 mmol), and the suspension was vigorously stirred at room temperature for 24 h. Water (300 mL) was added to the reaction mixture, and the suspension was extracted with methylene chloride (3 x 200). The combined organics were dried (Na_2SO_4) and the solvent was removed under reduced pressure. The crude residue was purified by silica flash chromatography (65:35 hexanes:ethyl acetate) to yield **Fmoc-L-Serine allyl ester** as a white solid: ^{1}H NMR (400 MHz, $CDCl_3$) δ = 7.77 (d, J = 7.3 Hz, 2 H), 7.62 (br.d., J = 4.6 Hz, 2 H), 7.41 (t, J = 7.5 Hz, 2 H), 7.32 (t, J = 7.5 Hz, 2 H), 5.92 (tdd, J = 5.6, 11.0, 16.9 Hz, 1 H), 5.84 (d, J = 7.8 Hz, 1 H), 5.35 (d, J = 17.1 Hz, 1 H), 5.27 (dd, J = 1.1, 10.4 Hz, 1 H), 4.69 (d, J = 5.4 Hz, 2 H), 4.53 - 4.46 (m, 1 H), 4.46 - 4.37 (m, 2 H), 4.23 (t, J = 7.0 Hz, 1 H), 4.04 (dd, J = 3.1, 11.1 Hz, 1 H), 3.94

(dd, J = 2.9, 11.2 Hz, 1 H), 2.37 (br. s., 1 H). Exact mass calculated for $C_{21}H_{21}NO_5$ 367.14; found (ESI+, m/z) 368.1 $(M + H)^+$, 390.1 $(M + Na)^+$.

DMNB trichloroacetimidate

4,5-dimethoxy-2-nitrobenzyl alcohol (8.97 g, 42.08 mmol) and anhydrous K_2CO_3 (14.2 g, 102.74 mmol) were stirred in anhydrous CH_2Cl_2 (120 mL) under N_2 atmosphere. To the above mixture, trichloroacetonitrile (10 mL, 99.73 mmol) and anhydrous triethylamine (6 mL, 43.01 mmol) were added and the reaction mixture stirred at room temperature for 24 h. CH_2Cl_2 (300 mL) was added to the reaction mixture. The organic layer was collected and washed with 0.5 N HCl followed by solvent removal. The dried crude residue was purified by silica flash chromatography (75:25 hexanes:ethyl acetate) to give **DMNB trichloroacetimidate**: ^{1}H NMR (400 MHz, $CDCl_3$) δ = 8.51 (s, 1 H), 7.75 (s, 1 H), 7.23 (s, 1 H), 5.78 (s, 2 H), 3.97 (s, 3 H), 3.96 (s, 3 H). Exact mass calculated for $C_{11}H_{11}C_{l3}N_2O_5$ 355.97; found (ESI+, m/z) 374.9 $(M + H_3O)^+$.

Fmoc-L-Serine(DMNB) allyl ester

Fmoc-L-Serine allyl ester (1.74 g, 4.75 mmol) and the **DMNB trichloroacetimidate** (3.22 g, 9.04 mmol) were dissolved in CH_2Cl_2 (40 mL) and mixed under N_2 atmosphere at room temperature. To the above solution was slowly added a solution of triflic acid in CH_2Cl_2 (75 µL triflic acid in 5 mL CH_2Cl_2). The reaction mixture was stirred at room temperature for 30 min after the completion of the triflic acid addition. N,N-diisopropylethylamine (DIPEA, 150 µL) in CH_2Cl_2 (10 mL) and silica gel were added to the reaction mixture and then concentrated under reduced pressure. The crude residue, adsorbed on silica, was purified by silica flash chromatography (67:33 hexanes:ethyl acetate) to afford **Fmoc-Serine(DMNB) allyl ester**: ^{1}H NMR (400 MHz, $CDCl_3$) δ= 7.77 (d, J = 7.5 Hz, 2 H), 7.72 (s, 1 H), 7.61 (t, J = 6.7 Hz, 2 H), 7.41 (t, J = 7.3 Hz, 2 H), 7.31 (t, J = 6.6

Hz, 2 H), 7.18 (s, 1 H), 5.97 - 5.82 (m, 1 H), 5.71 (d, J = 8.4 Hz, 1 H), 5.33 (d, J = 17.1 Hz, 1 H), 5.23 (d, J = 10.4 Hz, 1 H), 4.98, 4.92 (ABq, JAB = 15.4 Hz, 2 H), 4.71 (d, J = 5.1 Hz, 2 H), 4.68 - 4.62 (m, 1 H), 4.48, 4.39 (ABXqd, JAB = 10.5 Hz, JAX = 6.8 Hz, JBX = 6.9 Hz, 2 H), 4.24 (t, J = 7.1 Hz, 1 H), 4.18 - 4.04 (m, 2 H), 3.96 (s, 3 H), 3.95 (s, 3 H), 3.94 - 3.89 (m, 1 H). Exact mass calculated for $C_{30}H_{30}N_2O_9$ 562.20; found (ESI+) 563.2 $(M + H)^+$, 585.2 $(M + Na)^+$.

Fmoc-L-Serine(DMNB)-OH

Fmoc-Serine(DMNB) allyl ester (1.00 g, 1.78 mmol) was dissolved in $CHCl_3$ (40 mL) containing acetic acid (21 mL) and N-methylmorpholine (3 mL). To the above solution was added $Pd(Ph_3P)_4$ (0.97 g, 0.84 mmol). The reaction mixture was stirred for 4 h at room temperature and neutralized by the addition of 0.1 N HCl until pH 4 and then the suspension was extracted with CH_2Cl_2 (twice) and ethyl acetate (three times). The organic extracts was dried (Na_2SO_4), and concentrated under reduced pressure. The crude residue was purified by silica flash chromatography (CH_2Cl_2 and then 48:2 CH_2Cl_2:CH_3OH) to yield **Fmoc-L-Serine(DMNB)-OH**: ^{1}H NMR (400 MHz, $CDCl_3$) δ = 7.76 (d, J = 7.6 Hz, 2 H), 7.66 (s, 1 H), 7.60 (t, J = 5.9 Hz, 2 H), 7.40 (t, J = 7.5 Hz, 2 H), 7.31 (dt, J = 1.2, 6.4 Hz, 2 H), 7.10 (s, 1 H), 5.69 (d, J = 8.3 Hz, 1 H), 4.97, 4.87 (ABq, J_{AB} = 15.29, 2 H), 4.68 (br.s., 1 H), 4.53 - 4.37 (m, 2 H), 4.23 (t, J = 6.7 Hz, 1 H), 4.12 (d, J = 9.2 Hz, 1 H), 3.93 (s, 3 H), 3.90 (s, 3 H), 3.89 - 3.83 (m, 1 H). ^{1}H NMR (400 MHz , acetone-d_6) □ = 7.86 (d, J = 7.6 Hz, 2 H), 7.73 (dd, J = 3.8, 7.4 Hz, 2 H), 7.70 (s, 1 H), 7.44 - 7.37 (m, 3 H), 7.35 - 7.28 (m, 2 H), 4.98, 4.92 (ABq, JAB = 15.7 Hz, 2 H), 4.58 (t, J = 4.5 Hz, 1 H), 4.41 - 4.29 (m, 2 H), 4.28 - 4.21 (m, 1 H), 4.09 (dd, J = 4.9, 9.6 Hz, 1 H), 3.98 - 3.94 (m, 1 H), 3.93 (d, 6 H). Exact mass calculated for $C_{27}H_{26}N_2O_9$ 522.16; found (ESI+, m/z) 523.2 $(M + H)^+$, 545.1 $(M + Na)^+$.

Synthesis of fluorophore-labeled peptides

Solid phase peptide synthesis was performed on a Prelude automatic peptide synthesizer from Protein Technology using Fmoc protected amino acids (amino acids 3 eq, HCTU 2.95 eq, DIPEA 10 eq in DMF, double coupling in 20 and 40 min). The 4,5-dimethoxy-2-nitrobenzyl (DMNB) modified Ser residue was double-coupled to resin as follows: Fmoc-Ser(DMNB)-OH (3.2 eq.), HCTU (3 eq.), DIPEA (10 eq.) for 30 min and then Fmoc-Ser(DMNB)-OH (1.5 eq.), HCTU (1.5 eq.), DIPEA (10 eq.) for 40 min. Fmoc deprotection was performed using 25% piperidine in DMF (3 times, 10 min each). Preactivated fluorophores were coupled to peptides on resin for 4 h using 1 eq. of the preactivated fluorophore, 10 eq. DIPEA, and an excess amount of peptide. Fluorophores with a free carboxylic acid moiety were coupled to the peptides on resin for 4 h using 1 eq. of the fluorophore, 1.1 eq. of HCTU, 10 eq. DIPEA, and an excess amount peptide. 5Fam was coupled to peptides on resin using 1.5 eq. of 5Fam, 1.7 eq. of diisopropylcarbodiimide, and 10 eq. of HOBt in DMF for 2 h followed by 30 min treatment with 25% piperidine in DMF (2 times). Labeled peptides were cleaved with trifluoroacetic acid (TFA):H_2O:triisopropylsilane in a ratio of 95:2.5:2.5, and purified by HPLC using H_2O:CH_3CN with 0.1 % TFA.

Purification and LC-MS Characterization

Flash chromatography purification was performed on an Isolera One instrument (Biotage) using a silica or C18 column (Biotage). HPLC purifications were performed on a Waters HPLC instrument. Peptides were purified using a C18 HPLC (Apollo C18, 5 µm, 250 x 22 mm column). LC-MS analytical characterizations were run on an Agilent instrument equipped with UV-VIS, fluorescence, and quadrupole mass detectors using either a Viva C4 column (5 µm, 50 x 2.1 mm) from Restek or a Prevail C18 column (3 µm, 50 x 2.1 mm)

from Alltech Associates, Inc. All LC-MS experiments were conducted using H_2O-CH_3CN solvents with 0.1% formic acid.

Fluorescence Measurements

200 µL 96 well plate fluorescence assays were performed using a Molecular Devices SpectraMax Gemini EM Dual-Scanning Microplate Spectrofluorometer. Data was collected using SoftMax Pro Software. Alternatively, protein kinase activities were monitored using a PTI Technologies QuantMaster-40 equipped with cooled PMT housing. The data was collected using FelixGX Software. Sensor monitoring studies were performed using a plate reader in a 96 well format (200 µL/well) in Tris-HCl (25 mM, pH 7.5), $MgCl_2$ (1 mM), PKA (10 nM), peptide (1 µM), and quencher. Reactions were initiated with the addition of ATP (final concentration of 1 mM).

Screening of the Dye Library

Kinase buffer (200 µL) containing Tris-HCl (25 mM, pH 7.5), $MgCl_2$ (1 mM), ATP (1 mM) and fluorophore-peptide (2.5 or 5 µM) were added to wells of a 96-well plate. Dyes (concentration ranging from 5 µM to 60 µM) were then added to each well and the initial fluorescence recorded. Phosphorylation was initiated by the addition of PKA (10 nM) into each well and fluorescence was monitored over time. Dyes that produced a fluorescent increase upon the PKA addition were selected for further confirmation by replication in the plate reader or spectrofluorometer. Phosphorylation products were confirmed by LC-MS.

Comparison of Kinase Reporter Assay Using Various Salt Concentrations

Fluorophore-labeled peptides were added to 200 µL of either “no salt” buffer containing Tris-HCl (25 mM, pH 7.5), $MgCl_2$ (1 mM), ATP (1 mM) or “with salt” buffer containing Tris-HCl (25 mM, pH 7.5), $MgCl_2$ (1 mM), ATP (1 mM), and NaCl (150 mM)

followed by incubation (5 min at 30 °C). Various quenchers were then added to the solutions followed by incubation (5 min at 30 °C) and the addition of PKA (to 10 nM) to initiate phosphorylation. Fluorescence fold change = F_f/F_q, and fluorescent quenching = $100*(F_i-F_q)/F_i$, where F_i, F_q, F_f are the fluorescence of the reaction mixture in the absence of quencher, in the presence of quencher, and after the phosphorylation reaction is completed, respectively.

Job Plots

Various ratios of peptide (TAMRA-Aoc-GRTGRRFSY) and quencher dye (Acid Blue 80 or Evans Blue) at a fixed total concentration of peptide and quencher dye (5 μM) were added to 200 μL kinase buffer containing Tris-HCl (25 mM, pH 7.5), $MgCl_2$ (1 mM), ATP (1 mM), and NaCl (150 mM). Mixtures were then incubated at room temperature for 10 min before the absorbance measurements were taken.

Dynamic Light Scattering

Dynamic light scattering experiments were performed on a DynaPro Plate Reader (Wyatt Technology). Buffer (1 mL) containing Tris-HCl pH 7.5 (25 mM), NaCl (150 mM), $MgCl_2$ (1 mM), and ATP (1 mM) was added 5Tam-Aoc-GRTGRRFSY-amide (1 μM) or Evans Blue (2 μM) or both 5Tam-Aoc-GRTGRRFSY-amide (1 μM) + Evans Blue (2 μM), followed by incubation at room temperature for 10 min. The solutions were then centrifuged at 14,000 g for 10 min. The solutions (100 μL) were then transferred to wells of a 384-well plate, followed by light scattering measurement.

Initial Phosphorylation Rates of Reporter/Quencher Pairs

Buffer (200 μL) containing Tris-HCl (25 mM, pH 7.5), $MgCl_2$ (1 mM), ATP (1 mM), peptide (5 μM), and quencher was added to individual wells of a 96-well plate. The plate was incubated at 30 ^oC for 5 min followed by addition of PKA (2 nM) to initiate

phosphorylation. The concentration of the phosphorylated peptide was calculated by the formula: [phosphopeptide] (μM) = $5(F_t - F_q)/(F_f - F_q)$, where F_t is the fluorescence at time *t*, F_f and F_q are the final fluorescence after the addition of PKA and the initial fluorescence, respectively.

Initial Phosphorylation Rate Determined by Capillary Electrophoresis

Buffer (200 μL) containing Tris-HCl (25 mM, pH 7.5), $MgCl_2$ (1 mM), ATP (1 mM), 5Fam-KRRRLASLAA-amide (5 μM), and Acid Green 27 (20 μM) was added PKA (2 nM). At different time points, aliquots were quenched with HCl (10 M). Phosphopeptide and peptide were then separated by capillary electrophoresis and quantified by fluorescence.

PKA Activity in Erythrocyte Lysate

Peripheral erythrocytes were washed three times in PBS 1X [sodium phosphate (8.06 mM), potassium phosphate (1.94 mM), KCl (2.7 mM) and NaCl (137 mM); pH 7.4] by centrifuging at 1400 g for 10 min. After each centrifugation the supernatant was removed by aspiration and replaced with PBS 1X buffer. After the final wash, erythrocytes were suspended to 50% hematocrit levels and lysed in the presence of DTT (20 mM) with mechanical shearing. The lysed erythrocytes were then centrifuged at 10,000 rpm for 3 min and the subsequent supernatant was used for assay measurements. Kinase assays were performed in a 200 μL cuvette using a PTI spectrofluorometer. Solutions contained PBS with fluorophore labeled peptide (1 μM), $MgCl_2$ (5 mM), Halt protease and phosphatase inhibitors (1), and lysed erythrocytes (10%). Reactions were initiated with the addition of cAMP and ATP to a final concentration of 1 mM each.

Fluorescence Signal Loss Study due to Erythrocyte Lysate

A two-chambered cuvette (Precision Cells, LT125ES10) was filled with PBS 1X or PBS 1X and 10% lysate in one chamber and PBS 1X containing 5Fam-, 5Tam-, or Atto633-

Aoc-GRTGRRFSY-amide (1 μM) in the sec chamber. The fluorescence spectrum was measured for each peptide using their corresponding maximum excitation and emission wavelengths.

Photoactivation of DMNB-bearing Sensor

Photolysis of **Atto633-Aoc-GRTGRRFS(DMNB)Y-amide** was conducted in PBS 1X or in PBS containing 10% erythrocyte lysate, DTT (20 mM), and Halt protease and phosphatase inhibitors (1X). Photolysis was performed using a Zeiss Colibri 1 LED light source (365 nm light at 100% power) for 5 min or using an Oriel Hg arc lamp (426 mW/cm2) for 2 min. PBS 1X containing Atto633-Aoc-GRTGRRFSY-amide (1 μM), Evans Blue (2 μM), and PKA (10 nM) was photolyzed. Following photolysis, activity was monitored using fluorescence by the addition of ATP (1 mM) to initiate the phosphorylation.

Kinase Reporter Loading into Erythrocytes

Erythrocytes were loaded with peptide and dye quencher via a hypotonic dilution method. Briefly, whole peripheral erythrocytes were washed three times in PBS 1X. Erythrocytes were then stored overnight at 4 °C to deplete any remaining ATP. Washed erythrocytes (50 μL, 50%) were added to a solution containing **Atto633-Aoc-GRTGRRFS(DMNB)Y-amide** (1 μM), Evans Blue (2 μM), ATP (5 mM), CPT-cAMP (1 mM), Tris-HCl (10 mM, pH 7.5), and Halt protease and phosphatase inhibitor cocktail (1X) to a final volume of 500 μL. The solution was incubated on ice (10 min) and turned a transparent red. 52.7 μL of 10X buffer [KCl (1.22 M), $MgCl_2$ (180 mM), glucose (100 mM), and Tris-HCl (100 mM, pH 7.5)] was then added to the erythrocyte solution, which changed from transparent to opaque. At this point erythrocytes were allowed to recover at 4 °C for 30 min. 5 μL of DTT (1 M) and 5 μL of Evans Blue (400 μM) were then added to

the erythrocyte solution to completely quench fluorescence outside erythrocytes . Several studies have demonstrated that, upon resealing, erythrocytes are unable to completely reseal the membrane. To prevent loss of smaller molecules (ATP, cAMP, or quencher) the erythrocytes were not washed. For microscopy experiments, 7 µL of the final erythrocyte solution was placed between two cover slips. Erythrocytes added to the cover slips were allowed to rest for 10 min, and subsequently imaged using confocal microscopy.

Confocal Microscopy

All microscopy experiments were performed at room temperature on an Olympus FV1000 scanning confocal with an IX81 microscope base. Laser and region of photolysis were controlled via Fluoview software. Photolysis was performed using the stimulation mode with images collected before and after stimulation. A photolytic dwell time of 20 µs/pixel in tornado mode was employed for the defined region of interest using 25 frames at 405 nm and 2% power level. All imaging was performed with a 100X at 1.9X digital zoom objective using 635 nm at 2% laser power and a dwell time of 12 µs/pixel. The Atto633-peptide, in the absence of dye quencher, was used to generate a photobleaching curve. ImageJ software was employed for image analyses. Final fluorescence intensity changes of Atto633 were corrected for photobleaching effect by the following equation.

F_t (corrected) = F_t x f_o/f_t

Where F_t are fluorescence values measured at time t, f_o and f_t are fluorescence values of bleaching curve at t = 0 and at t.

CHAPTER 3: PEPTIDE STABILIZATION AND KINASE ASSAY BASED ON PHOSPHORYLATION-INDUCED PEPTIDE DEGRADATION

Using small peptides is an appealing approach in developing biosensors given the ease of synthesis, modification, and optimization. However, this type of biosensor, with the exception of negatively charged peptides, possess a critical drawback in term of stability when using in living cells or cell lysates.[43, 44, 84] For example, Proctor et al. showed that a PKB peptide substrate, 6Fam-GRPRAATFAEG-amide, is 50% degraded after 20 min in HeLa cell lysate. Depending on the preparation of cell lysate, this half-life value might be significantly shorter. Moreover, in intact LNCap cells, little of the peptide is detected at 1.5 min after the microinjection.[43]

A tremendous effort has been put into stabilizing small peptides in general, such as substitution or cyclization. When applied to peptide therapeutics such as inhibitors, agonists and antagonists, those strategies have led to some successes.[85] However, in the case of peptide enzyme substrates, the task becomes more challenging since the requirement of maintaining the ability of the enzyme to process the modified substrates.[43] In addition to the chemical modification approach, introducing a mixture of various protease inhibitors into the studied system is an alternative to prevent degradation of the peptide substrates. This approach, however, unfavorably requires a large excess of protease inhibitors and protection is not always sufficiently achieved. For example, for fluorophore-KRRRLASLAA-amide peptide sensors described in Chapter 2, various protease inhibitor cocktails were employed but significant degradation was still observed.

As demonstrated in Chapter 2, negatively charged quenchers interact with the positively charged peptides; and the phosphorylation of the peptides disrupt those interactions. It has also been suggested that the arginine residues in a peptide play an important role in the peptide proteolytic instability.[43, 44] Those basic residues are further away from the phosphorylation site compared to the proteolytic cleavage sites to which they are usually adjacent to. Additionally, we found that the presence of negatively charged quencher slows down the phosphorylation process of the peptide sensors, fluorophore-KRRRLASLAA-amide and fluorohore-Aoc-GRTGRRFSY-amide. Therefore, we hypothesized that quenchers-peptide interaction might prevent proteases from processing the peptide while still allow the kinase to phosphorylate the substrate. Upon phosphorylation, the peptide-quencher interactions are disrupted leading to the digestion of the phosphorylated peptide. The complete fragmentation of the peptide is expected to result in a significant fluorescence dequenching since all binding sites are destroyed. We decided to investigate the possibility of stabilizing the positively charged peptides using the negatively charged quenchers and developing fluorescent sensors based on phosphorylation-induced peptide destabilization mechanism (Figure 3.1).

Results and Discussion

Protection of Peptide 5Tam-Aoc-GRTGRRFYS-amide from Trypsinolysis by Evans Blue

We first investigated the hypothesis that binding of a negatively charged quencher to the peptide protects the peptide from proteolysis. Since the Evans Blue quencher binds tightly to the peptides fluorophore-Aoc-GRTGRRFSY-amide, we examined the stability of the peptide 5Tam-Aoc-GRTGRRFSY-amide toward trypsinolysis in the presence and

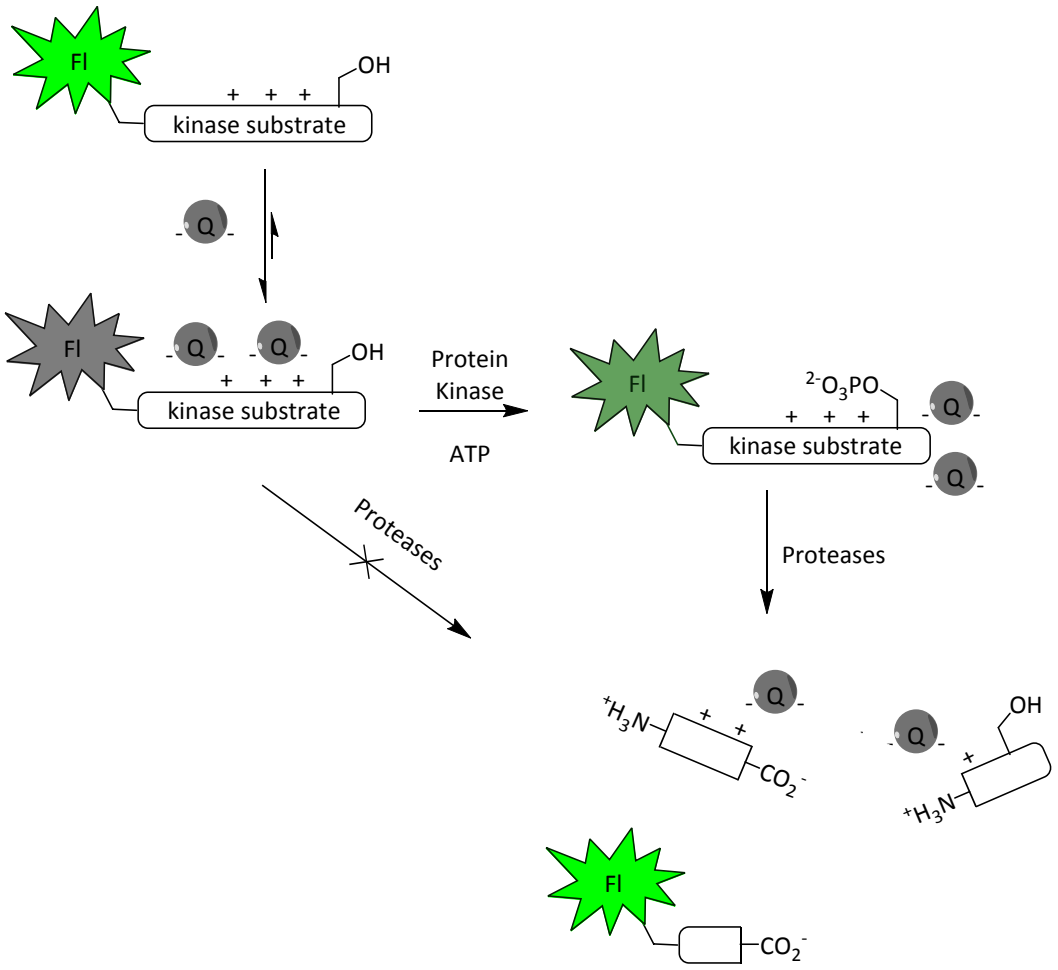

Figure 3.1: General strategy for the stabilization and phosphorylation induced peptide degradation leading to dequenching of fluorescent kinase substrates. Negatively charged quenchers (Q) interact with a positively charged fluorescent kinase substrate. The interaction leads to both the quenching of the peptide's fluorescence and the stabilization of the peptide against proteolysis. Kinase-catalyzed phosphorylationof the peptide disrupts Q-peptide interaction leading to peptide degradation and fluorescence dequenching.

absence of Evans Blue using LC-MS. As expected, the peptide is significantly more stable under trypsinolysis condition when Evans Blue (5 µM and 20 µM) is added to the assay buffer (Figure 3.2a). No significant peptide protection at 5 µM of Evans Blue and 30 µM of peptide (Figure 3.2b) further confirms that the protection is due to the peptide-Evans

Blue association since at that high peptide concentration, the majority of the peptide does not bind to the quencher, and thus is susceptible to proteolysis.

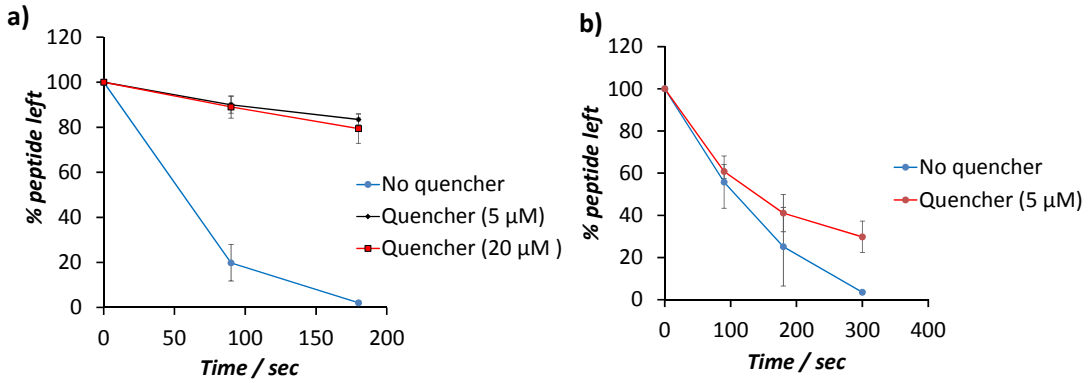

Figure 3.2: Protection of 5Tam-Aoc-GRTGRRFSY-amide 2.5 µM (a) and 30 µM (b) from trypsinolysis by Evans Blue. Tris buffer [150 µL total, Tris-HCl (25 mM, pH 7.5)] containing peptide 5Tam-Aoc-GRTGRRSFY-amide (2.5 or 30 µM) and Evans blue (5 or 20 µM) was preincubated at 37 °C for 5 min, followed the addition of trypsin (5 nM). At various time points, reaction aliquots were quenched and analyzed by LC-MS.

Trypsinolysis of 5Tam-Aoc-GRTGRRFSY-amide and its phosphorylated peptide in the presence of Evans blue

We next examined if, upon phosphorylated by PKA, the phosphopeptide is more susceptible to trypsinolysis in the presence of Evans Blue. Since we noticed that degradation of the peptides also disrupts the fluorescence quenching, we used the fluorescence readout as an indication of peptide degradation. The peptide 5Tam-Aoc-GRTGRRFSY-amide and its phosphorylated counterpart were incubated with trypsin in the presence of Evans Blue and fluorescence was monitored. The 10 times higher rate of fluorescence increase with phosphopeptide compared to that of nonphosphorylated peptide suggests that the phosphopeptide is less protected by Evans Blue (Figure 3.3).

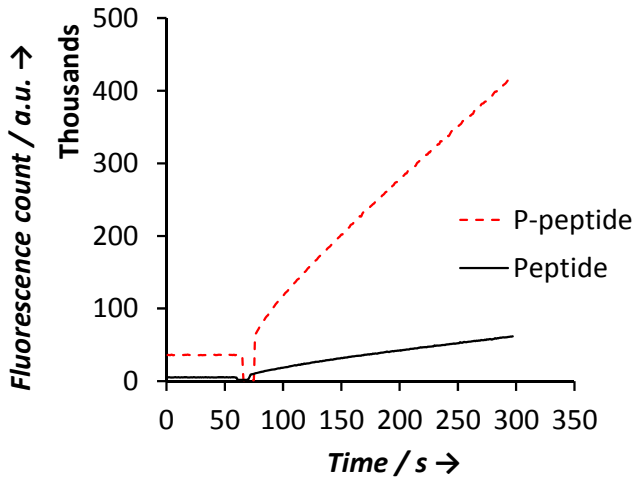

Figure 3.3: Degradation of 5Tam-Aoc-GRTGRRFSY-amide and its phosphorylated counterpart by trypsin in the presence of Evans Blue. Peptide (2.5 µM), Evans Blue (5 µM). Fluorescence was followed in a spectrofluorometer, λ_{ex} - λ_{em} = 550 - 587 nm.

Screening for Quenchers Which Protect the Peptide but not Phosphorylated Peptide from Proteolysis in Erythrocyte Lysate

Given the promising results obtained from the 5Tam-peptide/Evans Blue quencher pair with PKA and trypsin, we decided to rescreen all quenchers in our library to find quenchers which slow or prevent degradation of the unphosphorylated peptide while permitting degradation of the phosphorylated peptide. We used erythrocyte lysates, which contain endogenous proteases, as the protease model. The lysate was used at 2.4% concentration to reduce the inner filter effect of hemoglobin. No protease inhibitors were added to the lysate to preserve the protease activity of the lysate, whereas phosphatase inhibitors were added to prevent the newly formed phosphorylated peptide from dephosphorylation. In the presence of a number of quenchers, little fluorescence change is observed with the unphosphorylated peptide, whereas significant fluorescence increase is observed with phosphorylated one (Figure 3.4). The acceleration in

fluorescence increase of the phosphorylated samples compared to that of unphosphorylated ones suggests that the newly introduced phosphate group destabilizes the peptide in the lysate, while little fluorescence increase observed in unphosphorylated samples suggests that the peptide might be stabilized in the investigated conditions.

Among the forty eight quenchers screened, eight were selected for further study based on the background fluorescence increase of unphosphorylated samples and the difference in the fluorescence increase rate between phosphorylated and unphosphorylated samples. Further studies were conducted to eliminate quenchers which, upon association with the peptide, prevent the peptide from getting phosphorylated by PKA. The 5Tam-peptide was preincubated with a selected quencher followed by the addition of erythrocyte lysate. Br-cAMP was added to the buffer to activate endogenous PKA. A number of peptide-quencher pairs show significant fluorescence increase only when PKA is activated by 8-Br-cAMP (Figure 3.5). The fluorescence increase was abolished in the presence of the PKA inhibitor, H89, further confirming the phosphorylation induced fluorescence response.

Stability of 5Tam-peptide in Erythrocyte Lysate in the Presence and Absence of Quenchers as Assessed by LC-MS

The protection of peptide from proteolysis in erythrocyte lysate by four selected quenchers (Acid Green 27, Disperse Yellow 3, Brilliant Blue R, and Acid Blue 129) was further confirmed using LC-MS. The peptide 5Tam-Aoc-GRTGRRFSY-amide was incubated with erythrocyte lysate in the presence and absence of a listed quencher. At various time points, the samples were quenched and analyzed by LC-MS. As demonstrated in Figure 3.6, in the absence of quencher, the peptide gets degraded quickly in 2.4% erythrocyte lysate with a half-life of about 16 min, whereas under the same conditions in the presence

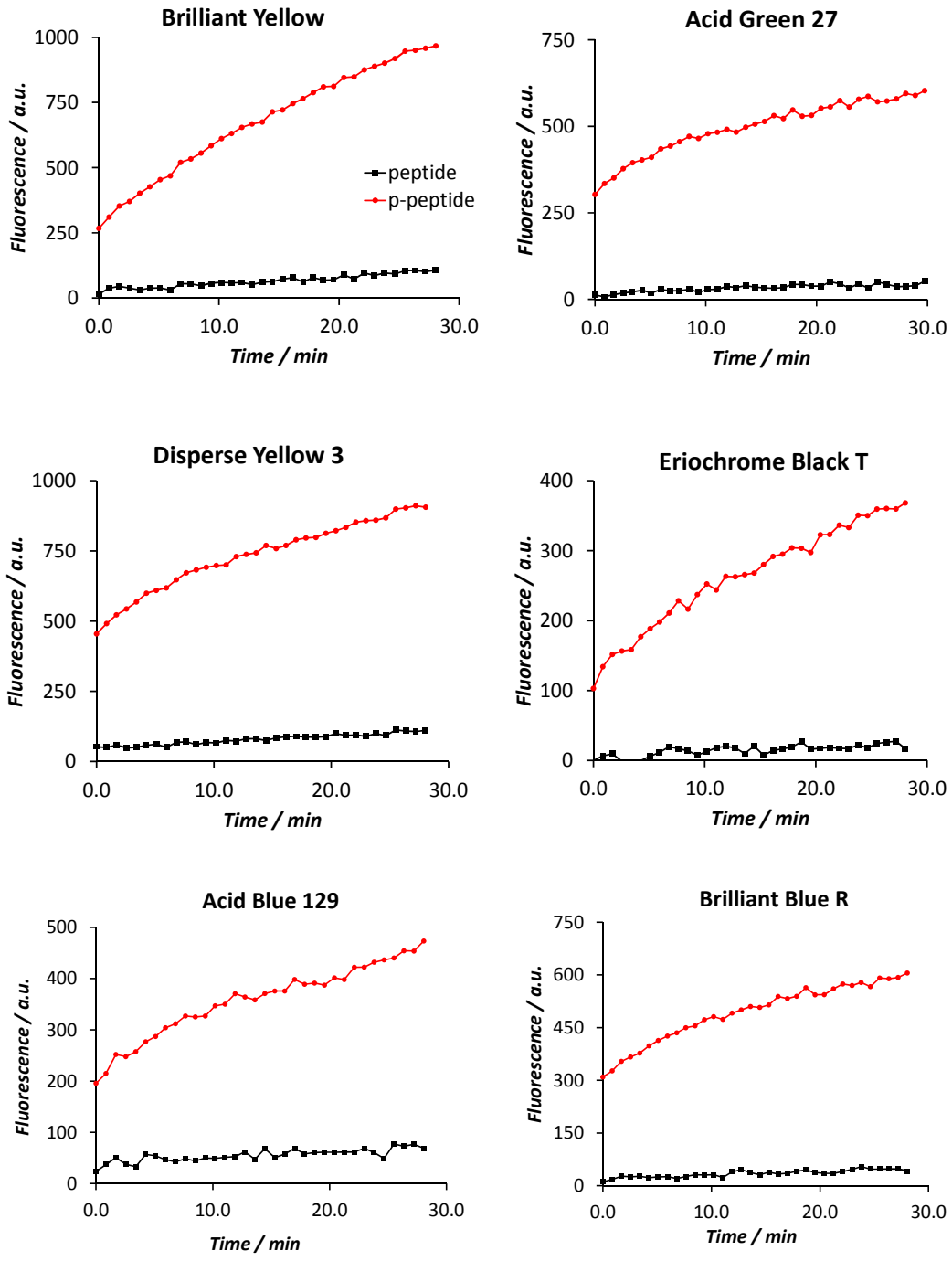

Figure 3.4: Degradation difference of phosphorylated and unphosphorylated peptides in erythrocyte lysate (2.4% lysate in PBS 1X buffer) in the presence of quenchers, Acid Green 27 (18.75 µM) or other dyes (37.5 µM) and peptide (2.5 µM). Fluorescence was followed in a plate reader. λ_{ex} - λ_{em} = 550 - 587 nm.

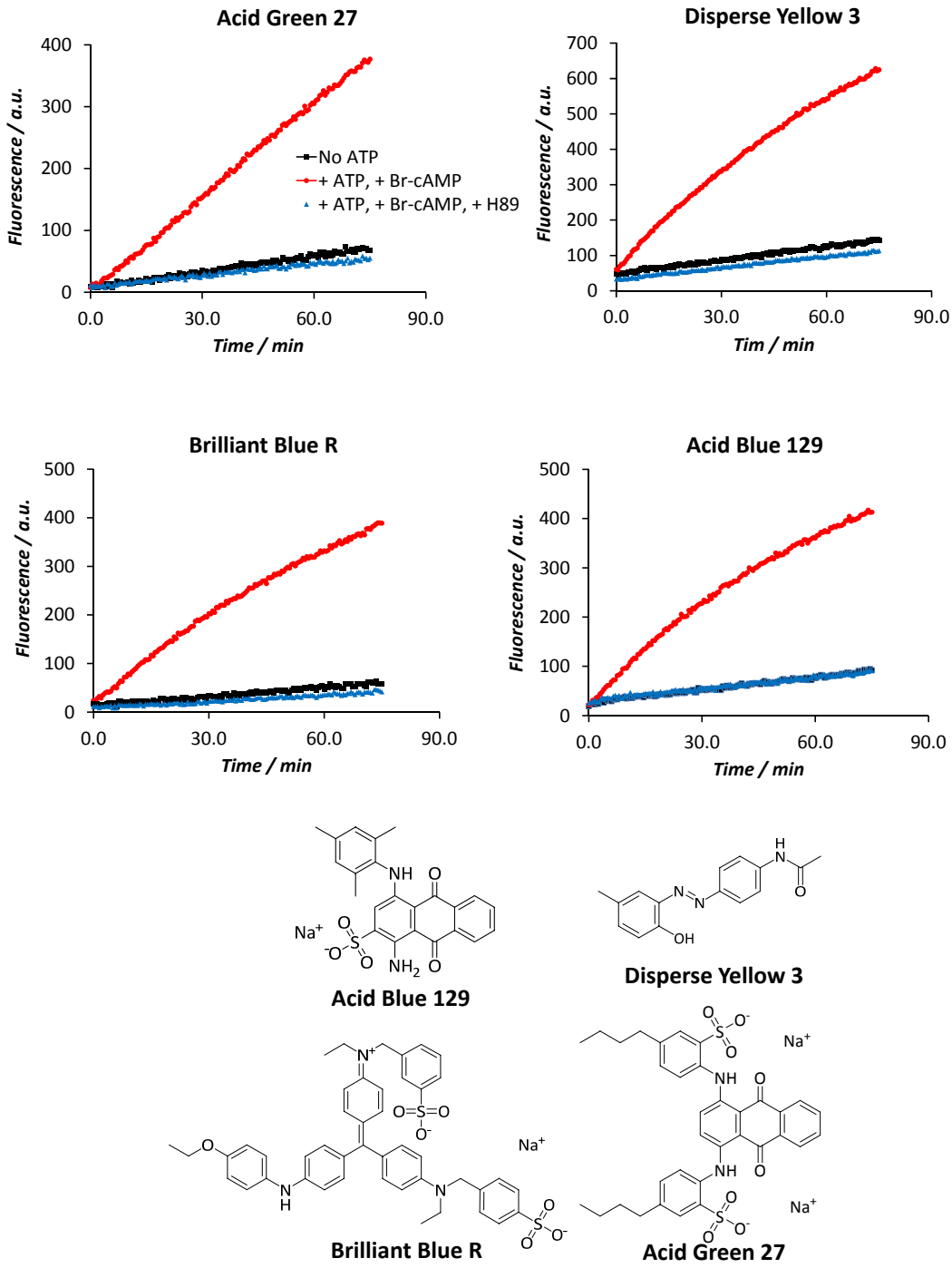

Figure 3.5: Fluorescence increase induced by phosphorylation-degradation in erythrocyte lysate (2.4% lysate in PBS 1X buffer) in the presence of quenchers, Acid Green 27 (18.75 µM) or other dyes (37.5 µM) and peptide (2.5 µM). ATP (1 mM), $MgCl_2$ (1mM) and phosphatase inhibitors was added to the lysate. Phosphorylation was initiated by the addition of 8-Br-cAMP (100 µM). Fluorescence was followed in a plate reader. λ_{ex} - λ_{em} = 550 - 587 nm.

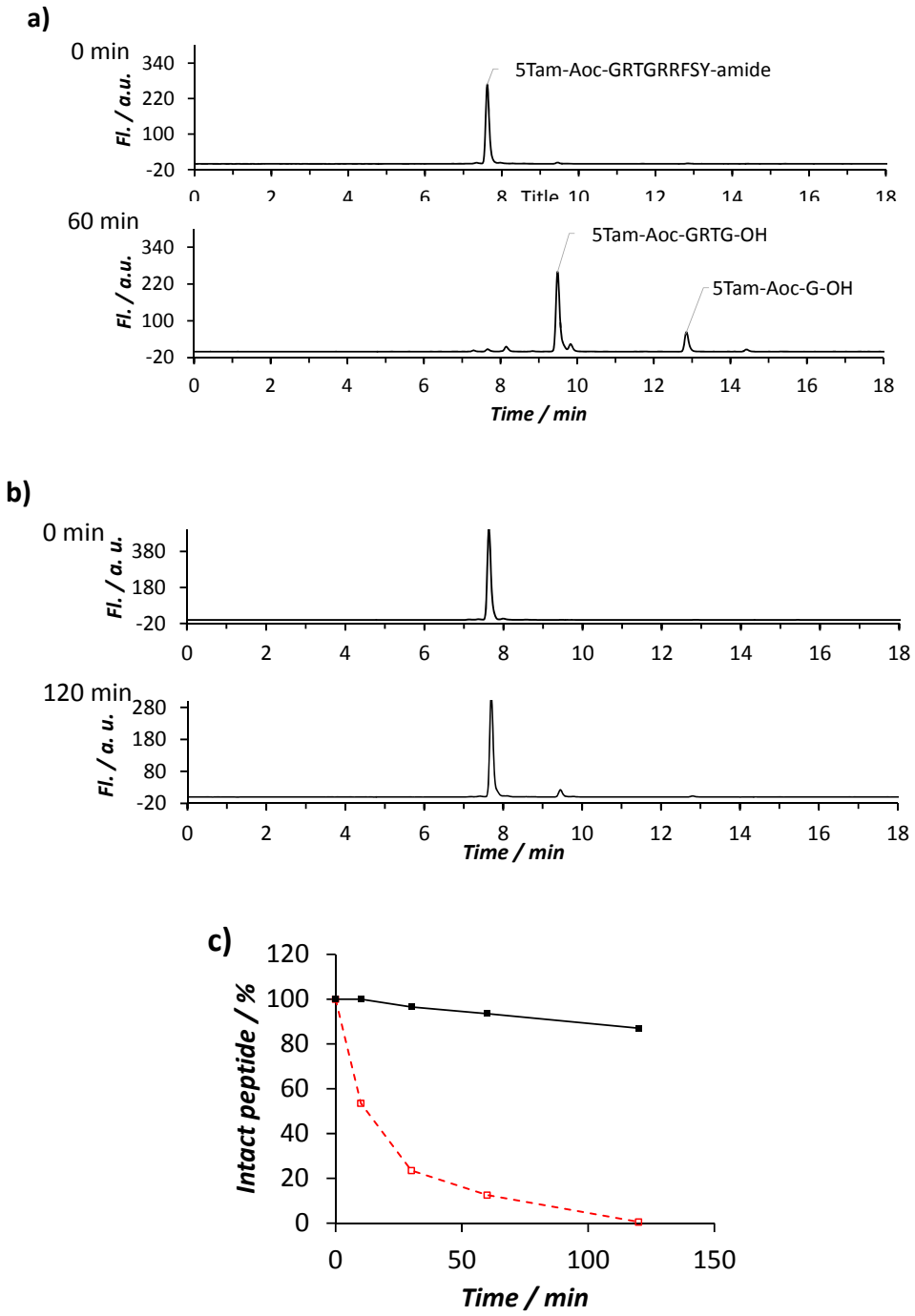

Figure 3.6: Degradation of 5Tam-Aoc-GRTGRRFSY-amide in erythrocyte lysate in the absence and presence of Acid Green 27. LC-Fluorescence trace (λ_{ex} - λ_{em} = 550 - 590 nm) of peptide 5Tam-Aoc-GRTGRRFSY-amide (2.5 µM) incubated in erythrocyte lysate (2.4% lysate in PBS 1X buffer) in the absence (a) and presence of Acid Green 27 (18.75 µM) (b). 5Tam-Aoc-GRTGRRYSY-amide remains in the lysate vs time (c). Red: No quencher, black: 18.75 µM Acid Green 27.

of quencher Acid Green 27, more than 85% of the intact peptide is still detected after 120 min. Similar levels of protection are also observed with the other three quenchers, Disperse Yellow 3, Brilliant Blue R, and Acid Blue 129 (Figure 3.6, 3.7).

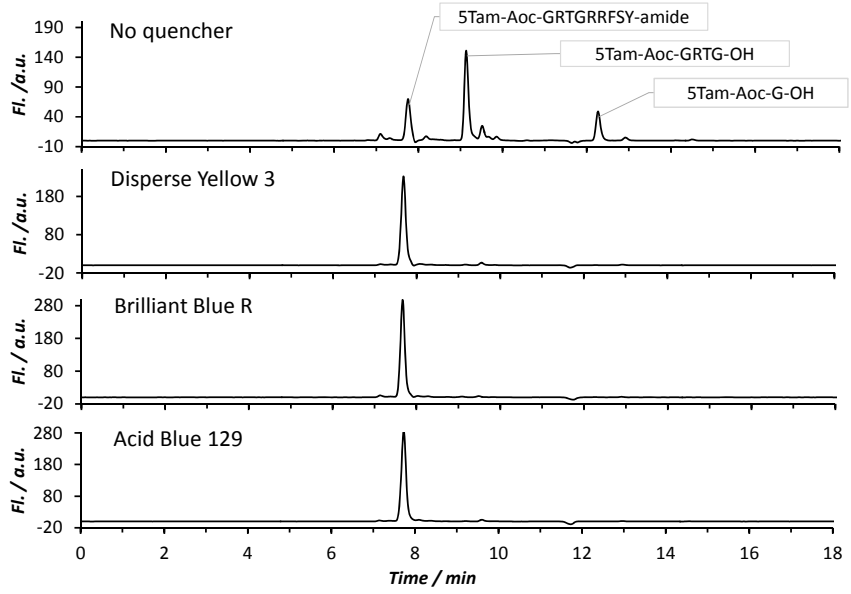

Figure 3.7: Protection of 5Tam-Aoc-GRTGRRFSY-amide against proteolysis in erythrocyte lysate by quenchers. LC fluorescence trace of 5Tam-Aoc-GRTGRRFSY-amide incubated with erythrocyte lysate (2.4% lysate in PBS 1X buffer) in the absence (30 min incubation) and presence of quencher (60 min incubation). Peptide (2.5 µM), quencher (37.5 µM), 30 ^{o}C.

Phosphorylation-Induced Degradation of the Peptide in the Presence of Quencher as Assessed by LC-MS

We investigated if phosphorylation destabilizes the peptide in the lysate. The peptide was incubated with erythrocyate lysate in the presence of a selected quencher. Phosphorylation of the peptide by endogenous PKA was stimulated by the addition of 8-Br-cAMP and ATP. After 90 min of incubation at the 30 ^{o}C, the assays were analyzed by LC-MS. The fluorescence traces from LC-MS experiment demonstrate that the peptide, upon phosphorylation, was degraded rapidly, whereas the unphosphorylated peptide was intact during the time course of the experiments (Figure 3.8, 3.9).

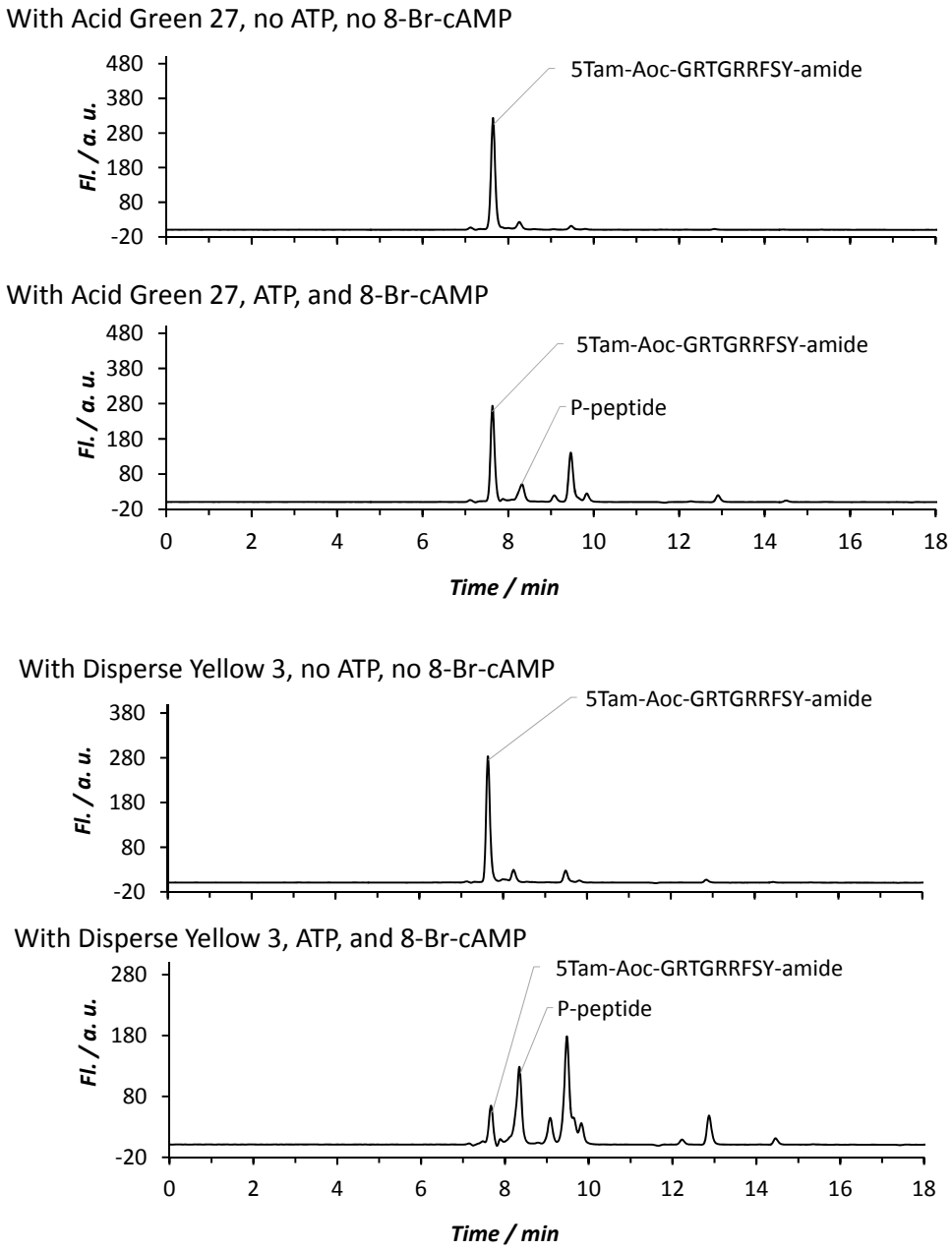

Figure 3.8: Phosphorylation-induced degradation of 5Tam-Aoc-GRTGRRFSY-amide in the presence of quencher in erythrocyte lysate. The peptide and quencher were incubated with erythrocyte lysate with and without the activation of PKA. After 90 min of incubation, assay samples were analyzed by LC-MS. Fl = Fluorescence. λ_{ex} - λ_{em} = 550 nm - 590 nm.

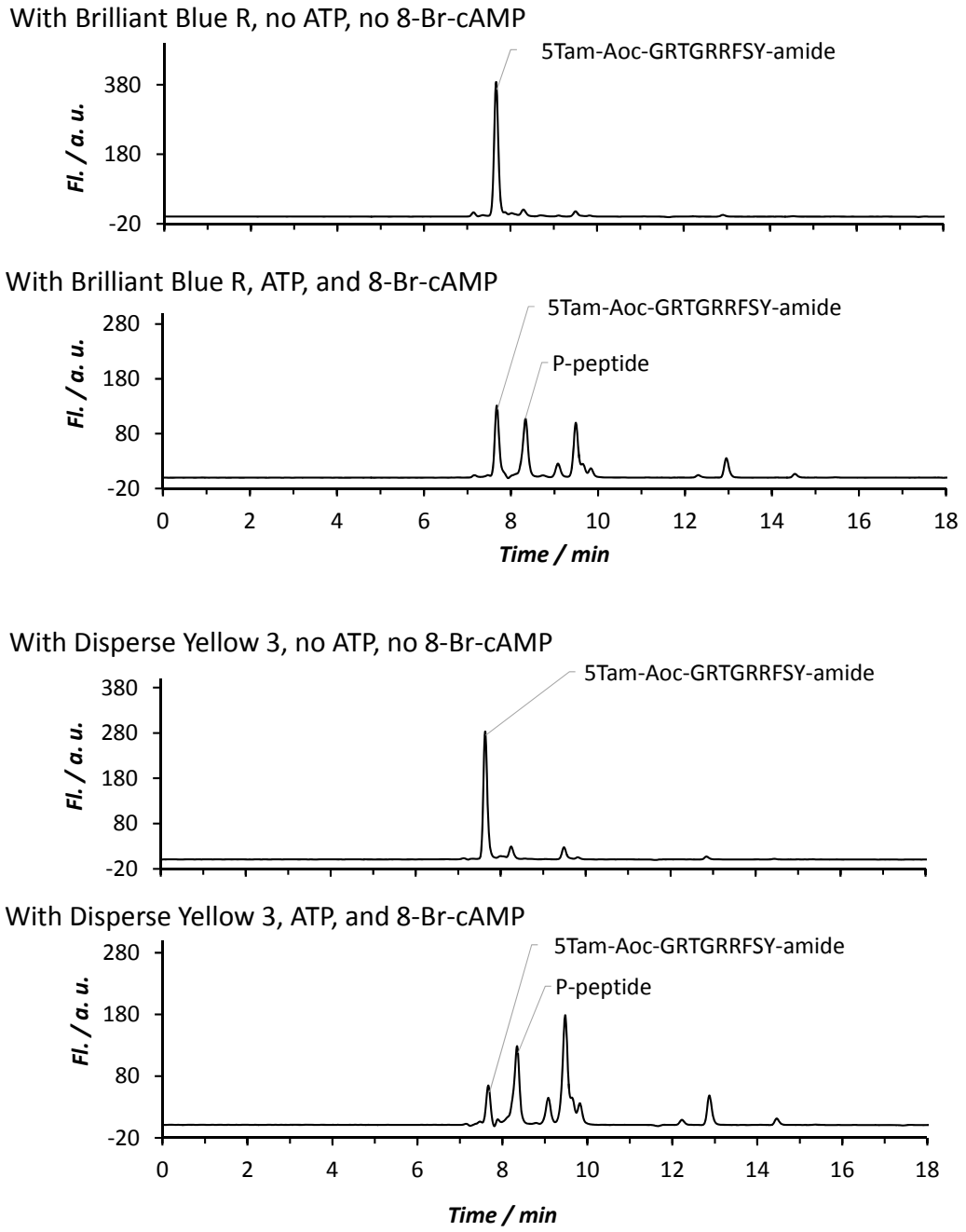

Figure 3.9: Phosphorylation-induced degradation of 5Tam-Aoc-GRTGRRFSY-amide in the presence of quencher in erythrocyte lysate. The peptide and quencher were incubated with erythrocyte lysate with and without the activation of PK. After 90 min of incubation, assay samples were analyzed by LC-MS. Fl = Fluorescence. λ_{ex} - λ_{em} = 550 nm - 590 nm.

Conclusion

We have demonstrated a strategy for creating enhanced fluorescent kinase sensors based on phosphorylation and degradation-induced fluorescence dequenching. Four developed sensors have been demonstrated to be capable of monitoring PKA activity in erythrocyte lysate. Additionally, we have shown a strategy to stabilize a peptide sensor in cell lysate without the necessity of adding protease inhibitors.

Materials and Method

General reagents and solvents were purchased from Fisher or Sigma-Aldrich. 8-bromoadenosine-3',5'-cyclic monophosphate (8-Br-cAMP), ATP, H89, and phosphatase inhibitor cocktail were purchased from Sigma-Aldrich. PKA was obtained from Promega.

Peptide Synthesis and Purification

Peptide synthesis and purification was conducted as described in Chapter 2 (Materials and Method).

LC-MS Analysis

All LC-MS analyses were performed on an Agilent liquid chromatography instrument which is coupled to a fluorescence and a mass detector. An Agilent C18 Eclipse 4.5 x 150 mm column was used for the separation. Peptide degradation was quantified by the area under the curve of the fluorescence traces.

Protection Peptide 5Tam-Aoc-GRTGRRFYS-amide from Trypsinolysis by Evans Blue

Tris buffer [150 µL total, Tris-HCl (25 mM, pH 7.5)] containing peptide 5Tam-Aoc-GRTGRRSFY-amide (2.5 or 30 µM) and Evans blue (5 or 20 µM) was preincubated at 37 ^{o}C for 5 min before the addition of trypsin (final 5 nM). At various time points, reaction aliquots were quenched with HCl (10 M) and analyzed by LC-MS.

Trypsinolysis of 5Tam-Aoc-GRTGRRFSY-amide and Its Phosphorylated Counterpart in the Presence of Evans Blue

A quartz cuvette containing a buffer [200 µL of Tris.HCl (25 mM, pH 7.5)], $MgCl_2$ (1 mM), ATP (1 mM), and peptide 5Tam-Aoc-GRTGRRFSY-amide (2.5 µM) was added PKA (10 nM) and incubated at 30 ^{o}C. After a 45 min incubation when all the peptide was phosphorylated, Evans Blue (5 µM) was added to the cuvette. The mixture was then equilibrated for 10 min followed by the addition of trypsin (5 nM). A parallel cuvette,

which contained a buffer [200 µL of Tris.HCl (25 mM, pH 7.5)], $MgCl_2$ (1 mM), ATP (1 mM), and peptide 5Tam-Aoc-GRTGRRFSY-amide (2.5 µM) was incubated at 30 ^oC for 45 min without the addition of PKA. Evans Blue (5 µM) was then added to the cuvette followed by a 10 min equilibrium and a trypsin addition (5 nM). The fluorescence after the trypsin addition was monitored in a spectrofluorometer.

Degradation Screening with Erythrocyte Lysate (Primary Screening)

Erythrocyte Lysate Preparation. Erythrocytes were washed three times with Gibco® PBS 1X buffer. Packed erythrocytes (625 µL) was then added to H_2O [3875 µL containing 198 µL phosphatase inhibitor cocktail 100X (product P0044 Sigma-Aldrich)]. The mixture was sonicated on ice in a water bath sonicator (5 times, 10 - 20 sec each) or by anultrasonic sonicator probe (3 times, 3-5 sec each). Gibco® PBS 10X (500 µL) was then added to the sonicated lysate to yield erythrocyte lysate (12% in PBS 1X buffer).

Screening. PBS 1X buffer (150 µL), 5Tam-Aoc-GRTGRRFSY-amide (2.5 µM), $MgCl_2$ (1 mM), ATP (1 mM), and PKA (10 nM) were added to 48 wells of a clear-bottom, black, 96-well plate were added. PBS 1X buffer (150 µL), 5Tam-Aoc-GRTGRRFSY-amide (2.5 µM), no $MgCl_2$, no ATP, and kinase dilution buffer were added to the other 48 wells. The plate was incubated at 30 ^oC for over 30 min then dyes (25 µM) in the 48-dye library were added to each well. Following a 15 min equilibration, the erythrocyte lysate (40 µL) was added to each well and the fluorescence monitored (λ_{ex} - λ_{em}: 555 nm - 586 nm). Fluorescence increase rates were compared between wells containing phosphorylated peptide and unphosphorylated peptide of the same dye. Thirteen promising peptide-dye pairs which showed minimal fluorescence increase in the unphosphorylated sample and accelerated fluorescence increase in phosphorylated sample were further screened at 37.5 µM dye. Evans Blue was further screened at 9.375 µM.

Screening the phosphorylation in erythrocyte lysate (Secondary Screening)

Among the forty eight dyes in the screened library, eight were selected for further phosphorylation screening. An additional dye, Chrysophenine, was also added to the list because of its structural similarity to the dye Brilliant Yellow. PBS 1X buffer (150 µL), 5Tam-Aoc-GRTGRRFSY-amide (2.5 µM), $MgCl_2$ (1 mM), ATP (100 µM), and 8-Br-cAMP (100 µM) each were added to a 96-well plate. Two sets of control wells # 1: PBS 1X buffer (150 µL), 5Tam-Aoc-GRTGRRFSY-amide (2.5 µM), $MgCl_2$ (1 mM), no ATP, and no 8-Br-cAMP; # 2: PBS 1X buffer (150 µL), 5Tam-Aoc-GRTGRRFSY-amide (2.5 µM), $MgCl_2$ (1 mM), ATP (100 µM), 8-Br-cAMP (100 µM), and H89 (10 µM)] were prepared in parallel. To each well was then added the selected dye (37.5 µM for all dyes, additional screening concentration at 18.75 µM for Acid Green 27 and Chrysophenine). The plate was then incubated at 30 ^oC for 30 min followed by the addition of erythrocyte lysate (40 µL, 12% lysate). Fluorescence increase rates were compared between the assay wells and the two control wells.

Confirmation of Peptide Stabilization by Quencher in Erythrocyte Lysate by LC-MS

Five Eppendorf vials containing PBS 1X buffer (450 µL), the peptide 5Tam-Aoc-GRTGRRFSY-amide (2.5 µM) were added quenchers or water as a control (18.75 µM for Acid Green 27 and 37.5 µM for Disperse Yellow 3, Brilliant Blue R, Acid Blue 129). The vials were then preincubated at 30 ^oC for 5 - 10 min followed by the addition of erythrocyte lysate (120 µL, 12% lysate) and further incubation at 30 ^oC. At different time points, reaction aliquots (100 µL) were quenched with HCl (10 M, 10 µL), then dilluted by MeOH (100 µL) and filtered through 3K molecular-weight-cut-off centrifugal filters (Amiconultra-0.5 mL Centrifugal Filters, 14,000 g, 30 min). After the first round of centrifugation, the filters were washed with another solution of MeOH-H_2O (200 µL, 50-50 by volume, 14,000

g. 30 min). Filtrates were collected and dried under vacuum. The residue were then dissolved in DMSO (100 µL), diluted with H_2O (100 µL), and analyzed by LC-MS.

Confirmation the Phosphorylation-Induced Degradation of the Peptide in the Presence of Quencher by LC-MS

PBS 1X buffer (150 µL) containing the peptide 5Tam-Aoc-GRTGRRFSY-amide (2.5 µM), $MgCl_2$ (1 mM), ATP (100 µM), and 8-Br-cAMP (100 µM), was added to 4 wells of a 96-well plate. Two other sets of wells were used for control samples # 1: PBS 1X buffer (150 µL), 5Tam-Aoc-GRTGRRFSY-amide (2.5 µM), $MgCl_2$ (1 mM), no ATP, and no 8-Br-cAMP; # 2: PBS 1X buffer (150 µL), the peptide 5Tam-Aoc-GRTGRRFSY-amide (2.5 µM), $MgCl_2$ (1 mM), ATP (100 µM), 8-Br-cAMP (100 µM), and H89 (10 µM)]. Quenchers were then added to each well (18.75 µM for Acid Green 27 and 37.5 µM for Disperse Yellow 3, Brilliant Blue R, and Acid Blue 129) and the plate was preincubated at 30 ^oC for 10 - 15 min, followed by the addition of erythrocyte lysate (40 µL, 12% lysate) and fluorescence monitoring. At 90 min after the addition of the lysate, reaction mixtures were quenched with HCl (20 µL, 10 M), diluted with MeOH (200 µL) and filtered through 3K molecular-weight-cut-off centrifugal filters (Amiconultra-0.5 mL Centrifugal Filters, 14,000 g, 30 min). After the first round of centrifugation, the filters were washed with another solution of MeOH-H_2O (200 µL, 50-50 by volume, 14,000 g. 30 min). Filtrates were collected and dried under vacuum. The residue were then dissolved in DMSO and analyzed by LC-MS.

CHAPTER 4: MEMBRANE SEQUESTRATION AND THE DESIGN OF LIGHT-ACTIVATABLE BIOAGENTS

Light-controllable agents have been widely used in drug delivery and chemical biology as they provide a unique means to orthogonally manipulate the biological systems with a high degree of spatial and temporal resolution. The principles of designing and constructing these species are well-defined. Prior to light exposure, the agent is biologically/biochemically/chemically inert. Upon light-activation, the active agent is rapidly produced and drives the desired process with the high degree of spatiotemporal control. One strategy for constructing such light-controllable reagents involves using photolabile groups. In this case, a key functional group (e.g. alcohol, amine, carboxylate) of the bioactive agents is covalently modified with a photocleavable moiety (e.g. nitrobenzyl, phenacyl, coumarin). The modification renders the bioagent inactive until photolysis removes the photolabile group and activates the bioagent. However, in a number of instances, a key functional group is not well defined or the modification of only a single functional group is not sufficient to eliminate biological activity. Modification of a phosphorylable hydroxyl group in kinase peptide sensors, for example, is sufficient to block its phosphorylation susceptibility but insufficient to protect the peptide from being processed by other enzymes (e.g., proteases). Upon entering a biological environment, the sensor might be degraded before any light-activation event. With the aim of controlling the initiation of phosphorylation and protecting peptide sensors from degradation inside living cells, we have developed a strategy to create light-activatable bioagents based on the compartmentalized nature of cells and organelles. The light-

activatable bioagents can be constructed from active agents of which no functional group is absolutely essential. Additionally, activation of those bioagents can be attained by a single photolytic event.

Hypothesis

Biological membranes are composed of a lipid bilayer decorated by proteins. Cells commonly employ hydrophobic moieties, such as fatty acids, terpenes, cholesterol, and peptides to direct proteins to membranes. We hypothesize that lipidated bioactive species, upon anchoring to the membrane will be embedded within the protein layer, and thus hidden from enzymatic species might be prevented from acting on or being acted upon by their intracellular targets. Placing a photolabile group between the membrane targeting moiety and the bioactive agent provides a way to control the release of the bioactive species from the membrane in a light-dependent fashion (Figure 4.1).

Results and Discussion

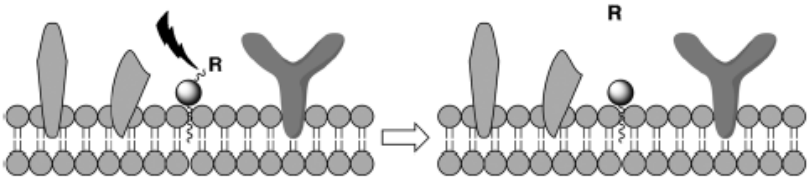

Figure 4.1: General strategy for lipid pool-anchored light-activatable bioagents. The active species (R), when appended to a lipid, is embedded within the densely populated protein sheath and thus unavailable for interaction with its biological target. Photolysis releases R from the membrane and thus renders the bioagent active.

Design of Photolabile Lipid Anchor

The membrane anchoring linker (**C18-bn-COOH**) was synthesized with a lipophilic C18 alkyl moiety which serves as membrane directing group and a carboxylate functionality to which the bioactive active species can be appended (Figure 4.2). The

nitrobenzyl moiety is inserted in between the lipophilic and carboxylate moieties to facilitate the release of appended bioactive species from the membrane upon photolysis.

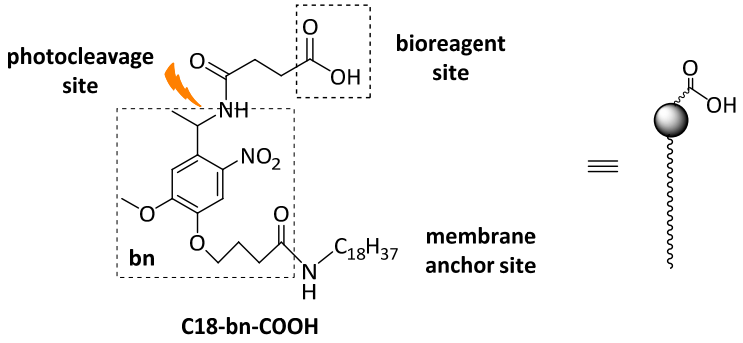

Figure 4.2: Structure of the photolabile lipid linker C18-bn-COOH. bn denotes the photolabile group where the cleavage site is on the n-site and the nitroso by-product goes with the moiety on the b-site.

Study of a Lipidated Fluorophore

For our initial studies, a fluorophore was appended to the **C18-bn-COOH** and membrane association as well as light-triggered membrane-release was investigated. The 5Tam fluorophore was appended to the side chain of a lysine residue. The fluorophore-labeled lysine was then appended to the carboxylate moiety of the membrane anchoring group to produce **C18-bn-K(5Tam)** (Figure 4.3). LC-MS data confirmed that photolysis of **C18-bn-K(5Tam)** produces the corresponding lipid-free (5-Tam)-labeled lysine (Figure 4.4).

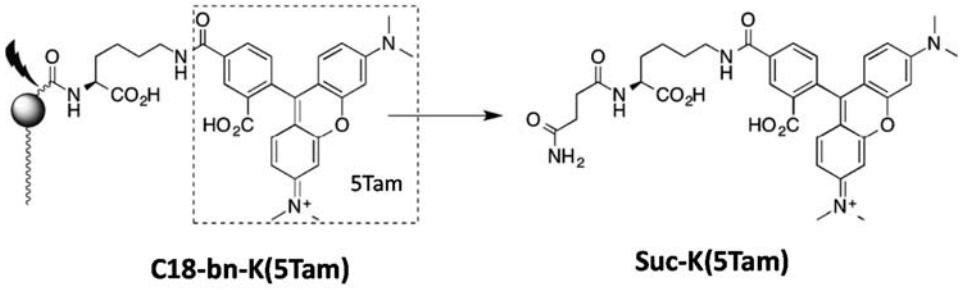

Figure 4.3: Structure of the photolabile lipidated fluorophore C18-bn-K(5Tam) and its photolyzed product Suc-K(5Tam).

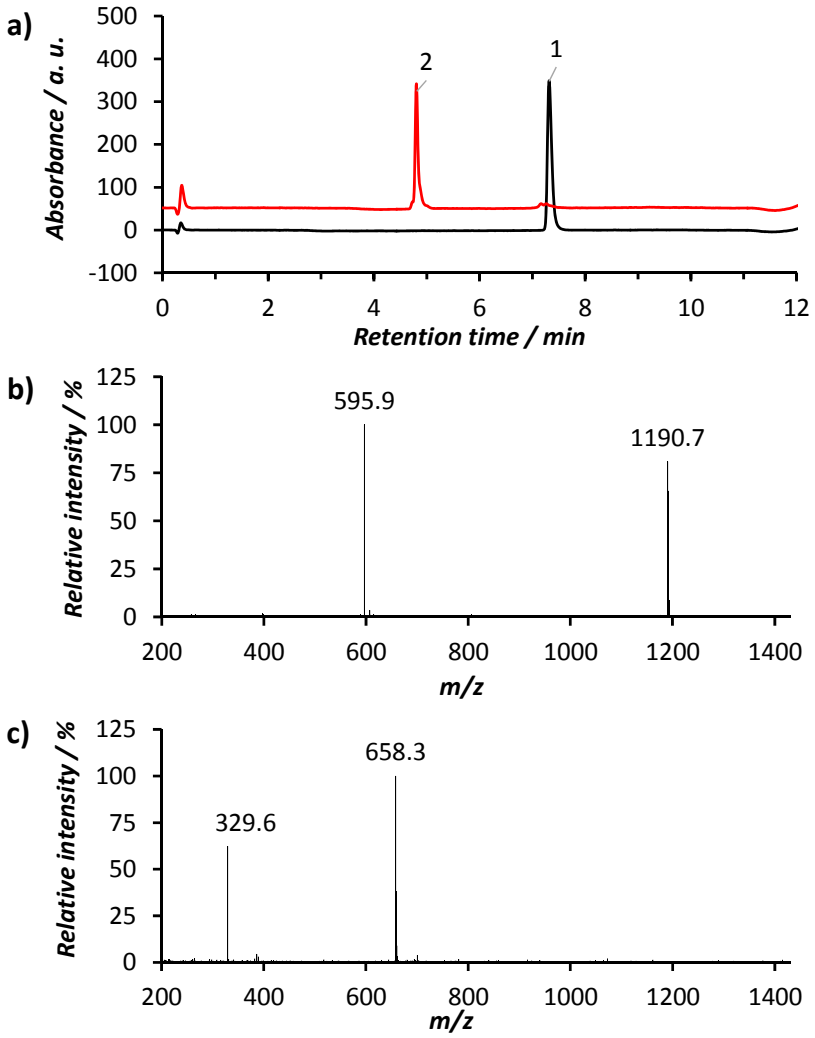

Figure 4.4: (a) LC-MS trace of **C18-bn-K(5Tam)** before (black) and after (red) photolysis. ESI+ MS data of peak 1 (b) and peak 2 (c). 90 µL solution containing PBS 1X (45 µL), MeOH (45 µL), DTT (5 mM), and **C18-bn-K(5Tam)** (4 µM) was photolyzed at 360 nm for 2 min. The sample was run on the C4 column after removal of MeOH by vacuum. Pure **C18-bn-K(5Tam)** was run as a reference. Absorbance was monitored at 550 nm. Photolyzed product **Suc-K(5Tam)** (peak 2): $C_{35}H_{40}N_5O_6^+$, calculated $(M)^+$ 658.3, found (ESI+, m/z) 658.3 $(M)^+$, 329.6 $(M + H)^{2+}$.

Octanol/water partition experiments revealed that **C18-bn-K(5Tam)** exclusively resides in the octanol phase prior to photolysis and migrates to the aqueous phase after photolysis (Figure 4.5a). Studies with biological membrane models showed that **C18-bn-K(5Tam)** is completely associated with both mitochondria (Figure 4.5b, 4.6) and erythrocyte ghosts (Figure 4.5c). Photolysis subsequently triggers the release of the

peptide from the organelles/cells into the aqueous solution (Figure 4.5b, c, ii). Given the lipophilic characteristics of **C18-bn-K(5Tam)**, it was surprising that **C18-bn-K(5Tam)** stays exclusively on the outer leaflet of erythrocytes even after hours of incubation at 37 ^{o}C. This suggests that **C18-bn-K(5Tam)**, upon binding to the outer leaflet of the bilayer membrane, was unable to flip to the other side due to the energy barrier associated with the transfer of positively charged 5Tam moiety.

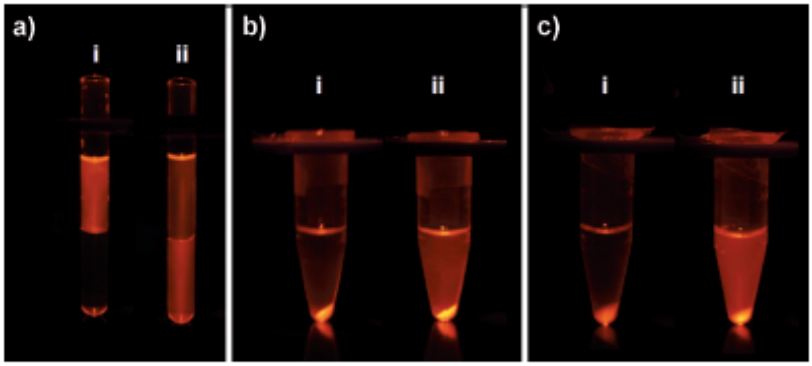

Figure 4.5: Light-dependent distribution studies with C18-bn-K(5Tam). a) Distribution of C18-bn-K(5Tam) in octanol (top) and water (bottom) prior to (i) and after (ii) photolysis. b) Distribution of C18-bn-K(5Tam) in mitochondria (pellet) and buffer prior to (i) and after (ii) photolysis. c) Distribution of C18-bn-K(5Tam) in erythrocytes (pellet) and buffer prior to (i) and after (ii) photolysis.

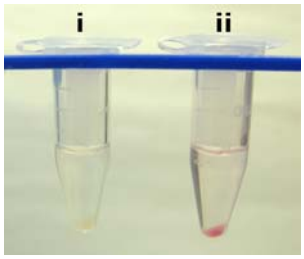

Figure 4.6: Mitochondria stained with C18-bn-K(5Tam) prior to (i) and after (ii) loading of C18-bn-K(5Tam). Image acquired with ambient light.

Using 2-hydroxypropyl-β-cyclodextrin and buffer tonicity manipulation, we were able to load **C18-bn-K(5Tam)** onto the inner leaflet of erythrocytes. Briefly, **C18-bn-K(5Tam)** was dissolved in a solution of 2-hydroxypropyl-β-cyclodextrin (100 mg/mL)

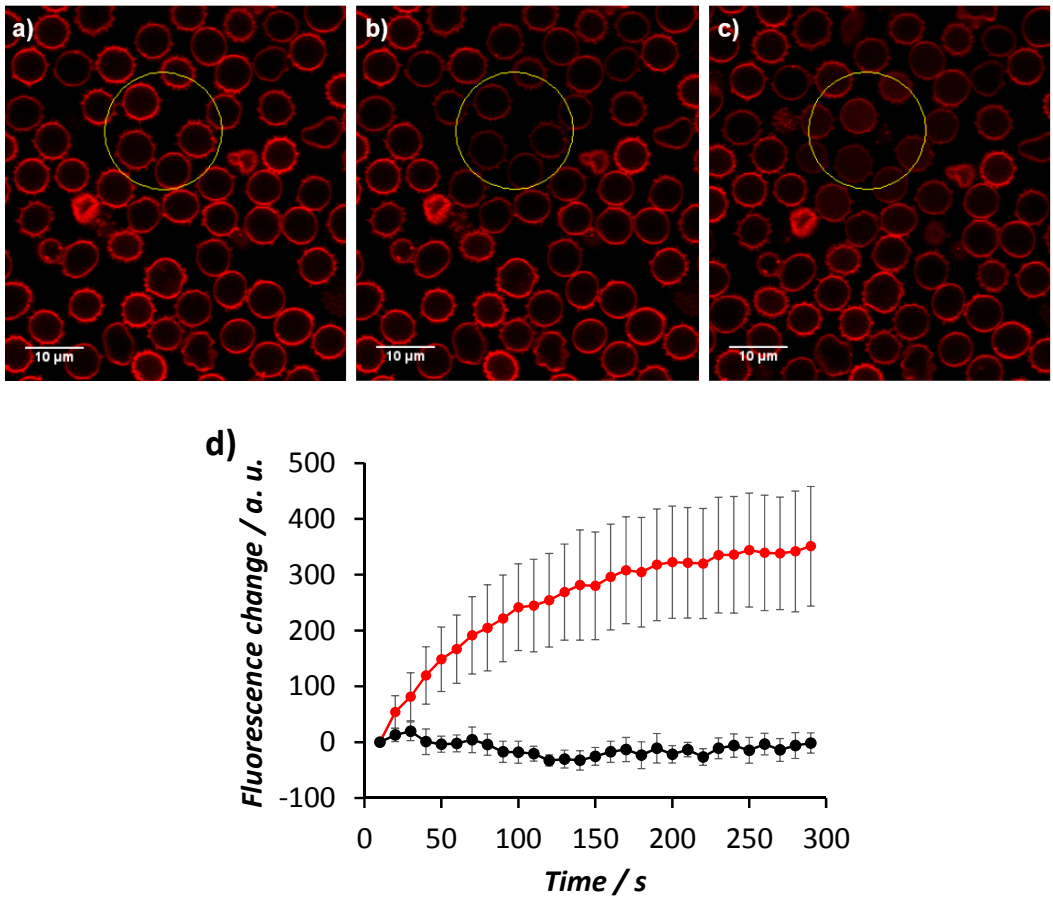

Figure 4.7: Confocal microscopy of erythrocyte ghosts loaded C18-bn-K(5Tam) with and without photolysis. (a) Before photolysis, (b) immediately after photolysis, and (c) 8.5 min after photolysis. (d) Changes of average fluorescence inside erythrocytes loaded with C18-bn-K(5Tam) with (red) and without photolysis (black). n = 8 for photolyzed cells, n = 7 for non-photolyzed cells. Photolysis was performed with 100 mW, 355 nm laser at the power level of 1 mW, tornado mode, dwell time of 10 µs/pixel, and 5 frames. Images were acquired by excitation at 559 nm and data collected using spectral PMTs set for the 5-Tam fluorophore.

followed by the addition of washed erythrocytes. Cold deionized water was added to the mixture to reduce the tonicity of the solution and open the erythrocytes' membranes. After adequate equilibrium, the tonicity of the solution was restored to that of PBS 1X to seal the erythrocytes. Confocal microscopy confirmed that the lipidated fluorophore **C18-bn-K(5Tam)** is retained by the erythrocyte membrane prior to photolysis. By irradiating with a UV laser, we demonstrated the ability to selectively photolyze and release the

fluorescent moiety into the interior of erythrocytes (Figure 4.7). However, we noticed that it takes more than 5 min after photolysis for the fluorescence to completely migrate to erythrocyte interior. Since the photolysis of 2-nitrobenzyl group involves acid/base catalyzed steps,[86] the delay in fluorescence release might indicate that the photolabile group is positioned away from hydrophilic environment.

Study of Lipidated Protease Substrate

We subsequently investigated if bioactive species can be rendered biologically/biochemically inert by membrane sequestration and then activated upon photolysis-triggered membrane releasing. The FRET-based peptide **Ac-K(Tam)--K(Fam)** was synthesized, which serves as a generic protease substrate. The corresponding lipidated derivative **C18-bn-K(Tam)--K(Fam)**, was prepared by acetylating the N-terminal of the peptide NH_2-K(5Tam)RRRLAALAAK(5Fam)-amide with the lipidated photolabile linker **C18-bn-COOH** (Figure 4.8).

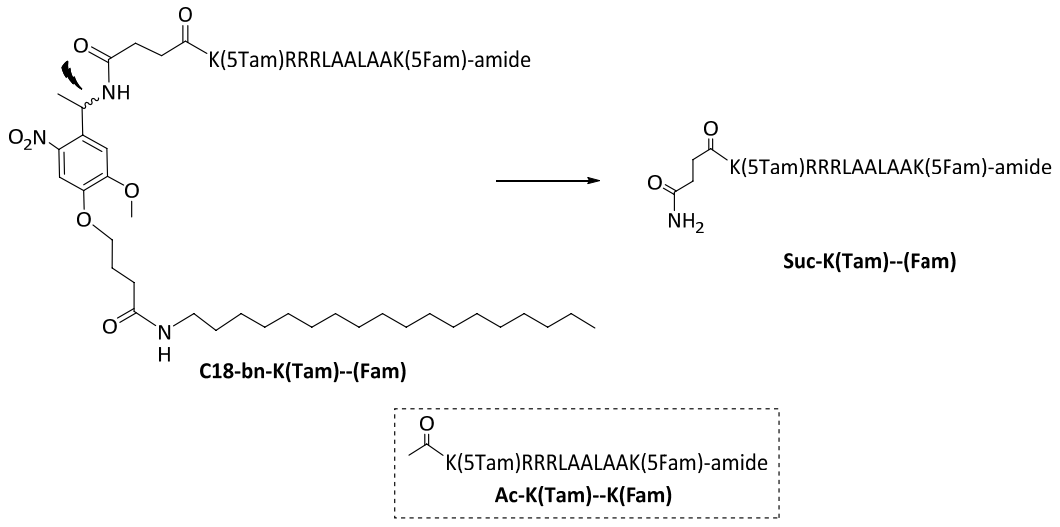

Figure 4.8: Structure of the photolabile lipidated protease sensor C18-bn-K(Tam)--K(Fam), the corresponding light-activated membrane-released derivative Suc-K(Tam)--K(Fam), and a control non-lipidated sensor Ac-K(Tam)--K(Fam).

The fluorescence of 5Fam fluorophore is completely quenched by 5Tam, provides the means to monitor substrate proteolysis at the 5Fam emission wavelength (492 nm - 525 nm). Moreover, the partially quenched 5Tam fluorescence signals the location of the peptide (555 nm - 587 nm) both prior to and following photolysis (Figure 4.9).

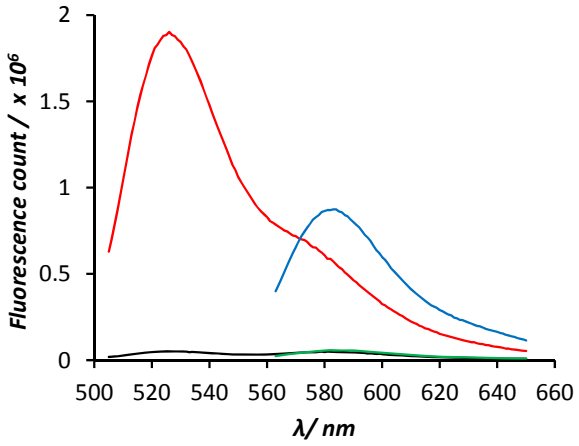

Figure 4.9: Fluorescence response from trypsin digestion of Ac-K(Tam)--K(Fam). Tris-HCl buffer (200 µL, 25 mM pH 7.5) containing $MgSO_4$ (4 mM) and Ac-K(Tam)--K(Fam) (1 µM) was incubated at 37 °C for 5 min followed by addition of trypsin (20 nM) and fluorescence was scanned over time. Emission scan with 495 nm excitation prior to (black) and 20 min after the addition of trypsin (red). Emission scan with 553 nm excitation prior to (green) and 20 min after the addition of trypsin (blue).

LC-MS analysis demonstrated the formation of the lipid-free peptide from **C18-bn-K(Tam)--K(Fam)** upon photolysis (Figure 4.10). An octanol/water partition study of **C18-bn-K(Tam)—K(Fam)** showed that, prior to photolysis, the lipidated peptide resides in the octanol phase and is not susceptible to trypsinolysis even when trypsin is present in the aqueous phase. Upon photolysis, the lipid-free protease substrate peptide is released into the aqueous phase and processed by trypsin (Figure 4.11). Further investigation with mitochondria demonstrated that **C18-bn-K(Tam)--K(Fam)** is completely associated with the mitochondria and protected from trypsinolysis. Subsequent photolysis triggers the release of the substrate from the mitochondria and renders it susceptible to trypsin-

catalyzed proteolysis (Figure 4.12 - 4.14). Furthermore, binding of **C18-bn-K(Tam)--K(Fam)** to erythrocyte ghosts prevent it from being digested by trypsin. Photolysis releases the substrate from the membrane leading to a rapid proteolysis (Figure 4.15 - 4.18).

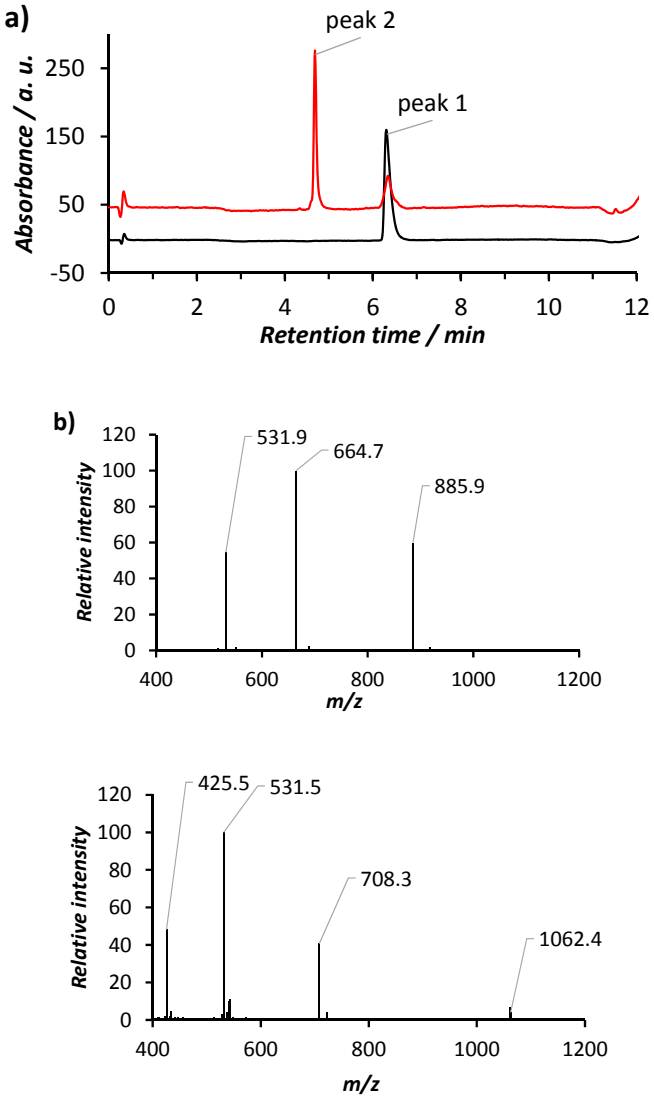

Figure 4.10: (a) LC-MS of **C18-bn-K(Tam)--K(Fam)** before (black) and after photolysis (red). ESI+ MS data of peak 1 (b) and peak 2 (c) in (a). PBS 1X (100 µL) containing **C18-bn-K(Tam)--K(Fam)** (4 µM), DTT (5 mM) was photolyzed at 360 nm for 2 min. Sample was run on the C4 column. Absorbance was monitored at 550 nm. Photolyzed product **Suc-K(5Tam)RRRLAALAAK(5Fam)-amide** (peak 2): $C_{104}H_{140}N_{25}O_{24}^{+}$, calculated $(M)^{+}$ 2123.0, found (ESI+, m/z) 1062.4 $(M + H)^{2+}$, 708.3 $(M + 2H)^{3+}$, 531.5 $(M + 3H)^{4+}$, 425.5 $(M + 4H)^{5+}$.

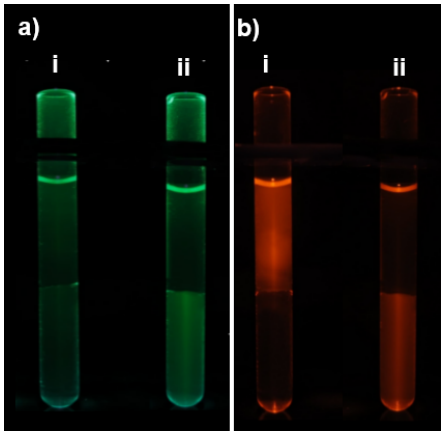

Figure 4.11: Trypsin cleavage of **C18-bn-K(Tam)--K(Fam)** distributed in octanol and water with and without photolysis as assessed by fluorescence. Samples were excited by 360 nm UV light from a Hg-Arc lamp source, images were acquired with X-Nite 525 filter (a) and X-Nite 590 filter (b). **C18-bn-K(Tam)--K(Fam)** (4 µM) without photolysis (i) and with photolysis (ii) after 2.5 h incubation with trypsin (20 nM) at room temperature. Top layer octanol and bottom layer PBS 1X.

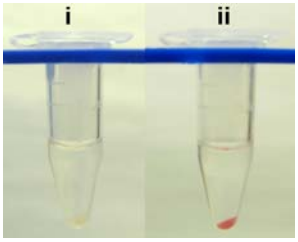

Figure 4.12: Mitochondria prior to (i) and after (ii) loaded with **C18-bn-K(Tam)--K(Fam)**. Images acquired with ambient light.

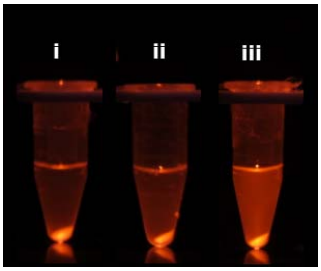

Figure 4.13: Trypsin cleavage of **C18-bn-K(Tam)--K(Fam)** loaded on mitochondria with and without photolysis as assessed by fluorescence. Samples were excited by 360 nm UV light from a Hg-Arc lamp source, images were acquired using the X-Nite 590 filter. **C18-bn-K(Tam)--K(Fam)** (4 µM) without photolysis and with trypsin (i); with photolysis and no trypsin (ii); with photolysis and with trypsin (iii) after 40 min incubation at 37 ^{o}C. Trypsin (10 nM) was used in with trypsin experiments.

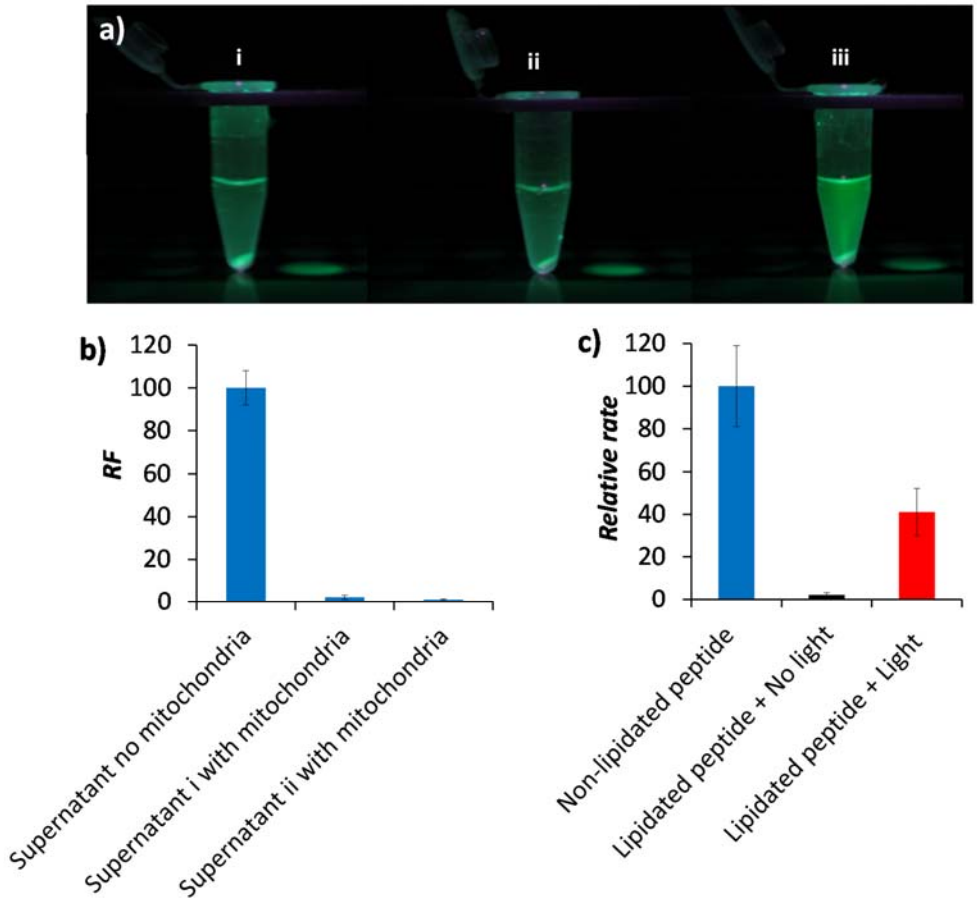

Figure 4.14: a) Trypsin cleavage of **C18-bn-K(Tam)--K(Fam)** loaded onto mitochondria in the absence and presence of illumination as assessed by fluorescence. Samples were illuminated with 360 nm UV light from a Hg-Arc lamp source, images were acquired with the X-Nite525 filter. i) In the dark with trypsin; ii) with photolysis and no trypsin; and iii) with photolysis and trypsin after 40 min incubation at 37 °C. b) Relative amount of **C18-bn-K(Tam)--K(Fam)** in the supernatant in the absence and presence of mitochondria (**supernatant i with mitochondria**), and after a mitochondria wash (**supernantant ii with mitochondria**). c) Relative rate of trypsinolysis of **C18-bn-K(Tam)--K(Fam)** in the presence of mitochondria with and without photolysis compared to that of **Ac-K(Tam)--K(Fam) (with mitochondria**) as determined by fluorescence increase 492 nm - 525 nm. RF = relative fluorescence.

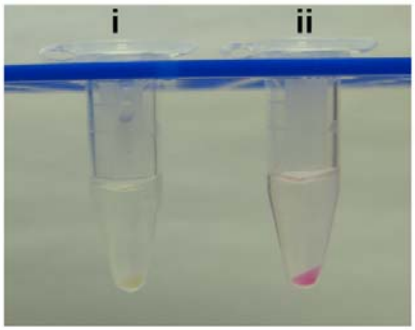

Figure 4.15: Erythrocyte ghosts prior to (i) and after (ii) loaded with **C18-bn-K(Tam)--K(Fam)**. Image acquired with ambient light.

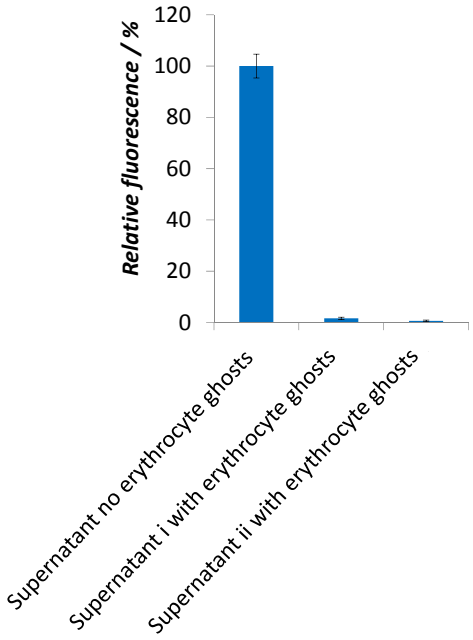

Figure 4.16: Distribution of **C18-bn-K(Tam)--K(Fam)** in aqueous phase in the presence of erythrocyte ghosts. Cold ghost buffer (200 µL) containing **C18-bn-K(Tam)--K(Fam)** (4 µM) and 20% hematocrit was incubated on ice for 30 min followed by centrifugation (5000 g for 5 min) to give **supernatant i**. The pellet resuspended in cold ghost buffer (200 µL) was centrifuged to **give supernatant ii**. Supernatants were diluted in MeOH (1:1 ratio by v:v) and the fluorescence (λ_{ex} - λ_{em} = 555 nm - 587 nm) of the solutions were compared to corresponding fluorescence of **C18-bn-K(Tam)--K(Fam)** (4 µM) by the identical dilution.

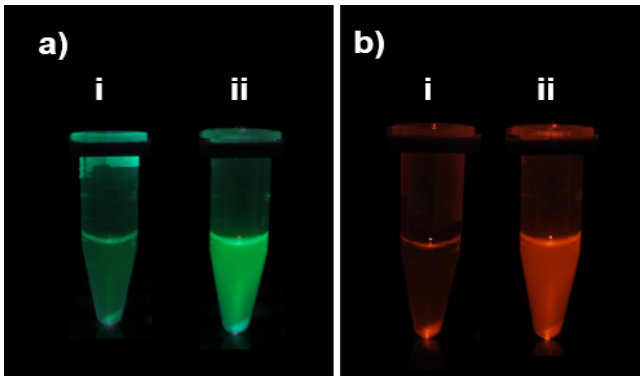

Figure 4.17: Trypsin cleavage of **C18-bn-K(Tam)--K(Fam)** loaded on erythrocyte ghosts with and without photolysis as assessed by fluorescence. Samples were excited by 360 nm UV light from a Hg-Arc lamp source, images were acquired with the X-Nite 525 filter (a) and X-Nite 590 filter (b). **C18-bn-K(Tam)--K(Fam)** (4 µM) without photolysis and with trypsin (i); with photolysis and with trypsin (ii) after 45 min incubation at 37 °C. Trypsin (10 nM) was used in the trypsin experiments.

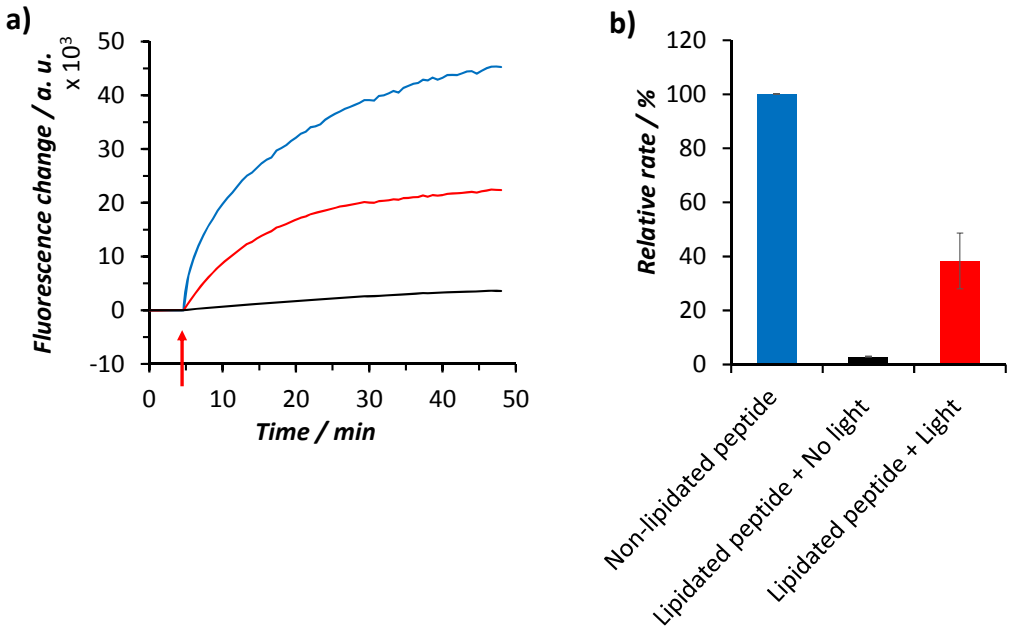

Figure 4.18: **C18-bn-K(Tam)--K(Fam)** (4 µM) with erythrocyte ghosts (20% hematocrit) and trypsin (10 nM) in the presence (red) and absence (black) of photolysis (3 min). **Ac-K(Tam)--K(Fam)** (4 µM) with erythrocyte ghosts and trypsin (10 nM) was performed in parallel as reference (blue). Data from a single experiment (a) and average of three experiments (b). Trypsin addition indicated by the arrow.

Finally, we used the light-activatable sensor, **C18-bn-K(Tam)--K(Fam)**, to assess endogenous intracellular proteolytic activity of erythrocytes in a light-dependent fashion. The control non-lipidated sensor, **Ac-K(Tam)--K(Fam)**, is rapidly proteolyzed in erythrocyte lysates as demonstrated by LC-MS analysis (Figure 4.19). Various combinations of protease inhibitors were used to confirm the activity and inhibition of endogenous proteases acting on the peptide in erythrocyte lysate (Figure 4.20). Subsequently, the lipidated protease sensor, **C18-bn-K(Tam)--K(Fam)** was loaded into the inner leaflet of erythrocytes using 2-hydroxypropyl-β-cyclodextrin and buffer tonicity manipulation [see loading of C18-bn-K(5Tam) into erythrocyte]. Confocal images of the loaded erythrocytes revealed that the lipidated peptide is localized onto erythrocyte membrane as indicated by the 5Tam fluorescence (Figure 4.21b). Photolysis with a UV light separates the protease peptide substrate from the membrane anchoring moiety leading to the release of the unlipidated peptide into the erythrocyte interior (Figure 4.21e). By contrast, there is no observable presence of the sensor in the interior of unphotolyzed erythrocytes. Additionally, photoactivated cells showing a robust increase in 5Fam fluorescence indicates degradation of photolyzed protease sensor in the interior of erythrocytes (Figure 4.21a, c). The potent combination of protease inhibitors [(EDTA (10 mM), leupeptin (100 μM), and MG-132 (100 μM)] blocking the 5Fam fluorescence increase in the interior of erythrocytes further confirms the proteolytic activity inside erythrocytes (Figure 4.21c).

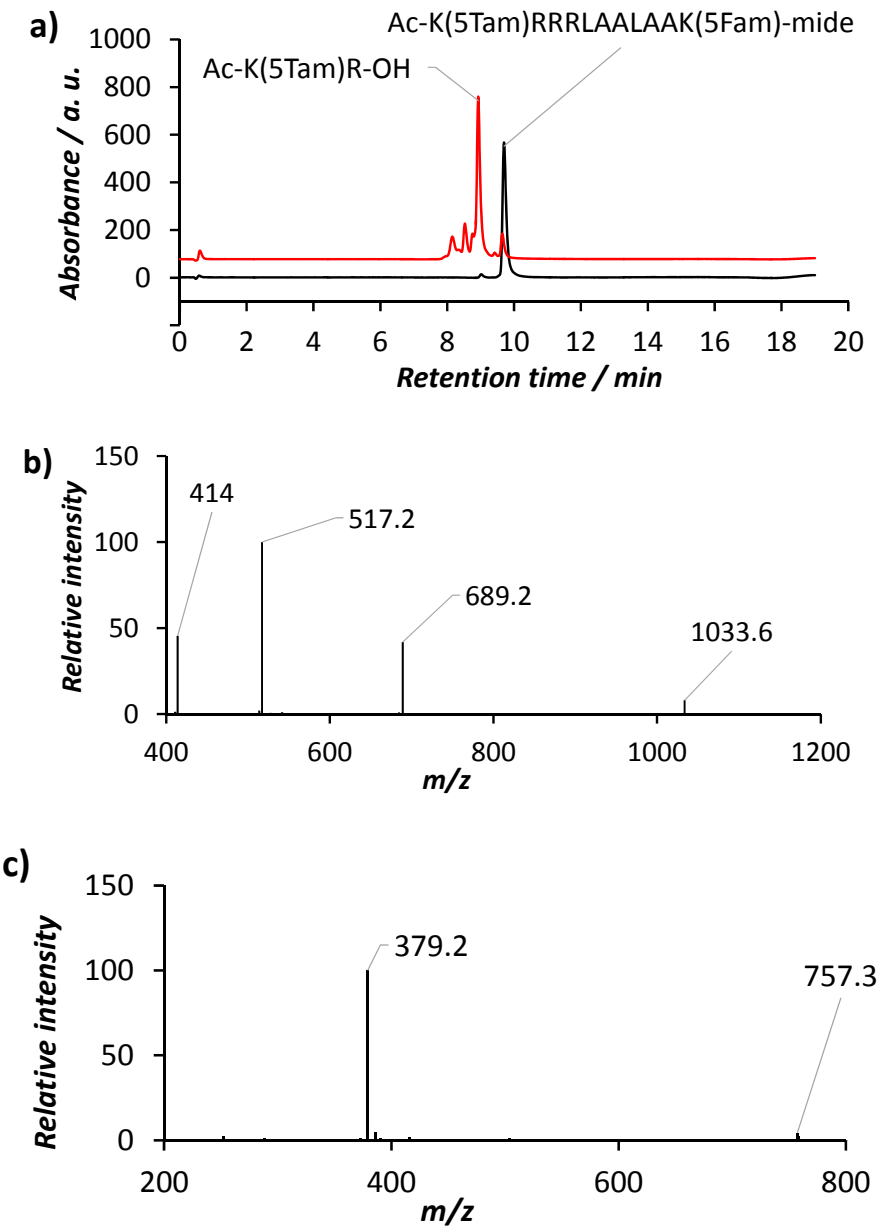

Figure 4.19: (a) LC-MS analysis of **Ac-K(Tam)--K(Fam)** before (black) and after (red) incubation with erythrocyte lysates. ESI+ MS data of (b) peak before and (c) peak after incubation. **Ac-K(Tam)--K(Fam)** (20 µM) was added to 37 °C-preincubated erythrocyte whole lysates (200 µL) and fluorescence (λex 495 nm, λem 525 nm) was monitored in the plate reader until the fluorescence plateaued. HCl (20 µL, 10 M) and MeOH (160 µL) were then added to the reaction mixture followed by centrifugation filtration (14,000 g for 30 min) using a 3K cutoff filter (Invitrogen). The collected solution was dried and analyzed by LC-MS on a C18 column. Absorbance was monitored at 550 nm. Major cleaved product was **Ac-K(5Tam)R-OH**: $C_{39}H_{49}N_8O_8^+$ exact mass calculated 757.4, found (ESI+, m/z) 757.3 $(M)^+$ and 379.2 $(M + H)^{2+}$.

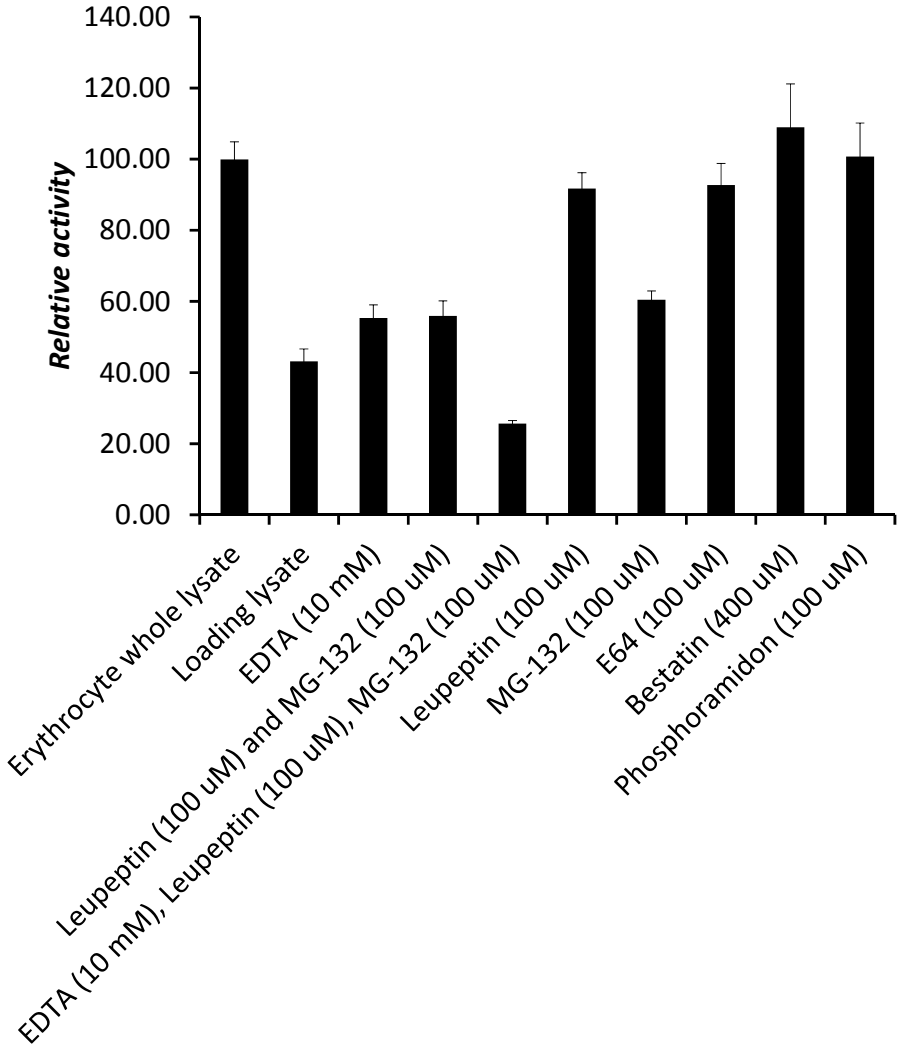

Figure 4.20: Inhibition of protease activities in erythrocyte lysate by different protease inhibitors. Erythrocyte whole lysates were prepared by sonication of PBS 1X-containing 10% hematocrit. "Loading lysates" were the supernatant containing-materials that leaked out of erythrocyte during the loading of **C18-bn-K(Tam)--K(Fam)** (4 µM). Protease activity was determined by the rate of cleavage of the fluorescent sensor **Ac-K(Tam)--K(Fam)** (1 µM) monitored at λ_{ex} - λ_{em} = 495 nm - 525 nm. Lysates with or without inhibitors were preincubated at 37 ^{o}C for 5 min before the addition of **Ac-K(Tam)--K(Fam)** to start the reaction.

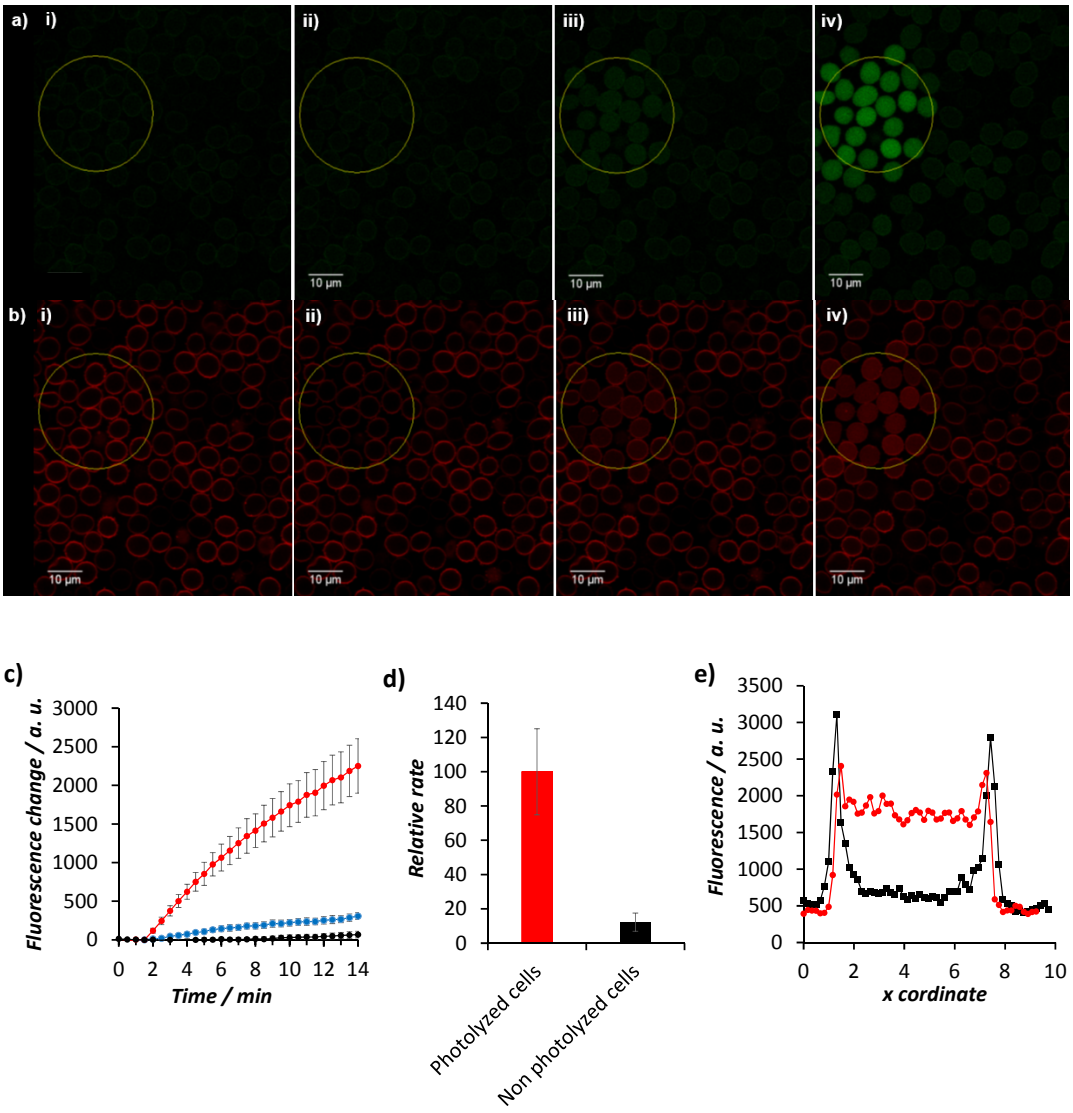

Figure 4.21: Confocal images of erythrocytes loaded with **C18-bn-K(Tam)--K(Fam)**. (i) before photolysis, (ii) immediate after photolysis, (iii) 1.5 min after photolysis, and (iv) 13 min after photolysis. Photolysis was performed with 100 mW, 355 nm laser at the power level of 1 mW, tornado mode, dwell time of 10 µs/pixel, and 5 frames. Images were acquired by excitation at (a) 448 nm (5Fam), (b) 559 nm (5Tam) and data collected using spectral PMTs set for the fluorophores. c) Average fluorescence (5Fam) inside photolyzed erythrocytes (red; n = 30), unphotolyzed erythrocytes (blue; n = 30), and photolyzed erythrocytes in the presence of a protease inhibitor cocktail (black; EDTA (10 mM), leupeptin (100 µM), and MG-132 (100 µM); n = 14). d) Relative fluorescence increase rate of photolyzed and unphotolyzed cells. e) Line scanning fluorescence profile in 5Tam wavelengths of an erythrocyte loaded with **C18-bn-K(Tam)--K(Fam)** before (black) and 13 min after photolysis (red).

Study of Cholesterol-Conjugated Coumarin-Based Protease Substrate

We also examined the light-dependent behavior of a lipidated coumarin-based trypsin sensor, **5Tam-K(Chol)-nb-R-AMC**. In this case, the lipid anchor is cholesterol and the hydrolysis is followed by the coumarin fluorescence (Figure 4.22). The 5Tam fluorophore was appended to signal the membrane binding of the lipidated substrate and help in analysis with LC-MS. Photolysis of **5Tam-K(Chol)-R-AMC** releases the lipid anchor from the coumarin trypsin substrate (Figure 4.23). In analogy to the lipidated protease substrate **C18-bn-K(Tam)--K(Fam)**, erythrocyte-bound **5Tam-K(Chol)-nb-R-AMC**, is not susceptible to trypsinolysis. Upon light-exposure of the **5Tam-K(Chol)-nb-R-AMC** loaded erythrocyte, the trypsin substrate is released from the membrane and rapidly proteolyzed by trypsin as indicated by the increase in fluorescence of at coumarin's wavelengths (λ_{ex} - λ_{em} = 354 nm - 442 nm*)* (Figure 4.24).

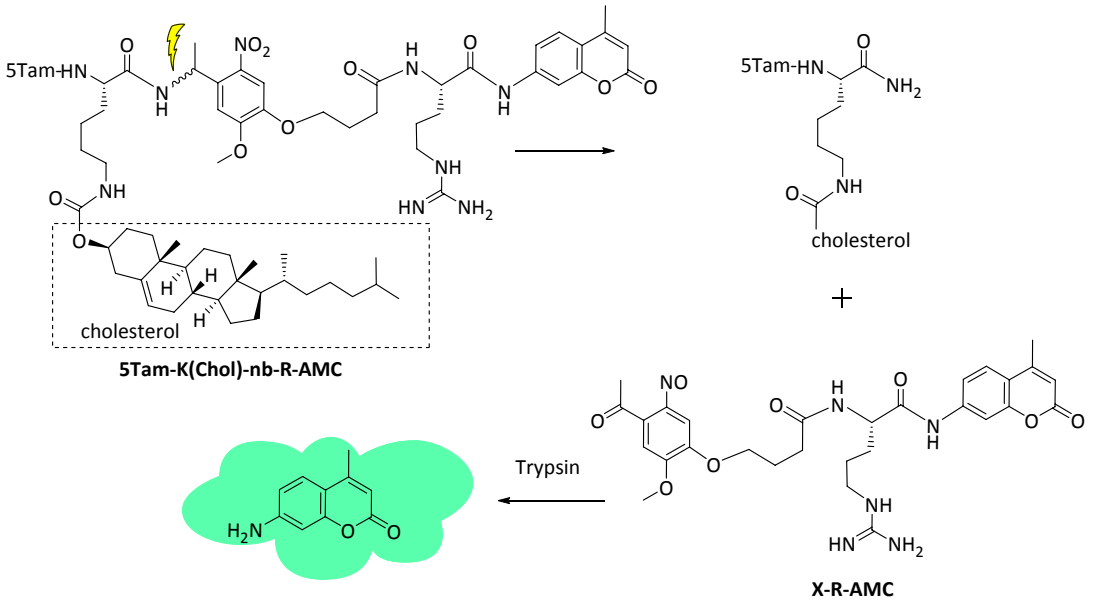

Figure 4.22: The inert trypsin sensor 5Tam-K(Chol)-nb-R-AMC is anchored to erythrocyte membranes using cholesterol. Photolysis releases the active sensor X-R-AMC that, upon trypsinolysis, release fluorescent coumarin derivative.

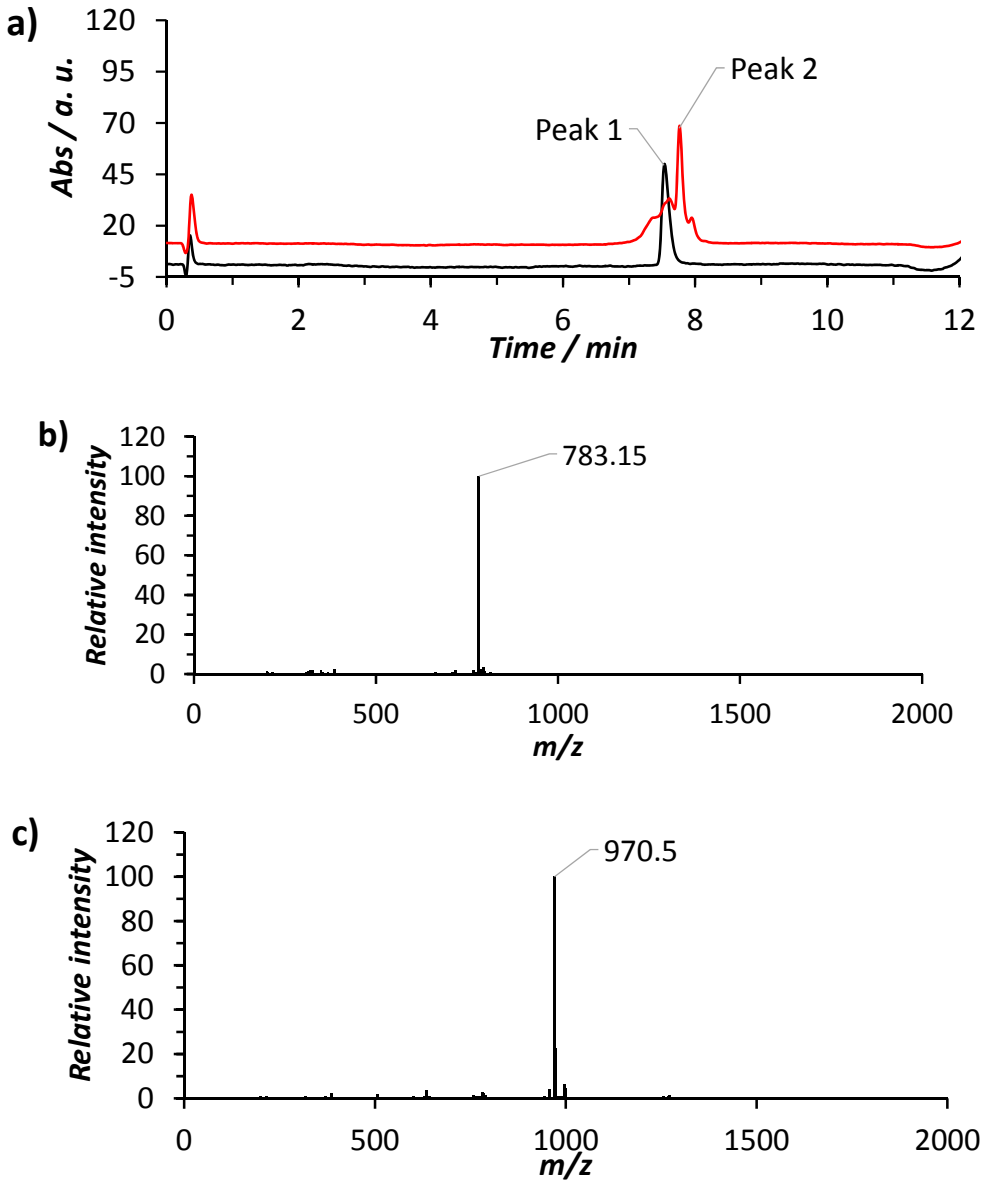

Figure 4.23: (a) LC-MS trace of **5Tam-K(Chol)-nb-R-AMC** before (black) and after (red photolysis. ESI+ MS data of pure **5Tam-K(Chol)-nb-R-AMC** (peak 1, b) and 5Tam-labelled photolyzed product (peak 2, c). PBS 1X (100 µL) containing DTT (5 mM) and **5Tam-K(Chol)-nb-R-AMC** (2.5 µM) was photolyzed at 360 nm for 2 min. The sample was then run on the C4 column. Pure **5Tam-K(Chol)-nb-R-AMC** was run as a reference. Absorbance was monitored at 550 nm. 5Tam-labelled photolyzed product (peak 2): $C_{59}H_{80}N_5O_7^+$, exact mass calculated $(M)^+$ 970.6, found (ESI+, m/z) 970.5 $(M)^+$.

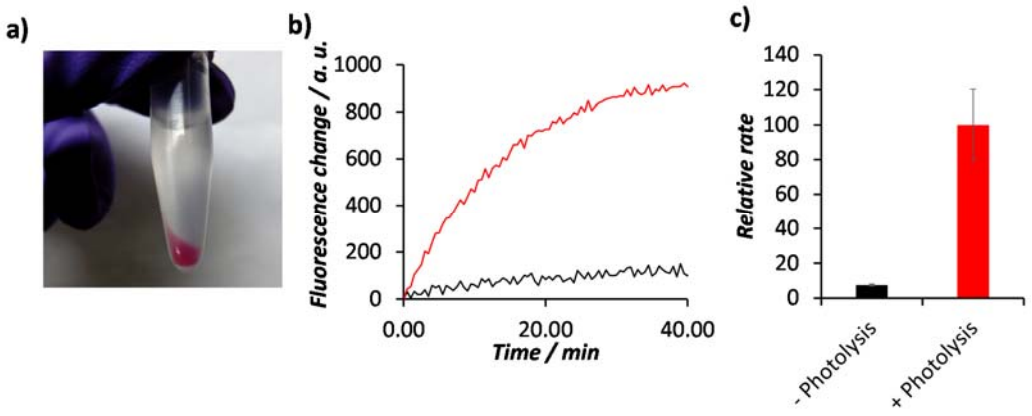

Figure 4.24: Study of 5Tam-K(Chol)-nb-R-AMC with trypsin and erythrocyte ghosts. (a) Erythrocyte ghosts loaded with 5Tam-K(Chol)-nb-R-AMC *(2.5 μM).* (b) Digestion of 5Tam-K(Chol)-nb-R-AMC *b*y trypsin as assessed by fluorescence in the presence of erythrocyte ghosts and no light (black); in the presence of erythrocyte ghosts and 3 min photolysis at 360 nm (red). (c) Relative digestion rate of 5Tam-K(Chol)-nb-R-AMC bound erythrocyte ghosts in the presence and absence of ligtht. PBS 0.1X (200 μL) containing 5Tam-K(Chol)-nb-R-AMC (2.5 μM) and DTT (5 mM) was added erythrocyte ghosts (20% hematocrit) followed by incubation at 37 ^{o}C for 20 min. The suspension was then kept in dark (- photolysis) or photolyzed (3 min, 360 nm) (+ photolysis) followed by addition of trypsin (200 nM). Fluorescence of the reaction mixture was monitored in the plate reader (λ_{ex} - λ_{em} = 354 - 442 nm, cut-off 435 nm) at 37 ^{o}C.

Study of Lipidated Kinase Substrate

In addition to protease substrates, we also investigated the susceptibility of a membrane-bound protein kinase substrate to phosphorylation. As described in Chapter 2, the peptide sequence KRRRLASLAA is efficiently phosphorylated on the serine residue by PKA. Since the N-terminal lysine residue is not important for substrate recognition,[81] we prepared a lipidated analogue of this sequence, **C12-bn-PKA** (Figure 4.25). In a manner similar to the lipidated protease substrates, more than 98% of the lipidated PKA substrate associates with mitochondria after 1 h on-ice incubation (Figure 4.26a). 2 min of 360 nm photolysis releases approximately 50% of the mitochondria-embedded peptide (Figure 4.26b). Furthermore, the relative PKA-catalyzed phosphorylation rates of **C12-bn-PKA** in

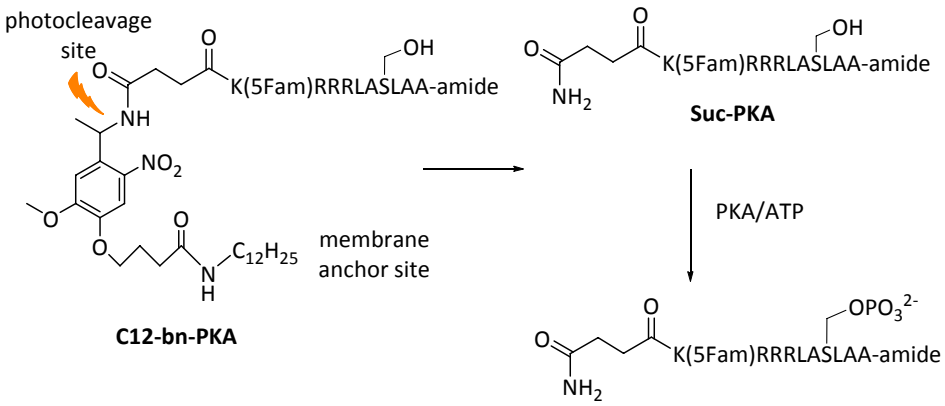

Figure 4.25: The structure of lipidated PKA sensor C12-bn-PKA and its photolyzed product, Suc-PKA. When anchoring to biological membranes, the lipidated PKA sensor is not susceptible to phosphorylation. Upon photolysis, the active sensor Suc-PKA is released and phosphorylated by PKA.

the absence of mitochondria, in the presence of mitochondria, and in the presence of mitochondria followed by photolysis were assessed by capillary electrophoresis and compared. When **C12-bn-PKA** is free in solution, it is efficiently phosphorylated by PKA. On the contrary, mitochondria-bound lipidated PKA substrate is not susceptible to PKA-catalyzed phosphorylation. The latter, upon photolysis, generates an active PKA sensor that undergoes PKA-dependent phosphorylation at a rate 50% of that displayed by **C12-bn-PKA** that is free in solution (Figure 4.26d, e).

Role of peptide charge, lipid, and biological membrane in binding and protection

We also investigated the role of peptide charge in membrane binding and the role of membrane itself in rendering bioagents from active to inactive upon its binding. Three additional lipidated molecules, **5Tam-EEK(Chol)-nb-R-AMC**, **5Tam-K(Stear)-nb-R-AMC**, and **5Tam-EEK(Stear)-nb-R-AMC**, which varies in lipid moiety and total molecular charge, were synthesized (Figure 2.27)). Interestingly, **5Tam-K(Chol)-nb-R-AMC** binds tightly to erythrocyte ghosts whereas **5Tam-EEK(Chol)-nb-R-AMC** favorably resides in aqueous solution (Figure 4.28a, b). In an analogous pattern, a stearoyl group is sufficient to anchor

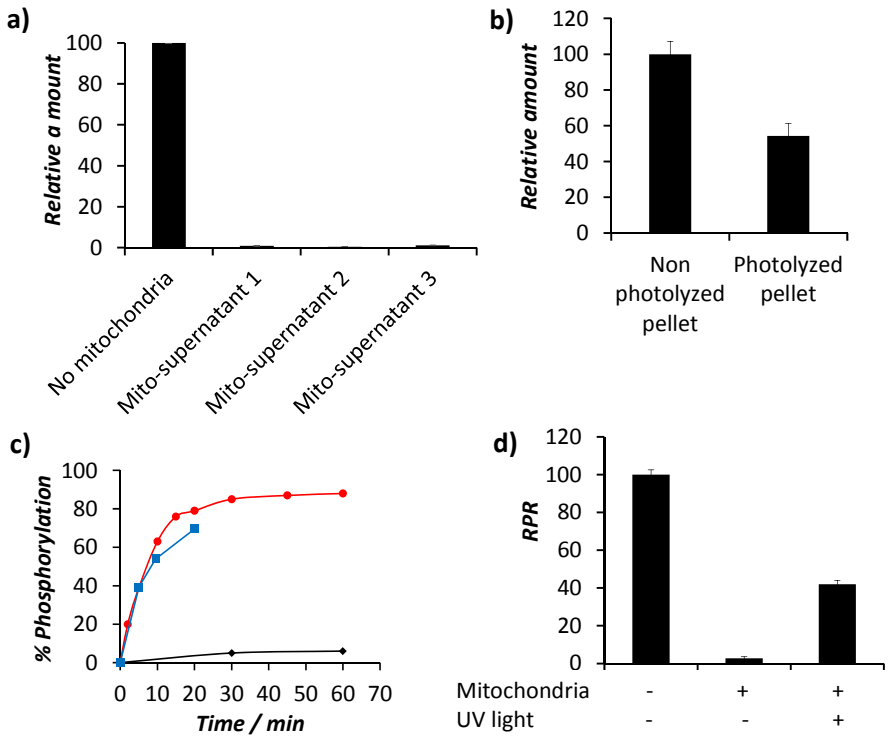

Figure 4.26: Study of lipidated PKA sensor with mitochondria and PKA. (a) Distribution of C12-bn-PKA in aqueous phase in the presence of mitochondria. (b) Relative amount of the lipidated PKA sensor remaining on mitochondria without and with photolysis as assessed by fluorescence. Mitochondria loaded with the lipidated PKA sensor was kept in the dark or exposed to 2 min of illumination (360 nm) followed by washings with mito buffer, pellet solublization in mito buffer and dilution buffer (1:1 by v:v) and fluorescence measurement (λ_{ex} - λ_{em} = 492 - 525 nm). (c) Phosphorylation of lipidated PKA sensor by PKA in the presence of mitochondria and no light (black); in the presence of mitochondria and UV light (red); and in the absence of both mitochondria and UV light (blue) as assessed by capillary electrophoresis. (d) Quantification of experiments in (b, c).

the **5Tam-K-bn-R-AMC** peptide to erythrocyte ghosts whereas this anchor is not enough to recruit the peptide analog to erythrocyte ghosts when two negatively charge glutamate residues is added to the peptide (Figure 4.28 c, d).

Additionally, liposomes are unable to render the lipidated kinase substrate resistant to phosphorylation (Figure 4.29). This data is consistent with the hypothesis that negatively charge protein layer, which covers the erythrocyte membrane, plays a role in binding and rendering the peptides inert toward the corresponding enzymes. It is also

interesting to note that **C18-bn-K(5Tam)** tightly binds to mitochondria and erythrocyte membranes, even though it has the same total charge as **5Tam-EEK(Chol)-nb-R-AMC** and **5Tam-EEK(Stear)-nb-R-AMC**. This observation together with the delay in the release of fluorophore from erythrocyte-bound **C18-bn-K(5Tam)** upon photolysis (Figure 4.7) implies that the photolabile linker is likely inserted in the membrane.

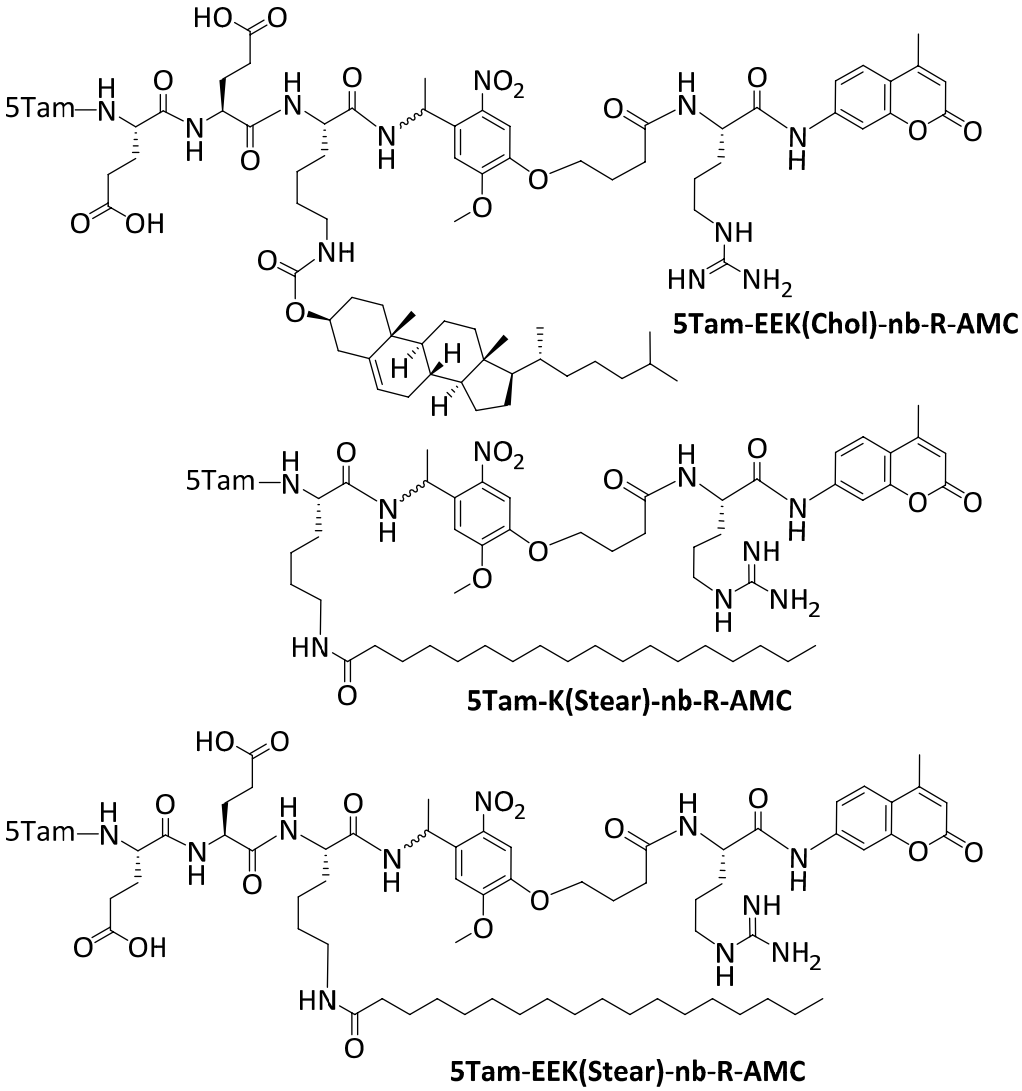

Figure 4.27: Structures of 5Tam-EEK(Chol)-nb-R-AMC, 5Tam-EEK(Stear)-nb-R-AMC, and 5Tam-K(Stear)-nb-R-AMC.

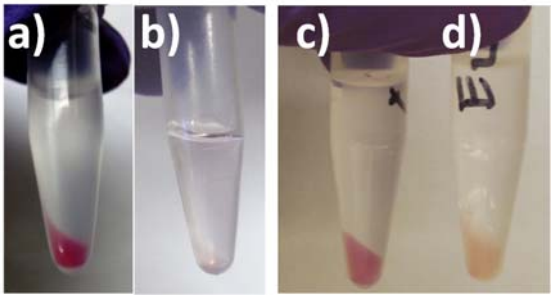

Figure 4.28: Binding of 5Tam-K(Chol)-nb-R-AMC (a), 5Tam-EEK(Chol)-nb-R-AMC (b), 5Tam-K(Stear)-nb-R-AMC (c), and 5Tam-EEK(Stear)-nb-R-AMC (d) to erythrocyte ghosts. Erythrocyte ghosts (1 mL, 10% hematocrit) in PBS 0.1X (a, b) or PBS 1X (c, d) were added to ethanol solution (10 uL) containing a lipidated peptide (final peptide concentration 2.5 µM). The suspension was then mixed at room temperature for 30 min, followed by centrifugation (5000 g / 5 min in a, b, or 2000 g / 2 min in c, d). The pellets were washed two more times with PBS buffer (1 mL, 0.1X in a, b and 1 mL, 1X in c, d), and resuspended in the buffer before imaging.

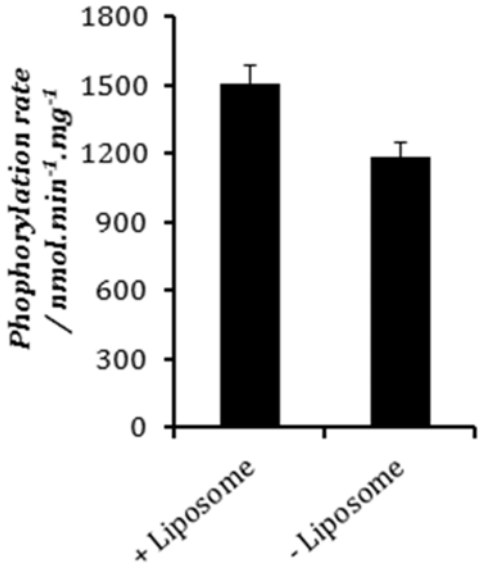

Figure 4.29: Phosphorylation of C12-bn-PKA by PKA in the presence and absence of liposomes as assessed by capillary electrophoresis. HEPES buffer (100 mM, pH 7.3, 20 µL) containing liposomes (total lipid concentration 24 mM) or containing no liposome was added C12-bn-PKA (9.5 µM). Mixtures were incubated at 28 °C followed by addition of PKA (5 nM). Reaction samples were quenched with HCl at 3 min and analyzed by capillary electrophoresis.

Lipidated Peptides and Cellular Uptake Studies with HeLa Cells

We also synthesized and investigated the cellular uptake of a lipidated peptide, **C18-bn-K(5Tam)RRRLAALAA-amide** (Figure 4.30).

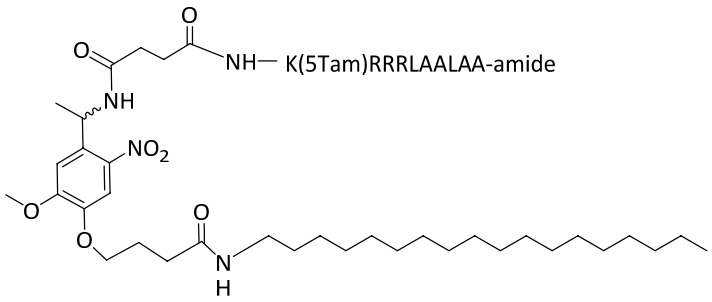

C18-bn-K(5Tam)RRRLAALAA-amide

Figure 4.30: Structure of lipidated fluorescent peptide C18-bn-K(5Tam)RRRLAALAA-amide.

As expected, upon incubation at 4 ^{o}C with HeLa cells, the peptide binds to and resides on plasma membrane as endocytotic processes are inhibited at low temperature (Figure 4.31a, b). Photolyzed cells showing no observable fluorescence increase in the interior of the cell compared to that of unphotolyzed cells suggesting that the peptide locates exclusively on the outer leaflet of the plasma membrane (Figure 4.31c, d). Incubation of the peptide with HeLa cells at 37 ^{o}C results in cells containing punctate fluorescence (Figure 4.32a), which shows no clear change in fluorescence pattern upon photolysis (Figure 4.32b). The observation suggests that the peptide still resides on the membrane's outer leaflet of lipid vesicles and, upon photolysis, the cleaved peptide is trapped inside lipid vesicles. Interestingly, treatment of the cells with an endosomal disrupting agent, chloroquine, shows no apparent difference in fluorescence pattern before and after photolysis (Figure 4.32c, d). The study needs further investigation.

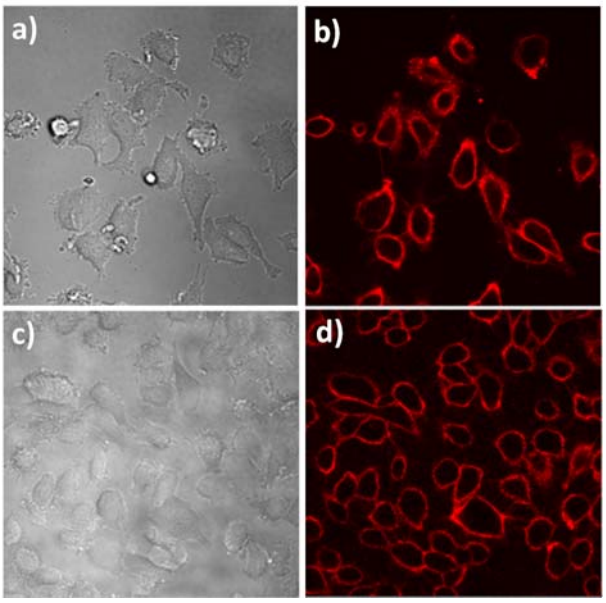

Figure 4.31: Confocal images of HeLa cells treated with **C18-bn-K(5Tam)RRRLAALAA-amide** (500 nM) for 2 h at 4 °C. (a, b) before photolysis, (c, d) after 5 min photolysis with a Hg-Arc lamp using a 360 nm bandpass filter. (b, d) Confocal images acquired with standard filter setting for 5Tam fluorophore. HeLa cells were incubated with L-15 media containing the peptide, washed, and imaged.

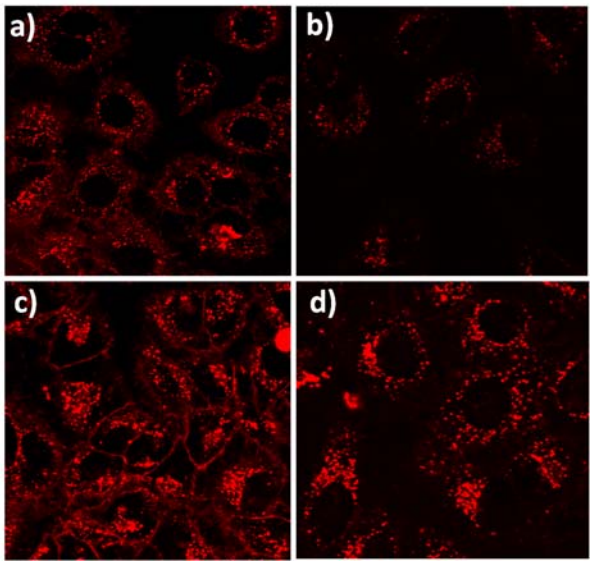

Figure 4.32: HeLa cells treated with **C18-bn-K(5Tam)RRRLAALAA-amide** (500 nM) at 37 °C for 0.5 h in the absence of UV light (a), followed by 5 min photolysis (b). HeLa cells treated with **C18-bn-K(5Tam)RRRLAALAA-amide** (500 nM) and chloroquine (100 μM) at 37 °C for 1.5 h in the absence of UV light (c), followed by 5 min photolysis (d). Photolysis was performed with a Hg-Arc lamp using a 360 nm bandpass filter. Confocal images acquired with standard filter setting for 5Tam fluorophore.

Peptide Deliver Using Doubly Labeled Transmembrane Helical Peptides

We also investigated delivery and photoactivation of peptides using doubly labeled transmembrane helical peptides. Since incubation of lipidated peptides with HeLa cells (at 4 ^{o}C) and erythrocytes shows no detectable outer-to-inner leaflet flipping of the peptide, we hypothesized that a transmembrane helical peptide which has bioagents on both termini, upon inserting into membrane, will pull one of the cargos across the membrane. The energy gained by the helical formation in the membrane's hydrophobic interior would produce the force to drive the cargo across cell membrane (Figure 4.33).

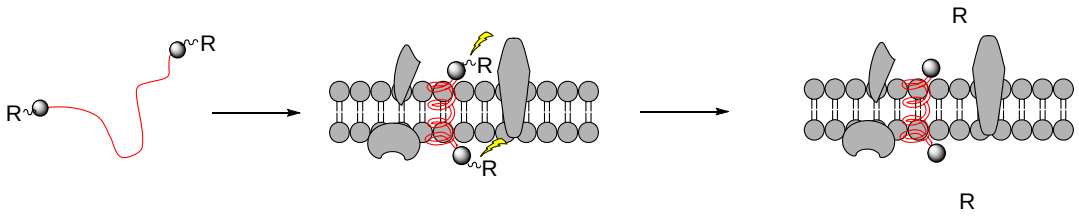

Figure 4.33: Transmembrane peptide as a membrane inserting agent. A transmembrane helical peptide appended a bioactive molecule on both sides, upon insertion into the cell membrane, evenly distributes the bioactive molecule on both sides of the membrane. Photolabile linkers placed between the transmembrane peptide and bioactive species furnishes a means to control the release of the bioactive molecule in a light-dependent fashion.

Two 25-amino acid peptides were synthesized where the length should be sufficient to form transmembrane helices. Lipophilic amino acids, leucine and alanine, are two major components of the peptides. Leucine residues are separated by five alanine residues to further facilitate helix formation upon membrane insertion. In one of the peptides, four terminal alanine residues were replaced by arginine to improve peptide solubility in aqueous environment. Additionally, two cysteine residues were appended on both termini to allow attaching maleimide containing cargos through maleimide-thiol conjugation (Figure 4.34).

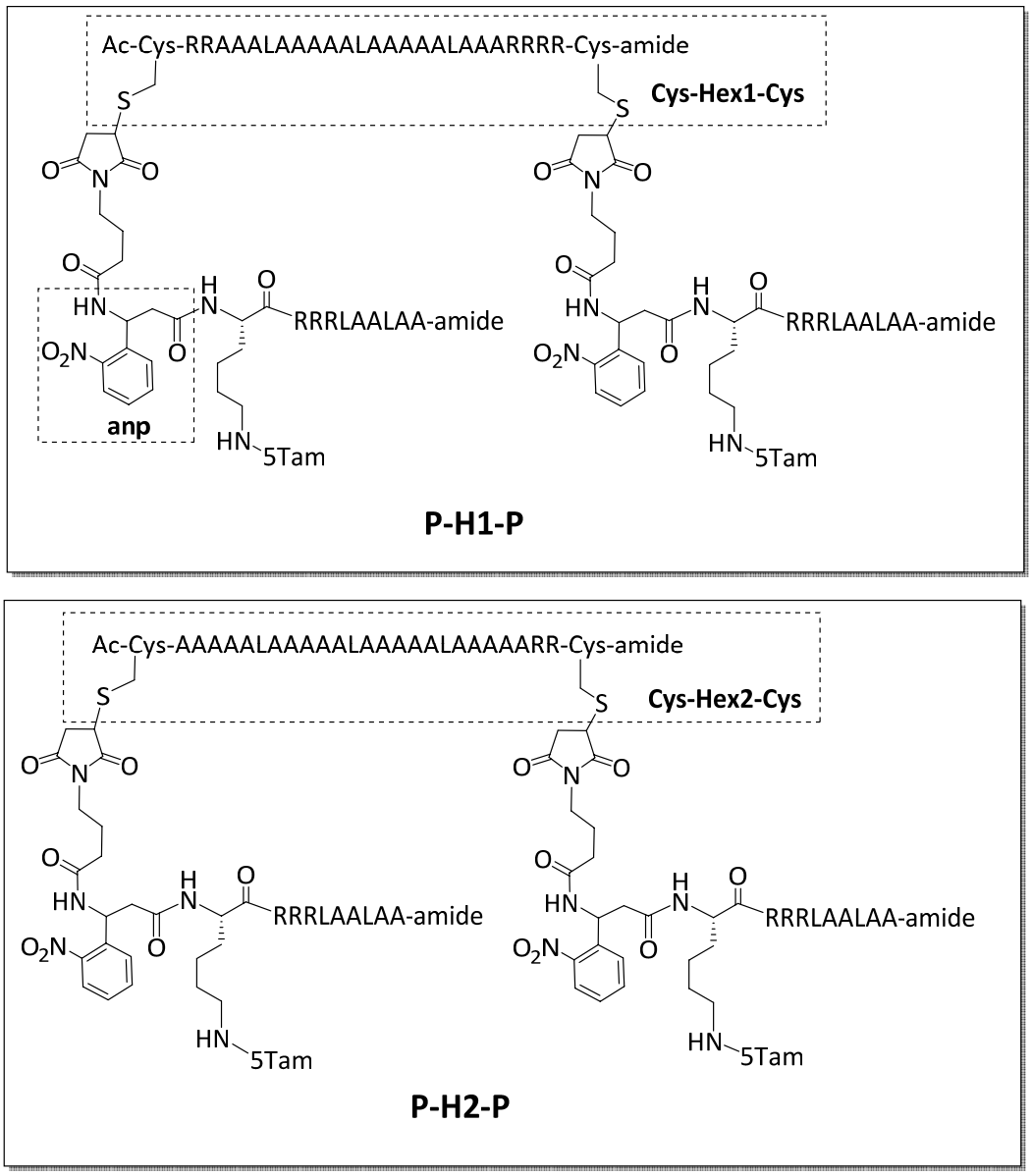

Figure 4.34: Structures of doubly labeled transmembrane helices.

Two doubly labelled transmembrane helical peptides were synthesized, **Peptide-anp-Helix1-anp-Peptide** and **Peptide-anp-Helix2-anp-Peptide** by appending the peptide sequence K(5Tam)RRRLAALAA-amide to two 25-amino peptides**, Cys-Hex1-Cys and Cys-Hex2-Cys** (Figure 4.34, 4.35). Photolabile linkers (**anp**) were placed between the fluorophore-containing peptide and the transmembrane peptide to furnish a means to

release the peptide from the transmembrane helix in a light-dependent fashion (Figure 4.34).

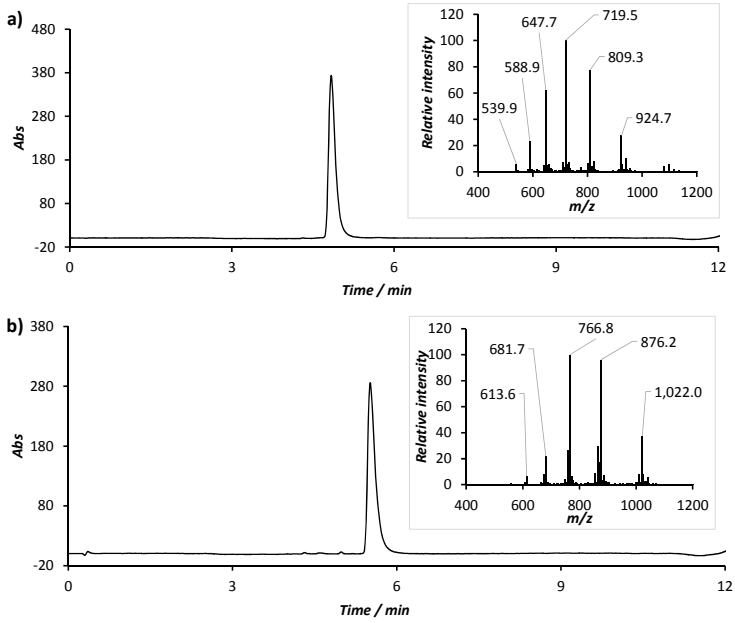

Figure 4.35: LC-MS data of doubly labeled transmembrane peptides **P-H1-P** (a) and **P-H2-P** (b). Left: LC-UV traces, right: ESI+ data of the peak in the left.

Confocal images of HeLa cells incubated with **P-H1-P** and **P-H2-P** shows cells with punctate fluorescence (Figure 4.36). Interestingly, photolysis with a 405 laser leads to an obvious increase in fluorescence at those spots whereas no detectable fluorescence increase was observed in cell's interior (Figure 4.36, circled region). One explanation is based on the presumed self-quenching of the two fluorophores on the peptide. Upon endocytosis and subsequent photolysis, the two fluorophores are separated, leading to the noticeable fluorescence dequenching. We, however, do not eliminate the possibility that the peptides inserts properly and distributes the cargo evenly on both side of cell membrane. Photolysis releases half of the labeled peptide into cell interior. The brightness of the fluorescence spots as well as the dilution effect once the peptide is

released into cell's interior might, however, prevent the signal from being captured by the confocal microscope. The study needs further investigation.

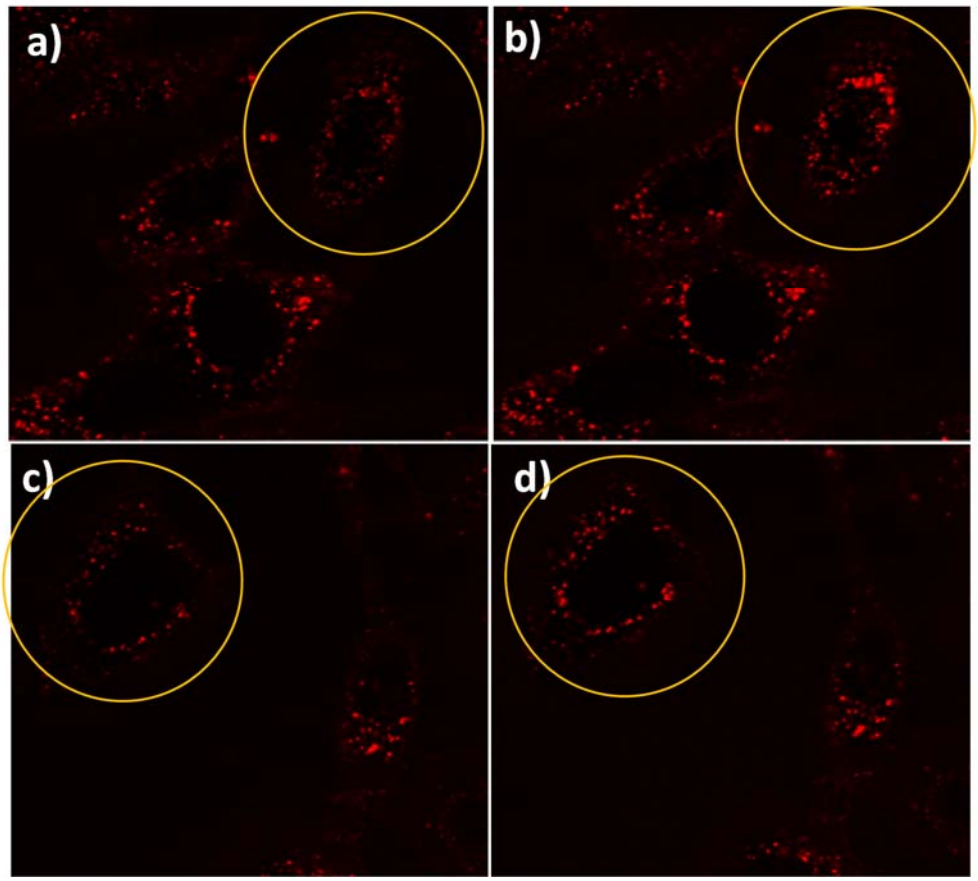

Figure 4.36: HeLa cells incubated with P-H1-P (1 μM) before photolysis (a) and after photolysis in the circle (b); with P-H2-P (1 μM) before photolysis (c) and after photolysis (d). HeLa cells incubated with peptide for 30 min. Photolysis was performed in circled region using 405 nm laser, 100 us/pixel, 100 frames turnado mode. Fluorescence confocal images were acquired using standard filter setting for 5Tam fluorophore.

Conclusion

We have developed a strategy for constructing light-activatable bioagents by cellular membrane sequestration. An active bioagent appended to a lipid binds to cells/organelles' membrane and is resistant to processing by its biological target. Photolysis releases it from the membrane anchor and renders it biologically active. This

strategy provides a means to control the release of active biomolecules with a high degree of spatiotemporal resolution. The construction, however, needs further investigation in term of cellular delivery if the bioagent of interest functions inside cells. The role of linker's length between membrane anchoring moiety and bioagent as well as the nature of anchor itself in membrane binding and rendering biomolecules inactive is also in need of further examination.

Materials and Method

Reagents were purchase as described before unless noted otherwise. Fmoc-Lys($NH_3^+Cl^-$)-OH was obtained from Bachem; Fmoc photolabile linker, **Fmoc-nb-COOH**, was acquired from Advanced Chemtech. Protease inhibitors were purchased from Sigma-Aldrich, Enzo Life Science, and Selleckchem. Mitochondria were ordered from Mitoscience.

Purifications

HPLC purifications were run on Waters HPLC instrumentation. Flash chromatography purifications were run on an Isolera One instrument (Biotage) using a silica or C18 column (Biotage). Lipidated molecules, unless otherwise specified, were purified by HPLC on a Viva C4 preparative column (5 μM, 250 x 21.2 mm) from Restek. Non-lipidated molecules were either purified by C18 flash chromatography or C18 HPLC (Apollo C18, 5 μM, 250 x 22 mm column). LC-MS analytical characterizations were run on an Agilent instrument equipped with a UV-VIS, fluorescence, and quadrupole mass detectors using either a Viva C4 column (5 μM, 50 x 2.1 mm) from Restek or a Prevail C18 column (3 μM, 50 x 2.1 mm) from Alltech Associates, Inc. All LC-MS experiments were conducted using H_2O-CH_3CN solvents with 0.1% formic acid.

Fluorescence Assays

Fluorescence assays were performed on 96 or 384-well clear bottom plates on a SpectraMAX Gemini EM instrument from Molecular Devices or in a cuvette on a spectroflurometer from PTI.

Capillary Electrophoresis

Capillary electrophoresis was performed on a ProteomeLab PA800 system equipped with a laser-induced fluorescence (LIF) detector (Beckman Coulter). The LIF was

excited using a 488 nm argon laser. A fused-silica capillary (30/20 cm total/effective length, 30 or 50 μM inner diameter) was used for separation (Polymicro Technologies). Capillaries were pretreated with 0.1 M NaOH for 12 h, distilled water for 1 h, 0.1 M HCl for 6 h and water for 12 h before installation. The samples were hydrodynamically injected and separated at a constant voltage of 15 kV using a separation buffer containing 350 mM tris, 175 mM tricine, and 20 mM sodium cholate pH 8.5. Before each run, the capillary was rinsed with 1 M NaOH (1 min), distilled water (2 min), and the running buffer for 2 min under 20 psi pressure. Data was collected and analyzed using 32 Karat Software (Version 8.0, Beckman Coulter).

Octanol - Water Partition Studies

*Partition Studies with **C18-bn-K(5Tam)***

Octanol (300 μL) containing **C18-bn-K(5Tam) (**4 μM) was mixed with of PBS 1X (300 μL) containing DTT (5 mM) by pipetting then centrifuged (1000 g for 5 min). An image of the tube being excited by the UV light from the top was acquired. The test tube was then photolyzed for 30 min with mixing every 5 min followed by centrifugation (1000 g for 5 min) and reimaging. All images were acquired using the X-Nite 590 filter.

*Partition Study with **C18-bn-K(Tam)--K(Fam)***

Octanol (300 μL) containing **C18-bn-K(Tam)--K(Fam)** (4 μM) was mixed with 300 μL of PBS 1X containing DTT (5 mM) by pipetting followed by centrifugation (1000 g for 5 min). Trypsin (20 nM) was gently added to the aqueous phase. The tube was then incubated at room temperature for 2.5 h and imaged. The test tube was then photolyzed for 10 min with one time mixing at 5 min. After photolysis, the test tube was centrifuged at 1000 g for 5 min and then reimaged. Fluorescence images were acquired using X-Nite 525 and X-Nite 590 filters while the tube was being excited by the UV light from the top.

Studies with Mitochondria

C18-bn-K(5Tam) *and mitochondria*

Mito buffer: 10 mM Tris 7.5, 0.25 M Sucrose, 0.2 mM EDTA.

Mitochondria were washed 3 times with mito buffer and resuspended in mito buffer to a concentration of 5.5 mg/mL. A 150 µL cold solution of mito buffer containing C18-bn-K(5Tam) was sonicated for 3 min to which 50 µL of washed mitochondria (5.5 mg/mL) was added. The final concentration of **C18-bn-K(5Tam)** was 4 µM. The suspension was gently mixed and incubated on ice for 30 min. Mitochondria were pelleted by centrifugation at 5000 g for 5 min and imaged under ambient light. The pellet was then washed with cold mito buffer (200 µL) and resuspended in cold mito buffer (200 µL) containing DTT (5 mM). The fluorescence of the contents was imaged after 5 min of centrifugation. The contents were then resuspened followed by photolysis (3 min), centrifugation, and reimaging.

C18-bn-K(Tam)--K(Fam)*, mitochondria, and trypsin*

A cold mito buffer solution (150 µL) containing **C18-bn-K(Tam)--K(Fam)** (4 µM) was sonicated for 1 min and then 50 µL of washed mitochondria (5.5 mg/mL) was added. The suspension was gently mixed and incubated on ice for 30 min. Mitochondria were pelleted by centrifugation at 5000 g for 5 min. The supernatant (named **supernatant i**) was collected. The pellet resuspended in 200 µL cold mito buffer, centrifuged to collect **supernatant ii**, and then resuspended in 200 µL cold mito buffer containing DTT (5 mM). 100 µL of the above suspension was photolyzed for 3 min. 80 µL of the photolyzed or non-photolyzed suspension was transferred to a 384-well plate and equilibrated at 37 ^{o}C for 5 min. Trypsin (10 nM) was added and the fluorescence change was monitored (λ_{ex} 492 nm, λ_{em} 525 nm). A well containing mito buffer (80 µL), mitochondria (1.375 mg/mL), DTT (5

mM), **Ac-K(Tam)--K(Fam) (**4 μM), and trypsin (10 nM) was prepared as a reference. The experiments were performed in triplicate.

C12-bn-K(5Fam)RRRLASLAA-amide, mitochondria and PKA

Dilution buffer: 190 mM Tris 7.5, 0.25 M sucrose, 0.25 mM EDTA, 2% SDS.

Loading study

Washed mitochondria (final concentration of mitochondria 0.917 mg/mL) was added to mito buffer containing peptide **C12-bn-PKA** (9.5 μM, 100 μL total volume) followed by incubation on ice 1 h and centrifugation (5000 g for 10 min) to get **mito-supernatant i** and pellet. The pellet was then washed twice with mito buffer (100 μL) to get **mito-supernatant ii** and **mito-supernatant iii**. The mito-supernatants were then diluted with dilution buffer (1:1 by v:v) and the fluorescence of the diluted solution (λ_{ex} 492 nm, λ_{em} 525 nm) compared to fluorescence of a standard solution of **C12-bn-PKA** in the same final buffer.

Photorelease assessment

The peptide mitochondria pellet loaded with **C12-bn-PKA** was resuspended in DTT-contaning mito buffer (100 μL, 5 mM DTT) and photolyzed for 2 min. After centrifugation (5000 g / 10 min) the pellet was washed twice by 100 μL mito buffer and then dissolved in 50 μL mito buffer + 50 μL dilution buffer. The dissolved photolyzed mitochondria solution (10 μL) was diluted in 35 μL mito buffer + 35 μL dilution buffer and the solution's fluorescence was measured (λ_{ex} 492 nm, λ_{em} 525 nm). A parallel sample without photolysis was performed as a reference.

Phosphorylation studies

The **[C12-bn-PKA**]-loaded mitochondria pellet was suspended in mito buffer (420 μL) containing DTT (5 mM), ATP (1 mM), and $MgCl_2$ (1 mM). The final concentrations were

9.5 μM(peptide) and 0.917 mg/mL (mitochondria). An aliquot (40 μL) was quenched with HCl 1M (40 μL) followed by photolysis (2 min) and capillary electrophoresis (CE) analysis. The suspension was then photolyzed for 2 min followed by addition of PKA (20 nM) and the reaction aliquots were quenched and analyzed by CE over time. Another sample [420 μL mito buffer containing **C12-bn-PKA** (9.5 μM), DTT (5 mM), ATP (1 mM), and $MgCl_2$ (1 mM)] was also performed in parallel in which no photolysis was employed before the addition of PKA (20 nM). The reaction aliquots were quenched at 30 and 60 min after the PKA addition and photolyzed for 2 min followed by CE analysis. A solution of **C12-bn-PKA** (9.5 μM) in mito buffer containing DTT (1 mM), ATP (1 mM), and $MgCl_2$ (1 mM) was added PKA (20 nM) and phosphorylation was monitored over time by quenching followed by photolysis and CE analysis. Phosphorylated peptide of **C12-bn-PKA** was generated enzymatically and confirmed by LC-MS. Standard photolyzed products were generated by 3 min photolysis and confirmed by LC-MS. Phosphorylation rates were calculated from the percentages of phospho peak over total peptide and the amount of peptide released after photolysis acquired from the photorelease studies.

Studies of C12-bn-PKA with Liposomes

DSPC (18:0 PC,1,2-distearoyl-*sn*-glycero-3-phosphocholine)/CHOL (cholesterol) liposomes (55/45 mol/mol, lipid concentration 60 ± 2.5 mM, mean particle diameter 87.3 ± 0.5 nm) were purchased from Formumax. The liposomes were diluted in HEPES buffer (100 mM pH 7.3) containing 10% sucrose to a lipid concentration of 24 mM. To a 20 μL solution of the liposome was added **C12-bn-PKA** (9.5 μM), $MgCl_2$ (1 mM), and ATP (1 mM). The solution was incubated at 28 ^oC for 30 min followed by the addition of PKA (5 nM). Reaction was quenched at 3 min and analyzed by capillary electrophoresis. A parallel

sample in which 20 μL of HEPES buffer (100 mM, pH 7.3) was used instead of liposome suspension was also performed as the reference.

Studies with Erythrocyte Ghosts

Erythrocyte ghosts preparation

Ghost buffer: PBS 0.1X and 50 mM Tris pH 7.5. Erythrocyte ghosts were prepared by washing erythrocytes with cold PBS 0.1X until centrifugation (5000 g for 5 min) gave a white to white-yellow pellet. The pellet was then resuspended in the ghost buffer to a concentration corresponding to 40% hematocrit.

C18-bn-K(5Tam) *and erythrocyte ghosts*

Ghost buffer (100 μL) containing **C18-bn-K(5Tam)** was sonicated for 3 min. To that solution was added erythrocyte ghosts (100 μL, 40% hematocrit). The final concentration of **C18-bn-K(5Tam)** was 4 μM. The suspension was incubated on ice for 30 min followed by centrifugation (5000 g for 5 min). The supernatant was discarded, the pellet washed with ghost buffer (200 μL), and then resuspended in 200 μL ghost buffer containing 5 mM DTT. Images were acquired before and after of photolysis (3 min) using X-Nite 590 filter.

C18-bn-K(Tam)--K(Fam)*, erythrocyte ghosts, and trypsin*

A 100 μL ghost buffer containing **C18-bn-K(Tam)--K(Fam)** was sonicated for 1 min. To that solution were added erythrocyte ghosts (100 μL, 40% hematocrit). The final concentration of **C18-bn-K(Tam)--K(Fam)** was 4 μM. The suspension was incubated on ice for 30 min followed by centrifugation (5000 g for 5 min). The supernatant (**supernatant i**) was collected, the pellet was suspended in cold ghost buffer (200 μL), centrifuged to collect **supernatant ii**, and then suspended in 200 μL ghost buffer containing DTT (5 mM). 100 μL of the above suspension was photolyzed for 3 min. 80 μL of the photolyzed or non photolyzed suspension was transferred to a 384-well plate, equilibrated at 37 ^{o}C for 5 min

followed by addition of trypsin (10 nM) and the fluorescence change was monitored (λ_{ex} 492 nm, λ_{em} 525 nm). A well containing 80 µL of ghost buffer (20% hematocrit), DTT (5 mM), **Ac-K(Tam)--K(Fam)** (4 µM), and trypsin (10 nM) was prepared as a reference. The experiments were performed in triplicate.

Determination of Peptide Concentration in Supernatants

Supernatants [**C18-bn-K(Tam)--K(Fam)** loading on mitochondria and erythrocyte ghosts] were diluted with MeOH (1:1 by volume) and the fluorescence of the solution compared to the fluorescence of standard **C18-bn-K(Tam)--K(Fam) (**4 µMin 200 µL mito buffer or ghost buffer diluted with 200 µL MeOH; λ_{ex} 555 nm, λ_{em} 587 nm). Standard curves were built showing a linear relationship between fluorescence and concentration of **C18-bn-K(Tam)--K(Fam)** (in 50% MeOH and 50% mito buffer or ghost buffer, when the concentration of the peptide < 2 µM).

Studies with Erythrocyte Lysates

Erythrocyte Whole Lysate Preparation

Erythrocytes were washed twice with PBS 1X. 100 µL of washed erythrocytes were diluted in 850 µL of cold deionized water. The mixture was sonicated (3 times, 30 s each). 105.4 µL of PBS 10X was then added to the mixture followed by two additional cycles of 30 s sonication to obtain whole lysate. The lysate was kept on ice and was made fresh before use each day.

Inhibition of protease activity in erythrocyte lysate

To a 200 µL of erythrocyte lysates preincubated at 37 ^{o}C for 5 min (with and without different protease inhibitors) was added **Ac-K(Tam)--K(Fam)** (1 µM) and the fluorescence changes monitored (37 ^{o}C, λ_{ex} 492 nm, λ_{em} 525 nm) over time.

*LC-MS Confirmation of Digestion of **Ac-K(Tam)--K(Fam)** by Erythrocyte Whole Lysates*

Proteolysis of **Ac-K(Tam)--K(Fam)** (20 μM, 200 μL total volume) in whole lysate was monitored in the plate reader until the fluorescence plateaued. HCl (20 μL, 10 M) and MeOH (160 μL) were then added to the reaction mixture followed by filtration by centrifugation 14,000 g for 30 min using 3K cutoff filter (Invitrogen). The collected solution was then dried and analyzed by LC-MS on the C18 column.

Confocal Microscopy

All microscopy experiments were performed at 37 ^{o}C on an Olympus FV1000 scanning confocal with an IX81 microscope base. A Coherent Genesis CX355-100 STM 355 nm, 100 mW continuous wave UV laser was coupled to the confocal via an installed UV port. Laser and region of photolysis were controlled via Fluoview software. Photolysis was performed using the stimulation mode of the Fluoview software with images collected before and after stimulation. A photolytic dwell time of 10 μs/pixel in tornado mode was employed for the defined region of interest using 5 frames at 355 nm and 1 mW power level. All imaging was performed with a 100X objective using 488 nm and 559 nm lasers. 5-Fam was used to generate photobleaching curve. ImageJ software was employed for image analyses. Final fluorescence intensity changes of 5-Fam were corrected for photobleaching effect by the formula

$$F_{t\,(corrected)} = F_t \times f_o/f_t$$

Where F_t were fluorescence value measured at time t, f_o and f_t were fluorescence values of bleaching curve at $t = 0$ and at t.

Loading of C18-bn-K(5Tam) and C18-bn-K(Tam)--K(Fam) into erythrocytes

Erythrocytes were washed 2 times with PBS 1X, centrifuged at 1,400 g for 10 min. The supernatant was discarded to furnish the erythrocytes (100% hematocrit). The C18-

lipidated peptide (4 μM) was dissolved in H_2O (125 μL) containing (2-hydroxypropyl)-β-cyclodextrin (100 mg/mL). To this solution was added the washed erythrocytes (50 μL). The mixture was then incubated on ice for 30 min. Cold deionized H_2O was added to the mixture until centrifugation at 1000 g for 5 min gave no observable pellet (added 300 μL of H_2O). The mixture was then incubated on ice for 40 min followed by addition of PBS 10X (52.7 μL) and incubation on ice for additional 2 h. The mixture was then centrifuged at 1400 g for 10 min and most of the supernatant collected (475 μL - loading lysate). 2 μL of the remaining erythrocyte suspension was resuspended in of PBS 1X (200 μL) containing DTT (5 mM) for confocal imaging.

Loading of C18-bn-K(Tam)--K(Fam) into erythrocytes with protease inhibitors

The procedure was identical to loading of **C18-bn-K(Tam)--K(Fam)** into erythrocytes except, in this case, 125 μL H_2O containing (2-hydroxypropyl)-β-cyclodextrin (100 mg/mL) also contains EDTA (10 mM), leupeptin (100 μM), and MG-132 (100 μM).

Syntheses

*Synthesis of Lipidated Photolabile Linker **C18-bn-COOH***

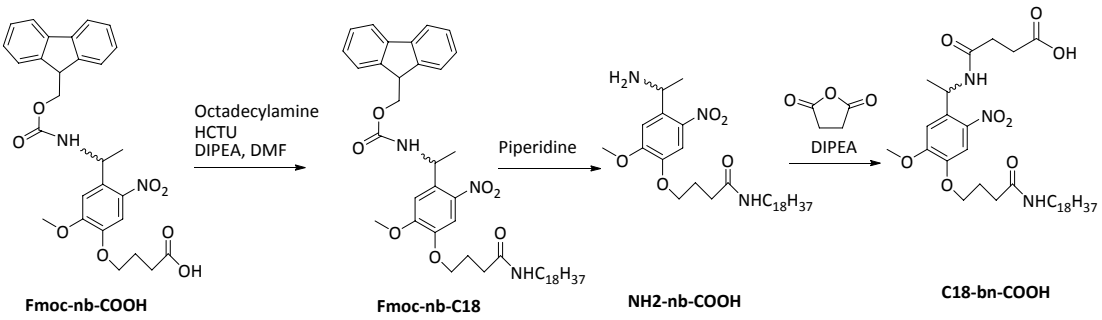

Scheme 4.1: Synthesis of lipidated photolabile linker C18-bn-COOH.

Octadecylamine (270 mg, 1.00 mmol) was dissolved in 5 mL DMF (with a small amount of CH_2Cl_2 to help dissolve the compound). To the above solution was added DIPEA (1.65 mL, 10 mmol) and a DMF solution containing **Fmoc-nb-COOH (**580 mg, 1.11 mmol)

and HCTU (463 mg, 1.12 mmol). The reaction was mixed for 30 min and stopped by addition of H_2O (2 mL). The mixture containing product **Fmoc-nb-C18** was added piperidine (2 mL, 20 mmol) and mixed for 1 h to deprotect the Fmoc group. The reaction mixture containing **NH_2-nb-C18** was dried under vacuum and redissolved in DMF (5 mL). DIPEA (1.65 mL, 10 mmol) was added to the crude solution of **NH_2-nb-C18** in DMF followed by addition of succinic anhydride (1 g, 10 mmol). The mixture was stirred for 4 h then extracted with H_2O:EtOAc after neutralizing the pH of the aqueous phase to 5 with HCl 10 M. The EtOAc extract containing **C18-bn-COOH** was dried and purified by flash chromatography using silica column and CH_2Cl_2:MeOH= 90:10 with 0.1% TFA. ^{1}H NMR (600 MHz, DMSO-d_6) δ 12.03 (s, 1 H), 8.57 (d, *J* = 7.4 Hz, 1 H), 7.83 (t, *J* = 5.4 Hz, 1 H), 7.47 (s, 1 H), 7.16 (s,1 H), 5.34 (quin, *J* = 6.8 – 7.1 Hz, 1 H), 4.00 (t, *J* = 6.4 Hz, 2 H), 3.91 (s, 3 H), 3.01 (q, *J* = 6.2 – 6.6 Hz, 2 H), 2.40-2.32 (comp, 4 H), 2.21 (t, *J* = 7.4 Hz, 2 H), 1.93 (quin, *J* = 6.6 – 7.1 Hz, 2 H), 1.38 (d, *J* = 6.9 Hz, 3 H), 1.36 (comp, 2H), 1.22 (comp, 30 H), 0.85 (t, *J* = 6.9 Hz, 3 H); ^{13}C NMR (600 MHz, DMSO-d6) δ 173.8, 171.2, 170.4, 153.4, 146.2, 139.8, 135.7, 109.3, 108.2, 68.3, 56.1, 44.2, 40.1, 38.4, 31.6, 31.3, 29.8, 29.1-29.0 (comp), 28.8, 28.7 (comp), 26.4, 24.8, 22.1, 21.9, 14.0; $C_{35}H_{59}N_3O_8$. Exact mass calculated (M) 649.43, found (ESI+, m/z) 650.4 $(M + H)^+$, 672.4 $(M + Na)^+$.

*Synthesis of **C18-bn-K(5Tam)***

*Synthesis of **NH2-K(5Tam)***

To a solution of 5Tam (17.8 mg, 41.3 µmol) in DMF was added HCTU (41.2 µmol) and DIPEA (200 µmol) dissolved in DMF. The reaction mixture was incubated at room temperature for 2 min to preactivate 5Tam. To a DMF solution containing Fmoc-Lys($NH_3^+Cl^-$)-OH (40.9 mg, 101 µmol) was added DIPEA (200 µmol) followed by addition of HCTU-activated 5Tam solution above (final volume ~ 3 mL). The reaction was shaken at

room temperature for 30 min followed by the addition of H_2O (1 mL) to stop the reaction. Piperidine (700 µmol) was then added to the reaction mixture, which was shaken for 30 min to deprotect the Fmoc group on Lys. DMF and piperidine were removed by lyophilization. The crude mixture was then purified by flash chromatography using a C18 column with a H_2O:CH_3CN gradient from 0% to 50% of CH_3CN in 15 column void volumes to afford **NH_2-K(5Tam)**. ^{1}H NMR (600 MHz, D_2O) δ 8.41 (d, *J* = 1.7 Hz, 1 H), 8.06 (dd, *J* = 7.8, 1.7 Hz, 1 H), 7.52 (d, *J* = 7.8 Hz, 1 H), 7.13 (d, *J* = 9.5 Hz, 2 H), 6.81 (dd, *J* = 9.5, 2.3 Hz, 2 H), 6.38 (s, 2 H), 3.84 (t, *J* = 6.1 Hz, 1 H), 3.47 (t, *J* = 6.9 Hz, 2 H), 3.07 (s, 12 H), 1.99 - 1.89 (comp, 2 H), 1.72 (quin, *J* = 7.2 – 7.7 Hz, 2 H), 1.58 – 1.44 (comp, 2 H); $C_{31}H_{35}N_4O_6^+$ Exact mass calculated 559.26; found (ESI+, m/z) 559.2 $(M)^+$, 280.1 $(M + H)^{2+}$.

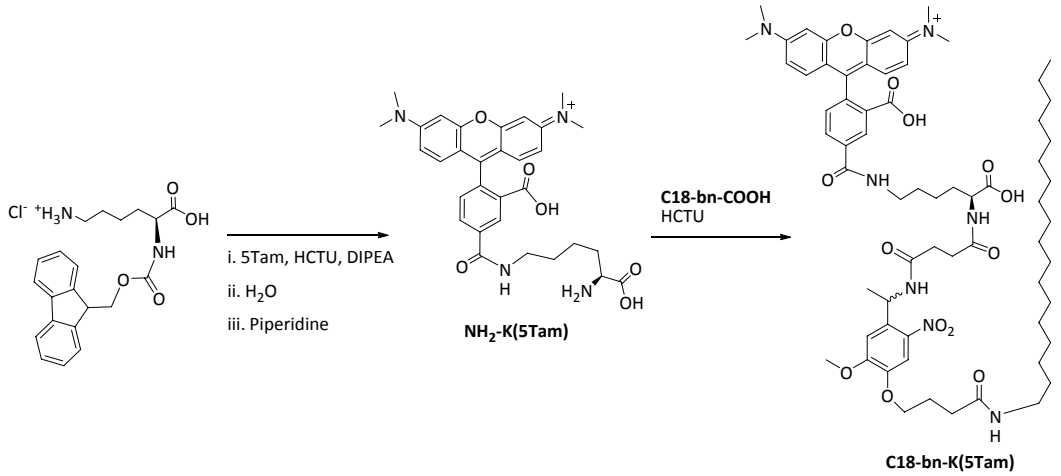

Scheme 4.2: Synthesis of C18-bn-K(5Tam).

*Synthesis of **C18-bn-K(5Tam)***

To a 500 µL DMF solution (with a small amount of CH_2Cl_2 to help dissolve the compound) containing **C18-bn-COOH** (7 mg, 10.77 µmol) was added DIPEA (21 µmol) and HCTU (8.5 µmol). The reaction mixture was shaken for 2 min. To a 5 mL DMF solution of **NH_2-K(5Tam)** (8.5 µmol) was added DIPEA (85 µmol) followed by addition of HCTU-activated **C18-bn-COOH** solution above. The reaction mixture was shaken for 5 min then

quenched by addition of H_2O (1 mL). Solvent and excess reagents were removed under vacuum. The crude material was purified by HPLC on the C4 column using H_2O:CH_3CN with 0.1% TFA to afford **C18-bn-K(5Tam)**. $C_{66}H_{92}N_7O_{13}^+$. Exact mass calculated 1190.67, found (ESI+, m/z) 1190.7 $(M)^+$, 595.9 $(M + H)^{2+}$.

*Synthesis of Protease Fluorescent Substrates **Ac-K(Tam)--K(Fam)** and **C18-bn-K(Tam)--K(Fam)***

Solid phase peptide synthesis (SPPS) was performed on a Prelude peptide synthesizer from Protein Technology using Fmoc-protected amino acids (amino acids 3 eq., HCTU 2.95 eq., DIPEA 10 eq. in DMF, double coupling in 20 and 40 min). Fmoc deprotection was performed using piperidine (25%) in DMF (3 times, 10 min each). The peptide containing a Lys side chain protected with the acid sensitive 4-methyltrityl group (Mtt), Boc-K(Fmoc)RRRLAALAAK(Mtt), was synthesized on a NovaSyn TGR resin using SPPS. The Fmoc protecting group on the lysine residue was deprotected by piperidine (25%) in DMF followed by coupling of 5-Tam fluorophore using 5-Tam (1.5 eq.), HCTU (1.5 eq.), and DIPEA (10 eq.) in DMF for 4 h. The Mtt was removed with 1% trifluoroacetic acid (TFA) in CH_2Cl_2 followed by coupling 5-Fam using 5-Fam (1.5 eq.), *N,N'*-diisopropylcarbodiimide (DIC, 1.7 eq.), and 1-hydroxybenzotriazole (HOBt, 10 eq.) in DMF for 2 h. The peptide was then cleaved from the resin with TFA:H_2O:Triisopropylsilane in a ratio of 95:2.5:2.5, and purified by HPLC using H_2O:CH_3CN with 0.1% TFA to afford **NH_2-K(5Tam)RRRLAALAAK(5Fam)-amide**. Solution of pure **NH_2-K(5Tam)RRRLAALAAK(5Fam)-amide** was acidified with HCl and dried. $C_{100}H_{135}N_{24}O_{22}^+$. Exact mass calculated 2024.02, found (ESI+, m/z) 675.3 $(M + 2H)^{3+}$, 506.6 $(M + 3H)^{4+}$, 405.6 $(M + 4H)^{5+}$.

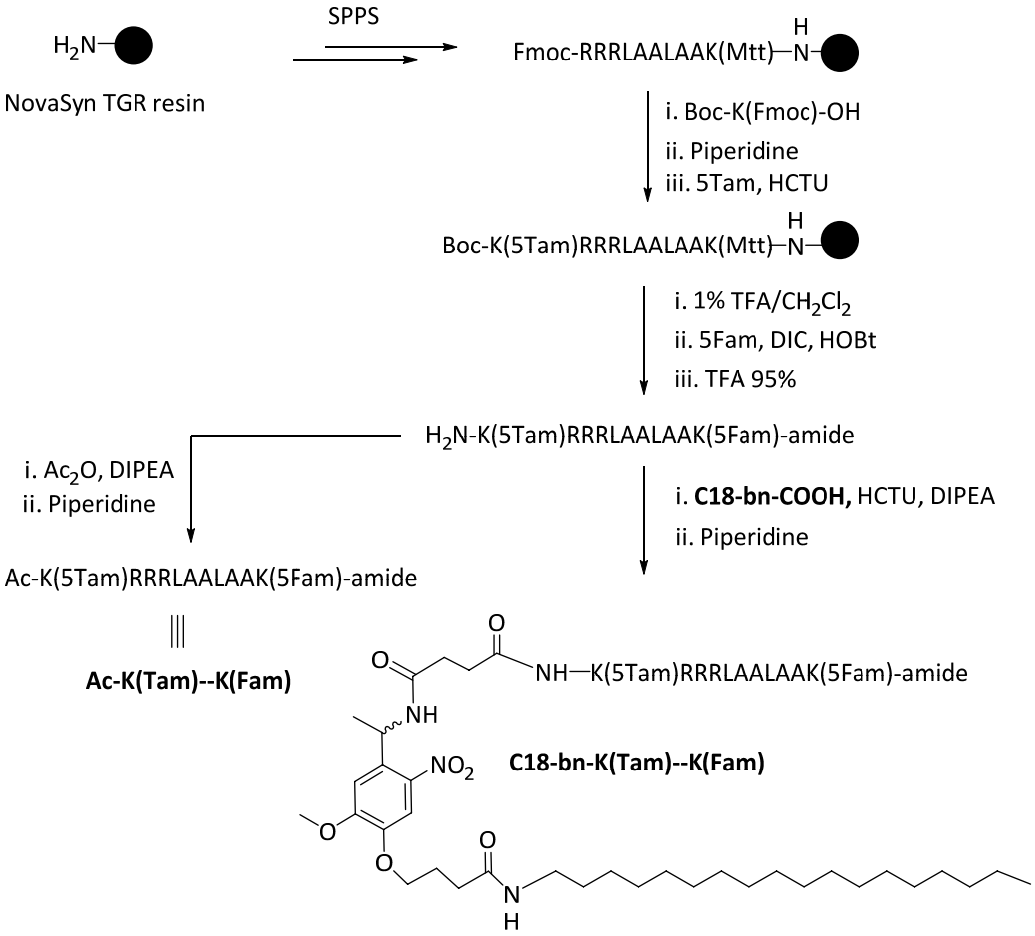

Scheme 4.3: Synthesis of protease fluorescent substrates Ac-K(Tam)--K(Fam) and C18-bn-K(Tam)--K(Fam).

*Synthesis of **Ac-K(Tam)--K(Fam)***

Dried **NH_2-K(5Tam)RRRLAALAAK(5Fam)-amide** (0.55 µmol) was redissolved in DMF (500 µL). To this solution was then added DIPEA (5.5 µmol) and Ac_2O (5.5 µmol). The reaction mixture was shaken at room temperature for 1 h. H_2O (500 µL) was then added and the mixture shaken for 30 min. Piperidine (27.5 µmol) was then added and the mixture shaken for 30 min. Solvent and excess reagents were removed under vacuum and the crude product purified by HPLC using the C18 column to afford pure **Ac-K(Tam)--K(Fam).** $C_{102}H_{137}N_{24}O_{23}^{+}$. Exact mass calculated 2066.03, found (ESI+, m/z) 1033.6 $(M + H)^{2+}$, 689.2 $(M + 2H)^{3+}$, 517.2 $(M + 3H)^{4+}$, 414.0 $(M + 4H)^{5+}$.

*Synthesis of **C18-bn-K(Tam)--K(Fam)***

C18-bn-COOH (21.5 mg, 33 µmol), HCTU (12.4 mg, 30 µmol), and DIPEA (10.9 µL, 66 µmol) were dissolved in minimum amount of DMF (with a small amount of CH_2Cl_2 to help dissolve the compound) and the solution was stirred for 2 min. The HCTU-activated **C18-bn-COOH** was then added to DMF (20 mL) containing **NH_2-K(5Tam)RRRLAALAAK(5Fam)-amide** (22 µmol) and DIPEA (220 µmol). The reaction mixture was shaken at room temperature for 20 min. H_2O (0.5 mL) was then added to the reaction mixture, which was then shaken for 30 min followed by addition of piperidine (110 µL, 1.1 mmol) and 30 min stirring. Solvent and excess reagents were then removed under high vacuum and crude product purified by HPLC on the C4 column to afford pure **C18-bn-K(Tam)--K(Fam).** $C_{135}H_{192}N_{27}O_{29}^+$. Exact mass calculated 2655.44, found (ESI+, m/z) 1328.3 $(M + H)^{2+}$, 885.9 $(M + 2H)^{3+}$, 664.6 $(M + 3H)^{4+}$, 531.9 $(M + 4H)^{5+}$.

*Synthesis of **5Tam-K(Chol)-nb-R-AMC***

*Synthesis of **Fmoc-K(Chol)-OH**.*

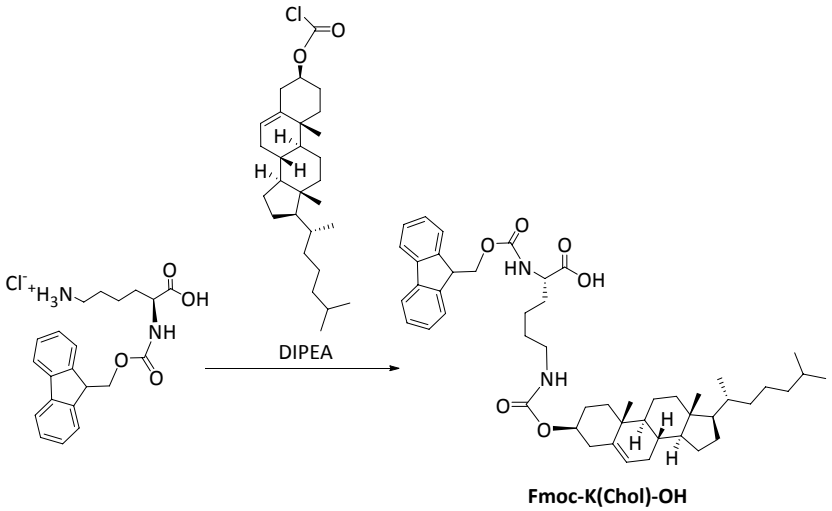

Fmoc-K(Chol)-OH

Scheme 4.4: Synthesis of Fmoc-K(Chol)-OH.

To a DMF solution containing Fmoc-Lys($NH_3^+Cl^-$)-OH (1.00 g, 2.47 mmol) was added DIPEA (10 mmol) followed by the addition of cholesteryl chloroformate (554 mg, 1.23 mmol). The reaction was shaken at room temperature for 2 h followed by the addition of H_2O and extraction with CH_2Cl_2. Organic extract was dried and the residue was purified by flash chromatography using a silica column and CH_2Cl_2 95:5 with 0.1% acetic acid to afford **Fmoc-K(Chol)-OH**. $C_{49}H_{68}N_2O_6$. Exact mass calculated (M) 780.5, found (ESI+, m/z) 803.5 $(M + Na)^+$.

Synthesis of ***NH_2-R(pbf)-AMC***

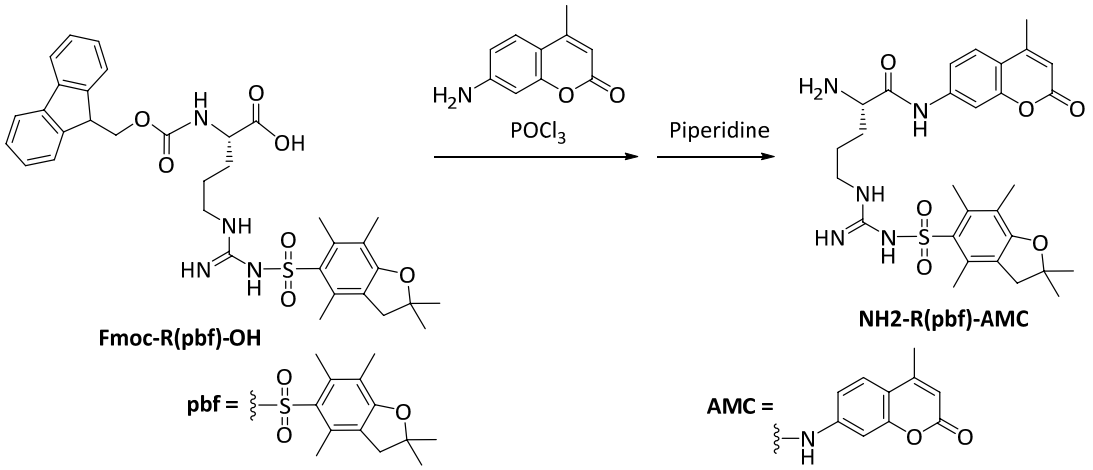

Scheme 4.5: Synthesis of NH_2-R(pbf)-AMC.

NH_2-R(pbf)-AMC was synthesized followed the procedure reported in Pept. Res. 9(2): 92-6. Briefly, 7-amino-4-methylcoumarine (250 mg, 1.43 mmol) and Fmoc-R(pbf)-OH (670 mg, 1.43 mmol) were dissolve in pyridine, which was dried over KOH pellets and redistilled right before use. This solution was cooled by dried ice and $POCl_3$ (1.7 mmol) was added dropwise under vigorous stirring. Crushed ice was added after 30 min followed by extraction with ethyl acetate. The organic phase was washed 3 times with water followed by solvent removal. The residue was then redisolved in DMF containing piperidine (25%) to deprotect the Fmoc group. The reaction was mixed at room

temperature for 30 min followed by solvent removal and purification using C18 flash chromatography with H_2O:CH_3CN gradient to afford **NH_2-R(pbf)-AMC**. $C_{29}H_{37}N_5O_6S$. Exact mass calculated (M) 583.2, found (ESI+, m/z) 1167.5 (2 M + H)$^+$, 584.2 (M + H)$^+$, 292.6 (M + 2H)$^{2+}$.

*Synthesis of **5Tam-K(Chol)-nb-R-AMC***

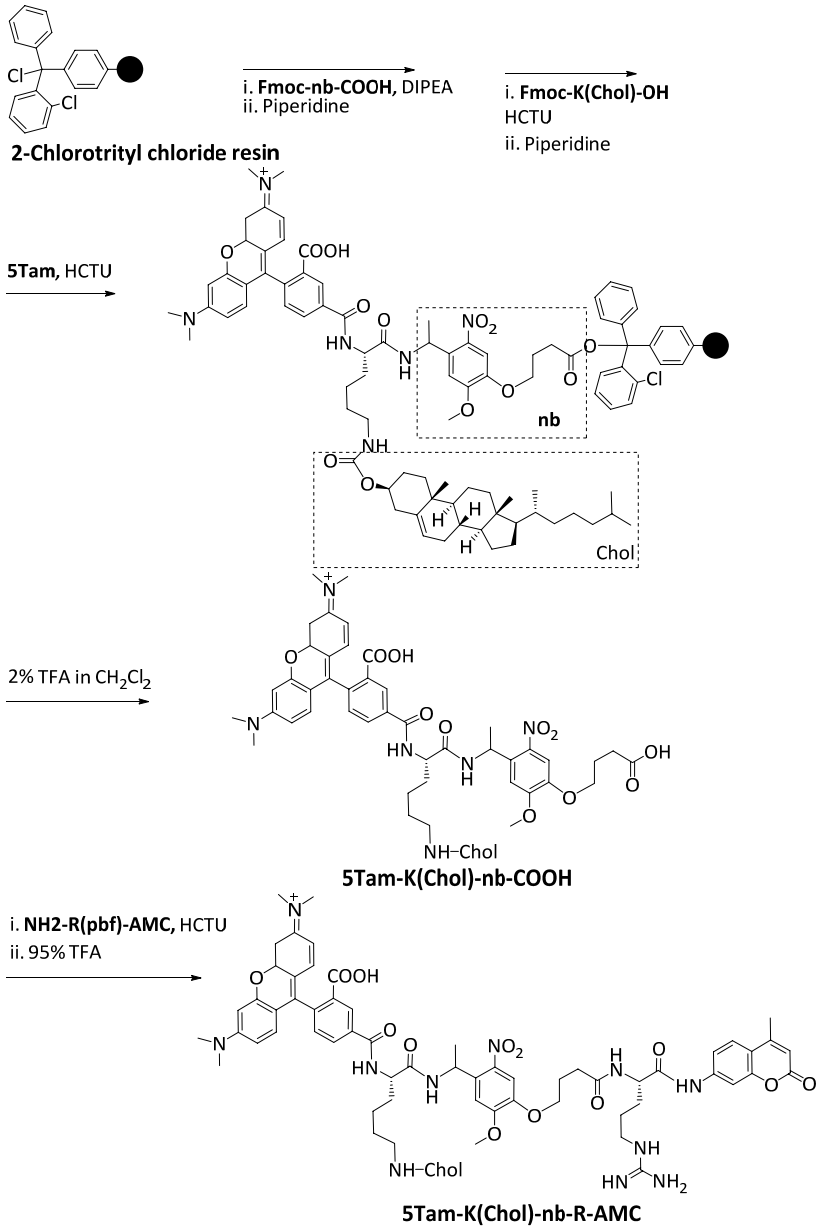

Scheme 4.6: Synthesis of 5Tam-K(Chol)-nb-R-AMC.

5Tam-K(Chol)-bn-COOH was synthesized on resin using 2-chlorotrityl chloride resin (Novabiochem). Briefly, **Fmoc-nb-COOH** (1.2 eq.) was dissolved in dried CH_2Cl_2 (with the help of a small amount of dried DMF). This solution was then added to the 2-chlorotrityl chloride resin (1 eq.) followed by the addition of DIPEA (5 eq.). The reaction was then shaken at room temperature for 2 h. Fmoc were removed by piperidine (25% in DMF, 3 times, 10 min each). Fmoc-K(chol)-OH was coupled using amino acid (3 eq.), HCTU (2.95 eq.), and DIPEA (10 eq.) in DMF (with a small amount of CH_2Cl_2) for 4 h. 5Tam was coupled using 5Tam (1.5 eq.), HCTU (1.5 eq.), and DIPEA (10 eq.) in DMF for 4 h. **5Tam-K(Chol)-bn-COOH** was cleaved off the resin using 2% TFA and 5% TIS in CH_2Cl_2. Following the neutralization of TFA with DIPEA, CH_2Cl_2 was removed and the residue was purified by flash chromatography using C18 column and H_2O:MeOH gradient containing 0.1 % TFA to afford **5Tam-K(Chol)-bn-COOH**. $C_{72}H_{95}N_6O_{13}^+$, exact mass calculated $(M)^+$ 1251.7, found (ESI+, m/z) 1251.8 $(M)^+$.

5Tam-K(Chol)-bn-COOH (1 eq.) was coupled to **NH_2-R(pbf)-AMC** in DMF using **NH_2-R(pbf)-AMC** (1.5 eq.), HCTU (1.1 eq.), and DIPEA (10 eq.) for 30 min followed by water precipitation and extraction with CH_2Cl_2. The organic extract was washed with H_2O three times, dried, and treated with TFA:TIS:H_2O = 95:2.5:2.5 for 1 h followed by another cycle of water precipitation and extraction with CH_2Cl_2. The organic phase was washed with H_2O 3 times, dried and purified on C4 column afforded **5Tam-K(Chol)-bn-R-AMC.** $C_{88}H_{114}N_{11}O_{15}^+$, exact mass calculated $(M)^+$ 1564.8, found (ESI+, m/z) 783.2 $(M + H)^{2+}$.

*Synthesis of **5Tam-K(Stear)-nb-R-AMC***

5Tam-K(Stear)-nb-COOH was synthesized on resin using 2-chlorotrityl chloride resin (Novabiochem, **Fmoc-nb-COOH** (1.2 eq.) was dissolved in dried CH_2Cl_2 (with the help

of a small amount of dried DMF). This solution was then added to the 2-chlorotrityl chloride resin (1 eq.) followed by the addition of DIPEA (5 eq.). The reaction was then shaken at room temperature for 2 h. Following Fmoc removal with piperidine (25% in DMF, 3 times, 10 min each), Fmoc-K(ivDde)-OH (5 eq.) was coupled using HCTU (4.9 eq.) and DIPEA (10 eq.) in DMF for 1 h. 5Tam (1.5 eq.) was coupled using HCTU (1.5 eq.) and DIPEA (10 eq.) in DMF for 4 h. The ivDde protecting group was then removed (2% hydrazine in DMF, 5 min, 5 times) and stearic acid (10 eq.) was coupled using HCTU (9.5 eq.) and DIPEA (20 eq.) for 2 h. **5Tam-K(Stear)-nb-COOH** was cleaved off the resin using 2% TFA and 5% TIS in CH_2Cl_2. Following the neutralization of TFA with DIPEA, CH_2Cl_2 was removed and the residue was purified by reverse phase chromatography using H_2O:MeOH gradient containing 0.1 % TFA. **5Tam-K(Stear)-nb-COOH**, $C_{62}H_{85}N_6O_{12}^+$, exact mass calculated $(M)^+$ 1105.6, found (ESI+, m/z) 1105.7 $(M)^+$, 553.5 $(M+H)^{2+}$.

5Tam-K(Stear)-nb-COOH (1 eq.) was coupled to NH_2-R(pbf)-AMC (1.5 eq.) in DMF using HCTU (1.1 eq.) and DIPEA (10 eq.), for 30 min, followed by water precipitation and extraction with CH_2Cl_2. The organic extract was washed with H_2O three times, dried and roughly purified by C18 reverse phase flash chromatography using H_2O:MeOH with 0.1% of TFA solvent system. The formation of **5Tam-K(Stear)-nb-R(pbf)-AMC** was confirmed by LC-MS. **5Tam-K(Stear)-nb-R(pbf)-AMC**, $C_{91}H_{120}N_{11}O_{17}S^+$, exact mass calculated $(M)^+$ 1670.9, found (ESI+, m/z) 836.0 $(M+H)^{2+}$.

The fraction containing **5Tam-K(Stear)-nb-R(pbf)-AMC** was dried and treated with TFA:TIS:H_2O = 95:2.5:2.5 for 1 h. The reaction was then dried and the residue was purified purified on C4 column to yield **5Tam-K(Stear)-nb-R-AMC**. $C_{78}H_{105}N_{11}O_{14}^{2+}$, exact mass calculated 1419.8, found (ESI+, m/z) 1418.9 $(M-H)^+$, 710.2 $(M)^{2+}$.

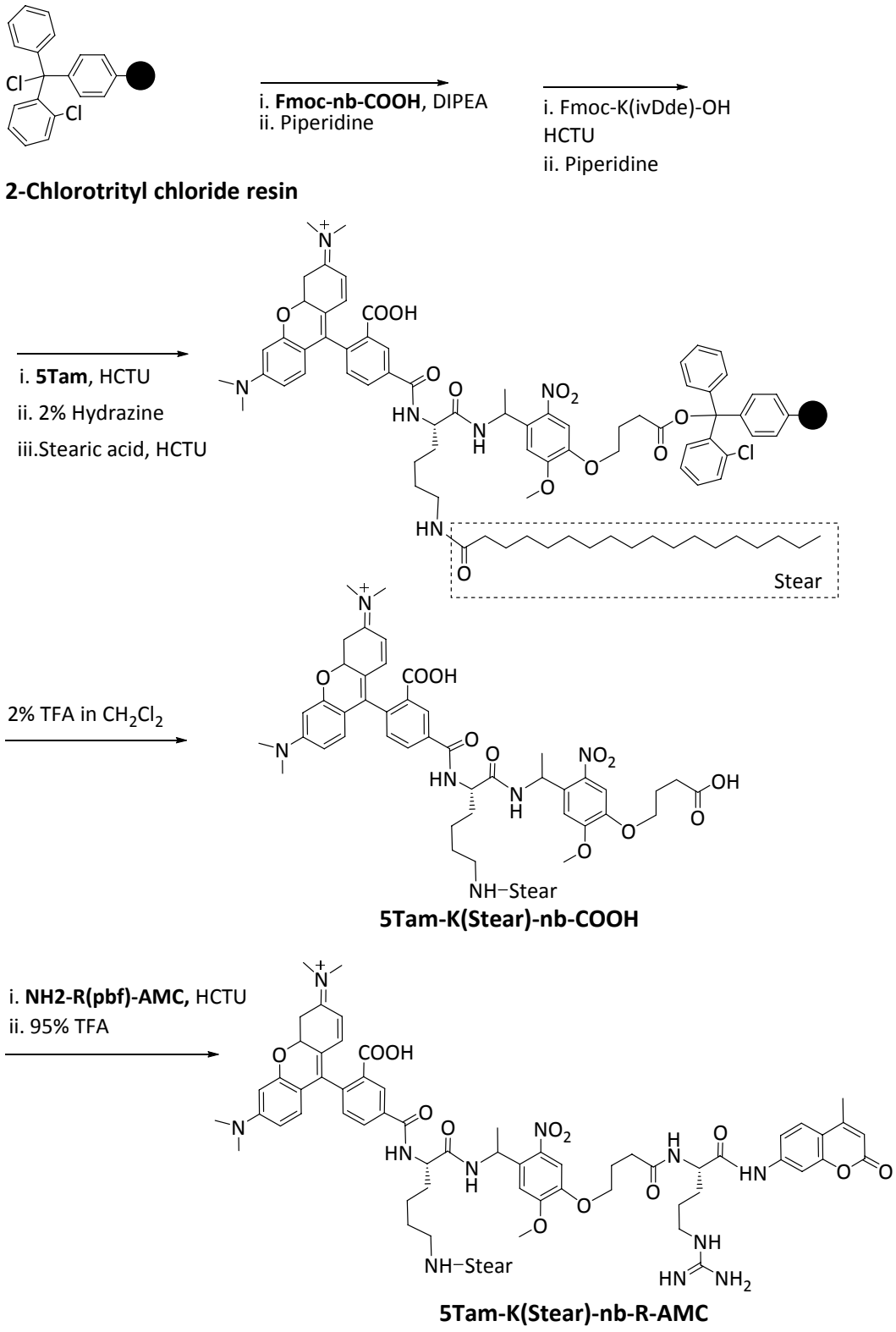

Scheme 4.7: Synthesis of 5Tam-K(Stear)-nb-R-AMC.

*Synthesis of **5Tam-EEK(Stear)-nb-R-AMC** and **5Tam-EEK(Chol)-nb-R-AMC***

5Tam-EEK(Stear)-nb-R-AMC and **5Tam-EEK(Chol)-nb-R-AMC** were synthesized following procedures similar to that of **5Tam-K(Stear)-nb-R-AMC** and **5Tam-K(Chol)-nb-R-AMC**, respectively, except that the two glutamate residues were coupled to the peptide before the coupling of 5Tam. Glutamate residues were coupled to the peptide using Fmoc-Glu(OtBu)-OH (5 eq.), HCTU (4.9 eq.), DIPEA (10 eq.), 1 h coupling. **5Tam-EEK(Stear)-nb-R-AMC**, $C_{88}H_{117}N_{13}O_{20}$, exact calculated mass 1675.9, found (ESI+, m/z) 839.3 $(M+2H)^{2+}$, **5Tam-EEK(Chol)-nb-R-AMC**, $C_{98}H_{127}N_{13}O_{21}$, exact calculated mass 1821.9, found (ESI+, m/z) 912.2 $(M+2H)^{2+}$.

*Synthesis of **C12-bn-PKA***

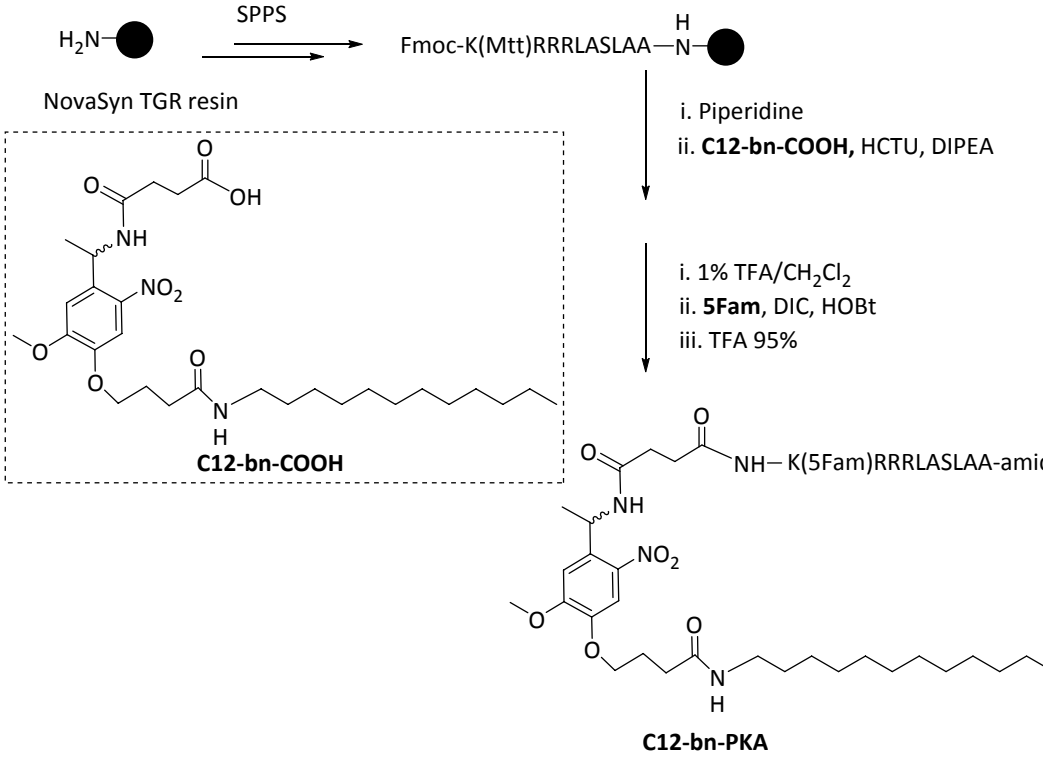

Scheme 4.8: Synthesis of **C12-bn-PKA**.

*Synthesis of **C12-bn-COOH***

Procedure used to synthesize **C18-bn-COOH** was applied to synthesized **C12-bn-COOH**, in which dodecylamine was used instead of octadecylamine. **C12-bn-COOH**: ^{1}H NMR (400 MHz, DMSO-d_6) δ 8.56 (d, *J* = 7.6 Hz, 1 H), 7.82 (t, *J* = 5.4 Hz, 1 H), 7.48 (s, 1 H), 7.17 (s,1 H), 5.35 (quin, *J* = 6.8 – 7.2 Hz, 1 H), 4.02 (t, *J* = 6.4 Hz, 2 H), 3.92 (s, 3 H), 3.02 (q, *J* = 6.0 – 6.8 Hz, 2 H), 2.42-2.32 (comp, 4 H), 2.22 (t, *J* = 7.4 Hz, 2 H), 1.94 (quin, *J* = 6.0 – 7.2 Hz, 2 H), 1.38 (d, *J* = 7.2 Hz, 3 H), 1.36 (comp, 2H), 1.23 (comp, 18 - 20 H), 0.86 (t, *J* = 6.8 Hz, 3 H); $C_{29}H_{47}N_3O_8$, exact mass calculated (M) 565.34, found (ESI+, m/z) 566.3 $(M + H)^+$, 588.3 $(M + Na)^+$.

*Synthesis of **C12-bn-PKA***

Fmoc-K(Mtt)RRRLASLAA, was synthesized on a NovaSyn TGR resin using SSPPS. The Fmoc group was deprotected by piperidine (25%) in DMF followed by coupling of **C12-bn-COOH** (5 eq.), HCTU (4.9 eq.), and DIPEA (10 eq.) in DMF for 4 h. The Mtt was removed with 1% TFA in CH_2Cl_2 followed by coupling 5Fam using 5Fam (1.5 eq.), *N,N'*-diisopropylcarbodiimide (DIC, 1.7 eq.), and 1-hydroxybenzotriazole (HOBt, 10 eq.) in DMF for 2 h. The resin was treated with piperidine then dried. The peptide was then cleaved from the resin with TFA: H_2O:Triisopropylsilane in a ratio of 95:2.5:2.5, and purified by HPLC on C18 using H_2O:CH_3CN with 0.1% TFA to afford **C12-bn-PKA**. $C_{98}H_{148}N_{24}O_{24}$, exact mass calculated (M) 2045.11, found (ESI+, m/z) 1024.1 $(M + 2H)^{2+}$, 683.0 $(M + 3H)^{3+}$, 512.5 $(M + 4H)^{4+}$.

Synthesis of ***Mal-anp-K(5Tam)RRRLAALAA-amide***

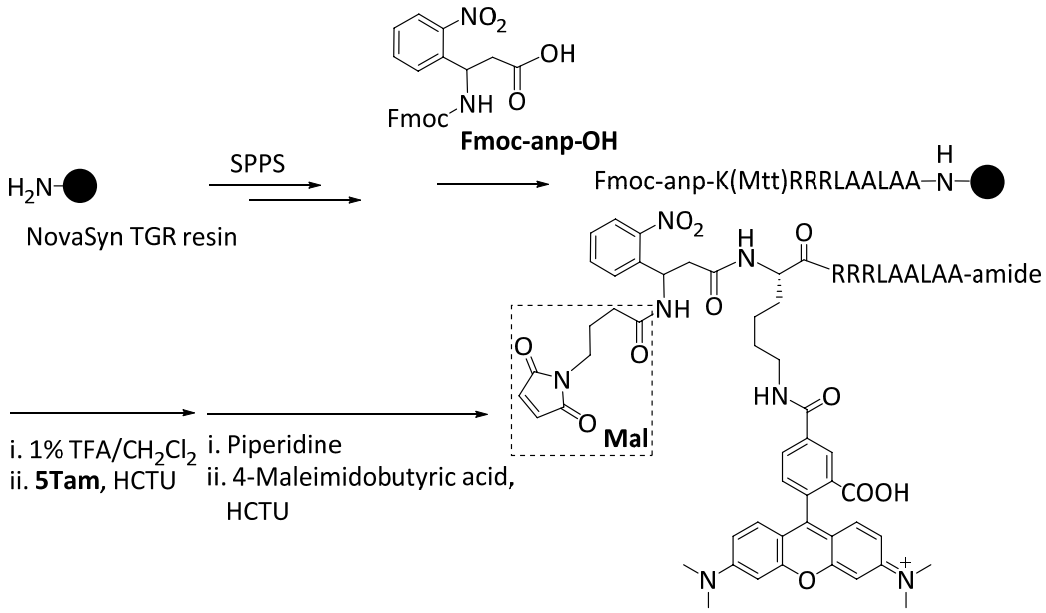

Scheme 4.9: Synthesis of Mal-anp-K(5Tam)RRRLAALAA-amide.

Fmoc-anp-K(Mtt)RRRLAALAA sequence was synsthesized on resin using Fmoc-protected amino acids (amino acids 3 eq., HCTU 2.95 eq., DIPEA 10 eq. in DMF, double coupling in 20 and 40 min). Fmoc deprotection was performed using piperidine (25%) in DMF (3 times, 10 min each). The lysine residue is side chain protected with the acid sensitive 4-methyltrityl group (Mtt). The Mtt group was deprotected with 1% of TFA in CH_2Cl_2 followed by coupling of 5Tam fluorophore using 5Tam (1.5 eq.), HCTU (1.5 eq.), and DIPEA (10 eq.) in DMF for 4 h. The Fmoc protecting group was then deprotected with piperidine (25%) followed by coupling of 4-maleimidobutyric acid (carboxylic acid 5 eq., HCTU 4.9 eq., DIPEA 10 eq. in DMF, 1 h coupling). The peptide was then cleaved from the resin with TFA:H_2O:TIS in a ratio of 95:2.5:2.5 (by volume), and purified by HPLC using H_2O:CH_3CN with 0.1% TFA to yield **Mal-anp-K(5Tam)RRRLAALAA-amide**. $C_{90}H_{129}N_{26}O_{20}^+$, Exact mass calculated $(M)^+$ 1894.0, found (ESI+, m/z) 948.1 $(M+H)^{2+}$, 632.2 $(M+2H)^{3+}$, 474.4 $(M+3H)^{4+}$.

*Synthesis of **Cys-Hex1-Cys and Cys-Hex2-Cys***

Cys-Hex1-Cys 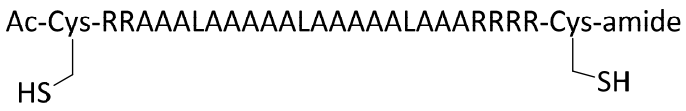

Cys-Hex2-Cys 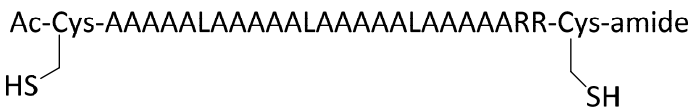

Cys-Hex1-Cys and **Cys-Hex2-Cys** were synthesized on NovaPEG Rink Amide resin and DMF solvent. The first Cys amino acid was coupled to NovaPEG Rink Amide resin (1 eq.) using Fmoc-Cys(Trt)-OH (8 eq.) 3.5 min-preactivated with HOBt (16 eq.) and DIC (8 eq.), 1 h coupling. Other amino acids were coupled using amino acid (4 eq.), HCTU (3.92 eq.), and DIPEA (10 eq.), double coupling for 20 and 40 min. Deprotection was accomplished by treatment with piperidine (25%) in DMF for 30 min. Acetylation was performed using acetic anhydride (10 eq.) and DIPEA (25 eq.) for 30 min. After the acetylation step, the peptides were cleaved off the resin using mixture TFA:TIS:H_2O = 95:2.5:2.5 (by volume). The formation of peptides was confirmed by LC-MS. Crude peptide was dried and stored for further synthesis. **Cys-Hex1-Cys**, $C_{110}H_{200}N_{46}O_{28}S_2$, exact mass calculated (M) 2677.5, found (ESI+, m/z) 894.0 $(M+3H)^{3+}$, 670.8 $(M+4H)^{4+}$, 536.7 $(M+5H)^{5+}$, 447.5 $(M+6H)^{6+}$. **Cys-Hex2-Cys**, $C_{98}H_{172}N_{34}O_{28}S_2$, exact mass calculated (M) 2337.3, found (ESI+, m/z) 1170.2 $M+2H)^{2+}$, 780.3 $(M+3H)^{3+}$.

*Synthesis of **P-H1-P** and **P-H2-P***

Mal-anp-K(5Tam)RRRLAALAA-amide was dissolved in PBS 1X solution containing EDTA (10 mM) to which crude **Cys-Hex1-Cys** or **Cys-Hex2-Cys** (dissolved in DMF right before the reaction) was slowly added. The reaction was followed by LC-MS until no **Mal-anp-K(5Tam)RRRLAALAA-amide** was detected. The reaction mixtures were then purified by HPLC [C18 column, CH_3CN:H_2O gradient containing TFA (0.1%)]. **P-H1-P**,

$C_{290}H_{458}N_{98}O_{68}S_2^{2+}$, exact mass calculated $(M)^{2+}$ 6465.5, found (ESI+, m/z) 1078.7 $(M+4H)^{6+}$, 924.7 $(M+5H)^{7+}$, 809.3 $(M+6H)^{8+}$, 719.5 $(M+7H)^{9+}$, 647.7 $(M+8H)^{10+}$, 588.9 $(M+9H)^{11+}$, 539.9 $(M+10H)^{12+}$. **P-H2-P**, $C_{278}H_{430}N_{86}O_{68}S_2^{2+}$, exact mass calculated $(M)^{2+}$ 6125.2, found (ESI+, m/z) 1022.0 $(M+4H)^{6+}$, 876.2 $(M+5H)^{7+}$, 766.8 $(M+6H)^{8+}$, 681.7 $(M+7H)^{9+}$, 613.6 $(M+8H)^{10+}$.

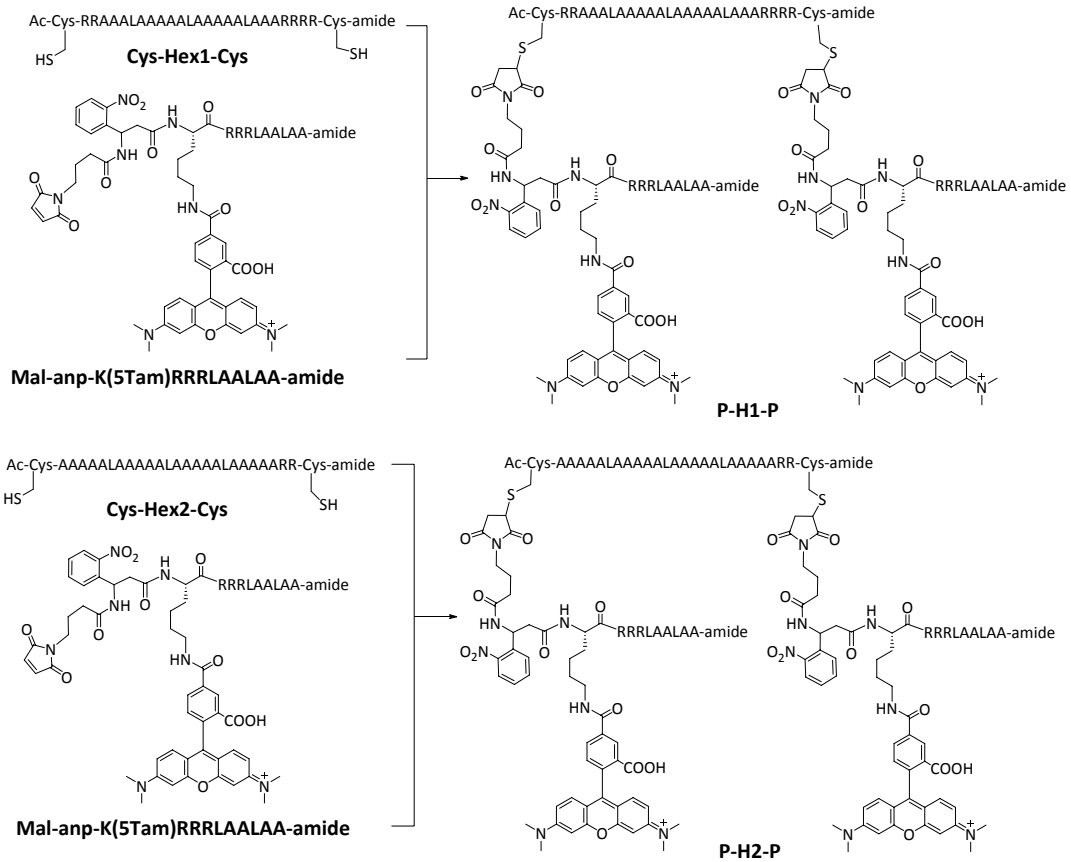

Scheme 4.10: Synthesis of P-H1-P and P-H2-P.

CHAPTER 5: ERYTHROCYTES AS CARRIERS FOR LIGHT-ACTIVATABLE THERAPEUTICS

Over the past few years, peptides have gained significant attention as drugs.[87] The ready availability of peptides as initial scaffolds for further modification accelerates the process of finding and optimizing peptides as potential drug candidates. Additionally, large peptide libraries, which can be conveniently produced both chemically and biochemically provide an alternative way to screen for new drugs. Peptides, however, possess poor oral availability, mainly due to their poor stability and poor intestinal adsorption. Intravenous administration, which delivers peptides directly into blood stream, is insufficient since peptides can be degraded by peptidases in plasma and cleared from blood stream by renal filtration. The bloodstream half-life of peptides is very short, typically a few minutes.

Significant effort has been put into extending the circulation time of peptides. Peptides have been rendered resistant to proteolytic processing by chemical substitution/intramolecular cyclization.[87] Confining peptide drugs within liposomes or nanoparticles to prevent them from being degraded and cleared before releasing them at the site of action is also an appealing approach.[88] Finally, both covalent and noncovalent conjugation of peptides to macromolecules such as polyethylene glycol or plasma proteins to stabilize them and prevent them from renal clearance have also been explored.[87, 89] These strategies, however, still have some limitations. For instance, making peptides resistant to peptidases, on one hand lengthens their circulation time, but on the other hand could potentially increase the toxicity since they can now have off-target

effects and accumulate in specific organs such as the kidney and liver. Liposome and nanoparticle carriers, in addition to toxicity, also potentially trigger immune response.

In this Chapter, we report the results of an on-going project to stabilize and photodeliver peptide therapeutics using erythrocytes as carriers. Sequestration of peptide therapeutics to the erythrocyte membranes by lipidation protects them from proteolysis. Insertion of a photolabile linker between the lipid anchor and peptide drugs furnishes the means to control the release of active drug using light.

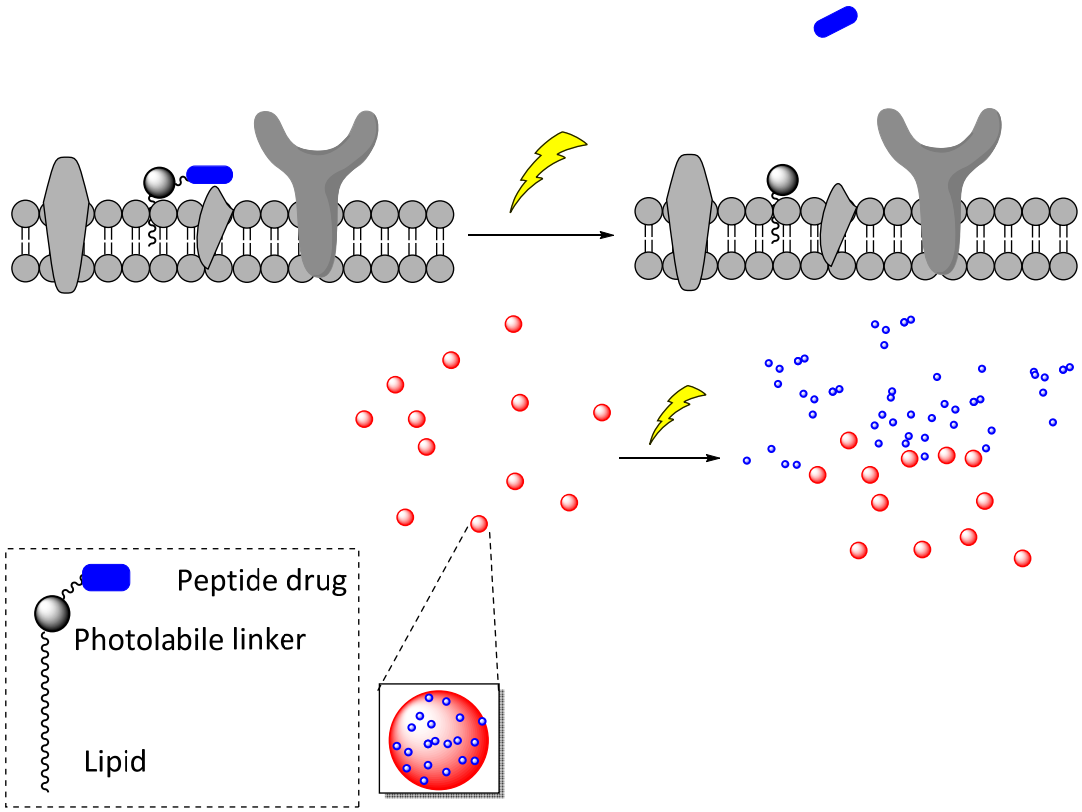

Figure 5.1: General strategy of delivery peptide drug using erythrocytes as carriers.

Results and Discussion

Studies of CP-nb-Stear

We first investigated if a cell permeable peptide can be kept from entering cells by sequestration to the cell membrane of erythrocytes, followed by controlled release with

light using a photolabile group. This would represent an appealing strategy to selectively deliver potent cell-permeable drugs to a specific location. Based on Dr. Melanie Priestman's observation that the peptide 5Tam-Aoc-GRTGRRFSY-amide was taken up by HeLa cells, a lipidated version of this peptide was synthesized, **CP-nb-Stear** (Figure 5.2). A stearoyl moiety was appended to the peptide's C-terminal to facilitate membrane binding. A 2-nitrobenzyl photolabile linker (**nb**) was inserted between the peptide and lipid to furnish a means to release the peptide from the membrane in a light-dependent fashion. The fluorophore 5Tam is attached to the peptide's N-terminal to allow degradation detection by fluorescence (Figure 5.2). Photolysis of **CP-nb-Stear** produced peptide 5Tam-Aoc-GRTGRRFYS-amide (Figure 5.2, 5.3).

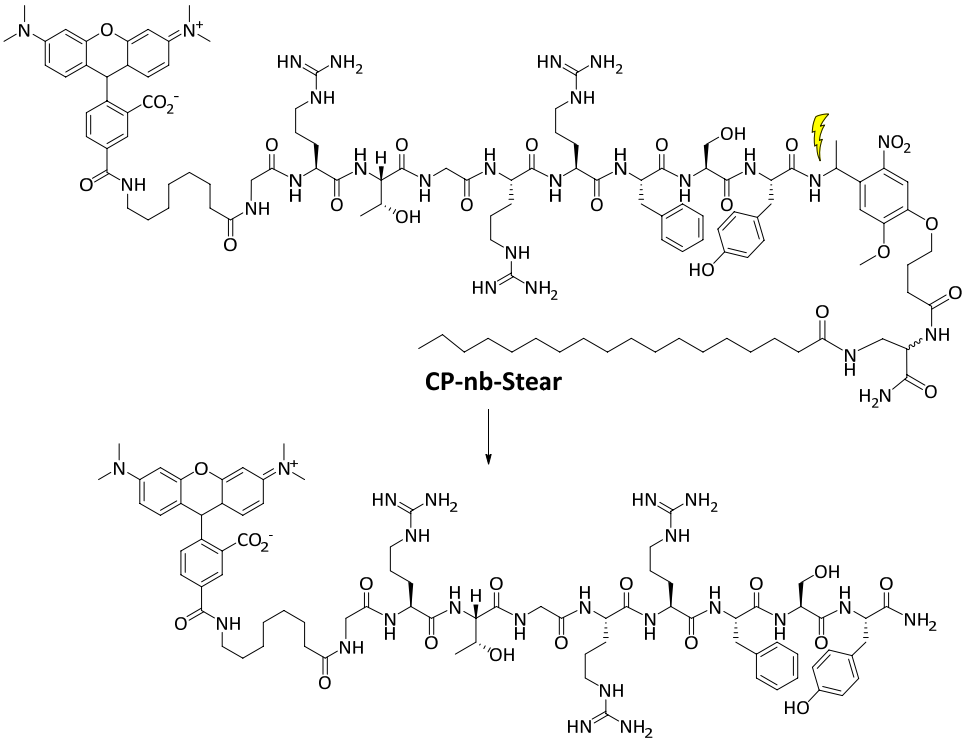

CP-nb-Stear

5Tam-Aoc-GRTGRRFSY-amide

Figure 5.2: Structures of cell-permeable peptide 5Tam-Aoc-GRTGRRFSY-amide and its photolabile lipidated counterpart CP-nb-Stear.

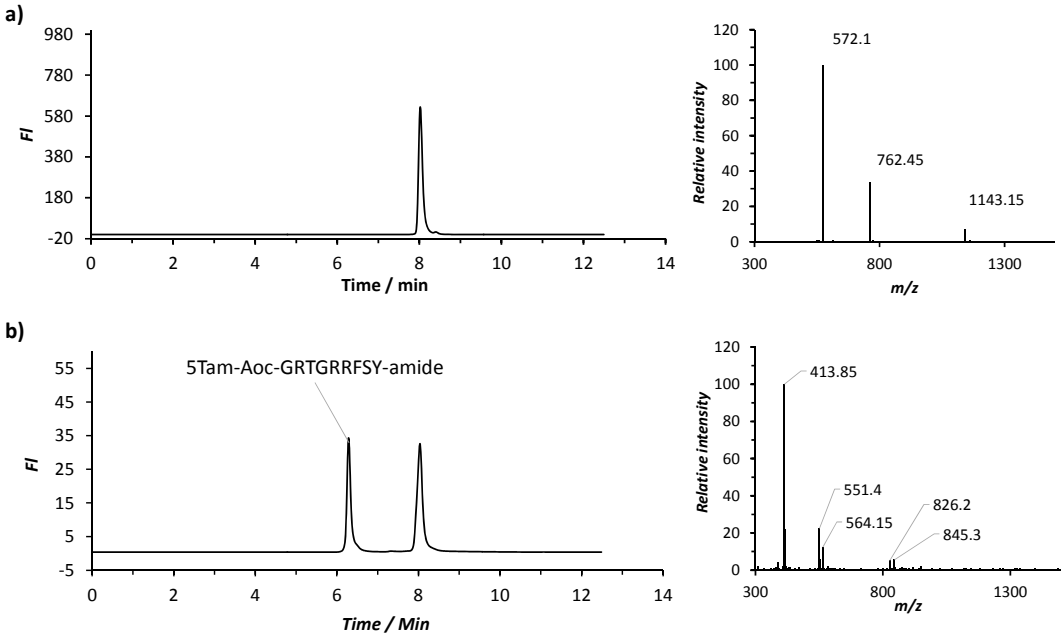

Figure 5.3: LC-MS analysis of **CP-nb-Stear** before (a) and after (b) 2 min photolysis. PBS 1X (200 µL) containing **CP-nb-Stear** (2.1 µM) was photolyzed for 3 min using a Hg-Arc lamp with 360 nm bandpass filter. Left: fluorescence traces; right: ESI+ mass data of the peak in the left.

Though protection from proteolysis was confirmed when **CP-nb-Stear** was bound to erythrocyte membranes (Figure 5.4), significant transfer of the peptide from the erythrocyte to HeLa cells in the absence of UV light is also observed (Figure 5.5). This observation together with the noticeable residual degradation of the peptide in the presence of erythrocyte without light is consistent with the hypothesis that the peptide dissociates from membrane-bound state. When the peptide is free in solution, it can associate with HeLa cells and/or be processed by proteases in solution.

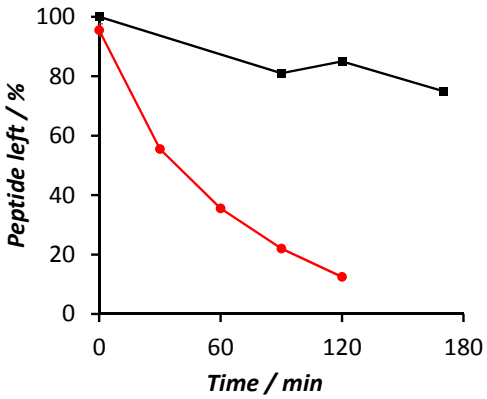

Figure 5.4: Degradation of 5Tam-Aoc-GRTGRRFSY-amide (red) and **CP-nb-Stear** (black) in human plasma (5% in PBS 1X) in the presence of erythrocytes as assessed by LC-MS coupled to a fluorescence detector. Peptide concentration is 2.5 µM. See Materials and Method for details.

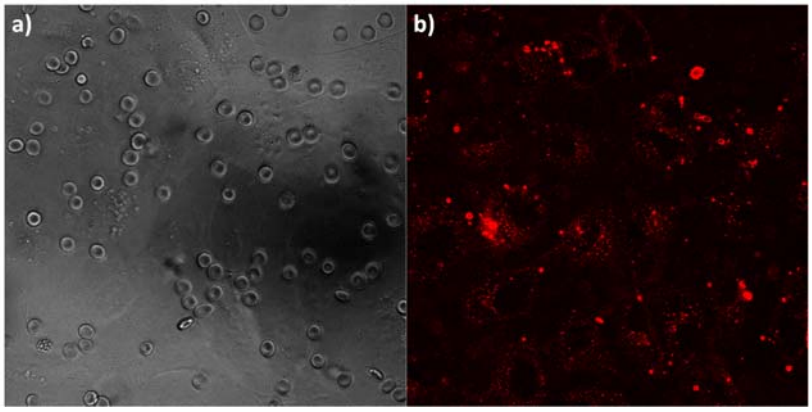

Figure 5.5: Transfer of erythrocyte-bound **CP-nb-Stear** to HeLa cells upon incubation in the absence of UV light. (a) DIC image, (b) Fluorescence image.

Study with Phospholipid-Conjugated Peptide

Construction of Phospholipid-Conjugated Counterpart of 5Tam-Aoc-GRTGRRFSY-amide

We investigate if increasing the hydrophobicity of the lipid anchor prevents the membrane-bound peptide from transferring between cells and undergoing proteolysis in the dark. A phospholipid appended maleimide, **Dipal-Mal**, was synthesized (Figure 5.6).

The maleimide group provides a convenient way of conjugating the phospholipid to any peptide with a free thiol residue (Figure 5.6).

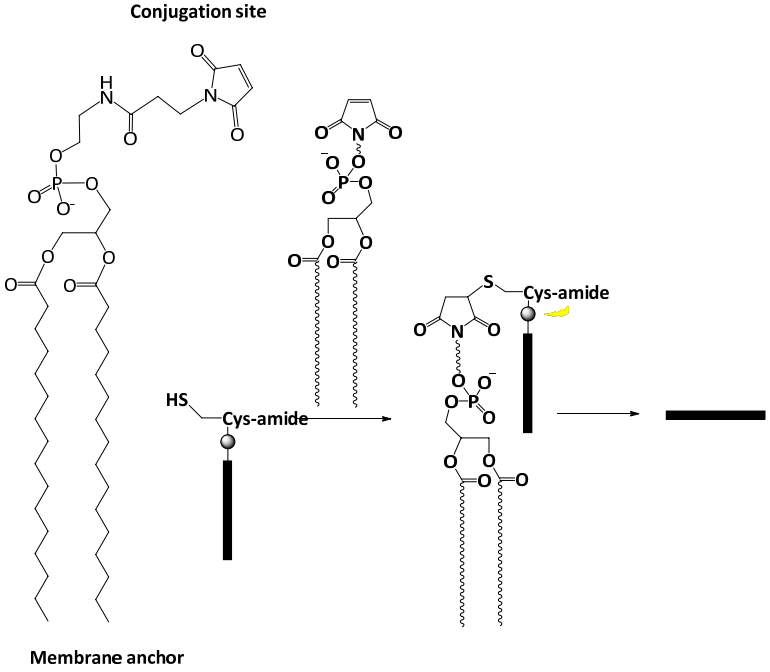

Figure 5.6: General strategy of synthesis phospholipid-conjugate peptide.

With this strategy of construction, we synthesized peptide **CP-nb-Dipal** (Figure 5.7a). Formation of the conjugated peptide was confirmed by LC-MS. Photolysis of **CP-nb-Dipal** produced the cell-permeable peptide **5Tam-Aoc-GRTGRRFSY-amide** (Figure 5.7).

As expected, in the absence of UV light, peptide transfer from erythrocytes to HeLa cells was not detected when erythrocytes loaded with **CP-nb-Dipal** are incubated with HeLa cells. Upon photolysis with UV light, the peptide 5Tam-Aoc-GRTGRRFSY-amide is cleaved from erythrocyte membrane and readily taken up by HeLa cells (Figure 5.8).

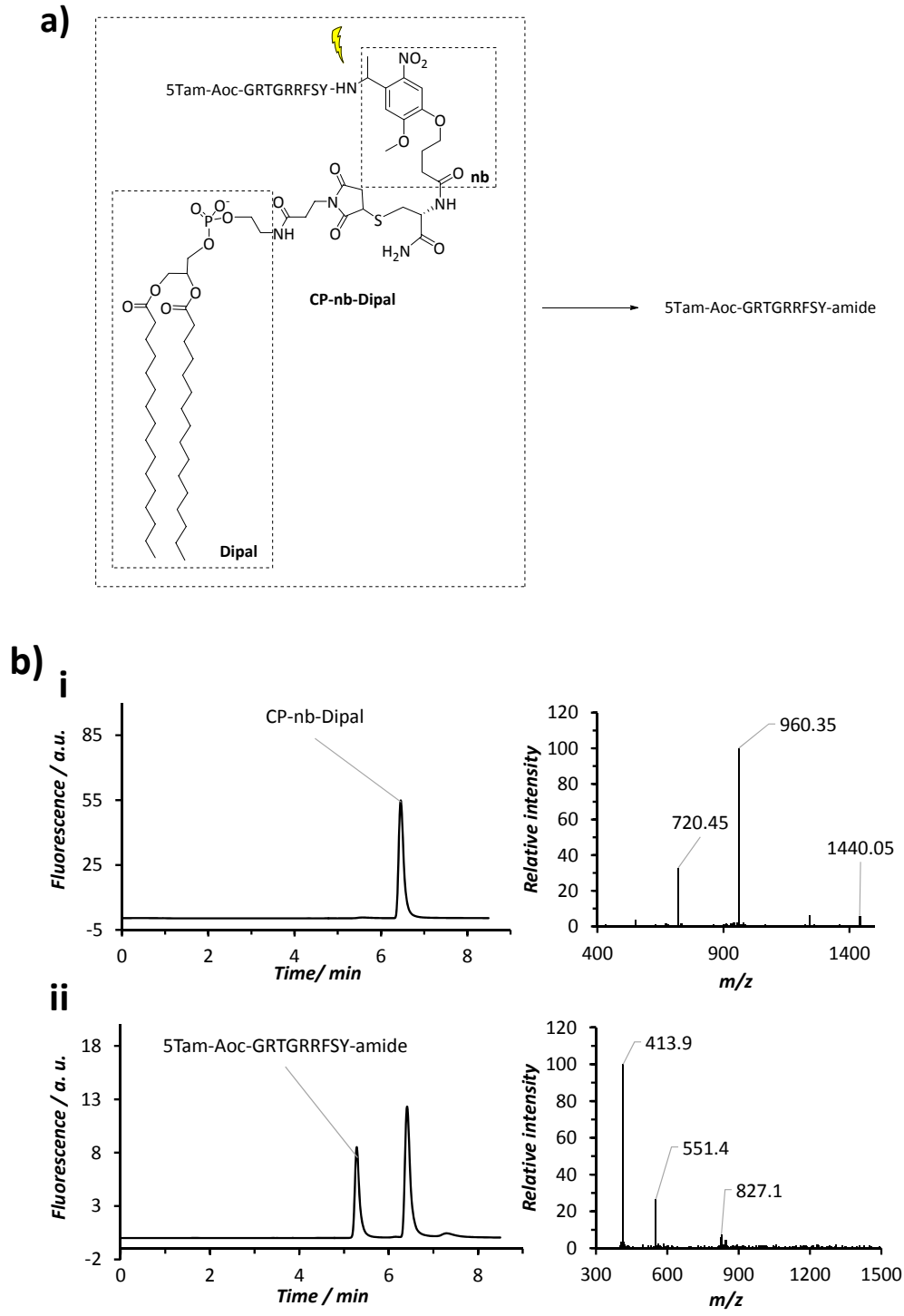

Figure 5.7: Photolysis of **CP-nb-Dipal** as assessed by LC-MS. Structure of **CP-nb-Dipal** and its photolyzed product (a), LC-MS of **CP-nb-Dipal** before (i) and after photolysis (ii). **CP-nb-Dipal** (1 µM) in water (200 µL) was photolyzed using a Hg-Arc lamp and a 360 nm bandpass filter.

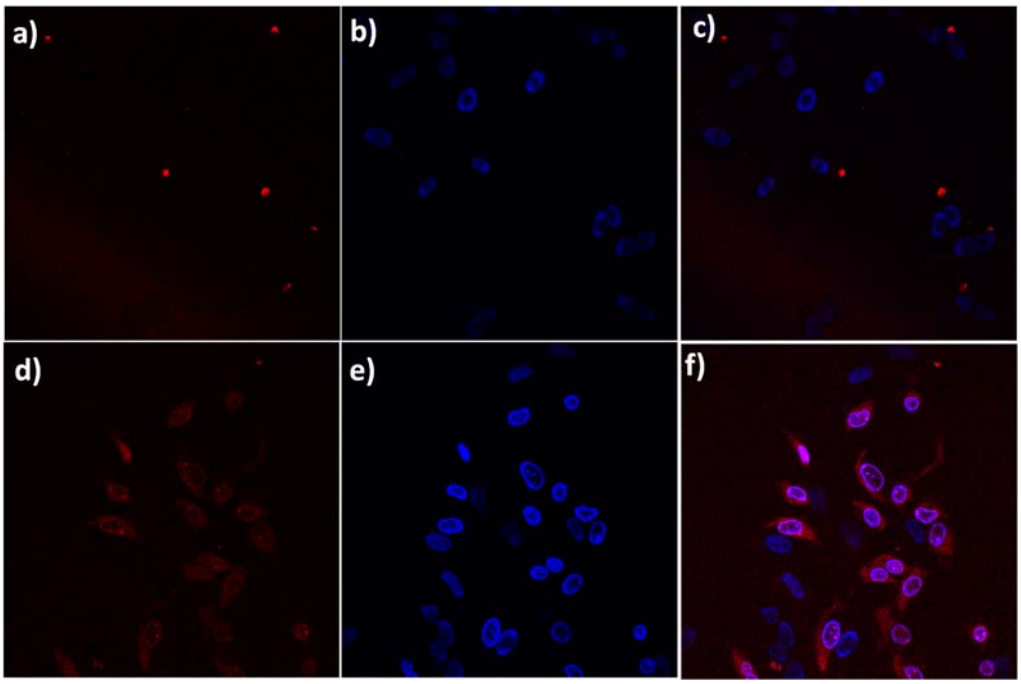

Figure 5.8: Study of hemoglobin-free erythrocytes loaded with CP-nb-Dipal and HeLa cells with and without photolysis. Confocal images of HeLa cells after incubating with erythrocytes loaded with CP-nb-Dipal peptide in the presence and absence of UV light. (a, d) 5Tam fluorescence; b, e) Hoechst 33342 fluorescence; (c, f) overlay. (a, b, c) no UV light; d, e, f) 30-minute UV photolysis using a Hg-Arc lamp and a 360 nm bandpass filter.

Furthermore, **CP-nb-Dipal** was protected from degradation by trypsin (1 nM) and chymotrypsin (5 nM) when bound to erythrocytes, whereas the nonlipidated counterpart was completely processed after few mininutes of incubation under the same conditions (Figure 5.9). When the concentration of trypsin was increased to 5 nM, detectable degradation of the phospholipid-conjugated peptide was observed even in the presence of erythrocytes and without UV light. However, under these conditions, the protein layer covering erythrocyte membrane might be compromised due to proteolysis.

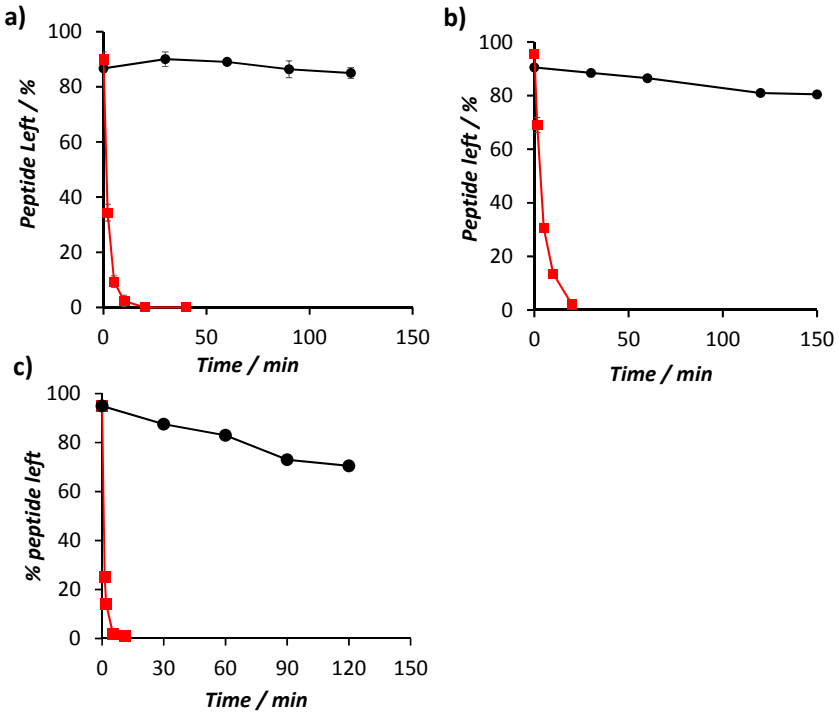

Figure 5.9: Degradation of 5Tam-Aoc-GRTGRRFSY-amide (red) and CP-nb-Dipal (black) by chymotrypsin and trypsin in the presence of hemoglobin-free erythrocytes. (a) Chymotrypsin (5 nM), (b) trypsin (1 nM), and (c) trypsin (5 nM). Corresponding peptide concentration (1.25 µM) in 5% hematocrit.

Study with Phospholipid-Conjugated Alpha-Melanocyte-Stimulating Hormone (α-MSH)

We also examined protection and activation of alpha-melanocyte-stimulating hormone (α-MSH) using the membrane sequestration strategy. There is compelling data suggesting that α-MSH will be a potent anti-inflammatory agent.[90-93] α-MSH affects various pathways regulating inflammatory responses such as NF-κB activation, expression of adhesion molecules and chemokine receptors, production of pro-inflammatory cytokines and other mediators. The anti-inflammatory effects of alpha-MSH have been confirmed in a variety of animal models of inflammation (e.g., vasculitis, fibrosis, uveitis, inflammatory bowel disease, rheumatoid arthritis, brain inflammation, etc.).[92, 93] The peptide, however, has a short half-life in blood circulation due to renal clearance and

proteolytic degradation.[94] Prolylcarboxypeptidase (PRCP) was identified as an enzyme which removes α-MSH's C-terminal Val residue and inactivates the hormone.[95] While stabilization of the hormone against peptidase degradation by cyclization and chemical modification has been extensively studied,[96-98] the physiological consequences of such stabilization *in vivo* remain to be explored. Protection by membrane sequestration and release by light could be beneficial since the hormone could be controllably activated at a specific site.

We synthesized 5Fam-labeled lipidated α-MSH, **MSH-nb-Dipal** (Figure 5.10a) via thiol-maleimide conjugation. LC-MS analysis demonstrated the formation of **MSH-nb-Dipal**. Photolysis with UV light generated 5Fam-labelled α-MSH from the lipidated counterpart (Figure 5.10b).

Stability of α-MSH and Fluorophore-Labelled α-MSH toward PRCP Enzyme

We performed a control experiment to confirm the degradation of α-MSH by PRCP enzyme. The recombinant human lysosomal Pro-X carboxypeptidase/PRCP was purchased from R&D systems. To our surprise, however, we were unable to confirm degradation of the nonlipidated fluorophore-label hormone **5Fam-α-MSH** and native α-MSH, Ac-SYSMEHFRWGKPV-amide (Abcam), by the commercial PRCP (Figure 5.11). One explanation for this observation could be due to the difference of enzymes produced from different sources. It is also interesting to note that, for the dipeptide N-Carbobenzyloxy-Pro-Phe, the enzyme only recognizes it as a substrate if the peptide's C-terminus is a COOH group. The same sequence bearing a methyl ester or an amide group at the C-terminus was not hydrolyzed by the enzyme.[99]

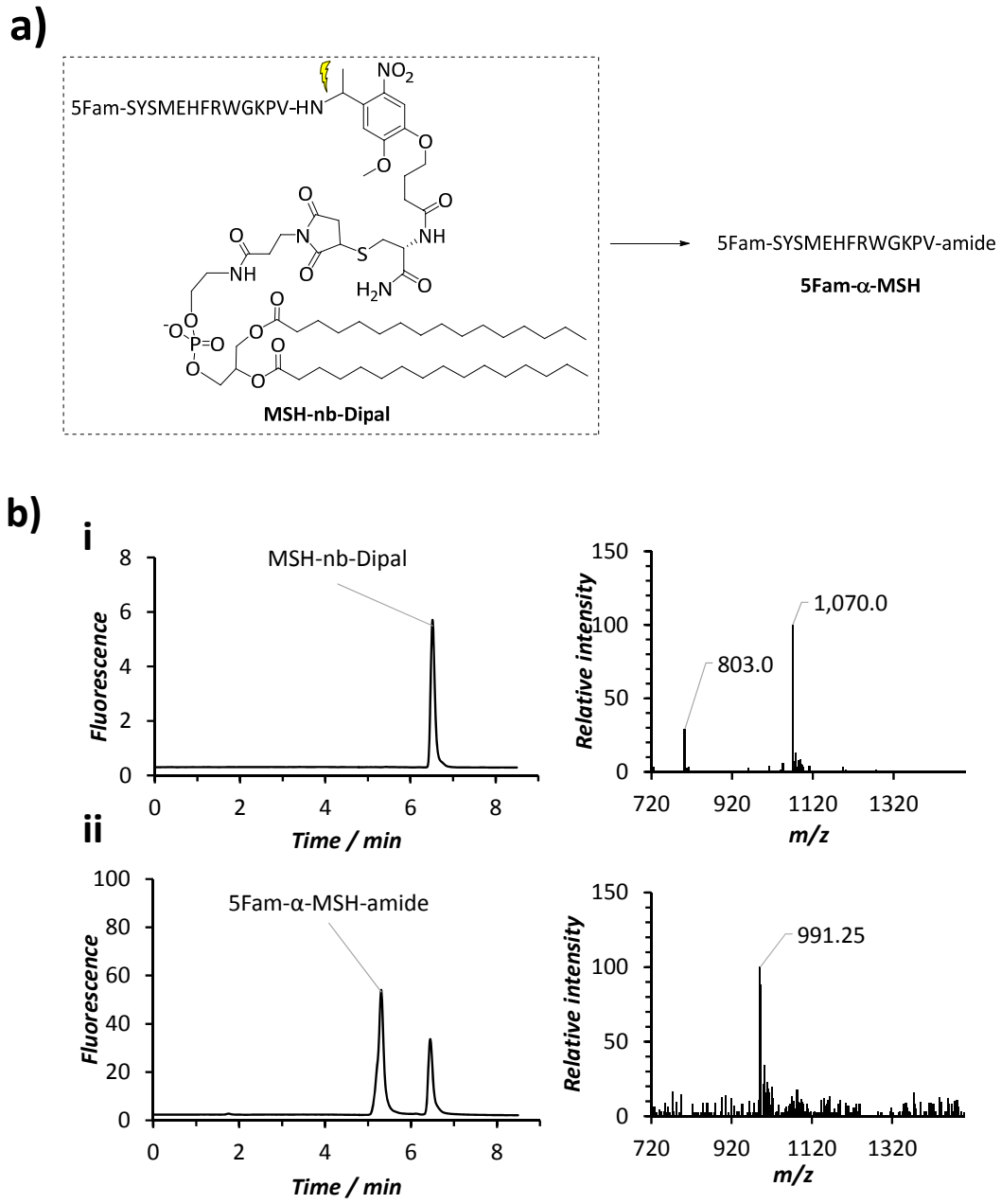

Figure 5.10: Photolysis of MSH-nb-Dipal as assessed by LC-MS. Structure of MSH-nb-Dipal and its photolyzed product (a), LC-MS of MSH-nb-Dipal before (i) and after 5 min photolysis (ii). MSH-nb-Dipal (1 µM) in water (200 µL) was photolyzed using a Hg-Arc lamp with a 360 nm bandpass filter.

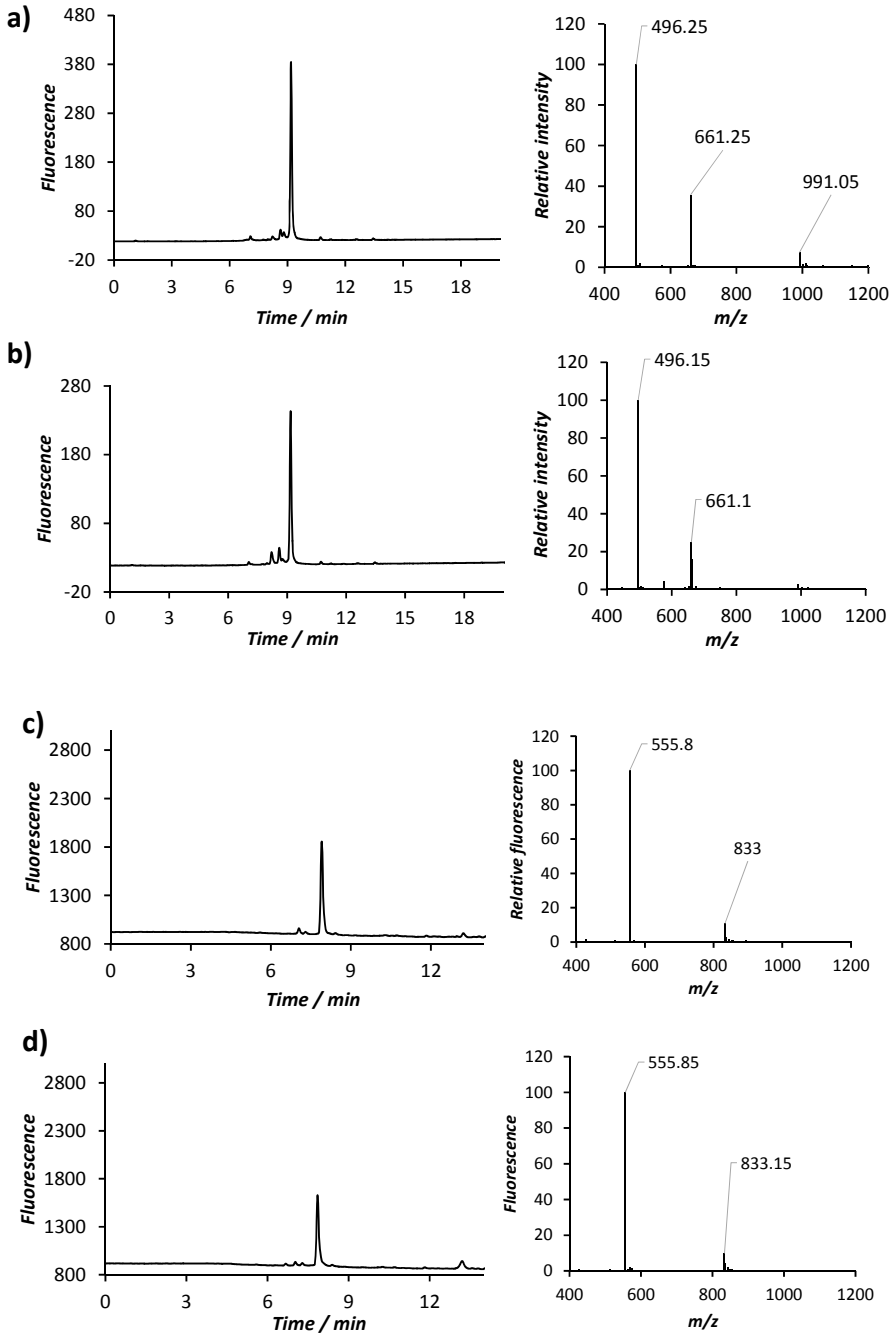

Figure 5.11: Stability of 5Fam-labelled and native α-MSH toward PRCP degradation as analyzed by LC-MS. (a) 5Fam-α-MSH control, (b) 5Fam-α-MSH after 30 min incubation with PRCP (20 nM, 37 ^{o}C), (c) Native α-MSH control, (d) 5Fam-α-MSH after 30 min incubation with PRCP (20 nM, 37 ^{o}C). Left: fluorescence trace, right: mass spectrum of the peak on the left trace. (a, b) monitored at (λ_{ex} - λ_{em}) 490nm - 525 nm; (c, d) monitored at 280 nm - 315 nm.

We also investigated the stability of **MSH-nb-Dipal**, against proteolysis when it was associated with erythrocytes. To our surprise, however, significant degradation was observed with trypsin, chymotrypsin, and plasmin even in the presence of erythrocytes and no photolysis (Figure 5.12). The peptide **C8-K(5Tam)-α-MSH-nb-Dipal** (see Scheme 5.5 page 151) was also synthesized in which a octanoyl group was appended the N-terminus to further facilitate the peptide-membrane association. Examination with chymotrypsin, however, shows that significant degradation of the peptide was still detected even in the presence of erythrocytes and absence of UV light. It is interesting to note that the thickness of erythrocytes' glycocalyx has been reported as about 5.9 nm.[100] The lipidated peptide was expected to be embedded within the glycocalyx and protected from proteolysis. These unexpected results are under further investigation.

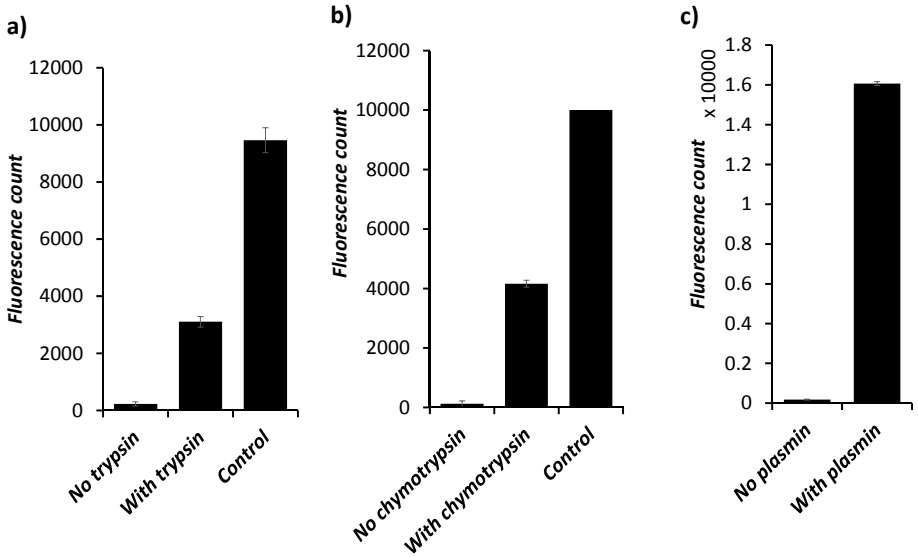

Figure 5.12: Degradation of MSH-nb-Dipal by (a) trypsin 5 nM, (b) chymotrypsin 5 nM, and (c) plasmin 40 nM in the presence of erythrocytes. Erythrocytes loaded with peptide MSH-nb-Dipal were incubated with the enzyme or without the enzyme at 37 ^{o}C. At t = 1 h (a, b), 0.5 h (c) the suspensions were centrifuged and supernatant's fluorescence measured. Control: fluorescence of supernatant when all of membrane bound peptide was cleaved. See Materials and Method for details.

Materials and Method

Reagents were purchased as described before (Chapter 2, 3, 4).

Hemoglobin-Free Erythrocyte Preparation

Peripheral human erythrocytes were washed with L-15 media upon receipt and stored in L-15 media containing FBS (10%) at 10% hematocrit. Hemoglobin-free erythrocyte ghosts were prepared fresh before all experiments. Briefly, the stored erythrocytes (1 mL) were washed with PBS 1X 3 times (1 mL PBS 1X, centrifuged at 2000 g for 2 min), followed by washes (five times) with PBS 0.1X (1 mL PBS 0.1X, centrifuged at 14,000 g for 2 min). The hemoglobin-free erythrocytes were then restored and kept in PBS 1X (1 mL) for 1 h, followed by three more washes with PBS 1X (1 mL PBS 1X, centrifuged at 10,000 g for 2 min) and suspended in PBS 1X (1 mL) for loading and further experiments.

Loading Lipidated Peptides on Hemoglobin-Free Erythrocytes

Lipidated peptide stock solution was predissolved in ethanol (10 μL). To this solution was then added hemoglobin-free erythrocytes in PBS 1X (1 mL, 10% hematocrit). The final peptide concentration was 2.5 μM. The solution was gently shaken at room temperature (30 min), followed by centrifugation (10,000 g for 2 min). The pellet was resuspended in PBS 1X (1 mL) and transferred to a new tube. The suspension was washed two more times with PBS 1X (1 mL, 10,000 g/2 min) and resuspended in PBS 1X (1 mL) to make hemoglobin-free peptide-loaded erythrocytes (1 mL, 10% hematocrit). All supernatants were collected for fluorescence measurement if needed.

Stability of 5Tam-Aoc-GRTGRRFSY-amide in the Presence of Human Plasma and Erythrocytes

Human plasma (solid form from 1 mL, Sigma) was dissolved in PBS 1X (1 mL). Erythrocytes were washed with PBS 1X three times.

PBS 1X solution (400 μL) containing 5Tam-Aoc-GRTGRRFSY-amide (final 2.5 μM) was preincubated at 37 ^{o}C for 10 min, followed by the addition of washed erythrocytes (100 μL, 100% hematocrit) and human plasma (25 μL). The mixture was then incubated at 37 ^{o}C. At various time points, aliquots (100 μL) were quenched with HCl (10 μL, 10 M). To the quenched solution MeOH (200 μL) and H_2O (100 μL) was added, followed by ultrafiltration (14,000 g/30 min with 3K Amicon filters, Invitrogen) and the wash was repeated one more time with MeOH:H_2O (50:50 v:v, 400 μL). Filtrates were collected, dried, dissolved in DMSO (200 μL), and analyzed by LC-MS using a C18 column.

Degradation of 5Tam-Aoc-GRTGRRFSY-amide by Trypsin and Chymotrypsin

Hemoglobin-free erythrocytes suspension (500 μL, 10% hematocrit) was added to a PBS 1X solution (500 μL) containing 5Tam-Aoc-GRTGRRFSY-amide (2.5 μM). An aliquot (100 μL) was quenched with HCl (10 μL, 10 M). The remainder (900 μL) was preincubated at 37 ^{o}C for 5 min before adding enzyme (chymotrypsin or trypsin at specified concentrations) added. At various time points, aliquots (100 μL) were quenched with HCl (10 μL, 10 M). MeOH (1 mL) was added to all quenched samples, followed by centrifugation at 21000 g/10 min. Supernatants were collected, dried, dissolved in DMSO, and analyzed by LC-MS.

Proteolytic Stability of CP-nb-Dipal in the Presence of Membrane

CP-nb-Dipal (0.417 μL, 3 mM) was dissolved in ethanol (5 μL). A suspension of hemoglobin-free erythrocytes (500 μL, 10% hematocrit in PBS 1X) was added to the

peptide solution. The suspension was then shaken at room temperature for 30 min, followed by centrifugation (10,000 g/2 min). The supernatant was discarded and the pellet was suspended in PBS 1X (500 µL) and transferred to a new vial. The loaded erythrocytes were then washed two more times with PBS 1X (500 µL, 10,000 g for 2 min centrifugation) before being suspended in PBS 1X (500 µL) to make lipidated-peptide-loaded erythrocytes (corresponding to 2.5 µM peptide, 10% hematocrit).

PBS 1X (500 µL) was added to the loaded erythrocyte suspension (500 µL 10% hematocrit, 2.5 µM peptide). One aliquot (100 µL) was quenched with HCl (10 µL, 10 M), another aliquot (100 µL) was transfer to a new vial and incubated at 37 ^{o}C for 2 h then quenched with HCl 10 µL, 10 M). The remainder (800 µL) was preincubated at 37 ^{o}C for 5 min before adding the enzyme (chymotrypsin or trypsin at specified concentrations). At various time points, aliquots (100 µL) were quenched with HCl (10 µL, 10 M). MeOH (1 mL) was added to all quenched samples were added followed by centrifugation at 21000 g for 10 min. Supernatants were collected, dried, dissolved in DMSO, and analyzed by LC-MS.

Study of α-MSH and 5Fam-labelled α-MSH with PRCP

Upon receipt, PRCP stock solution was diluted with cold enzyme dilution buffer (Tris.HCl 100 mM, pH 7.5 containing 10% glycerol by weight) to a concentration of 1 µM. Diluted enzyme was divided into PCR vials (10 µL each). Few aliquots were tested for activity, the remainder was stored in -80 ^{o}C for future experiments.

PBS 1X buffer containing 5Fam-α-MSH or native α-MSH (1.25 µM) was preincubated at 37 ^{o}C for 5 min. An aliquot was taken out as a control and PRCP (20 nM) was added to the remainder, followed by incubation at 37 ^{o}C for 30 min and analyzed by LC-MS.

Degradation was followed by mass and fluorescence (λ_{ex} - λ_{em} = 490 nm - 525 nm for 5Fam-peptide and 280 nm - 315 nm for native α-MSH).

Study of MSH-nb-Dipal with Chymotrypsin in the Presence of Erythrocytes

Hemoglobin-free erythrocytes were loaded with **MSH-nb-Dipal** as described before (10% hematocrit, 2.5 μM peptide). This suspension was then diluted in PBS 1X to 5% hematocrit and divided into three vials. One vial (1 mL) was incubated at 37 ^{o}C. Another vial was treated with chymotrypsin (5 nM), followed by incubation at 37 ^{o}C. At t = 1 h, aliquots (500 μL) were centrifuged (14,000 g for 10 min), followed by supernatant fluorescence assessment (200 μL) in a plate reader (λ_{ex} - λ_{em} = 490 nm - 525 nm). The third vial (1 mL) was treated with chymotrypsin (50 nM), followed by incubation at 37 ^{o}C for 2 h. The vial was then centrifuged (14,000 g for 10 min) and supernatant fluorescence was measured as control fluorescence (200 μL).

Study of MSH-nb-Dipal with Trypsin in the Presence of Erythrocytes

Hemoglobin-free erythrocytes were loaded with **MSH-nb-Dipal** as described before (10% hematocrit, 2.5 μM peptide). This suspension was then diluted in PBS 1X to 5% hematocrit and divided into three vials. One vial (1 mL) was incubated at 37 ^{o}C. Another vial was treated with trypsin (5 nM), followed by incubation at 37 ^{o}C. At t = 1 h, aliquots (500 μL) were centrifuged (14,000 g for 10 min), followed by supernatant fluorescence assessment (200 μL) in a plate reader (λ_{ex} - λ_{em} = 490 nm - 525 nm). To the third vial was added chymotrypsin (50 nM) followed by incubation at 37 ^{o}C for 2 h. The vial was then centrifuged (14,000 g for 10 min) and supernatant fluorescence was measured as control fluorescence (200 μL).

Study of MSH-nb-Dipal with Plasmin in the Presence of Erythrocytes

Erythrocytes (1 mL, 10% hematocrit) were washed three times with PBS 1X, followed by resuspension in PBS 1X to 10 % hematocrit. This erythrocyte suspension (1 mL) was then added to ethanol solution of MSH-nb-Dipal (10 μL, final concentration of peptide is 2.5 μM), followed by 30 min of gentle shaking at room temperature. The erythrocytes were then centrifuged at 2000 g for 2 min, resuspended in PBS 1X (1 mL) and transferred to a new vial, followed by two more wash cycles (1 mL PBS 1X, 2000g for 2 min). Peptide-loaded erythrocytes were then resuspended to 5% hematocrit in PBS 1X and divided into two vials (1 mL each). One vial was incubated at 37 ^{o}C, plasmin (40 nM) was added to the other vial followed by incubation at 37 ^{o}C. At t = 30 min, these vials was centrifuged (2000 g for 10 min) and supernatants' fluorescence measured in a plate reader (λ_{ex} - λ_{em} = 490 nm - 525 nm).

Confocal Microscopy Study of Hemoglobin-Free Erythrocytes Loaded with CP-nb-Dipal and HeLa Cells with and without Photolysis

HeLa cells were plated on 35 mm glass bottom dishes (MatTeck) the night before the experiment. Hemoglobin-free erythrocytes were prepared and loaded with **CP-nb-Dipal** (2.5 μM peptide, 10% hematocrit). The loaded erythrocyte were diluted to 5% hematocrit with L-15 media (Invitrogen) and then added to dishes containing HeLa cells (100 μL). The dishes were then kept on ice without photolysis or photolyzed on ice for 30 min using a Hg-Arc lamp with a 360 nm bandpass filter. HeLa cells were then washed with media, followed by incubation with Hoechst 33342 for 1-5 min. The HeLa cells were then washed 6 more times with media and imaged using confocal microscopy with filter settings corresponding to Hoechst 33342 and 5Tam fluorophores.

Syntheses

*Synthesis of **CP-nb-Stear***

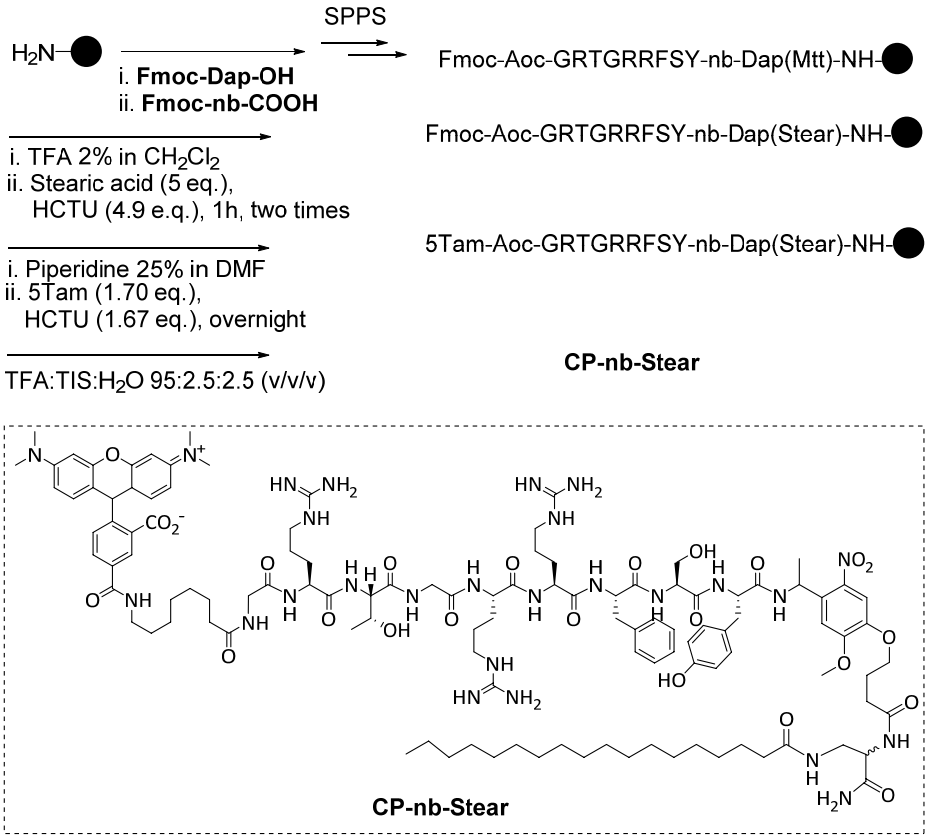

Scheme 5.1: Synthesis of CP-nb-Stear.

Peptide **CP-nb-Stear** was synthesized on resin using NovaPEG amide resin. Aoc, Dap, G, R, T, F, S, and Y residues were coupled using double coupling [Fmoc-Dap(Mtt)-OH (chempep), Fmoc building blocks of G, R, T, F, S, and Y residues (3 eq.), HCTU (2.94 eq.), DIPEA (10 eq.), coupling for 40 min and then amino acid (1.5 eq.), HCTU (1.47 eq.), DIPEA (7.5 eq.), coupling for 20 min]. Fmoc-nb-OH photolabile linker was coupled using Fmoc-nb-OH (2.05 eq.), HCTU (2.0 eq.), and DIPEA (7.5 eq.) for 2 h. Before the coupling of Fmoc-Aoc-OH, the peptide was capped with Ac_2O (10 eq.), DIPEA (20 eq.) for 20 min. Fmoc deprotection was performed using piperidine (25% in DMF) for 20 min. Before the

deprotetion of Fmoc group and coupling of 5Tam, the Mtt group was removed by TFA:TIS:CH_2Cl_2 (2:5:93 by v:v:v), the resin was washed with DMF (5 times), DMF with DIPEA 100 mM (2 times), then DMF, followed by the stearic acid coupling with stearic acid (5 eq.), HCTU (4.9 eq.) for 1 h, twice. 5Tam was coupled using 5Tam (1.7 eq.), HCTU (1.67 eq.), DIPEA (5 eq.) overnight. The resin was washed by DMF and dried. The peptide was leaved by TFA 95%, precipitated by cold ether, dried and purified on a C4 column using H_2O:CH_3CN solvents with 0.1% TFA. **CP-nb-Stear**, $C_{114}H_{168}N_{26}O_{24}$, exact mass calculated 2285.3, found (ESI+, m/z) 1143.1 $(M+2H)^{2+}$, 762.3 $(M+3H)^{3+}$, 572.1 $(M+4H)^{4+}$.

Synthesis of ***Dipal-Mal***

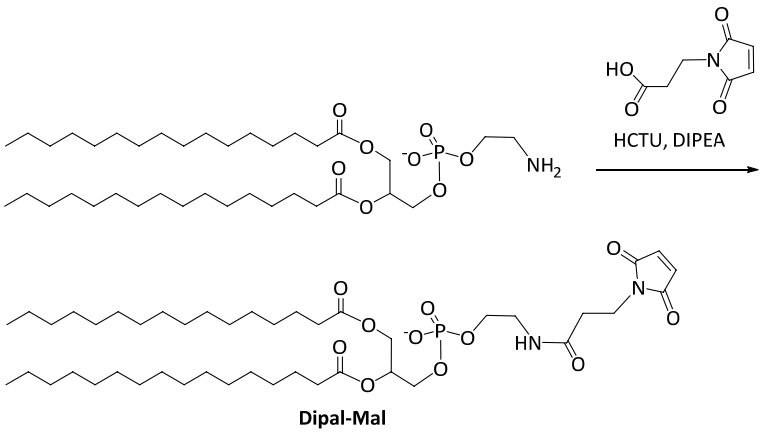

Scheme 5.2: Synthesis of Dipal-Mal.

1,2-Dipalmitoyl-*sn*-glycero-3-phosphoethanolamine (1.45 mmol, 1 eq.) was dissolved in CH_2Cl_2 and DMF. 3-Maleimido-propionic acid (1.2 eq.) and HCTU (1. 2 eq.) were dissolved in DMF in two separate glass vials. DIPEA (2 eq.) was added to the solution of 1,2-dipalmitoyl-*sn*-glycero-3-phosphoethanolamine immediately followed by the addition of the maleimide and HCTU solution. The reaction was shaken at room temperature for 30 min followed by addition of HCl (10 M) to pH 4. The reaction mixture was then extracted with EtOAc three times. The organic extract was dried and purified by

silica column using CH_2Cl_2:MeOH (MeOH with 0.5% CH_3COOH) as solvents, gradient from 0% to 50% MeOH. **Dipal-Mal**: ^1H NMR (400 MHz, $CDCl_3$) δ 7.53 (s, 1 H), 6.72 (s, 2 H), 5.19 (s, 1 H), 4.37 (d, J = 9.5 Hz, 1 H), 4.15-4.11 (m, 1 H), 3.91-3.79 (m, 6 H), 3.41 (bd, 2 H), 2.54 (t, J = 7 Hz, 2 H), 2.30-2.25 (m, 4 H), 2.01 (s, 4 H), 1.25 (s, 48 H), 0.88 (t, J = 6.8 Hz, 6 H). Molecular formula $C_{44}H_{78}N_2O_{11}P^-$.

*Synthesis of **CP-nb-Dipal***

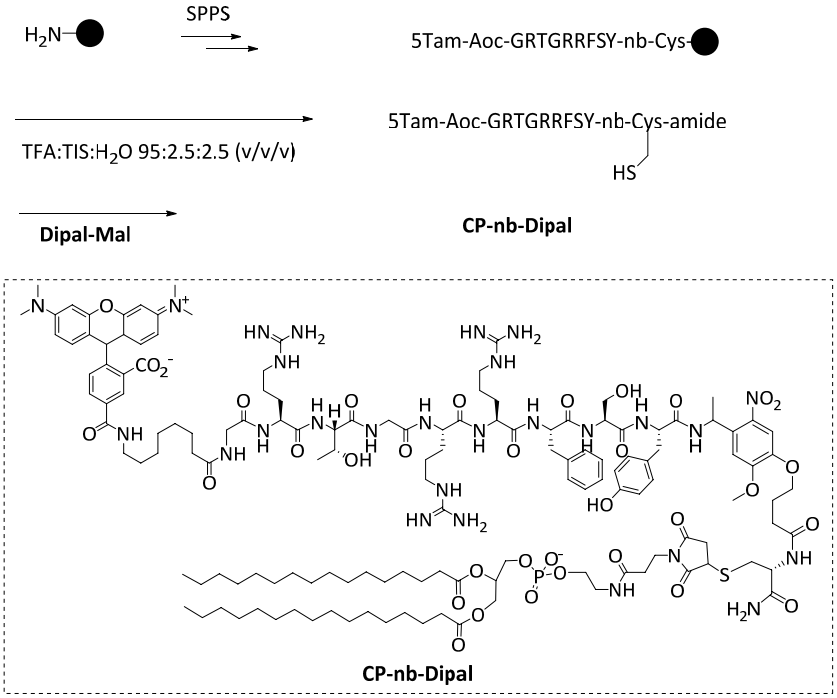

*Synthesis of **CP-nb-Cys***

Peptide **CP-nb-Cys** was synthesized on TGR resin. Briefly, all natural amino acids was coupled using double coupling with Fmoc-amino acid (5 eq.), HCTU (4.9 eq.), and DIPEA (10 eq.) for 20 and 30 min. Photolabile linker was coupled using **Fmoc-nb-OH** (3.2 eq.), HCTU (3.0 eq.), and DIPEA (6.5 eq.) for 59 min, then Fmoc-nb-OH (1.8 eq.), HCTU (1.5 eq.), and DIPEA (4.5 eq.) for 30 min. Aoc was coupled using Fmoc-Aoc-OH (5 eq.), HCTU (4.9 eq.), and DIPEA 10 (eq.) for 59 min. 5Tam was coupled using 5Tam (1.2 eq.), HCTU

(1.2 eq.), DIPEA (5 eq.) overnight. Fmoc deprotection was performed using piperidine (25% in DMF) for 20 min. After the coupling of 5Tam, the resin was washed by DMF and dried. The peptide was cleaved by TFA 95%, precipitated by cold ether, dried and purified on a C18 column using H_2O:CH_3CN solvents with 0.1% TFA. **5Tam-Aoc-RTGRRFSY-nb-Cys-amide**, $C_{96}H_{133}N_{25}O_{23}S$, exact mass calculated 2036.0 (M), found (ESI+, m/z) 1018.2 $(M+2H)^{2+}$, 679.2 $(M+3H)^{3+}$, 509.7 $(M+4H)^{4+}$.

*Synthesis of **CP-nb-Dipal***

CP-nb-Cys peptide (3.57 µmol) was dissolved in a minimum amount of MeOH. Dipal-Mal (6.17 µmol) was dissolved in $CHCl_3$. The two solutions were then mixed, bubbled with argon for 10 sec, sealed and shaken overnight. The reaction was then dried with air flow and vacuum and purified by the C4 column using H_2O:MeOH (each with 0.1 % TFA) as solvents. **CP-nb-Dipal**, $C_{140}H_{211}N_{27}O_{34}PS^-$, exact mass calculated 2877.5 $(M)^{1-}$, found (ESI+, m/z) 1440.1 $(M+3H)^{2+}$, 906.3 $(M+4H)^{3+}$, 720.5 $(M+5H)^{4+}$.

*Synthesis of **MSH-nb-Dipal***

*Synthesis of **5Fam- α-MSH-nb-Cys-amide***

Peptide **5Fam-α-MSH-nb-Cys-amide** was synthesized on TGR resin. Briefly, all natural amino acids were coupled using double coupling with Fmoc-amino acid (5 eq.), HCTU (4.9 eq.), and DIPEA (10 eq.) for 20 and 30 min. Photolabile linker was coupled using Fmoc-nb-OH (3.2 eq.), HCTU (3.0 eq.), and DIPEA (6.5 eq.) for 59 min, then **Fmoc-nb-OH** (1.8 eq.), HCTU (1.5 eq.), and DIPEA (4.5 eq.) for 30 min. 5Fam (1.5 eq.) was preactivated with HOBt (20 eq.) and DIC (1.7 eq.) for 10 min before being added to the resin. After the 5Fam coupling reaction was kept at room temperature for 2 h, the resin was washed with piperidine (25% in DMF) until no fluorescence was detected in DMF. The resin was dried and cleaved by TFA 95%, precipitated by cold ether, dried and purified on a C18 column

using H_2O:CH_3CN solvents with 0.1% TFA. **5Fam-α-MSH-nb-Cys-amide**, $C_{112}H_{138}N_{24}O_{30}S_2$, exact mass calculated 2363.0 (M), found (ESI+, m/z) 789.0 $(M+3H)^{3+}$, 592.0 $(M+4H)^{4+}$.

Synthesis of **MSH-nb-Dipal**

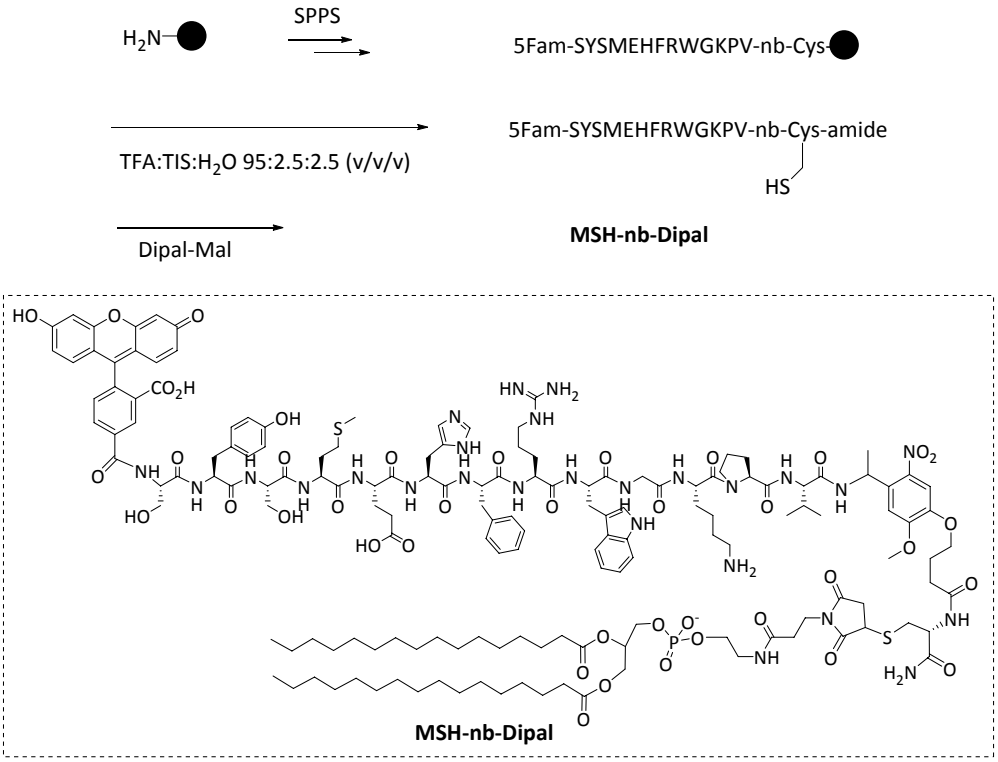

Scheme 5.4: Synthesis of MSH-nb-Dipal.

5Fam-α-MSH-nb-Cys-amide (1 eq.) was dissolved in a minimum amount of MeOH. **Dipal-Mal** (2 eq.) was dissolved in $CHCl_3$. The two solutions were then mixed, bubbled with Ar for 10 sec, sealed, and shaken overnight. The reaction was then dried with air flow and vacuum and purified on a C4 column using H_2O:MeOH as solvents (each with 0.1 % TFA). **MSH-nb-Dipal**, $C_{156}H_{216}N_{26}O_{41}PS_2^-$, exact mass calculated 3204.5 $(M)^{1-}$, found (ESI+, m/z) 1070.4 $(M+4H)^{3+}$, 802.9 $(M+5H)^{4+}$.

*Synthesis of **5Fam-SYSMEHFRWGKPV-amide (5Fam-α-MSH-amide)***

A solution of **5Fam-α-MSH-nb-Cys-amide** in H_2O was irradiated with UV light (from a Hg-Arc lamp using a 360 nm bandpass filter) for 30 min. The solution was then dried and

purified by HPLC using a C18 column. **5Fam-α-MSH-amide**, $C_{96}H_{117}N_{21}O_{24}S$, exact mass calculated (M) 1979.8, found (ESI+, m/z) 990.9 $(M+2H)^{2+}$, 661.2 $(M+3H)^{3+}$, 496.2 $(M+4H)^{4+}$.

*Synthesis of **C8-K(5Tam)-α-MSH-nb-Dipal***

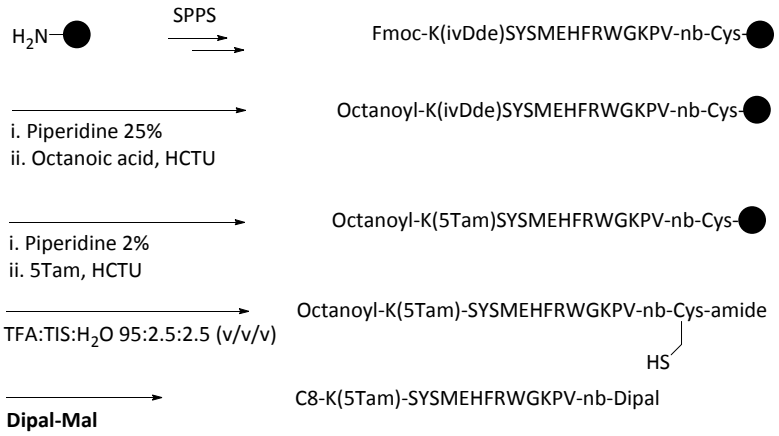

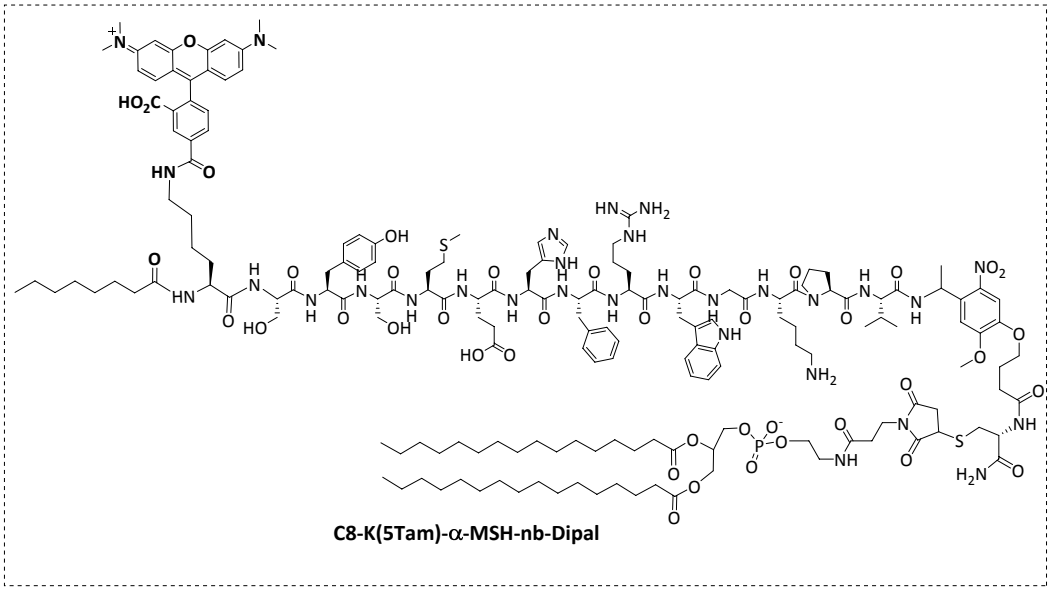

Scheme 5.5: Synthesis of C8-K(5Tam)-α-MSH-nb-Dipal.

*Synthesis of **C8-K(5Tam)-α-MSH-nb-Cys-amide***

Octanoyl-K(ivDde)SYSMEHFRWGKPV-nb-Cys-Resin was synthesized on TGR resin. Photolabile linker was coupled using **Fmoc-nb-COOH** (3.2 eq.), HCTU (3.0 eq.), and DIPEA (6.5 eq.) for 59 min, then **Fmoc-nb-COOH** (1.8 eq.), HCTU (1.5 eq.), and DIPEA (4.5

eq.) for 30 min. Octanoic acid (10 eq.) was coupled using HCTU (9.5 eq.), and DIPEA (20 eq.) for 1 h. All other amino acids were coupled using double coupling with Fmoc-amino acid (5 eq.), HCTU (4.9 eq.), and DIPEA (10 eq.) for 20 and 30 min. The ivDde protecting group was removed by hydrazine (2% in DMF, 5 min, 5 times) and 5Tam was coupled using 5Tam (1.2 eq.), HCTU (1.2 eq.), DIPEA (5 eq.) overnight. The resin was then dried and cleaved by TFA 95%, precipitated by cold ether, dried and purified on a C18 column using H_2O:CH_3CN solvents with 0.1% TFA. **C8-K(5Tam)-α-MSH-nb-Cys-amide**, $C_{130}H_{175}N_{28}O_{30}S_2$, exact mass calculated 2672.3 (M), found (ESI+, m/z) 891.6 $(M+3H)^{3+}$, 669.1 $(M+4H)^{4+}$.

*Synthesis of **C8-K(5Tam)-α-MSH-nb-Dipal***

C8-K(5Tam)-α-MSH-nb-Cys-amide (1 eq.) was dissolved in MeOH. **Dipal-Mal** (2 eq.) was dissolved in $CHCl_3$. The two solutions were mixed, bubbled with Ar for 10 sec, sealed, and shaken overnight. The reaction was then dried with air flow and vacuum and purified by the C4 column using H_2O:MeOH as solvents (each with 0.1 % TFA). **C8-K(5Tam)-α-MSH-nb-Dipal**, $C_{174}H_{253}N_{30}O_{41}PS_2$, exact mass calculated 3513.8 (M), found (ESI+, m/z) 1172.8 $(M+3H)^{3+}$, 880.2 $(M+4H)^{4+}$.

SUMMARY

In this dissertation we describe:

1. The development of the wavelength-tunable fluorescent reporters for monitoring protein kinase A activity. The developed sensors are powerful tools to investigate the roles of protein kinase A activity in erythrocyte biochemistry, for example, in *Plasmodium Falciparum* infection and propagation.

2. The design of light-activatable bioagents based on lipidation and membrane sequestration. The strategy provides a way to control the presence of a bioagents following a single photolytic event.

3. The further investigation of the membrane sequestration as a way to deliver peptide therapeutics into a specific region of the body. We propose to use erythrocytes as carriers and protectors of photoactivatable peptide therapeutics. The delivery of a cell permeable peptide, an anti-inflammatory agent, and a blood clotting agent are being investigated. The study will provide a powerful strategy toward the treatment of various diseases such as rheumatoid arthritis and cancer.

REFERENCES

1. Herschel, J. F. W., On a Case of Superficial Colour Presented by a Homogeneous Liquid Internally Colourless. *Philosophical Transactions of the Royal Society of London* **1845,** *135*, 143-145.

2. Stokes, G. G., On the Change of Refrangibility of Light. *Philosophical Transactions of the Royal Society of London* **1852,** *142*, 463-562.

3. *The Molecular Probes® Handbook—A Guide to Fluorescent Probes and Labeling Technologies* 11th Edition ed.; Invitrogen: 2010.

4. Lavis, L. D.; Raines, R. T., Bright ideas for chemical biology. *ACS Chem Biol* **2008,** *3* (3), 142-55.

5. Shimomura, O.; Johnson, F. H.; Saiga, Y., Extraction, purification and properties of aequorin, a bioluminescent protein from the luminous hydromedusan, Aequorea. *J Cell Comp Physiol* **1962,** *59*, 223-39.

6. Wang, Y.; Shyy, J. Y.; Chien, S., Fluorescence proteins, live-cell imaging, and mechanobiology: seeing is believing. *Annu Rev Biomed Eng* **2008,** *10*, 1-38.

7. Tsien, R. Y., The green fluorescent protein. *Annu Rev Biochem* **1998,** *67*, 509-44.

8. Chalfie, M.; Tu, Y.; Euskirchen, G.; Ward, W. W.; Prasher, D. C., Green fluorescent protein as a marker for gene expression. *Science* **1994,** *263* (5148), 802-5.

9. Shaner, N. C.; Steinbach, P. A.; Tsien, R. Y., A guide to choosing fluorescent proteins. *Nat Methods* **2005,** *2* (12), 905-9.

10. Heim, R.; Prasher, D. C.; Tsien, R. Y., Wavelength mutations and posttranslational autoxidation of green fluorescent protein. *Proc Natl Acad Sci U S A* **1994,** *91* (26), 12501-4.

11. Zhang, J.; Campbell, R. E.; Ting, A. Y.; Tsien, R. Y., Creating new fluorescent probes for cell biology. *Nat Rev Mol Cell Biol* **2002,** *3* (12), 906-18.

12. Tsien, R. Y., Fluorescent probes of cell signaling. *Annu Rev Neurosci* **1989,** *12*, 227-53.

13. Ueno, T.; Nagano, T., Fluorescent probes for sensing and imaging. *Nat Methods* **2011,** *8* (8), 642-5.

14. Nguyen, Q. T.; Tsien, R. Y., Fluorescence-guided surgery with live molecular navigation--a new cutting edge. *Nat Rev Cancer* **2013,** *13* (9), 653-62.

15. Urano, Y.; Kamiya, M.; Kanda, K.; Ueno, T.; Hirose, K.; Nagano, T., Evolution of Fluorescein as a Platform for Finely Tunable Fluorescence Probes. *J Am Chem Soc* **2005,** *127* (13), 4888-4894.

16. Nguyen, Q. T.; Olson, E. S.; Aguilera, T. A.; Jiang, T.; Scadeng, M.; Ellies, L. G.; Tsien, R. Y., Surgery with molecular fluorescence imaging using activatable cell-penetrating peptides decreases residual cancer and improves survival. *Proc Natl Acad Sci U S A* **2010,** *107* (9), 4317-22.

17. Wu, Y. I.; Frey, D.; Lungu, O. I.; Jaehrig, A.; Schlichting, I.; Kuhlman, B.; Hahn, K. M., A genetically encoded photoactivatable Rac controls the motility of living cells. *Nature* **2009,** *461* (7260), 104-8.

18. Sordillo, L. A.; Pu, Y.; Sordillo, P. P.; Budansky, Y.; Alfano, R. R. In *Deep tissue imaging of microfracture and non-displaced fracture of bone using the second and third near-infrared therapeutic windows*, 2014; pp 89263V-89263V-8.

19. Sordillo, L. A.; Pu, Y.; Pratavieira, S. o.; Budansky, Y.; Alfano, R. R., Deep optical imaging of tissue using the second and third near-infrared spectral windows. *Journal of Biomedical Optics* **2014,** *19* (5), 056004-056004.

20. Frangioni, J. V., In vivo near-infrared fluorescence imaging. *Curr Opin Chem Biol* **2003,** *7* (5), 626-34.

21. Pansare, V.; Hejazi, S.; Faenza, W.; Prud'homme, R. K., Review of Long-Wavelength Optical and NIR Imaging Materials: Contrast Agents, Fluorophores and Multifunctional Nano Carriers. *Chem Mater* **2012,** *24* (5), 812-827.

22. Boulnois, J.-L., Photophysical processes in recent medical laser developments: A review. *Lasers in Medical Science* **1986,** *1* (1), 47-66.

23. Zhang, J.; Yang, P. L.; Gray, N. S., Targeting cancer with small molecule kinase inhibitors. *Nat Rev Cancer* **2009,** *9* (1), 28-39.

24. Lahiry, P.; Torkamani, A.; Schork, N. J.; Hegele, R. A., Kinase mutations in human disease: interpreting genotype-phenotype relationships. *Nat Rev Genet* **2010,** *11* (1), 60-74.

25. Patterson, H.; Nibbs, R.; McInnes, I.; Siebert, S., Protein kinase inhibitors in the treatment of inflammatory and autoimmune diseases. *Clinical & Experimental Immunology* **2014,** *176* (1), 1-10.

26. Chico, L. K.; Van Eldik, L. J.; Watterson, D. M., Targeting protein kinases in central nervous system disorders. *Nat Rev Drug Discov* **2009,** *8* (11), 892-909.

27. Rothman, D. M.; Shults, M. D.; Imperiali, B., Chemical approaches for investigating phosphorylation in signal transduction networks. *Trends Cell Biol* **2005,** *15* (9), 502-10.

28. Ting, A. Y.; Kain, K. H.; Klemke, R. L.; Tsien, R. Y., Genetically encoded fluorescent reporters of protein tyrosine kinase activities in living cells. *Proc Natl Acad Sci U S A* **2001,** *98* (26), 15003-8.

29. Komatsu, N.; Aoki, K.; Yamada, M.; Yukinaga, H.; Fujita, Y.; Kamioka, Y.; Matsuda, M., Development of an optimized backbone of FRET biosensors for kinases and GTPases. *Mol Biol Cell* **2011,** *22* (23), 4647-56.

30. Chen, C. A.; Yeh, R. H.; Lawrence, D. S., Design and synthesis of a fluorescent reporter of protein kinase activity. *J Am Chem Soc* **2002,** *124* (15), 3840-1.

31. Shults, M. D.; Janes, K. A.; Lauffenburger, D. A.; Imperiali, B., A multiplexed homogeneous fluorescence-based assay for protein kinase activity in cell lysates. *Nat Methods* **2005,** *2* (4), 277-83.

32. Stains, C. I.; Tedford, N. C.; Walkup, T. C.; Lukovic, E.; Goguen, B. N.; Griffith, L. G.; Lauffenburger, D. A.; Imperiali, B., Interrogating signaling nodes involved in cellular transformations using kinase activity probes. *Chem Biol* **2012,** *19* (2), 210-7.

33. Shults, M. D.; Carrico-Moniz, D.; Imperiali, B., Optimal Sox-based fluorescent chemosensor design for serine/threonine protein kinases. *Anal Biochem* **2006,** *352* (2), 198-207.

34. Yeh, R. H.; Yan, X.; Cammer, M.; Bresnick, A. R.; Lawrence, D. S., Real time visualization of protein kinase activity in living cells. *J Biol Chem* **2002,** *277* (13), 11527-32.

35. Wang, Q.; Lawrence, D. S., Phosphorylation-driven protein-protein interactions: a protein kinase sensing system. *J Am Chem Soc* **2005,** *127* (21), 7684-5.

36. Wang, Q.; Cahill, S. M.; Blumenstein, M.; Lawrence, D. S., Self-Reporting Fluorescent Substrates of Protein Tyrosine Kinases. *J Am Chem Soc* **2006,** *128* (6), 1808-1809.

37. Wakata, A.; Cahill, S. M.; Blumenstein, M.; Gunby, R. H.; Jockusch, S.; Marti, A. A.; Cimbro, B.; Gambacorti-Passerini, C.; Donella-Deana, A.; Pinna, L. A.; Turro, N. J.; Lawrence, D. S., A mechanistic design principle for protein tyrosine kinase sensors: application to a validated cancer target. *Org Lett* **2008,** *10* (2), 301-4.

38. Wang, Q.; Zimmerman, E. I.; Toutchkine, A.; Martin, T. D.; Graves, L. M.; Lawrence, D. S., Multicolor monitoring of dysregulated protein kinases in chronic myelogenous leukemia. *ACS Chem Biol* **2010,** *5* (9), 887-95.

39. Sharma, V.; Agnes, R. S.; Lawrence, D. S., Deep Quench: An Expanded Dynamic Range for Protein Kinase Sensors. *J Am Chem Soc* **2007,** *129* (10), 2742-2743.

40. Agnes, R. S.; Jernigan, F.; Shell, J. R.; Sharma, V.; Lawrence, D. S., Suborganelle sensing of mitochondrial cAMP-dependent protein kinase activity. *J Am Chem Soc* **2010,** *132* (17), 6075-80.

41. Lee, C. L.; Linton, J.; Soughayer, J. S.; Sims, C. E.; Allbritton, N. L., Localized measurement of kinase activation in oocytes of Xenopus laevis. *Nat Biotechnol* **1999,** *17* (8), 759-62.

42. Meredith, G. D.; Sims, C. E.; Soughayer, J. S.; Allbritton, N. L., Measurement of kinase activation in single mammalian cells. *Nat Biotechnol* **2000,** *18* (3), 309-12.

43. Proctor, A.; Wang, Q.; Lawrence, D. S.; Allbritton, N. L., Development of a peptidase-resistant substrate for single-cell measurement of protein kinase B activation. *Anal Chem* **2012,** *84* (16), 7195-202.

44. Xu, W.; Allbritton, N.; Lawrence, D. S., SRC kinase regulation in progressively invasive cancer. *PLoS One* **2012,** *7* (11), e48867.

45. Kneissl, S.; Loveridge, E. J.; Williams, C.; Crump, M. P.; Allemann, R. K., Photocontrollable peptide-based switches target the anti-apoptotic protein Bcl-xL. *Chembiochem* **2008,** *9* (18), 3046-54.

46. Kneissl, S.; Loveridge, E. J.; Williams, C.; Crump, M. P.; Allemann, R. K., Photocontrollable Peptide-Based Switches Target the Anti-Apoptotic Protein Bcl-xL. *Chembiochem* **2008,** *9* (18), 3046-3054.

47. Banghart, M.; Borges, K.; Isacoff, E.; Trauner, D.; Kramer, R. H., Light-activated ion channels for remote control of neuronal firing. *Nat Neurosci* **2004,** *7* (12), 1381-6.

48. Volgraf, M.; Gorostiza, P.; Numano, R.; Kramer, R. H.; Isacoff, E. Y.; Trauner, D., Allosteric control of an ionotropic glutamate receptor with an optical switch. *Nat Chem Biol* **2006,** *2* (1), 47-52.

49. Tischer, D.; Weiner, O. D., Illuminating cell signalling with optogenetic tools. *Nat Rev Mol Cell Biol* **2014,** *15* (8), 551-8.

50. Lee, H. M.; Larson, D. R.; Lawrence, D. S., Illuminating the chemistry of life: design, synthesis, and applications of "caged" and related photoresponsive compounds. *ACS Chem Biol* **2009,** *4* (6), 409-27.

51. Klan, P.; Solomek, T.; Bochet, C. G.; Blanc, A.; Givens, R.; Rubina, M.; Popik, V.; Kostikov, A.; Wirz, J., Photoremovable Protecting Groups in Chemistry and Biology: Reaction Mechanisms and Efficacy. *Chemical Reviews 113* (1), 119-191.

52. Ellis-Davies, G. C., Caged compounds: photorelease technology for control of cellular chemistry and physiology. *Nat Methods* **2007,** *4* (8), 619-28.

53. Mayer, G.; Heckel, A., Biologically active molecules with a "light switch". *Angew Chem Int Ed Engl* **2006,** *45* (30), 4900-21.

54. Kaplan, J. H.; Forbush, B.; Hoffman, J. F., Rapid photolytic release of adenosine 5'-triphosphate from a protected analog: utilization by the sodium:potassium pump of human red blood cell ghosts. *Biochemistry* **1978,** *17* (10), 1929-1935.

55. Walker, J. W.; McCray, J. A.; Hess, G. P., Photolabile protecting groups for an acetylcholine receptor ligand. Synthesis and photochemistry of a new class of o-nitrobenzyl derivatives and their effects on receptor function. *Biochemistry* **1986,** *25* (7), 1799-805.

56. Wieboldt, R.; Gee, K. R.; Niu, L.; Ramesh, D.; Carpenter, B. K.; Hess, G. P., Photolabile precursors of glutamate: synthesis, photochemical properties, and activation of glutamate receptors on a microsecond time scale. *Proc Natl Acad Sci U S A* **1994,** *91* (19), 8752-6.

57. Cruz, F. G.; Koh, J. T.; Link, K. H., Light-Activated Gene Expression. *J Am Chem Soc* **2000,** *122* (36), 8777-8778.

58. Lin, W.; Albanese, C.; Pestell, R. G.; Lawrence, D. S., Spatially discrete, light-driven protein expression. *Chem Biol* **2002,** *9* (12), 1347-53.

59. Ellis-Davies, G. C. R.; Kaplan, J. H., A new class of photolabile chelators for the rapid release of divalent cations: generation of caged calcium and caged magnesium. *The Journal of Organic Chemistry* **1988,** *53* (9), 1966-1969.

60. Adams, S. R.; Kao, J. P. Y.; Grynkiewicz, G.; Minta, A.; Tsien, R. Y., Biologically useful chelators that release Ca2+ upon illumination. *J Am Chem Soc* **1988,** *110* (10), 3212-3220.

61. Ellis-Davies, G. C.; Kaplan, J. H., Nitrophenyl-EGTA, a photolabile chelator that selectively binds Ca2+ with high affinity and releases it rapidly upon photolysis. *Proceedings of the National Academy of Sciences* **1994,** *91* (1), 187-191.

62. Lawrence, D. S., The preparation and in vivo applications of caged peptides and proteins. *Curr Opin Chem Biol* **2005,** *9* (6), 570-5.

63. Walker, J. W.; Gilbert, S. H.; Drummond, R. M.; Yamada, M.; Sreekumar, R.; Carraway, R. E.; Ikebe, M.; Fay, F. S., Signaling pathways underlying eosinophil cell motility revealed by using caged peptides. *Proc Natl Acad Sci U S A* **1998,** *95* (4), 1568-73.

64. Nguyen, A.; Rothman, D. M.; Stehn, J.; Imperiali, B.; Yaffe, M. B., Caged phosphopeptides reveal a temporal role for 14-3-3 in G1 arrest and S-phase checkpoint function. *Nat Biotechnol* **2004,** *22* (8), 993-1000.

65. Veldhuyzen, W. F.; Nguyen, Q.; McMaster, G.; Lawrence, D. S., A light-activated probe of intracellular protein kinase activity. *J Am Chem Soc* **2003,** *125* (44), 13358-9.

66. Wang, Q.; Dai, Z.; Cahill, S. M.; Blumenstein, M.; Lawrence, D. S., Light-regulated sampling of protein tyrosine kinase activity. *J Am Chem Soc* **2006,** *128* (43), 14016-7.

67. Li, H.; Hah, J. M.; Lawrence, D. S., Light-mediated liberation of enzymatic activity: "small molecule" caged protein equivalents. *J Am Chem Soc* **2008,** *130* (32), 10474-5.

68. Chang, C.-y.; Fernandez, T.; Panchal, R.; Bayley, H., Caged Catalytic Subunit of cAMP-Dependent Protein Kinase. *J Am Chem Soc* **1998,** *120* (30), 7661-7662.

69. Zou, K.; Cheley, S.; Givens, R. S.; Bayley, H., Catalytic Subunit of Protein Kinase A Caged at the Activating Phosphothreonine. *J Am Chem Soc* **2002,** *124* (28), 8220-8229.

70. Ghosh, M.; Ichetovkin, I.; Song, X.; Condeelis, J. S.; Lawrence, D. S., A New Strategy for Caging Proteins Regulated by Kinases. *J Am Chem Soc* **2002,** *124* (11), 2440-2441.

71. Ghosh, M.; Song, X.; Mouneimne, G.; Sidani, M.; Lawrence, D. S.; Condeelis, J. S., Cofilin Promotes Actin Polymerization and Defines the Direction of Cell Motility. *Science* **2004,** *304* (5671), 743-746.

72. Goguen, B. N.; Hoffman, B. D.; Sellers, J. R.; Schwartz, M. A.; Imperiali, B., Light-Triggered Myosin Activation for Probing Dynamic Cellular Processes. *Angew Chem Int Ed Engl 50* (25), 5667-5670.

73. Lee, H. M.; Xu, W.; Lawrence, D. S., Construction of a photoactivatable profluorescent enzyme via propinquity labeling. *J Am Chem Soc* **2011,** *133* (8), 2331-3.

74. Wu, N.; Deiters, A.; Cropp, T. A.; King, D.; Schultz, P. G., A genetically encoded photocaged amino acid. *J Am Chem Soc* **2004,** *126* (44), 14306-7.

75. Endo, M.; Nakayama, K.; Kaida, Y.; Majima, T., Design and synthesis of photochemically controllable caspase-3. *Angew Chem Int Ed Engl* **2004,** *43* (42), 5643-5.

76. Endo, M.; Nakayama, K.; Majima, T., Design and synthesis of photochemically controllable restriction endonuclease BamHI by manipulating the salt-bridge network in the dimer interface. *J Org Chem* **2004,** *69* (13), 4292-8.

77. Deiters, A.; Groff, D.; Ryu, Y.; Xie, J.; Schultz, P. G., A genetically encoded photocaged tyrosine. *Angew Chem Int Ed Engl* **2006,** *45* (17), 2728-31.

78. Gautier, A.; Deiters, A.; Chin, J. W., Light-activated kinases enable temporal dissection of signaling networks in living cells. *J Am Chem Soc 133* (7), 2124-7.

79. Monroe, W. T.; McQuain, M. M.; Chang, M. S.; Alexander, J. S.; Haselton, F. R., Targeting Expression with Light Using Caged DNA. *Journal of Biological Chemistry* **1999,** *274* (30), 20895-20900.

80. Ando, H.; Furuta, T.; Tsien, R. Y.; Okamoto, H., Photo-mediated gene activation using caged RNA/DNA in zebrafish embryos. *Nat Genet* **2001,** *28* (4), 317-325.

81. Ubersax, J. A.; Ferrell, J. E., Jr., Mechanisms of specificity in protein phosphorylation. *Nat Rev Mol Cell Biol* **2007,** *8* (7), 530-41.

82. Hidaka, H.; Inagaki, M.; Kawamoto, S.; Sasaki, Y., Isoquinolinesulfonamides, novel and potent inhibitors of cyclic nucleotide dependent protein kinase and protein kinase C. *Biochemistry* **1984,** *23* (21), 5036-41.

83. D'Alessandro, A.; Righetti, P. G.; Zolla, L., The red blood cell proteome and interactome: an update. *J Proteome Res* **2010,** *9* (1), 144-63.

84. Proctor, A.; Wang, Q.; Lawrence, D. S.; Allbritton, N. L., Metabolism of peptide reporters in cell lysates and single cells. *Analyst* **2012,** *137* (13), 3028-38.

85. Piekielna, J.; Perlikowska, R.; Gach, K.; Janecka, A., Cyclization in opioid peptides. *Curr Drug Targets* **2013,** *14* (7), 798-816.

86. Il'ichev, Y. V.; Schwörer, M.; Wirz, J., Photochemical Reaction Mechanisms of 2-Nitrobenzyl Compounds: Methyl Ethers and Caged ATP. *J Am Chem Soc* **2004,** *126* (14), 4581-4595.

87. Kaspar, A. A.; Reichert, J. M., Future directions for peptide therapeutics development. *Drug Discov Today* **2013,** *18* (17-18), 807-17.

88. Tan, M. L.; Choong, P. F.; Dass, C. R., Recent developments in liposomes, microparticles and nanoparticles for protein and peptide drug delivery. *Peptides* **2010,** *31* (1), 184-93.

89. Harris, J. M.; Chess, R. B., Effect of pegylation on pharmaceuticals. *Nat Rev Drug Discov* **2003,** *2* (3), 214-21.

90. Brzoska, T.; Bohm, M.; Lugering, A.; Loser, K.; Luger, T. A., Terminal signal: anti-inflammatory effects of alpha-melanocyte-stimulating hormone related peptides beyond the pharmacophore. *Adv Exp Med Biol* **2010,** *681*, 107-16.

91. Lipton, J. M.; Catania, A., Mechanisms of antiinflammatory action of the neuroimmunomodulatory peptide alpha-MSH. *Ann N Y Acad Sci* **1998,** *840*, 373-80.

92. Brzoska, T.; Luger, T. A.; Maaser, C.; Abels, C.; Bohm, M., Alpha-melanocyte-stimulating hormone and related tripeptides: biochemistry, antiinflammatory and protective effects in vitro and in vivo, and future perspectives for the treatment of immune-mediated inflammatory diseases. *Endocr Rev* **2008,** *29* (5), 581-602.

93. Luger, T. A.; Brzoska, T., alpha-MSH related peptides: a new class of anti-inflammatory and immunomodulating drugs. *Ann Rheum Dis* **2007,** *66 Suppl 3*, iii52-5.

94. Rudman, D.; Hollins, B. M.; Kutner, M. H.; Moffitt, S. D.; Lynn, M. J., *Three types of alpha-melanocyte-stimulating hormone: bioactivities and half-lives*. 1983; Vol. 245, p E47-E54.

95. Wallingford, N.; Perroud, B.; Gao, Q.; Coppola, A.; Gyengesi, E.; Liu, Z. W.; Gao, X. B.; Diament, A.; Haus, K. A.; Shariat-Madar, Z.; Mahdi, F.; Wardlaw, S. L.; Schmaier, A. H.; Warden, C. H.; Diano, S., Prolylcarboxypeptidase regulates food intake by inactivating alpha-MSH in rodents. *J Clin Invest* **2009,** *119* (8), 2291-303.

96. Akiyama, K.; Yamamura, H. I.; Wilkes, B. C.; Cody, W. L.; Hruby, V. J.; Castrucci, A. M.; Hadley, M. E., Relative stability of alpha-melanotropin and related analogues to rat brain homogenates. *Peptides* **1984,** *5* (6), 1191-5.

97. Sawyer, T. K.; Sanfilippo, P. J.; Hruby, V. J.; Engel, M. H.; Heward, C. B.; Burnett, J. B.; Hadley, M. E., 4-Norleucine, 7-D-phenylalanine-alpha-melanocyte-stimulating hormone: a highly potent alpha-melanotropin with ultralong biological activity. *Proc Natl Acad Sci U S A* **1980,** *77* (10), 5754-8.

98. Cody, W. L.; Mahoney, M.; Knittel, J. J.; Hruby, V. J.; Castrucci, A. M.; Hadley, M. E., Cyclic melanotropins. 9. 7-D-Phenylalanine analogues of the active-site sequence. *J Med Chem* **1985,** *28* (5), 583-8.

99. Yang, H. Y. T.; Erdos, E. G.; Chiang, T. S., New Enzymatic Route for the Inactivation of Angiotensin. *Nature* **1968,** *218* (5148), 1224-1226.

100. Linss, W.; Pilgrim, C.; Feuerstein, H., How Thick is the Glycocalyx of Human Erythrocytes. *Acta histochemica* **1991,** *91* (1), 101-104.